

Micro-tip chromatography; a route to an  
integrated strategy for high throughput  
bioprocess development

by

Marc David Wenger

A thesis submitted for the degree of

Doctor of Philosophy

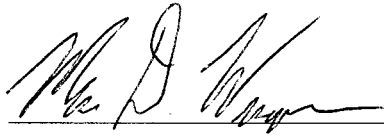
in

The Department of Biochemical Engineering

UCL

December 2010

I, Marc David Wenger, confirm that the work presented in this thesis is my own.  
Where information has been derived from other sources, I confirm that this has been  
indicated in the thesis.

A handwritten signature in black ink, appearing to read 'M. D. Wenger', written over a horizontal line.

Date 23 NOV 2010

## ABSTRACT

Bioprocessing groups must keep pace with the many biologics and vaccines entering development, while ensuring process robustness, controlling costs, and accelerating project timelines. Microscale techniques provide a means to cope with these challenges by enabling high-throughput investigations to identify problems early, reduce requirements for costly large-scale experiments, and promote quality-by-design approaches for process optimisation. Micro-tip columns (packed sorbent in a pipette tip) for chromatography and Adaptive Focused Acoustics (AFA) for cell disruption are two such techniques with potential to deliver high-throughput process development. This thesis characterises these platforms and integrates them as elements of the development workflow.

Firstly, the key parameters are defined for robust, automated micro-tip chromatography. Finite-bath methods for isotherms and kinetic measurements are demonstrated, with sorbent contact time found to be critical for uptake of proteins on porous adsorbents, consistent with pore diffusion being rate-determining. Based upon these micro-tip data, two data-driven models are applied to predict dynamic binding capacity, one employing a shrinking-core model, and the other, a staged-reaction model. Both show satisfactory agreement with experimental laboratory column results. Micro-tip chromatography is then illustrated as an accelerated process development strategy for a mixed-mode chromatography step, with the results found to be predictive of laboratory column-scale yield, purity and capacity. In a second application, micro-tip chromatography is used to evaluate the interaction of upstream fermentation changes upon the downstream chromatography. The microscale chromatography is predictive of laboratory-scale yield and purity, despite being 1000-times smaller, while increasing productivity by over ten-fold. The miniaturisation of the chromatography, however, necessitates the development of a microscale cell disruption method to fully realise the gains in throughput and volume reduction. The AFA technique meets this goal, providing representative feed material for chromatographic study. Together, micro-tip chromatography and AFA form the basis for a next-generation bioprocess development platform.

## **ACKNOWLEDGEMENTS**

I am grateful for the kind guidance and input by Dan Bracewell throughout this project. I would also like to thank Pete DePhillips for his support at Merck, without which this project would not have been possible. The contribution and expertise provided by the many people at Merck and UCL are warmly acknowledged, with specific appreciation given to Sunil Chhatre for his assistance with modelling, Colleen Price for her help with the laboratory-scale VLP purifications, Matt Woodling and Brad Thomas for their participation in the mixed mode chromatography work, Barry Buckland for his support from Merck BioProcess R&D, and Nigel Titchener-Hooker and Mike Hoare for their support at UCL. Last, but certainly not least, I would like to give a special thanks to my wife Sylvia for encouraging me to take on this endeavour and to my children, Matthew and Elena, for always helping to keep things in perspective.

In addition, I want to gratefully acknowledge the sponsorship of the Merck Doctoral Study Program and the support of the Innovative Manufacturing Research Centre (IMRC) in Bioprocessing. The IMRC is part of The Advanced Centre for Biochemical Engineering, University College London, with collaboration from a range of academic partners and biopharmaceutical and biotechnology companies.

# CONTENTS

<b>ABSTRACT</b> .....	<b>3</b>
<b>ACKNOWLEDGEMENTS</b> .....	<b>4</b>
<b>CONTENTS</b> .....	<b>5</b>
<b>LIST OF FIGURES</b> .....	<b>10</b>
<b>LIST OF TABLES</b> .....	<b>13</b>
<b>LIST OF SYMBOLS AND ABBREVIATIONS</b> .....	<b>15</b>
<b>1. INTRODUCTION</b> .....	<b>19</b>
<b>1.1. Motivation for the Project</b> .....	19
<b>1.2. Aims for the Project</b> .....	21
<b>1.3. Production of Recombinant Proteins</b> .....	22
<i>1.3.1. Fermentation and Cell Culture</i> .....	25
<i>1.3.2. Cell Disruption and Primary Recovery</i> .....	26
<i>1.3.3. Preparative Chromatography</i> .....	27
1.3.3.1. Modes of Operation.....	29
1.3.3.2. Sorbent Properties.....	30
1.3.3.3. Operational Parameters.....	33
<i>1.3.4. Membrane Separations</i> .....	33
<b>1.4. Theoretical Considerations in Preparative Liquid Chromatography</b> .....	35
<i>1.4.1. Adsorption</i> .....	36
1.4.1.1. Single-Component Adsorption Isotherms.....	36
1.4.1.2. Multi-Component Adsorption Isotherms.....	41
1.4.1.3. Adsorption Isotherm Models for Ion-Exchange Chromatography.....	42
1.4.1.4. Retention Factor.....	43
<i>1.4.2. Mass Transport</i> .....	44
1.4.2.1. Plate Models and Rate Theory.....	44
1.4.2.2. Mass Transfer in Porous Adsorbents.....	45
1.4.2.3. Intraparticle (Pore) Mass Transport.....	48
<i>1.4.3. Scale Considerations</i> .....	51
<i>1.4.4. Models of Nonlinear Chromatography</i> .....	52
<b>1.5. Microscale Bioprocess Development</b> .....	54
<i>1.5.1. Terminology</i> .....	54
<i>1.5.2. Goals of Microscale Bioprocessing Techniques</i> .....	56
<i>1.5.3. Techniques for Cell Culture and Fermentation</i> .....	58
<i>1.5.4. Techniques for Cell Disruption</i> .....	59
<i>1.5.5. Techniques for Primary Recovery</i> .....	60
<i>1.5.6. Techniques for Chromatography</i> .....	61
1.5.6.1. Micro-Batch Adsorption.....	62
1.5.6.2. Micro-Tip Chromatography.....	68
1.5.6.3. Miniature Column Chromatography.....	70

1.5.7. Workflow for High-Throughput Microscale Experiments.....	72
1.5.7.1. Experimental Design.....	72
1.5.7.2. High-Throughput Analytics.....	72
<b>1.6. Organisation of Thesis.....</b>	<b>74</b>
<b>2. MATERIALS AND METHODS.....</b>	<b>75</b>
<b>2.1. Materials.....</b>	<b>75</b>
2.1.1. Chromatographic Separation Media.....	75
2.1.2. Purification Reagents.....	75
<b>2.2. Protein Test Systems.....</b>	<b>75</b>
2.2.1. Human Papillomavirus (HPV) Virus-like Particles (VLPs).....	75
2.2.2. Monoclonal Antibodies.....	77
2.2.3. Purchased Proteins.....	78
<b>2.3. Analytical Methods.....</b>	<b>78</b>
2.3.1. Protein Quantification.....	78
2.3.1.1. Ultraviolet (UV) Spectrophotometry.....	78
2.3.1.2. Total Protein by the BCA Assay.....	78
2.3.1.3. Reversed-Phase Chromatography for HPV L1 Protein Quantification.....	79
2.3.1.4. Immunoassay for HPV VLP Quantification.....	79
2.3.1.5. Octet Protein A Assay for IgG Quantification.....	79
2.3.2. Purity.....	80
2.3.2.1. SDS-PAGE.....	80
2.3.2.2. Residual Host-Cell Protein Immunoassay.....	80
2.3.2.3. Quantification of Residual dsDNA with the PicoGreen Reagent.....	80
2.3.3. Characterisation of Yeast Lysate from Cell Disruption Experiments.....	81
2.3.3.1. Optical Density.....	81
2.3.3.2. Light Microscopy.....	81
<b>2.4. Description of Chromatographic Methods.....</b>	<b>81</b>
2.4.1. Column Chromatography.....	81
2.4.2. Micro-Tip Chromatography.....	82
2.4.3. Micro-Batch Adsorption.....	82
<b>2.5. Cell Disruption of Yeast.....</b>	<b>83</b>
<b>2.6. Statistical and Mathematical Software.....</b>	<b>84</b>
<b>3. OPERATION AND AUTOMATION OF MICRO-TIP CHROMATOGRAPHY.....</b>	<b>85</b>
<b>3.1. Introduction.....</b>	<b>85</b>
<b>3.2. Set-Up and Automation of Micro-Tip Chromatography.....</b>	<b>85</b>
3.2.1. Micro-Tip Column Preparation.....	85
3.2.2. Liquid-Handling Robot.....	90
3.2.3. Labware.....	90
3.2.4. Liquid-Handling Parameters (Liquid Classes).....	92
<b>3.3. General Procedure for Micro-Tip Chromatography.....</b>	<b>93</b>
<b>3.4. Considerations for Micro-Tip Column Operation.....</b>	<b>95</b>
3.4.1. Glossary of Key Operating Terms.....	95

3.4.2. <i>Flow Properties of Micro-Tip Chromatography</i> .....	97
3.4.2.1. Fundamental Characterisation of Micro-Tip Flow.....	97
3.4.2.2. Volumetric Flow Profile and Determination of Delay Times.....	99
3.4.3. <i>Micro-Tip Column Hold-Up Volume</i> .....	103
3.4.4. <i>Pre-Wash and Equilibration</i> .....	105
3.4.5. <i>Adsorption (Sample Loading)</i> .....	106
3.4.6. <i>Wash and Elution</i> .....	107
<b>3.5. Throughput of a Micro-Tip Purification</b> .....	111
<b>3.6. Summary</b> .....	112
 <b>4. ADSORBENT CHARACTERISATION BY MICRO-TIP CHROMATOGRAPHY</b> .....	 <b>114</b>
4.1. <b>Introduction</b> .....	114
4.2. <b>Equilibrium Adsorption Isotherms</b> .....	114
4.3. <b>Batch Uptake Experiments</b> .....	120
4.3.1. <i>Finite-Bath Experiments</i> .....	120
4.3.2. <i>Pre-Equilibrium Adsorption Isotherms</i> .....	129
4.3.3. <i>Shallow-Bed Adsorption</i> .....	132
4.4. <b>Prediction of Dynamic Binding Capacity From Micro-Tip Data</b> ..	139
4.4.1. <i>Modelling Data from Batch Uptake Experiments</i> .....	140
4.4.1.1. Modelling Approach.....	140
4.4.1.2. Application of Model to Micro-Tip Data.....	141
4.4.2. <i>Modelling Data from Pre-Equilibrium Adsorption Isotherms</i> ...	145
4.4.2.1. Modelling Approach.....	145
4.4.2.2. Application of Model to Micro-Tip Data.....	152
4.5. <b>Summary</b> .....	157
 <b>5. CAPTURING THE POTENTIAL OF MIXED-MODE LIGANDS WITH MICRO-TIP CHROMATOGRAPHY</b> .....	 <b>159</b>
5.1. <b>Introduction</b> .....	159
5.2. <b>Mixed Mode Chromatography: New Opportunities and Challenges</b> .....	159
5.3. <b>High-Throughput Development of Mixed Mode Chromatography</b> .....	163
5.3.1. <i>Developmental Workflow Using Micro-tip Chromatography</i> .....	163
5.3.2. <i>Design of High-Throughput Experiments</i> .....	165
5.4. <b>Demonstration of the High-Throughput Developmental Workflow</b> .....	165
5.4.1. <i>Experimental Details of Micro-Tip Chromatography</i> .....	167
5.4.2. <i>Range-Finding Study</i> .....	167
5.4.3. <i>Primary Evaluation: Capture Study</i> .....	171
5.4.3.1. Experimental Layout.....	171
5.4.3.2. Results of the Capture Study.....	174
5.4.3.3. Use of a Statistical Software for Selecting Lead Conditions.....	176

5.4.4. <i>Secondary Evaluation: Elution Study and Loading Optimisation</i> .....	178
5.4.4.1. Experimental Layout.....	180
5.4.4.2. Results of the Elution Study.....	180
5.4.4.3. Definition of the Final Purification Sequence.....	183
5.4.5. <i>Laboratory-Scale Column Verification of the Microscale Results</i> .....	185
<b>5.5. Experimental Throughput</b> .....	187
<b>5.6. Summary</b> .....	188
 <b>6. A MULTI-STEP CHROMATOGRAPHIC SCALE-DOWN WITH MICRO-TIP CHROMATOGRAPHY</b> .....	 <b>190</b>
6.1. Introduction.....	190
6.2. Chromatography of Viral Particles.....	191
6.3. Miniaturisation of the VLP Chromatographic Purification.....	194
6.4. Performance of the Microscale Chromatography.....	200
6.5. Throughput and Resource Benefits Using the Microscale Purification.....	204
6.6. Summary.....	205
 <b>7. A CELL DISRUPTION METHOD FOR INTEGRATED MICROSCALE BIOPROCESSING</b> .....	 <b>207</b>
7.1. Introduction.....	207
7.2. The Yeast Cell Wall.....	207
7.3. Small-Scale Disruption of Yeast Cells.....	208
7.4. Adaptive Focused Acoustics.....	212
7.4.1. <i>Experimental Details</i> .....	214
7.4.2. <i>Characterisation of Instrument Parameters</i> .....	217
7.5. <b>Optimisation of AFA for Yeast Cell Disruption</b> .....	220
7.5.1. <i>Fractional Factorial to Identify Critical Operating Parameters</i> .....	220
7.5.2. <i>Response Surface for the Optimisation of AFA Operating Parameters</i> .....	221
7.5.3. <i>Evaluation of Instrument Operating Modality</i> .....	222
7.5.4. <i>Addition of a Lytic Enzyme to Improve AFA Cell Disruption Efficiency</i> .....	225
7.5.5. <i>VLP Stability During AFA Cell Disruption</i> .....	227
7.5.6. <i>Evaluation of Cell Disruption by Light Microscopy</i> .....	228
7.6. <b>AFA Cell Disruption as a Component of a Fully Microscale Purification</b> .....	228
7.6.1. <i>Performance of the AFA Lysate Through the Chromatographic Purification</i> .....	230
7.6.2. <i>Sample Requirement, Experimental Throughput, and Labour Savings</i> .....	230
7.7. <b>Summary</b> .....	235
 <b>8. CONCLUSIONS AND FUTURE DIRECTIONS</b> .....	 <b>236</b>

<b>8.1. Conclusions</b> .....	236
8.1.1. <i>Micro-Tip Chromatography as a Platform for Microscale Chromatography</i> .....	236
8.1.2. <i>Adsorbent Characterisation by Micro-Tip Chromatography</i> ...	237
8.1.3. <i>Micro-Tip Chromatography Applied to High-Throughput Process Development</i> .....	238
8.1.4. <i>Adaptive Focused Acoustics for Microscale Cell Disruption</i> ...	239
<b>8.2. Future Directions</b> .....	240
8.2.1. <i>Future Directions in Micro-Tip Chromatography</i> .....	240
8.2.2. <i>Need for High Throughput Assays and a Comprehensive Analytical Strategy</i> .....	241
8.2.3. <i>Experimental Design to Best Utilise Increased Experimental Throughput</i> .....	241
8.2.4. <i>A Vision for Microscale Bioprocess Development</i> .....	242
8.2.4.1. <i>High-Throughput Examination of the Parameter Space</i> ....	242
8.2.4.2. <i>Validated Micro Scale-Down Models</i> .....	243
8.2.4.3. <i>An Integrated Strategy for Bioprocess Development</i> .....	244
<b>REFERENCES</b> .....	247

## LIST OF FIGURES

FIGURE 1.1	The process development spectrum, from platform to <i>de novo</i> processes.....	24
FIGURE 1.2	Typical bioprocess for protein production.....	28
FIGURE 1.3	Graphical example of three equilibrium adsorption isotherm models used to describe protein adsorption .....	38
FIGURE 1.4	Generalised van Deemter plot.....	46
FIGURE 1.5	Schematic of the mass transport of solute in porous adsorbents.....	47
FIGURE 1.6	Integration of microscale experiments into the process development workflow.....	57
FIGURE 1.7	Schematic representation of three formats for carrying out chromatography in a microtitre plate configuration.....	63
FIGURE 1.8	Iterative experimental design for high-throughput microscale experiments.....	73
FIGURE 3.1	Schematic illustration and dimensions of 10-, 40-, and 80- $\mu$ L micro-tip columns .....	87
FIGURE 3.2	Tecan Freedom EVO 200 workstation used for micro-tip chromatography.....	91
FIGURE 3.3	Example of pre-wash and purification plate layouts for a typical micro-tip column purification.....	94
FIGURE 3.4	Superficial linear velocity, Reynolds number, and Biot number as a function of column axial position for the 10-, 40-, and 80- $\mu$ L micro-tip columns.....	100
FIGURE 3.5	Volumetric flow profile through a 40- $\mu$ L UNOsphere S micro-tip column.....	101
FIGURE 3.6	Desorption of a huIgG from SP Sepharose FF.....	109
FIGURE 3.7	'Staircase' elution of a huIgG and its host-cell impurities from a 40- $\mu$ L micro-tip column.....	110
FIGURE 4.1	Determination of adsorption isotherms using micro-tip columns on a Tecan robotic workstation.....	118
FIGURE 4.2	Micro-tip method for performing batch uptake experiments.....	122
FIGURE 4.3	Binding of a huIgG on UNOsphere S as a function of residence time and contact time.....	124
FIGURE 4.4	Comparison of batch uptake curves generated by micro-batch adsorption and micro-tip chromatography.....	126
FIGURE 4.5	The effect of a four-fold difference in flow rate on protein uptake for three different cation-exchange adsorbents.....	128
FIGURE 4.6	Uptake of huIgG onto three different cation exchange adsorbents as a function of contact time .....	130
FIGURE 4.7	Pre-equilibrium adsorption isotherms of the binding of the test huIgG to UNOsphere S and POROS 50HS .....	131
FIGURE 4.8	Pre-equilibrium adsorption isotherms as a function of constant residence time and contact time.....	133
FIGURE 4.9	Conventional shallow-bed set-up and uptake curves.....	134
FIGURE 4.10	Scheme for performing shallow-bed adsorption (infinite-bath format) by micro-tip chromatography.....	136
FIGURE 4.11	Uptake curve from a shallow-bed experiment using micro-tip columns.....	138

FIGURE 4.12	Parity plot comparing the predicted $DBC_{10\%}$ of huIgG on UNOsphere S to experimental column breakthrough data.....	144
FIGURE 4.13	Example of data output when modelling column breakthrough with a staged reaction model.....	147
FIGURE 4.14	Breakthrough curves modelled from micro-tip pre-equilibrium adsorption isotherm data using a staged reaction model.....	149
FIGURE 4.15	Example of a calibration experiment used to relate micro-tip contact time to column contact time .....	151
FIGURE 4.16	Outline of the staged-reaction modelling approach for the prediction of column $DBC_{10\%}$ from micro-tip pre-equilibrium adsorption isotherm data .....	153
FIGURE 4.17	$K_D$ and $q_m$ constants as a function of micro-tip contact time derived from micro-tip pre-equilibrium adsorption isotherms in the binding of huIgG to UNOsphere S.....	154
FIGURE 4.18	Comparison of predicted dynamic binding capacities from micro-tip experiments using a staged reaction model to those of the experimental column.....	156
FIGURE 5.1	Binding capacity of two human monoclonal antibodies to Capto MMC as a function of sodium chloride and pH.....	162
FIGURE 5.2	High throughput workflow using microscale chromatography for the development of a mixed-mode chromatography process step.....	164
FIGURE 5.3	Factorial design to establish parameter ranges for the examination of mAb-1 binding to the multimodal weak cation-exchange adsorbent in sodium chloride and ammonium sulphate salts.....	169
FIGURE 5.4	Plate layout for the primary evaluation of product and host-cell impurity binding.....	172
FIGURE 5.5	Response surface graphs of capacity of the multimodal weak cation-exchange adsorbent (Capto MMC) for purified mAb-1 in four salt types as a function of salt concentration and pH.....	175
FIGURE 5.6	Contour plots showing the capacity of the multimodal weak cation-exchange adsorbent (Capto MMC) for purified mAb-1 and host cell proteins as a function of pH and salt concentration .....	177
FIGURE 5.7	Determination of desirable loading conditions from the ammonium sulphate screen using statistical software.....	179
FIGURE 5.8	Plate layout for the secondary evaluation in the development of a mixed-mode chromatography step.....	181
FIGURE 5.9	Evaluation of mobile phase conditions for the elution of mAb-1 from the multimodal weak cation-exchange adsorbent.....	182
FIGURE 5.10	Secondary evaluation of four loading conditions in the purification of mAb-1 from the clarified cell filtrate by multimodal weak cation-exchange chromatography.....	184
FIGURE 5.11	Verification of the microscale results for the multimodal weak cation-exchange chromatography at the laboratory column scale.....	186
FIGURE 6.1	Transmission electron micrographs of HPV 6, 11, 16, and 18 VLPs.....	192
FIGURE 6.2	Correlation of the VLP titre in lysate by immunoassay to the total protein recovery through a multi-step chromatographic purification.....	193

FIGURE 6.3	Purification scheme of HPV VLPs using micro-tip chromatography to provide feedback on fermentation performance.....	195
FIGURE 6.4	Binding of the column feed sample to the 80-μL CEX and the 40-μL CHT micro-tip columns as a function of cycle number and loading time.....	198
FIGURE 6.5	SDS-PAGE analysis of the HPV VLP multi-step chromatographic purification comparing the laboratory and micro-tip column scales.....	201
FIGURE 6.6	Correlation between the automated microscale purification and the laboratory-scale column purification in the assessment of fermentation productivity.....	203
FIGURE 7.1	Architecture of the yeast cell wall.....	209
FIGURE 7.2	Frequency range of the Adaptive Focused Acoustics device.....	213
FIGURE 7.3	The Covaris E210 instrument for Adaptive Focused Acoustics.....	215
FIGURE 7.4	Characterisation of instrument parameters in the disruption of yeast cells by Adaptive Focused Acoustics.....	218
FIGURE 7.5	Response surface contour plots of yeast cell disruption by Adaptive Focused Acoustics.....	223
FIGURE 7.6	Effect of the AFA operating modality on total soluble protein release.....	224
FIGURE 7.7	Timecourse of cell disruption by Adaptive Focused Acoustics with and without β1,3-glucanase pre-treatment.....	226
FIGURE 7.8	Light microscopy of yeast cells before and after cell disruption.....	229
FIGURE 7.9	SDS-PAGE of the clarified lysate following cell disruption and of the cation exchange and hydroxyapatite chromatographic products following the microscale purification.....	232
FIGURE 7.10	Final chromatographic recovery through the microscale VLP purification as a function of fermentation harvest time.....	233
FIGURE 8.1	Integration of microscale bioprocess techniques into the process development workflow.....	246

## LIST OF TABLES

TABLE 1.1	Methods for cell disruption in the recovery of intracellular proteins.....	27
TABLE 1.2	Types of ligand chemistries used in preparative protein chromatography.....	32
TABLE 1.3	Parameters affecting performance in preparative chromatography.....	34
TABLE 1.4	Models of non-linear chromatography.....	55
TABLE 1.5	Comparison of three microtitre-plate formats for microscale chromatography .....	64
TABLE 2.1	Properties of the chromatographic stationary phases used in this thesis .....	76
TABLE 3.1	Precision study to examine the reproducibility of micro-tip column preparation and operation.....	88
TABLE 3.2	Assessment of the accuracy of micro-tip column preparation by comparison to batch adsorption.....	89
TABLE 3.3	Flow-rate correction factors to compensate for the lag in fluid flow through a micro-tip column.....	103
TABLE 3.4	Breakdown of the run time in an example eight-column micro-tip purification.....	111
TABLE 3.5	Suggested operating ranges for micro-tip chromatography.....	113
TABLE 4.1	Allowed variable ranges for carrying out adsorption isotherms with micro-tip columns on a Tecan workstation.....	116
TABLE 4.2	Determination of equilibrium binding capacity by micro-tip and micro-batch adsorption methods.....	120
TABLE 4.3	Key model parameter inputs to predict DBC <sub>10%</sub> from micro-tip data using the approach outlined by Bergander et al. (2008).....	142
TABLE 4.4	Comparison of predicted DBC <sub>10%</sub> from micro-tip data to that of the experimental column data.....	143
TABLE 4.5	Prediction of column DBC <sub>10%</sub> using a staged reaction model and micro-tip pre-equilibrium adsorption isotherm data for the binding of huIgG to UNOsphere S.....	152
TABLE 5.1	Some commercially available mixed-mode chromatographic media.....	160
TABLE 5.2	Examination of mAb-1 solubility across a salt range from 0-2 M for multimodal weak cation-exchange chromatography development... ..	170
TABLE 5.3	Comparison of results between micro- and laboratory-scales for the purification of mAb-1 from cell filtrate using multimodal weak cation-exchange (Capto MMC) chromatography .....	187
TABLE 6.1	Run parameters for the CEX and CHT micro-tip chromatography for the purification of HPV VLPs.....	196
TABLE 6.2	Comparison of the micro-tip and laboratory column purifications of HPV VLPs for the assessment of fermentation performance.....	202
TABLE 6.3	Comparison of the experimental throughput, labour, and resources required for the microscale and laboratory-scale chromatographic purifications.....	206
TABLE 7.1	Overview of laboratory-scale methods for yeast cell disruption.....	210
TABLE 7.2	Instrument parameters for the Covaris E210.....	216

TABLE 7.3	Two-level fractional factorial to screen parameters affecting cell disruption by Adaptive Focused Acoustics.....	221
TABLE 7.4	Recovery of purified VLPs spiked into the yeast cell suspension prior to disruption and yeast lysate after disruption to assess product stability during AFA disruption.....	227
TABLE 7.5	Performance of the AFA cell lysate through the micro-tip chromatographic purification for three different fermentation pastes.....	231
TABLE 7.6	Experimental throughput and labour of the AFA cell disruption method when used as a component of the microscale HPV VLP purification.....	234

## LIST OF SYMBOLS AND ABBREVIATIONS

<b>a</b>	<i>i.</i> Numerical coefficient of the single-component Langmuir isotherm for component <i>i</i> used in the competitive Langmuir adsorption isotherm model; $a = K_{eq} * q_m$ <i>ii.</i> Selectivity factor
<b>A</b>	<i>i.</i> System constant in the three-parameter equation by Melander et al. (1989) to describe protein retention in chromatography. <i>ii.</i> Constant associated with eddy diffusion in the van Deemter equation.
<b>AFA</b>	Adaptive Focused Acoustics
<b>b</b>	Numerical coefficient of the single-component Langmuir isotherm for component <i>i</i> used in the competitive Langmuir adsorption isotherm model; $b = K_{eq}$
<b>B</b>	<i>i.</i> Electrostatic interaction parameter in the three-parameter equation by Melander et al. (1989) to describe protein retention in chromatography. <i>ii.</i> Constant associated with axial diffusion in the van Deemter equation.
<b>Bi</b>	Biot number
<b>C</b>	<i>i.</i> Solute (sample, adsorbate) concentration in mobile phase (bulk solution) <i>ii.</i> Hydrophobic interaction parameter in the three-parameter equation by Melander et al. (1989) to describe protein retention in chromatography. <i>iii.</i> Constant associated with mass transfer kinetics in the van Deemter equation.
<b>C<sub>0</sub></b>	Initial solute (sample, adsorbate) concentration
<b>cpb</b>	Cycles per burst (in Adaptive Focused Acoustics)
<b>CHT</b>	Ceramic hydroxyapatite chromatography
<b>CEX</b>	Cation exchange chromatography
<b>CV</b>	Coefficient of variation
<b>cyc</b>	Number of aspiration-dispense pipetting cycles (up, down) used in a micro-tip chromatographic operation
<b>d<sub>p</sub></b>	Average chromatographic particle size (diameter)
<b>D</b>	Molecular diffusivity
<b>D<sub>e</sub></b>	Effective pore diffusivity (may also be referred to as D <sub>p</sub> )
<b>D<sub>s</sub></b>	Effective adsorbed phase diffusivity (in surface diffusion)
<b>DBC</b>	Dynamic binding capacity

<b>DBC<sub>10%</sub></b>	Dynamic binding capacity at 10% of breakthrough
<b>dc</b>	Duty cycle (in Adaptive Focused Acoustics)
<b>F</b>	Fractional uptake to maximum equilibrium adsorbent binding: $q/q_m$
<b>DoE</b>	Design of experiment
<b>FTE</b>	Full-time equivalent (unit of labour)
<b>h</b>	Height; column height
<b>HETP</b>	Height equivalent of a theoretical plate
<b>HPV</b>	Human papillomavirus
<b>huIgG</b>	Human immunoglobulin
<b>i.d.</b>	Inner diameter
<b>IgG</b>	Immunoglobulin
<b>J</b>	Mass transfer flux from the bulk mobile phase to the adsorbent surface
<b>k'</b>	Retention (capacity) factor
<b>k<sub>1</sub> (or k<sub>a</sub>)</b>	Forward rate constant (adsorption)
<b>k<sub>2</sub> (or k<sub>d</sub>)</b>	Reverse rate constant (desorption)
<b>k<sub>f</sub></b>	Film mass transfer coefficient
<b>k<sub>p</sub></b>	Pore hindrance parameter
<b>K</b>	Constant in Freundlich adsorption isotherm model
<b>K<sub>D</sub></b>	Dissociation constant in adsorbate-adsorbent binding; constant in the Langmuir adsorption isotherm model
<b>K<sub>eq</sub></b>	Equilibrium binding constant; a constant in the linear and Langmuir adsorption isotherm models (may also be referred to as K <sub>A</sub> )
<b>K<sub>p</sub></b>	Partition coefficient (= $q/C$ )
<b>K<sub>SMA</sub></b>	Equilibrium binding constant derived from the steric mass action model
<b>L</b>	Column length
<b>m</b>	Adsorbate mass
<b>m<sub>s</sub></b>	Molality of salt
<b>mAb</b>	Monoclonal antibody
<b>M</b>	Molecular weight (also referred to as <b>MW</b> )
<b>n</b>	Exponential constant in Freundlich adsorption isotherm model
<b>N</b>	Number of theoretical plates; number of pore transfer units.

<b>q</b>	Concentration of the adsorbed species on an adsorbent (mass of adsorbate per volume of adsorbent)
<b>q<sub>m</sub></b>	Maximum equilibrium binding capacity of the adsorbent; can be derived from the Langmuir adsorption isotherm model; also referred to as q <sub>max</sub>
<b>Q</b>	Volumetric flow rate
<b>Re</b>	Reynolds number
<b>R<sub>p</sub></b>	Adsorbent particle radius
<b>Sc</b>	Schmidt number
<b>Sh</b>	Sherwood number
<b>STR</b>	Stirred tank reactor
<b>t<sub>0</sub></b>	Retention time of the unretained solute; used in the calculation of k'
<b>t<sub>r</sub></b>	Retention time of adsorbing solute; used in the calculation of k'
<b>T<sub>C</sub></b>	Total contact time (loading time) that the sorbent is in contact with liquid (sample) during a chromatographic loading step
<b>T<sub>D</sub></b>	Delay time following each micro-tip pipetting step
<b>T<sub>R</sub></b>	Column residence time; for micro-tip columns = $\frac{V_A}{Q} \times cyc \times 2$
<b>v</b>	Column interstitial linear velocity
<b>V<sub>A</sub></b>	Adsorbent (matrix particles, column) volume (may also be referred to as V <sub>M</sub> )
<b>V<sub>E</sub></b>	Elution volume
<b>V<sub>S</sub></b>	Sample or mobile phase solution volume (also referred to as V)
<b>V<sub>T</sub></b>	Total tank volume (mobile phase + adsorbent) in a staged reaction model
<b>VLP</b>	Virus-like particle
<b>z</b>	Characteristic charge of the solute
<b>α<sub>10%</sub></b>	Empirical correction factor used to relate micro-tip contact time to laboratory-column contact time
<b>δ</b>	Thickness of laminar sublayer around the adsorbent particle
<b>ε</b>	Column (extra-particle, interstitial) void fraction
<b>ε<sub>p</sub></b>	Intra-particle void fraction (pore porosity)
<b>φ</b>	Phase ratio, defined as the accessible surface area of the adsorbent per unit volume of mobile phase
<b>ν</b>	Kinematic viscosity

$\lambda$	Wavelength
$\mu$	Column superficial linear velocity
$\sigma$	Steric hindrance factor; used in the steric mass action model
$\tau$	Tortuosity factor (also represented as $\theta$ in Figure 1.5)
$\Lambda$	<i>i.</i> Parameter in the steric mass action model: Total ion exchange capacity of the stationary phase <i>ii.</i> Term in the shrinking core model

## **1. INTRODUCTION**

### **1.1. Motivation for the project**

The pharmaceutical industry is under increasing pressure to deliver safer yet cheaper medicines, with novel mechanisms of action. At the same time, one-size-fits-all blockbusters have become difficult to achieve because of safety and efficacy concerns in patient subpopulations, prompting a push for more personalised therapies. Biotech drugs, or biologics as they are often called, present new options for responding to these pressures. These biologics include therapeutic proteins, recombinant vaccines, peptide conjugates, gene therapy, RNA interference, and regenerative medicine. Increasingly, biologics are accounting for a larger share of the total pharmaceutical market. In 2000, there were only three blockbuster (defined as  $\geq$  \$1 billion in sales) biotech products, whereas in 2006 there were eight (Lawrence, 2007). Sales of biologics amounted to over \$75 billion in 2007, making up over 10% of the prescription drug market and defined by sales growth that was twice that of pharmaceuticals (Fiercebiotech.com). Furthermore, seven of the 26 new drugs approved by the FDA in 2009 were biotech therapies (Fiercebiotech.com). While overall progress in gene therapy and nucleic-acid based medicines has been slow, the therapeutic protein sector has exploded due to the success of monoclonal antibodies (mAbs), growth factors such as erythropoietin, and hormones like insulin. There were 29 mAbs approved in the US market in 2008 (Aggarwal, 2009) and more than 200 in the pipeline worldwide (Tuft Center for the Study of Drug Development, 2009), with projected sales growth of 14% per year through 2012 (Reichert, 2008). In addition to therapeutic proteins, vaccines, like the ones used to prevent pneumococcal and human papillomavirus infections, represent another important category of multi-billion dollar sales.

The present paradigm of bioprocess development must evolve to keep pace with the growing number of new biopharmaceutical candidates entering preclinical development while containing cost and reducing product development cycle time. Moreover, regulatory initiatives such as 'quality by design' (QbD) are raising the bar for biologics manufacture even higher, demanding a thorough understanding of the product and its manufacture design space (Rathore and Winkle, 2009). One solution has been to use platform bioprocesses for biomolecules within a same product class, such as mAbs (Shukla et al., 2007A). However, this is not a solution for the vast

number of therapeutic proteins and vaccines having unique structural and biochemical properties. Microscale bioprocessing techniques (Micheletti and Lye, 2006; Titchener-Hooker et al., 2008) offer a step change for bioprocess development. These techniques hold the promise of accelerating process development by enabling parallel experimentation and automation while requiring only small quantities of material. With less material required, quantitative bioprocess information can be obtained earlier in development so that critical process parameters can be better understood. Although these microscale systems do not need to perfectly emulate every aspect of large scale operation, they should be able to mimic the key engineering characteristics of that operation so that parameters affecting large-scale performance can be better understood and their impact predicted.

Development of a process chromatography step is usually performed empirically because of the complexity of the separation, meaning that the parameter space often is not fully explored at the laboratory scale due to time and resource constraints. However, with microscale methods, fundamental parameters that affect the operation, such as equilibrium binding and kinetic constants, can be obtained rapidly with small amounts of material and then be used to predict column scale performance using appropriate engineering correlations or *in silico* models. Alternatively, these techniques can be used qualitatively to probe the parameter space in the selection of adsorbent type and mobile phase conditions, narrowing the focus for subsequent larger-scale column optimisation. In this way, microscale techniques advance QbD initiatives while also accelerating process development. This thesis examines one such microscale technique for chromatography study, that being micro-tip chromatography and how it can be used as part of a strategy for accelerated bioprocess development. Micro-tip chromatography employs a packed chromatographic bed immobilised at the bottom of a pipette tip, thereby offering a number of operational advantages over other microwell methods such as micro-batch adsorption, in which adsorbent is statically mixed in a microwell.

With the miniaturisation of chromatography experiments, however, comes the need for integration with upstream microscale bioprocessing techniques along with low-volume, high-throughput analytical methods. New analytical technologies are increasingly becoming available for this purpose, while assay automation is reducing

the toll on analytical resources. For sample feed preparation, microscale disruption and/or primary recovery methods are essential for realising the advancements in throughput and low-volume processing provided by microscale chromatography. Therefore, in this project, the technique of Adaptive Focused Acoustics (AFA) is evaluated as a means for microscale cell disruption for the purpose of providing representative feed material for the downstream chromatography.

## **1.2. Aims for the Project**

This thesis seeks to demonstrate micro-tip chromatography as a platform for microscale chromatography and AFA as a platform for microscale yeast cell disruption. Each technique will be fully characterised, with critical operating parameters defined. The primary focus of this thesis will centre on micro-tip chromatography and determining how the format can be used to predict chromatography scale-up. The development of a small-scale cell disruption technique, in contrast to the goal of micro-tip chromatography, is not intended for the study and development of large-scale cell disruption, but rather to provide representative feed material for microscale chromatographic experiments, thereby yielding an integrated microscale purification. The use of these microscale techniques in the process development workflow will be examined, with the impact on developmental and analytical resources considered.

Specific aims of this project include:

- i. Automating the micro-tip column format on a robotic liquid-handling workstation (Tecan) and defining all critical operating parameters.
- ii. Characterising the flow and mass transport properties of the micro-tip format and describing how this approach differs from other microscale formats.
- iii. Developing and evaluating micro-tip methods for determining static binding capacity and uptake kinetics. Examining modelling approaches for predicting dynamic binding capacity from these data.

- iv. Demonstrating the use of micro-tip chromatography for high throughput process development, specifically in the case of a mixed-mode chromatography step, and considering strategies for efficient experimental design.
- v. Addressing the capability of the micro-tip format for studying the interplay between process unit operations. In particular, demonstrating the miniaturisation of a multi-step chromatographic purification as a scale-down mimic of the laboratory-scale chromatography for informing upstream fermentation development.
- vi. Developing a microscale disruption technique for yeast cells using Adaptive Focused Acoustics to provide a feedstock for chromatography experiments that is representative of the laboratory-scale homogenate. Combining this microscale cell disruption step with the multi-step micro-tip chromatography to yield an integrated microscale purification.

### **1.3. Production of Recombinant Proteins**

Bioseparations encompass the extraction or purification of natural products, live viruses and recombinant biomolecules. Bioprocesses used in the manufacture of biologics are typically divided into upstream and downstream processing, with the upstream process constituting the cell culture or fermentation and the downstream process dealing with its purification. However, these two components are not mutually exclusive and often strongly influence each other.

A typical protein purification process is comprised of a sequence of unit operations which exploit the chemical and physical properties of the molecule such as charge, hydrophobicity, size, and solubility. For a review of unit operations used in bioseparations, refer to Belter et al. (1988), Ladisch (2001), Harrison et al. (2003), and Lightfoot and Moscariello (2004). The unit operations of a purification can generally be divided into four stages based on their function: primary recovery, capture of the product, intermediate purification, and polishing. Primary recovery involves the removal of cells or cellular debris by filtration, sedimentation, or

centrifugation. For intracellular proteins, a cell disruption step is required as a first step in the primary recovery. Following the primary recovery, the bioproduct is isolated (captured) from impurities having different biophysical and chemical properties by ultrafiltration, extraction, fixed-bed chromatography, and/or precipitation. The product stream is then further purified by chromatography, affinity methods, crystallization, or fractional precipitation. Lastly, final product polishing is carried out by chromatography and/or membrane filtration. The purified bioproduct is then formulated for drug delivery.

Bioprocess development remains largely an empirical exercise, although process simulation and computer-aided design techniques have been developed for the evaluation of large numbers of process variables and to probe the interaction between unit operations (Jungbauer and Kaltenbrunner, 1996 and 1999; Zhou and Titchener-Hooker, 1999; Rouf et al., 2001; Vasquez-Alvarez et al., 2001). To reduce process development time and cost, platform bioprocesses have been applied for products having the same biophysical properties, such as those for monoclonal antibodies (Shukla et al., 2007A) and plasmid DNA (Prather et al., 2003; Murphy et al., 2006). However, *de novo* process development is usually required for completely new biologics. Hence, a spectrum of process development exists (Fig. 1.1), ranging from platform processes on one end to new developed processes on the other end.

The goal of any bioseparation from a regulatory perspective is to maximally purify the product while maintaining bioactivity and product stability, with the ultimate goal being to ensure product safety and efficacy. However, in practice, the design of a manufacturing process is also strongly driven by cost and productivity. Half of the cost of biopharmaceutical purification is typically associated with chromatography steps (Ladisch, 2001). Furthermore, material handling can drive the economics of a process, with Lightfoot and Moscariello (2004) contending that the overall processing cost is inversely proportional to the feed concentration of the bioseparation and independent of final purity. In the end, both cost and product quality must be considered in developing a commercially viable biopurification.

# The Process Development Spectrum

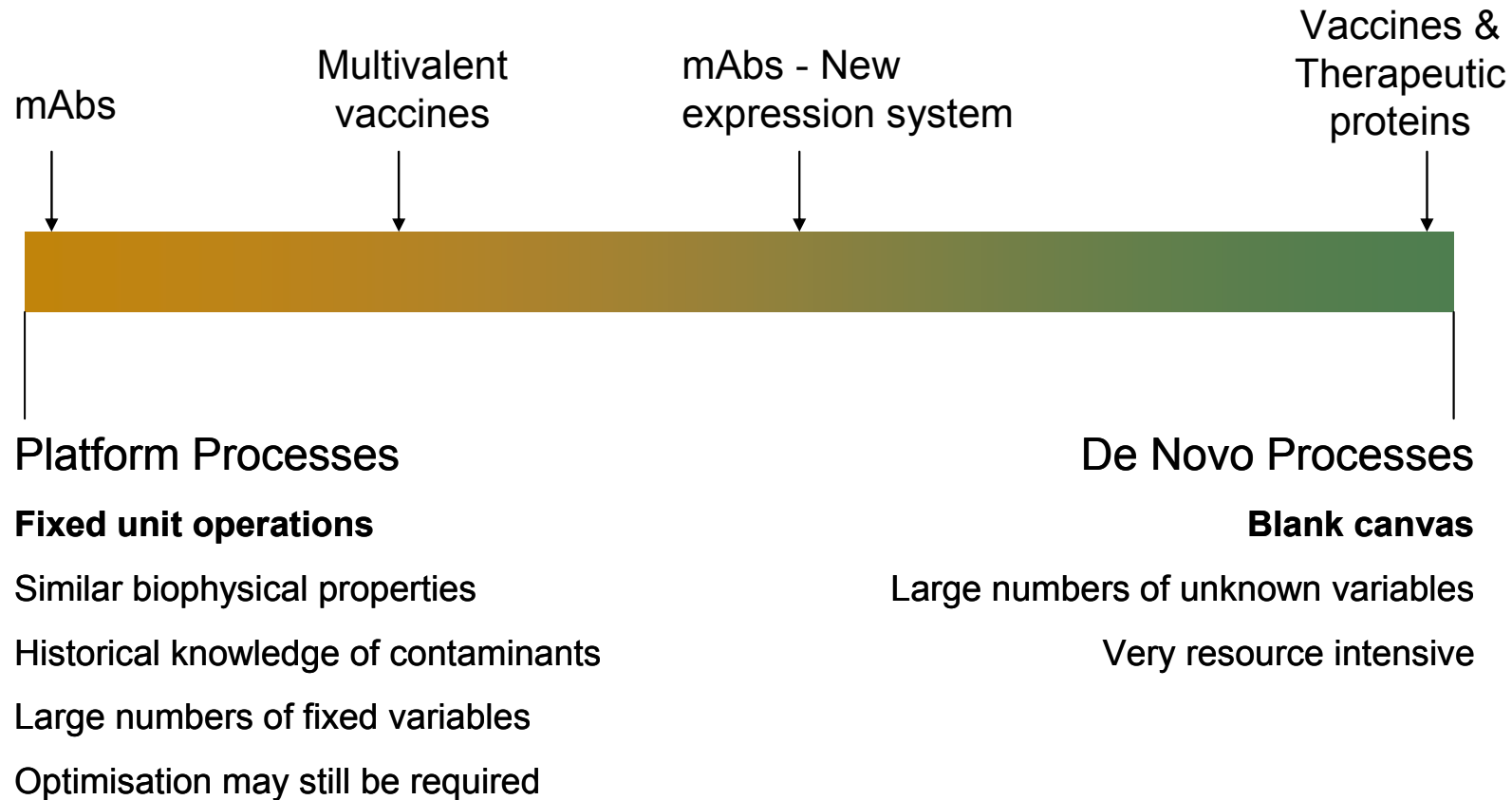


**Figure 1.1.** The process development spectrum, from platform to *de novo* processes.

### 1.3.1. Fermentation and Cell Culture

The choice of which expression system to use is one of the most important decisions in the production of a protein therapeutic or vaccine since it strongly influences the product quality, safety, and process economics. *Escherichia coli*, *Saccharomyces cerevisiae*, and immortalised Chinese hamster ovary (CHO) cell lines are the staple for biopharmaceutical production, although several new options have emerged, as reviewed by Schmidt (2004), Wurm (2004), and Walsh (2006). *E. coli* is the most widely used prokaryotic system because of historical experience, low cost, short generation times, high productivity, and ease of handling. However, proteins expressed in *E. coli* often may form insoluble aggregates known as inclusion bodies, which require additional processing for re-solubilisation. Consequently, there has been recent focus on designing secretory *E. coli* systems like those of mammalian cell lines (Choi and Lee, 2004), although with mixed results. Alternatively, *E. coli* and *Pseudomonas fluorescens* expression systems (Chae et al., 2002; Retallack et al., 2007) have been developed in which the expressed protein is transported to the periplasm, providing a simple way of recovering the protein in its soluble form. Disadvantages of prokaryotic systems are that they are not suitable for proteins requiring post-translational modification (such as N- and O-glycosylation), and there is a burden to clear pyrogenic or pathogenic impurities. Yeasts, like prokaryotes, can be grown cheaply and quickly with high product titres, yet they have little of the safety risk associated with prokaryotic systems. The most commonly used yeast host cells are *Saccharomyces cerevisiae* and *Pichia pastoris*. While most yeast systems are also not suitable for glycosylated protein expression since they do not naturally produce human glycans, *Pichia pastoris* strains have recently been engineered to do so (Li et al., 2006), thereby taking advantage of the fast processing times and high titres provided by yeast.

Despite the advances with glyco-engineered yeasts, mammalian cell lines are still the preferred system for producing human (or humanised) glycosylated proteins, especially for monoclonal antibodies. CHO cells are the most commonly used of these, although mouse myeloma (NS0), baby hamster kidney (BHK), human embryo kidney (HEK-293), and human retinal cells have also been used in the production of approved products (Wurm, 2004). Drawbacks of mammalian cell lines are their cost, the fact that their cultivation usually requires days to weeks, and that the resulting

product may have a heterogeneous glycan distribution. As a result, development of these cell lines typically centres on increasing productivity while achieving a desired glycan distribution for the product. The productivity of many of these cell lines has increased significantly since they were first introduced in the mid-1980s, with product titres now often exceeding 4 g/L in the production of monoclonal antibodies in CHO cells (Wurm, 2004).

### *1.3.2. Cell Disruption and Primary Recovery*

The first step in the purification of a recombinant protein is to harvest it from the cell suspension used in its production. For secretory systems, this means gently removing the cells and recovering the product in the resulting supernatant. However, for intracellular proteins, the cells must first be disrupted. An overview of some commonly used cell disruption techniques is shown in Table 1.1. Selection of the appropriate method must balance economic and operational considerations with cell breakage, product release and stability, and the impact on downstream processing. Disruption of prokaryotic and yeast cells at the industrial scale is almost always carried out by one of the mechanical methods, with the most common being solid-shear (bead-mill) and high pressure homogenisation (Middelberg, 1995; Garcia, 1999; Hopkins, 2001; Hatti-Kaul and Mattiasson, 2003.) Non-mechanical methods offer a gentler and sometimes more selective alternative that is based on physical, chemical, or enzymatic lysis. However, these methods are typically used only for laboratory experiments or to supplement mechanical disruption.

The primary recovery step constitutes a solid-liquid separation in which the cells and cellular debris are removed from the liquid phase. For soluble proteins, the product is recovered in the liquid medium; however, for inclusion bodies produced by *E. coli*, the insoluble protein must first be differentially recovered from the other cell solids and then the soluble form of the protein renatured from these inclusion bodies. Primary recovery is typically carried out by centrifugation, sedimentation, filtration, or microfiltration. Flocculation and filter aids are sometimes used to enhance the efficiency of these techniques (Sharma, 1999; Lightfoot and Moscariello, 2004). The choice of the specific technique and its operating conditions depends on the expression system, the solubility of the expressed protein, and whether or not whole cells or cellular debris are being removed.

**Table 1.1.** Methods for cell disruption in the recovery of intracellular proteins.

<b>Mechanical</b>	<b>Non-Mechanical</b>		
	<b>Physical</b>	<b>Chemical</b>	<b>Enzymatic</b>
Bead Mill	Osmotic shock	Detergents	Lytic Enzymes
Rotor-Stator Homogeniser	Thermolysis	Chelating Agents	Autolysis
High-Pressure Homogeniser	Freeze-fracturing	Chaotropes	
Ultrasonicator		Solvents	
		Antibiotics	

In addition to these techniques, expanded-bed adsorption (EBA; also known as fluidised bed chromatography) has been developed as a way of combining primary recovery with the initial capture chromatography (Chase, 1994). In EBA, a distribution of chromatographic particle diameters with varying densities is operated in a fluid field, resulting in an expansion of the bed by a factor of two- to three-fold. This expanded bed has a significantly increased void volume, allowing cellular debris and whole-cell broth to move through the column more easily as long as the feed is diluted to around 10-15% wet cell weight (Bierau et al., 1999). Although EBA has been demonstrated at the pilot scale, its deployment in industrial-scale production is still not commonplace due to concerns about fluid distribution, cleaning validation, and chromatographic performance.

### *1.3.3. Preparative Chromatography*

Preparative chromatography forms the backbone of most protein purification processes because of its high efficiency and selectivity, with many of these processes consisting of two to three chromatography steps (Fig. 1.2). An initial chromatography for product capture is carried out, followed typically by a second

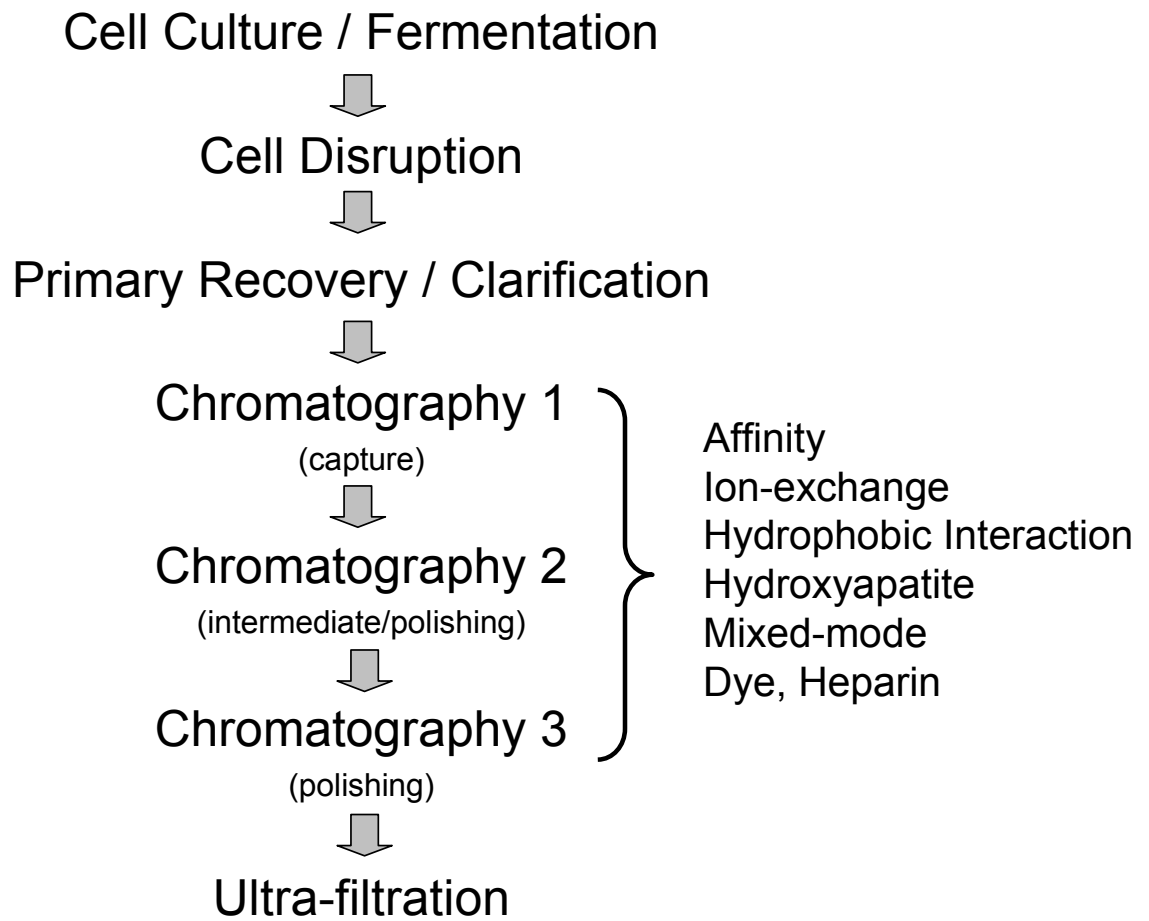


**Figure 1.2.** Typical bioprocess for protein production, consisting of two to three chromatographic steps.

chromatography for additional purification of the product from residual host-cell contaminants and process excipients. In some cases, a third chromatography may be performed as a polishing step to clear hard-to-remove residual impurities not purified away in the preceding steps.

#### 1.3.3.1. Modes of Operation

Process chromatography is a term encompassing all chromatographic separations in the manufacture of defined products. As opposed to analytical chromatography, process chromatography attempts to maximise throughput and capacity while achieving a defined purity. Therefore, the stationary phase is typically overloaded. Preparative chromatography may be operated in a packed-bed, stirred-tank, or expanded-bed configuration. In the case of packed-bed chromatography, the adsorbent may be packed in either an axial-flow or a radial-flow column, and may be operated as a single column or in a simulated-moving-bed format (Cramer and Jayaraman, 1993; Lyddiatt, 2002). Of these, a single axial-flow column is the most common.

Process chromatography is typically operated in one of two modes, 'bind-and-elute' or 'flow-through'. In bind-and-elute mode, the protein product is bound to the column and then separated across the length of the column under isocratic, linear-gradient, or step-gradient elution conditions (Harrison et al., 2003; Guiochon et al., 2006). A typical bind-and-elute chromatography step includes a column equilibration stage, sample loading, one or more wash steps, and product elution. In contrast, in flow-through mode, the feed (sample) is loaded continuously on the column with the goal being to bind contaminants to the column while the product passes through and is recovered. The typical stages in this mode include column equilibration and sample loading, with a column wash sometimes performed after the load. A slight variation to the typical flow-through mode is 'weak-partitioning chromatography', which was developed by Kelley and co-workers (2008A) for the purification of monoclonal antibodies. In weak-partitioning chromatography, the mobile phase conditions of the feed are adjusted so that the protein product binds weakly to the column, eluting isocratically during the load and in a short wash following the load. By carrying out the chromatography in this fashion, better separation can be achieved between the product and more tightly binding impurities.

An alternative to single column chromatography is simulated-moving-bed (SMB) chromatography, which seeks to improve production rates by providing a format for a continuous separation (refer to Guiochon, 2002, for a review of SMB). Here, the column is configured as a column train having four or more successive sections. A counter-current movement of the stationary phase is simulated by column switching of two successive columns in the train. SMB has found renewed interest in the industrial separation of enantiomers but is still used infrequently for bioseparations.

A chromatographic separation can also be carried out as a batch adsorption process in a continuously stirred tank, where the adsorbent is then recovered by settling, filtration or centrifugation (Belter et al., 1988; Lyddiatt, 2002). Unlike column chromatography, batch adsorption can be operated in the presence of cells or cellular debris and does not require a geometrically refined adsorbent particle. However, a significant limitation of this approach is that it offers only a single-stage of equilibrium adsorption as opposed to the rapid multistage processes achievable by packed-bed chromatography. Therefore, batch adsorption is used less frequently in protein purification processes, although it has been used in antibiotic purification, blood plasma fractionation, and hepatitis B vaccine processing (Beyzavi, 1999).

#### 1.3.3.2. Sorbent Properties

Chromatography sorbents are characterised by their base support and surface chemistry. The sorbents are functionalised by attaching a binding ligand to the base matrix, with or without a spacer. Use of a spacer can affect retention by impacting the accessibility of the biomolecule to the ligand, decreasing the effective pore volume, and providing a source of non-specific interaction. While the surface chemistry determines the primary separation mechanism, the base matrix can strongly influence the mass transport properties of the separation and contribute to secondary binding effects (Boschetti, 1994; Muller, 2005). The base matrix may either be porous or non-porous, with the majority of base matrices used in preparative protein chromatography being porous. Both inorganic and organic materials are used in the preparation of base matrices (Muller, 2005). Inorganic base matrices include hydroxyapatite, alumina, silica, and controlled pore glass. Organic polymers include cellulose, agarose-based matrices, cross-linked dextran, polyacrylates, and polyvinyl polymers (Beyzavi, 1999). Composite materials have

also been developed in order to combine the rigidity of one material with the biocompatibility and stability of another (Muller, 2005).

The ligand chemistries commonly used for process-scale protein purification are anion exchange (AEX), cation exchange (CEX), hydrophobic interaction (HIC), affinity, size-exclusion (SEC), and ceramic hydroxyapatite (CHT) chromatography. These are summarised in Table 1.2 along with their separation mechanism. Reversed phase chromatography is used only to a limited basis because of concerns about protein denaturation. In addition to the above chemistries, a new generation of ligands have recently emerged offering new modalities for purification. Specifically, these include biomimetic ligands for affinity chromatography (Roque et al., 2005; Clonis, 2006) and mixed-mode ligands with dual separation modalities, e.g. hydrophobic and ion-exchange properties (Burton and Harding, 1998; Johansson et al., 2003A; Johansson et al., 2003B; Chen et al., 2008A).

The properties of the chromatographic base matrix and their potential influence on the chromatography are summarised in Table 1.3 (Boschetti, 1994; Muller, 2005). Smaller sorbent particle sizes can increase dynamic binding capacity and improve the overall resolution of the chromatography; however, they usually lead to higher column back-pressures. Therefore, particles sizes of less than 20 microns are generally not used in process chromatography. In addition, sorbent properties such as the pore volume and pore size distribution can affect protein uptake rates (pore diffusivity) as well as protein retention (DePhillips and Lenhoff, 2001). Consequently, adsorbent design and optimisation must consider not only the ligand chemistry but also these physical properties of the base matrix.

Two major limitations of conventional preparative adsorbents are the slow diffusive mass transport within the pores and the stability of the packed bed (Cramer and Jayaraman, 1993; Guiochon, 2002). Consequently, new packing materials and modes of chromatography have been developed to address these concerns. Many manufacturers now offer resins with greater mechanical stability, such as the Capto resins by GE Healthcare (Uppsala, Sweden), thereby enabling more rapid processing and higher productivity. Radial flow chromatography also has been used as a way to avoid the instability, large pressure drops, and flow problems of large, axial-flow

columns. The geometry of the radial flow design increases the flow area and decreases the flow path; however, it is less effective for multistage separations (Cramer and Jayaraman, 1993). Monolithic columns offer the potential for fast mass transfer (Barut et al., 2008), which is of particular importance to large molecular

**Table 1.2.** Types of ligand chemistries used in preparative protein chromatography.

Type	Examples of Ligand Types	Mechanism of Separation
<b>Cation-exchange</b>	<i>Sulfopropyl (SP)</i> <i>Methylsulfonate (S)</i> <i>Carboxymethyl (CM)</i>	Electrostatic interaction
<b>Anion-exchange</b>	<i>Diethylaminoethylene (DEAE)</i> <i>Quaternary aminoethyl (QAE)</i> <i>Quaternary ammonium (Q)</i>	Electrostatic interaction
<b>Hydroxyapatite</b>	$(Ca_5(P0_4)_3OH)_2$	Cation-exchange and coordination bonds (between $Ca^{2+}$ and carboxyl/phosphoryl groups)
<b>Hydrophobic Interaction</b>	<i>Phenyl-</i> <i>Butyl-</i> <i>Octyl</i>	Hydrophobic complex formation
<b>Mixed Mode</b>	<i>N-benzyl-N-methyl-ethanolamine</i> <i>4-mercapto-ethyl-pyridine</i> <i>Phenylpropylamine</i> <i>MMC</i>	Multi-modal (e.g. hydrophobic interaction and ion exchange)
<b>Reversed phase</b>	<i>4-carbon alkyl (C4)</i> <i>18-carbon alkyl (C18)</i>	Hydrophobic complex formation
<b>Size-exclusion chromatography</b>	<i>N/A (porous inert base matrix)</i>	Steric exclusion
<b>Affinity, Pseudo-affinity</b>	<i>Protein A/G</i> <i>Glutathione</i> <i>Heparin</i> <i>Dye</i> <i>Antibody</i> <i>Recombinant protein</i> <i>Biomimetic</i> <i>Lectin</i> <i>Immobilised metal affinity</i>	Biospecific interaction, coordination complex formation

assemblies such as viruses, but only recently has the technology been available at process scale. Therefore, it has yet to find widespread use. Perfusion chromatography attempts to improve mass transfer by using a chromatographic support with very large through-pores for convective flow in addition to a network of short diffusive pores (Afeyan et al., 1990; Regnier, 1991). At high linear velocities ( $>1000$  cm/h), convective flow through these large pores is thought to dominate over diffusive transport. In addition, a number of chromatography manufacturers now produce adsorbents with a hydrogel structure, in which the pore is filled with a three dimensional network of ligands (the so-called "gel in a shell"). As a result, these resins have significantly higher binding capacities and improved mass transfer. Examples of these resins include Ceramic Hyper D and Hyper Q from Pall (Port Washington, NY, USA), Toyopearl Super Q from Tosoh Bioscience (Montgomeryville, PA, USA), and Capto S and Q from GE Healthcare (Uppsala, Sweden).

#### 1.3.3.3. Operational Parameters

In addition to the sorbent properties, chromatographic behaviour depends on the mobile phase composition and operating conditions of the chromatography (Table 1.3). These operational parameters include column geometry, flow rate, and temperature. Once an adsorbent is selected for a particular purification step, the mobile phase composition of the load, wash, and elution steps must then be optimised to maximise recovery and purity. This optimisation typically involves varying the pH, ionic strength, buffer type, and mobile-phase modifier (i.e. salt or solvent) type and concentration. Column height and flow rate are two other important factors that are optimised to increase the separation efficiency and dynamic binding capacity of the step.

#### 1.3.4. Membrane Separations

Membranes are used in protein purification processes for primary recovery (cell harvest and clarification), product purification or fractionation, product concentration, buffer exchange, sterile filtration, and virus removal. The most commonly used membrane processes are microfiltration and ultrafiltration. Microfiltration is used to remove solid particulates such as cells and cellular debris from the liquid medium. These membranes usually have pore diameters in the

micron range and may be classified as depth filters, surface filters, or screen filters (Kalyanpur, 1999). Depth filters are made of fibrous, granular, or sintered material with a random pore structure, whereas surface filters are comprised of layers of glass or polymeric microfibers (i.e. 'hollow fibres'). Screen filters are made of a porous matrix, often a polymeric material, with a well-defined pore size in the range of 0.1 to 1  $\mu\text{m}$  (Kalyanpur, 1999). Particles and solutes larger than the rated pore size are retained at the surface of these membranes. Therefore, membranes of this type are also used for sterile filtration, viral removal, and ultrafiltration. In the case of ultrafiltration, the pore sizes are usually rated by the molecular weight of the dissolved solute(s) rather than by their diameter.

**Table 1.3.** Parameters affecting performance in preparative column chromatography.

Parameter		Influence on
<b>Mobile Phase</b>	Buffer type	Retention, selectivity
	pH	Retention, selectivity
	Ionic Strength	Retention, selectivity
	Modifier (salt, solvent) type	Retention, selectivity
	Modifier (salt, solvent) conc.	Retention, selectivity
<b>Operational</b>	Flow rate	Efficiency
	Temperature	Efficiency, retention, selectivity
	Column length (geometry)	Efficiency
	Loading amount	Efficiency
	Elution gradient	Selectivity
<b>Sorbent</b>	Surface chemistry (ligand)	Retention, selectivity
	Ligand arrangement, Spacer arm	Efficiency, retention, selectivity
	Ligand density	Retention, selectivity
	Pore structure (geometry)	Efficiency, retention, selectivity
	Pore volume	Efficiency and retention
	Particle size	Efficiency
	Base matrix material	Efficiency, retention, selectivity

Adsorptive membrane chromatography (Ghosh, 2002) is a variation on a traditional membrane separation in which the membrane is functionalised with a charged group or affinity ligand. This offers an alternative to the slow diffusive mass transfer in porous resin since the flow through the membrane pores is convective, thereby allowing for fast on-off separations. This approach can be easily scaled up, and because membranes are cheaper to manufacture, they are potentially disposable. In addition, adsorptive membranes allows for the possibility of combining the lysate clarification with an initial purification. Disadvantages, however, are that these membranes have lower capacities than most chromatographic adsorbents and can be variable in their thickness, pore size distribution, and inlet flow distribution.

#### **1.4. Theoretical Considerations in Preparative Liquid Chromatography**

Chromatography was first developed by the Russian botanist Tswett at the turn of the 20<sup>th</sup> century in the separation of plant pigments (Tswett, 1906). It is defined as a separation process in which a solute interacts with a chromatographic stationary phase and is separated according to its distribution between the mobile phase and the stationary phase. Hence, the separation of a mixture depends on the differing migration velocities of each component, which in turn is defined by the unique structural properties and surface chemistry of these components.

Although the development of a bioprocess chromatographic step is often done empirically, development is aided by a fundamental understanding of the thermodynamics and kinetics (mass transfer) of the chromatographic process. Each of these concepts in turn requires the mode of contact to be considered, i.e. flow through a fixed bed or batch adsorption in a stirred vessel. Adsorption equilibrium between the solute and stationary phase are typically characterised by adsorption isotherms, which may be linear or nonlinear and which may model single-component or multi-component (competitive) systems (Belter et al., 1988; Ladisch, 2001; Harrison et al., 2003; Guiochon et al., 2006). However, column chromatography is not typically operated at equilibrium and is subjected to dispersive effects and mass transfer resistances. In porous resins, mass transport is affected not only by factors such as flow rate, bed packing quality, and sorbent particle size but also by the pore size distribution and the pore tortuosity. A variety of models of varying complexity

have been developed to describe mass transport, considering such components as axial dispersion, external film mass transfer, pore diffusion, surface diffusion, and surface reaction kinetics (Guiochon and Lin, 2003; Carta et al., 2005).

#### *1.4.1. Adsorption*

The adsorbent capacity, binding affinity, resolution, and selectivity of a chromatographic separation are affected strongly by the ligand chemistry, its density and distribution, and the accessible surface area of the stationary phase. Binding of a biomolecule to an adsorbent may involve electrostatic interactions (e.g. van der Waals or dipole-dipole forces), hydrophobic interactions, and hydrogen bonding. Consequently, the three dimensional structure of the protein (shape and size), its surface chemistry (e.g. charge), and the specific distribution of amino acids all contribute to binding. In addition, the physical properties of the base matrix can strongly influence retention. DePhillips and Lenhoff (2001 and 2004) in their work with cation-exchange adsorbents found that the anion type on the ligand, the adsorbent pore-size distribution, and local patches on the surface protein (instead of its overall net charge) were key determinants of protein retention. Interestingly, with respect to the pore size distribution, retention was enhanced for those adsorbents having pore dimensions similar to the size of the protein solute, presumably because the protein was surrounded by the charged ligand. Cramer and co-workers have used protein crystal structures and primary amino acid sequence information in combination with quantitative structure-property relationship (QSPR) models to predict chromatographic behaviour in ion-exchange (Tugcu et al. 2003; Yang et al., 2007A) and hydrophobic interaction chromatography (Chen et al., 2008B), as well as in the *a priori* design of mixed-mode ligands (Yang et al., 2007B). All of these studies attempt to gain a more comprehensive understanding of the underlying mechanisms of adsorption at the molecular level.

##### *1.4.1.1. Single-Component Adsorption Isotherms*

The thermodynamics of phase equilibria in liquid chromatography is described by adsorption isotherms. Knowledge of isotherms is important in understanding adsorption and integrating the differential mass balance equations used in chromatography models (Guiochon, 2002). Adsorption isotherm studies are carried out by having excess amounts of the binding species in the mobile phase close to the

surface of the stationary phase, with adsorption influenced by the chemical potential of each species. Isotherms are used in preparative chromatography for determining static binding capacity, revealing separation characteristics and the extent of purification, comparing the potential of different separation schemes, and modelling chromatographic separations. An incomplete understanding of isotherm curvature can often explain problems in scale-up of preparative chromatography (Guiochon, 2002). While bioseparations almost always involve multiple components, single-component isotherms still provide the simplest and most convenient means for understanding the thermodynamics of product binding and optimising the chromatographic step.

The simplest procedure for determining adsorption isotherms is by static batch adsorption, in which either the adsorbate (protein) or adsorbent concentration is varied across a concentration range and then mixed together in a vessel until equilibrium is reached (usually a few hours to a few days). The concentration of the adsorbate (binding species) in the liquid phase is measured following the incubation, with the concentration on the stationary phase (mass loaded per unit volume of adsorbate) calculated by material balance and graphed as a function of the equilibrium concentration in the mobile phase (Fig. 1.3). This approach can be time-consuming and laborious, unless automated, and does not guarantee an accurate reflection of dynamic column conditions. Alternatively, dynamic methods using a column configuration have been developed for faster and more accurate determination of adsorption isotherms. These methods attempt to solve the general inverse problem of chromatography, i.e. determining isotherm and rate constants by knowing the solution of the system of mass balance equations from band profiles and controlling boundary conditions (Guiochon et al., 2006). Commonly used dynamic methods include frontal analysis (FA), elution by characteristic point (ECP), frontal analysis by characteristic point (FACP), and pulse methods (as reviewed by Guiochon et al., 2006). Of these, only the pulse method is typically used for competitive adsorption isotherms.

A number of adsorption isotherm models exist to describe liquid-solid equilibria for single- and multi-component systems. A review of these is provided by Guiochon et

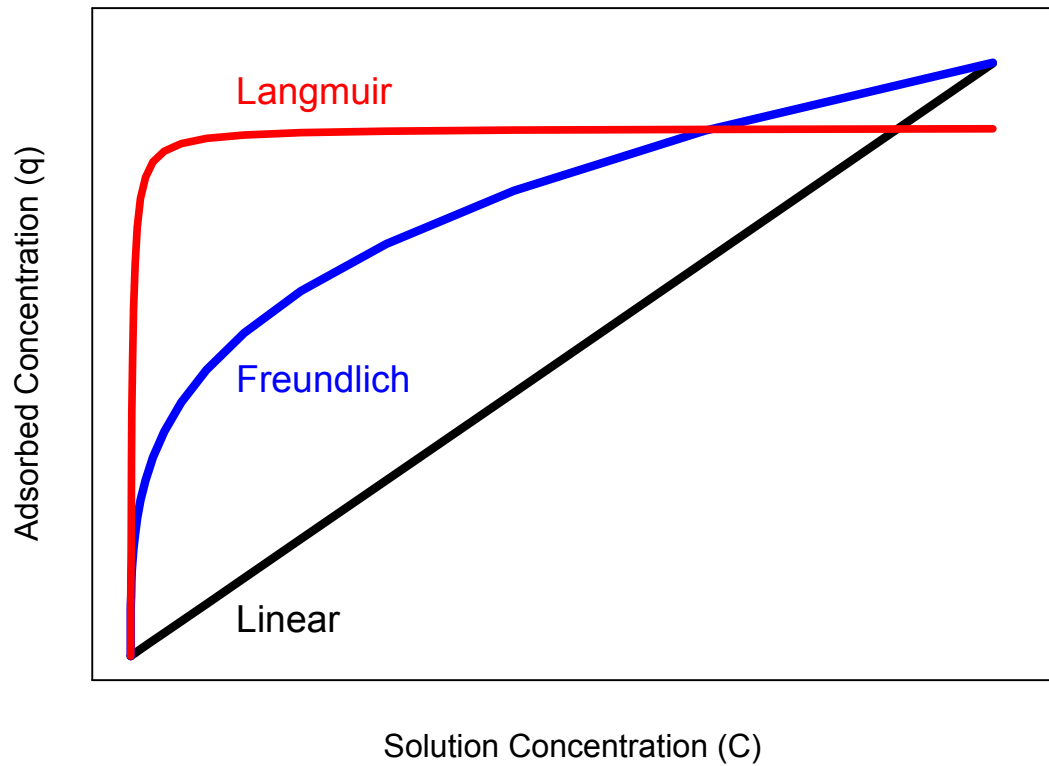


**Figure 1.3.** Graphical example of three equilibrium adsorption isotherm models used to describe protein adsorption: the Linear, Freundlich, and Langmuir models.

al. (2003 and 2006). While some of the models have a theoretical basis, others are simply empirical. Three commonly applied single-component isotherm models for protein adsorption are the Linear, Freundlich, and Langmuir models, as shown in Figure 1.3. In the ideal case, adsorption is assumed to be completely reversible, there is no non-specific binding, and the binding sites are homogeneous. When the concentration of adsorbent binding sites significantly exceeds the adsorbate concentration (i.e. adsorbent is vastly underloaded with adsorbate relative to its saturation concentration), the chromatography is linear and is given by:

$$q = q_m K_{eq} C , \quad \text{Equation 1.1}$$

where  $q$  is the concentration of adsorbed species on the resin,  $q_m$  is the maximum binding capacity,  $C$  is the concentration of the species in solution, and  $K_{eq}$  is the equilibrium constant for the adsorption reaction. This is typically the case in analytical chromatography, where baseline resolution and reproducible elution times are important. In contrast, preparative chromatography is rarely operated in the linear limits because the capacity of the adsorbent must be maximised for highest productivity.

Two classical adsorption isotherm models used to describe nonlinear chromatographic bioseparations are the Freundlich and Langmuir isotherms. The Freundlich isotherm describes the energetic heterogeneity on the surface of the resin (Harrison et al., 2003) and corresponds approximately to an exponential distribution of heats of adsorption (LeVan et al., 2008). It is used most often for antibiotic, steroid, and hormone adsorption (Belter et al., 1988; Harrison et al., 2003). It is given by:

$$q = K C^n , \quad \text{Equation 1.2}$$

where  $K$  and  $n$  are constants that are determined experimentally, typically from a log-log plot of  $q$  versus  $C$ . When the adsorption is favourable,  $n$  is less than 1, while when it is unfavourable,  $n$  is greater than 1.

The Langmuir isotherm was originally developed for the adsorption of gases to glass and mica surfaces but now is one of the most widely used models for protein adsorption in single-component systems on homogeneous surfaces. It postulates that a reversible binding reaction occurs between the adsorbate and the vacant sites of the

adsorbent, with these sites being equivalent, distinguishable, and independent (Belter et al., 1988; Zhu et al., 1991). It also assumes that only one solute molecule can bind per binding site and that this binding is localised and does not influence adsorption of another molecule at another site (Gritti et al, 2003). The Langmuir isotherm is described by:

$$q = \frac{q_m K_{eq} C}{1 + K_{eq} C}, \quad \text{Equation 1.3}$$

where  $q_m$  is the maximum binding capacity (monolayer) of the adsorbent. It can also be expressed as a function of  $K_D$ , the dissociation constant in adsorbate-adsorbent binding:

$$q = \frac{q_m C}{K_D + C}. \quad \text{Equation 1.4}$$

The consequence of the Langmuir isotherm in preparative chromatography is that adsorption depends not only on the equilibrium constant of the adsorbate but also on the binding capacity of the adsorbent. Typically, a process column is overloaded and is therefore operated in the nonlinear region of the isotherm, where baseline resolution may be difficult to achieve.

The assumptions of the Langmuir isotherm do not always hold, however. This can be the case if the adsorbent surface is not homogeneous, there are two or more different types of ligand functional groups, there is extensive non-specific interaction with the base matrix, or the binding is not localised (Guiochon et al., 2006). Therefore, other single-component isotherm models have been developed to addresses these situations, such as the bi-Langmuir, Fowler, Quadratic, Jovanovic, Jovanovic-Freundlich, Martire, Moreau, and Toth isotherms. Each of these models attempts to account for surface heterogeneity on the adsorbent and/or adsorbate-adsorbate interactions, although many of these are not relevant to the binding of large biomolecules onto preparative adsorbents. As a result, despite its limitations, the Langmuir isotherm remains the most commonly used isotherm model for describing single-component protein adsorption in preparative chromatography.

#### 1.4.1.2. Multi-Component Adsorption Isotherms

Competitive isotherm models have been developed for binary and multi-component systems, but these models are generally less rigorous than their single-component counterparts since a full understanding of multi-component interactions is incomplete (Guiochon et al., 2006). The Langmuir isotherm can be modified to deal with multi-component systems, in which the rate of desorption is considered along with the rate of adsorption. While the rate of adsorption of each component is proportional to its concentration and the free surface area, the rate of desorption is proportional to the surface area occupied by each component. Therefore, a system of linear equations can be written and solved. For the  $i$ th component of a multi-component system, the competitive isotherm is described by (Guiochon et al., 2006):

$$q_i = \frac{a_i C_i}{1 + \sum_{j=1}^n b_j C_j}, \quad \text{Equation 1.5}$$

where  $n$  is the number of components in the system and  $a$  ( $= q_m^* K_{eq}$ ) and  $b$  ( $= K_{eq}$ ) are the coefficients of the single-component Langmuir isotherm for component  $i$ , and their ratio ( $a/b$ ) is the column saturation capacity for component  $i$ .

The competitive Langmuir isotherm has a number of limitations. Although it provides a very useful first-order approximation of the experimental data, it lacks thermodynamic rigor and does not sufficiently predict overloaded elution profiles. Specifically, it cannot quantitatively predict competitive isotherm behaviour when the difference between the column saturation capacities for each component exceeds 5 to 10% (Felinger and Guiochon, 1996).

Other competitive adsorption isotherm models have been developed for multi-component systems where the competitive Langmuir falls short (reviewed by Zhu et al., 1991; Guiochon et al., 2006). These include the competitive bi-Langmuir model to deal with a surface covered with two different binding sites, the Ideal Adsorbed Solution model to account for differences in column capacities between two components in a binary mixture where the single-component adsorption is Langmuirian, and Statistical Isotherm models in which equilibrium binding is described by the ratio of two second-degree polynomial equations. In addition, the Fowler model has been modified to deal with binary mixtures, and the hybrid

Freundlich-Langmuir isotherm has been extended to address the situation of strong adsorption at low concentration in multi-component separations.

#### 1.4.1.3. Adsorption Isotherm Models for Ion-Exchange Chromatography

Several adsorption isotherm models have been developed for the special case of ion-exchange chromatography, in which the exchange between the solvent and the adsorbed molecules is considered to be stoichiometric rather than statistical. Classical stoichiometric theory of the salt elution of biomolecules in ion-exchange chromatography was developed by Boardman and Partridge (1955) and then expanded upon by Rounds and Regnier (1984) to correlate protein retention with mobile phase composition and protein charge in linear chromatography. Regnier and Mazsaroff (1987) later applied the theory to the competitive adsorption of proteins. These stoichiometric displacement models (SDM) assume binding by coulombic interaction at fixed sites but fail to consider other stationary phase interactions such as hydrophobic interaction.

Melander et al. (1989) considered hydrophobic effects in their mathematical treatment of the stoichiometric model, which is described by Langmuirian kinetics with a mobile phase modulator and is based on an adaptation of solvophobic theory. Solvophobic theory predicts that the contribution of hydrophobic interaction to the free energy of binding is proportional to the hydrophobic contact area and surface tension of the salt solution. Here, the salt is considered to be inert and the biomolecule is assumed to be retained by the electrostatic field at the surface of the stationary phase but retains some freedom of movement in the layer above it. The interplay of hydrophobic and electrostatic interactions is then described by a three-parameter equation:

$$\text{Log } k' = A - B \log m_s + C m_s, \quad \text{Equation 1.6}$$

where  $k'$  is the retention factor (capacity factor),  $m_s$  is the molality of the salt in the eluent, and  $A$  is a constant encompassing all characteristic system parameters. Parameter  $B$  is the electrostatic interaction parameter and depends on the charge of the protein and counter-ion. Parameter  $C$  is the hydrophobic interaction parameter and depends on the contact area of the protein with the stationary phase and on the properties of the salt.

Whitley *et al.* (1989) and Velayudhan (1990) observed that a macromolecule such as a protein shields a large number of charged binding sites due to its sizeable surface area, thereby reducing the capacity of the resin below its stoichiometric capacity. Accordingly, if an empirical shielding factor is incorporated into a mass action model, it provides a much better representation of ion-exchange isotherms for a number of model proteins. Brooks and Cramer (1992) extended this work to competitive systems, and then later Gallant *et al.* (1995) expanded the theory to the non-linear elution of proteins. In this steric mass action adsorption (SMA) model, the salt competes with the protein for available binding sites. The shielding factor used in the model depends not only on the ionic strength and composition of the solution but also on the adsorbent composition and on the properties and concentration of the protein. The SMA isotherm model for a single component (protein)  $i$  is given by:

$$C_i = \frac{q_i}{K_{SMA}} \times \left[ \frac{C_{salt}}{\Lambda - (\sigma_i + z_i)q_i} \right]^{z_i}, \quad \text{Equation 1.7}$$

where  $C_i$  is the protein concentration,  $K_{SMA}$  is the equilibrium constant,  $C_{salt}$  is the mobile phase salt concentration,  $z_i$  is the characteristic charge of the protein,  $\sigma_i$  is a steric hindrance factor,  $q_i$  is the adsorbed protein concentration, and  $\Lambda$  is the total ionic capacity of the stationary phase.

#### 1.4.1.4. Retention Factor

The retention of a protein across a chromatographic column can be characterised by its retention factor,  $k'$ , thereby providing an alternative method to adsorption isotherms for studying chromatographic adsorption. The retention (or capacity) factor is defined as the ratio of the time spent by the solute of interest in the stationary and mobile phases under *linear* conditions (Guiochon *et al.*, 2006):

$$k' = \frac{t_r - t_0}{t_0}, \quad \text{Equation 1.8}$$

in which the retention factor  $k'$  is a dimensionless value,  $t_r$  is the retention time of the solute of interest, and  $t_0$  is the time that it takes the unretained solute to pass through the column. The retention factor is related to the equilibrium constant,  $K_{eq}$ , by:

$$k' = K_{eq} \phi, \quad \text{Equation 1.9}$$

where  $\phi$  is the phase ratio defined as the accessible surface area of the adsorbent per unit volume of mobile phase. The retention factor is useful in that it reflects both the molecular interaction of binding and the physical characteristic of the stationary phase. Furthermore, the separation of two binding species, A and B, can then be described by comparing their retention factors. The separation between A and B is defined by the selectivity factor,  $\alpha$ :

$$\alpha = \frac{k'_B}{k'_A}, \quad \text{Equation 1.10}$$

where  $k'_B$  and  $k'_A$  are the retention factors for species B and A, respectively, with A being the faster eluting species.

#### 1.4.2. Mass Transport

The separation efficiency (i.e. peak resolution) and dynamic binding capacity (DBC) of column chromatography is impacted by the mass transport within the chromatographic bed. Mass transport factors include axial diffusion, eddy diffusion (resulting from variability in the flow path through the column), bed heterogeneity, and mass transfer kinetics (Guiochon et al., 2006). In porous adsorbents, the mass transfer kinetics depend on the external (extraparticle) mass transfer, pore (intraparticle) diffusion, pore surface (solid) diffusion, and surface reaction kinetics (adsorption/desorption kinetics). Consequently, the column packing efficiency, adsorbent particle size, pore size, and pore network all can impact mass transport and hence chromatographic performance.

##### 1.4.2.1. Plate Models and Rate Theory

Plate models (Martin and Synge, 1941; Craig, 1944) have been used to describe the band broadening and retention of a solute migrating through a column. In these models, a column is divided into a set of identical theoretical plates, representing stages of equilibrium. The height equivalent of a theoretical plate (HETP) for a column (L) with N theoretical plates is defined by:

$$HETP = \frac{L}{N}. \quad \text{Equation 1.11}$$

The number of theoretical plates, N, is determined by:

$$N = \frac{5.55t_r^2}{w_{1/2}^2}, \quad \text{Equation 1.12}$$

where  $w_{1/2}$  is the peak width of the eluting chromatographic peak at half-height. Plate models are empirical, with the number of theoretical plates correlated to the variance observed in the chromatographic profile.

Van Deemter et al. (1956) related plate height to the mobile phase linear velocity by considering the effects of axial diffusion, eddy diffusion, and mass transfer kinetics:

$$HETP = A + \frac{B}{\mu} + C\mu, \quad \text{Equation 1.13}$$

where  $\mu$  is the linear velocity, A is a constant associated with eddy diffusion, B is a coefficient associated with axial diffusion, and C reflects the mass transfer kinetics. (Note that although the same symbols are used, these do not refer to the same constants as those in Equation 1.6). Figure 1.4 shows the relationship between reduced plate height (HETP divided by the adsorbent particle diameter) and reduced velocity (product of the velocity and the adsorbent particle diameter divided by the solute diffusion coefficient). For the chromatography of proteins on preparative adsorbents, Carta et al. (2005) calculate that the reduced velocity is between 140-8000, implying that the efficiency of the separation is determined mostly by the mass transfer kinetics.

#### 1.4.2.2. Mass Transfer in Porous Adsorbents

The mass transfer of a solute onto a porous stationary phase is illustrated in Figure 1.5 (from Horvath and Lin, 1978). The chromatographic process proceeds by the following steps: (1) external transport of the solute from the bulk mobile phase to the surface of the particle; (2) diffusion within the pore; (3) adsorption to the ligand; (4) desorption; and (5) diffusion out of the pore (Guiochon et al., 2006). The external film mass transfer resistance in step (1) is due to the fact that each particle of the stationary phase is surrounded by a laminar sublayer having a stagnant film across which the solute must diffuse. Therefore, it is dependent on convection and affected by mobile phase velocity. Specifically, the mass transport flux (J) at the particle

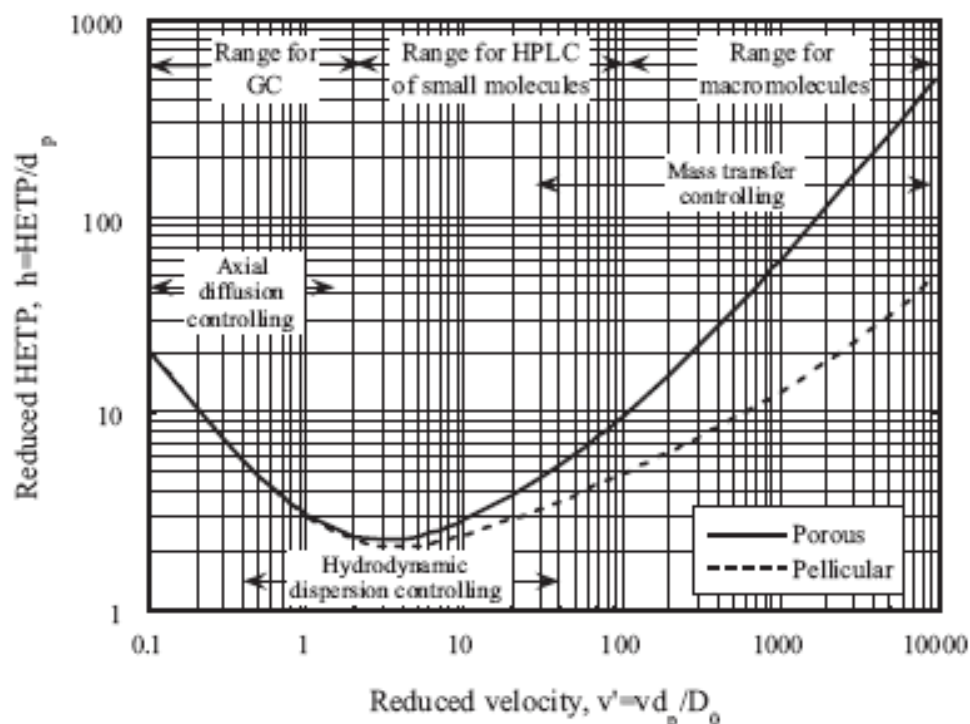


**Figure 1.4.** Generalised van Deemter plot showing the relationship between reduced plate height ( $h$ ) and reduced velocity ( $v'$ ), obtained from Carta et al. (2005). In this figure,  $v$  is the linear velocity (defined also as  $\mu$  in this thesis),  $d_p$  is the adsorbent particle diameter, and  $D_0$  is the solute diffusion coefficient. Based on calculations by Carta et al. (2005):  $v' = 140 - 8000$  for proteins separated on preparative stationary phases if  $D_0$  is  $\sim (1-10) \times 10^{-7} \text{ cm}^2/\text{s}$ ,  $d_p$  is  $\sim 50-100 \text{ }\mu\text{m}$ , and  $v$  is  $\sim 100-500 \text{ cm/h}$ .

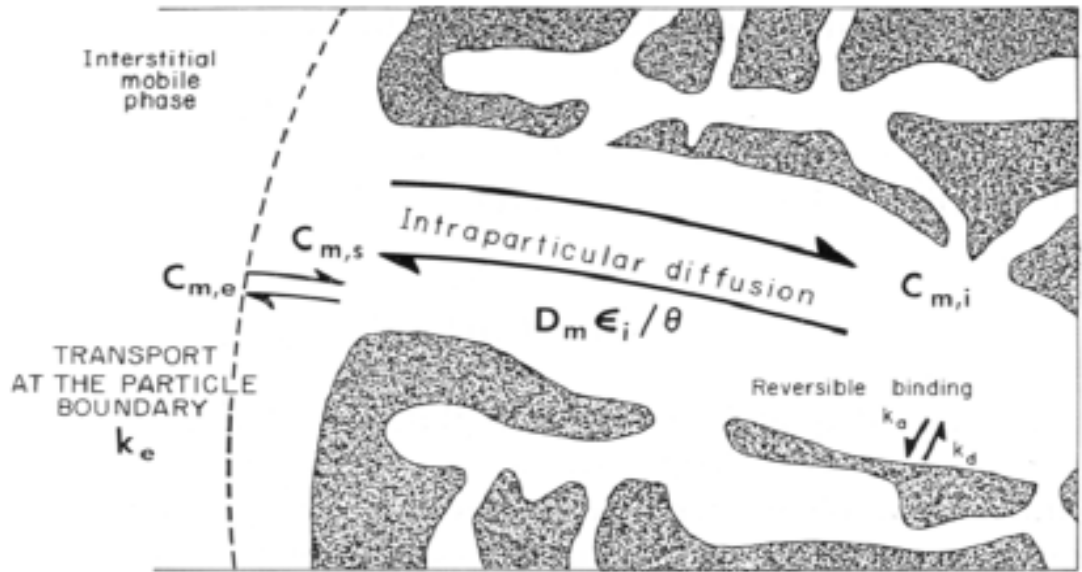


**Figure 1.5.** Schematic of the mass transport of solute in porous adsorbents, from Horvath and Lin (1978). In this figure,  $k_a$  and  $k_d$  are the rate constants for adsorption and desorption, respectively;  $k_e$  is the film mass transfer coefficient (referred to as  $k_f$  in equation 1.14),  $C_{m,e}$  and  $C_{m,s}$  are the concentrations of the solute in the bulk mobile phase and stationary phase, respectively (referred to as  $C$  and  $C_s$  in equation 1.14);  $\epsilon_i$  is the internal porosity;  $\theta$  is the tortuosity factor; and  $D_m$  is the intraparticle diffusion constant. (Note that these terms may differ from those used elsewhere in the text).

surface correlates to the effective film mass transfer coefficient,  $k_f$ , and the linear driving force (LeVan et al., 2008):

$$J = k_f(C - C_s), \quad \text{Equation 1.14}$$

where  $J$  is the mass transfer flux at the particle surface,  $C$  is the solute concentration in the bulk mobile phase and  $C_s$  is the solute concentration at the chromatographic particle surface. Generally speaking,  $k_f$  will increase with fluid velocity and solute diffusivity, and decrease with particle size. Differences in the film mass transfer resistance can also result between fixed bed and stirred tanks systems, with  $k_f$  increasing with the Reynolds number ( $Re$ ).  $k_f$  can be determined from the dimensionless Sherwood ( $Sh$ ) number (LeVan et al., 2008):

$$Sh = \frac{k_f d_p}{D}, \quad \text{Equation 1.15}$$

where  $D$  is the molecular diffusivity and  $d_p$  is the adsorbent particle diameter. In packed beds where  $0.0015 < Re < 55$ , the Sherwood number can be estimated from the  $Re$  and the Schmidt ( $Sc$ ) numbers using the following expression (Wilson and Geankoplis, 1996):

$$Sh = \frac{1.09}{\varepsilon} Re^{0.33} Sc^{0.33}, \quad \text{Equation 1.16}$$

where  $\varepsilon$  is the interstitial column voidage. The Reynolds number in a packed bed is defined by (LeVan et al., 2008):

$$Re = \frac{d_p \varepsilon v}{\nu}, \quad \text{Equation 1.17}$$

where  $v$  is the interstitial linear velocity in cm/s and  $\nu$  is the kinematic viscosity of the mobile phase (cm<sup>2</sup>/s).  $Sc$  is described by (LeVan et al., 2008):

$$Sc = \frac{\nu}{D}. \quad \text{Equation 1.18}$$

#### 1.4.2.3. Intraparticle (Pore) Mass Transport

The intraparticle transport of proteins in preparative ion-exchange adsorbents has been extensively studied. Within the adsorbent pores, transport has been shown to occur primarily by two different mechanisms: molecular diffusion in the pore liquid

(referred to as pore diffusion) and surface diffusion (also referred to as homogenous or solid diffusion) on the adsorbed phase (Carta et al., 2005). There is typically no convective flow within the pores because of their small diameter. One exception, however, is in the case of the very large through-pores (600-800 nm) of perfusive resins (Afeyan et al., 1990). Pore diffusion requires that the pore be large enough that the biomolecule can diffuse freely from the surface and is driven by the concentration gradient in the pore liquid. Surface diffusion occurs along surfaces and in pores filled with a hydrogel structure (Hunter and Carta, 2002) and is driven by the solute concentration gradient on the adsorbed phase. General diffusional transport models for spherical particles exist for describing pore diffusion (Carta et al., 2005). A simplification of the general pore diffusion model, known as the shrinking core model, is frequently used when the adsorption isotherm is highly favourable (Weaver and Carta, 1996; Dziennik et al., 2005). In this case, protein uptake occurs as a sharp front moving inward with increasing load amounts. Semi-empirical models have also been used, such as the linear driving force model, which lumps the sources of mass transfer resistance into one equation (Fernandez and Carta, 1996; Guiochon et al., 2006).

In practice, intraparticle diffusion is difficult to describe because it depends on the pore structure (its size distribution and tortuosity) and network connectivity, which are difficult to characterise. Therefore, the diffusivity ( $D$ ) in pores is often expressed as the effective pore diffusivity ( $D_e$  or  $D_p$ ) and effective adsorbed phase diffusivity ( $D_s$ ). The pore diffusivity can be described by (Carta, 2006; Guiochon et al., 2006):

$$D_e = k_p \frac{\varepsilon_p D}{\tau}, \quad \text{Equation 1.19}$$

where  $k_p$  is a pore hindrance parameter ( $<1$ ),  $\varepsilon_p$  is the intra-particle void fraction, and  $\tau$  is a tortuosity factor ( $>1$ ). Tortuosity has to do with the fact that the pores are rarely perfect cylinders but instead are convoluted, resulting in slower solute diffusion. The intraparticle void volume and tortuosity factor can be determined experimentally by methods such as mercury porosimetry, nitrogen adsorption, or inverse size-exclusion chromatography (Hagel et al., 1996; DePhillips and Lenhoff, 2000). The hindrance parameter depends on the ratio of the solute size and pore size, and is inversely related to size exclusion effects (steric exclusion of the solute from

the immediate vicinity of the pore walls) and viscous drag. Therefore,  $k_p$  should generally decrease as protein size increases.  $D_e/D$  is always less than one, and often ranges from 0.1 to 0.2 when the pore size is at least 5 times larger than the protein size (Carta, 2006).

Intraparticle diffusivities for proteins can be determined by macroscopic methods, in which the mass transfer rate is measured, or by microscopic methods, in which the intraparticle concentration profile is followed (Carta et al., 2005). Macroscopic methods include dynamic column approaches such as frontal analysis, isocratic pulse response, and gradient elution response as well as batch adsorption in stirred tanks or shallow beds. Determination of the effective diffusivity from the resulting data then requires a pre-established model. The isocratic pulse response method determines the intraparticle diffusivity by carrying out an injection and measuring the moment of the response peak in an isocratic elution. In the gradient method, the diffusivity is determined from the retention factor in a set of experiments in which the gradient slope and flow rate are varied. Batch methods are carried out with either well-mixed suspensions of the stationary phase or in very small packed (shallow) beds through which the sample is re-circulated at high flow rates. Protein uptake is determined by measuring the concentration of the solute in the mobile phase or on the adsorbed phase (following elution).

Microscopic techniques offer an advantage over macroscopic methods in that the effective diffusivity can be determined directly without requiring a pre-established model (Carta et al., 2005). Moreover, qualitative observations can be made that are reflective of the transfer mechanism, i.e. sharp concentration profiles associated with the shrinking core model and diffuse profiles associated with homogeneous transport. A commonly used microscopic technique is confocal laser scanning microscopy (CLSM), in which optically transparent, whole sorbent particles can be observed. Protein transport is then followed over time in optical sections using a fluorescently-labelled protein. To avoid quenching effects, the labelled protein is first diluted with unlabelled protein. However, since the observed protein is labelled, care must be given to ensure that the binding properties of the protein have not been altered by the fluorescent dye. A number of research groups have reported over the last decade on the use of CLSM for the determination of protein mass transport kinetics and the

elucidation of transport mechanisms in ion-exchange chromatography (Linden et al., 1999; Dziennik et al., 2003 and 2005; Hubbuch et al., 2003A and 2003B; Yang et al., 2006; Zhou et al., 2006). These researchers have observed pore and/or surface diffusion mechanisms, and in some cases the mechanism appeared to change with the mobile phase conditions. In addition, some of these researchers postulate that a non-diffusive mechanism such electrokinetic-based transport might be at play (Dziennik et al., 2003), although this remains controversial (Carta et al., 2005).

#### *1.4.3. Scale Considerations*

Ideal column chromatography assumes a homogeneous bed, yet columns are never perfectly homogeneous, with the extent of their heterogeneity influenced by the packing conditions and the mechanical stress on the bed (Guiochon, 2002). In the axial direction, the top part of the column is usually less densely packed than the bottom part, although this usually has only a minimal effect on band variance (Guiochon et al., 1997). This being said, for a compressible gel with a broad particle size distribution, the packing quality can be more of a concern since the particles have a tendency to separate according to Stoke's law (Jungbauer, 1993). Distortions in the radial distribution, in contrast to variance in the axial distribution, can lead to a significant decrease in column performance, with column efficiency lowest in the region closest to the wall (Knox et al., 1976; Guiochon et al., 1997; Shalliker et al., 2000 and 2003). This results in a perturbation of the flow profile and an increase in band broadening.

Radial heterogeneity in the local packing density are generally attributed to wall effects, which are proposed to extend a distance of about 30 particle diameters into the column (Knox et al., 1976). Using optical on-column visualisation of the migration of sample bands, Shalliker and co-workers (2000) found physical evidence of two wall effects. The first has to do with the geometry of the particles. Because the wall is flat and smooth, the particles cannot penetrate it, so the void volume increases along the wall. As a result, the mobile phase velocity is higher there than the bulk flow velocity, leading to band dispersion. While the effect of this wall effect is usually negligible in large-diameter preparative columns, it can be significant in micro-bore columns like those used for analytical HPLC, where the column diameter may only be about 10 to 15 times greater than the particle radii

(Knox, 1999). The second wall effect identified by Shalliker et al. (2000) arises from the friction between the bed and the column wall. This strong friction results in a heterogeneous stress distribution during column packing, leading to a packing density that is higher along the walls and lower at the column core. Consequently, this causes differential migration.

Approaches for scaling up chromatographic production include carrying out repeated chromatographic cycles, overloading the column, changing the adsorbent particle size, and increasing the column size (Jungbauer, 1993). With respect to increasing the column size, the conventional way of doing so is to increase the column diameter while maintaining a fixed bed length, adsorbent particle size, and residence time. This approach generally avoids distortions in resolution and a significant rise in column back pressure. However, the flow distribution and packing efficiency can deteriorate as the column diameter becomes larger, leading to band broadening and a decrease in performance. The column size can also be increased by keeping its aspect ratio constant, but this approach can lead to unexpected changes in performance and is usually avoided.

Many of the same scale effects associated with the scale-up of a chromatographic separation must also be considered when scaling down the chromatography. For batch adsorption, the scaled down system must ensure that the resin is uniformly mixed and efficiently recovered. Incubation times for adsorption and desorption have to be optimised accordingly. For separations carried out across a fixed bed, wall effects and packing efficiency must be carefully considered, especially in small-bore or capillary columns (Knox et al., 1976; Shalliker et al., 2000). Furthermore, it may not always be possible to keep either the column length or the aspect ratio fixed in scale down. All of these factors can impact chromatographic performance and should be considered accordingly.

#### *1.4.4. Models of Nonlinear Chromatography*

Models to describe chromatography have been around at least since the 1940s, although they still are not routinely used for bioprocess development. Three broad categories of models have emerged to describe linear chromatography, as reviewed by Guiochon (2002): (1) plate models, (2) rate models (i.e. solutions to the

differential equations that describe the mass balance and mass transfer kinetics), and (3) statistical models. Preparative chromatography, however, is rarely performed under linear conditions since the column is typically overloaded to maximise productivity. Therefore, versions of the linear models have been adapted for nonlinear chromatography, in which the equilibrium isotherms no longer behave linearly and become competitive with other components in the mixture. This situation makes the mathematical description of the chromatography considerably more complex.

While the thermodynamics of phase equilibria and the kinetics of mass transport will vary with experimental conditions, the mass of each component should remain constant throughout a chromatographic separation since it is assumed that no chemical reaction occurs (Guiochon et al., 2006). Consequently, a series of partial differential equations can be derived to describe the mass balance of the solute in the mobile phase and adsorbed on the stationary phase. An assumption is then made as to the relationship between the concentration of the stationary and mobile phases since the system is rarely at equilibrium. Different forms of these equations were derived by Wicke (1939), Wilson (1940), and DeVault (1943). In addition, a set of heat balance equations may be required if the process is not isothermal, although this is rarely the case in process chromatography. Upon setting initial and boundary conditions, several models can then be derived from the solution of these differential equations, with the thermodynamics of the separation described by the equilibrium adsorption isotherm.

Since column chromatography is subjected to dispersive effects and mass transfer resistances, different modelling approaches of varying complexity have been developed to account for one or more of these mass transport components, ranging from simple equilibrium models to multi-component general rate models which attempt to account for multiple sources of mass transfer resistance. Most of these models assume that the column is homogeneous in the radial direction, the mobile phase is incompressible, the column is run under isothermal conditions, and the phase ratio remains constant (Jungbauer and Kaltenbrunner, 1999). Reviews of models for nonlinear chromatography are provided by Guiochon et al. (2002, 2003,

and 2006) and by Jungbauer and Kaltenbrunner (1999). Some of the more commonly used models are summarised in Table 1.4.

## **1.5. Microscale Bioprocess Development**

Conventional bioprocess development involves performing early development and optimisation experiments at the laboratory scale with milligram-to-gram quantities and millilitre-to-litre volumes. This is followed by increasing the scale to pilot and production scales. Traditionally, this process has been slow and resource intensive. Furthermore, it does not always lead to the most robust process since the parameter space cannot be fully explored. Microscale and ultra scale-down techniques (Titchener-Hooker et al., 2008) enable a platform for next-generation bioprocess development that decreases cycle times while increasing process understanding.

### *1.5.1. Terminology*

Microscale bioprocess methods are defined here as techniques for bioprocess study carried out with microlitre-to-low-millilitre volumes (i.e. <10 mL). The term *microscale* is often associated in the literature with microfluidic separations. In this thesis, the term has been broadened to also include microwell formats since they too are carried out with microlitre volumes. Another term that is sometimes used interchangeably with microscale when referring to bioprocess techniques is *ultra scale-down*. However, this is a slightly different term that refers to the significant scale-down of a bioprocess unit operation or some feature of that operation, often with the goal being to directly simulate a critical parameter of the operation (e.g. shear during centrifugation). These techniques may use volumes that range from microscale volumes to 100s of millilitres. Finally, the term *high-throughput process development* is sometimes used synonymously with microscale or ultra scale-down methods, although this is not always the case. This term refers specifically to methods that can be carried out with a high degree of experimental parallelisation and usually with automation, such as experiments carried out in 96-well microtitre plates. Many microscale bioprocess techniques are indeed high throughput, but this need not necessarily be the case.

**Table 1.4.** Models of non-linear chromatography (as reviewed by Guiochon et al., 2002).

<b>Model</b>	<b>Description</b>	<b>Assumptions / Considerations</b>
<b>Ideal (Equilibrium)</b>	Band profile depends only on the equilibrium thermodynamics. Other sources of mass transfer resistance and axial dispersion are neglected.	Assumes column has infinite efficiency.
<b>Equilibrium-Dispersive</b>	Accounts for axial dispersion and relates it to column HETP but treats column efficiency as only a small correction.	Assumes mass transfer is infinitely fast. Less useful for the chromatography of proteins.
<b>Lumped Kinetic</b>	A simplistic model for mass transfer kinetics in which the local deviation from equilibrium is taken into account. Completes the mass balance of the ideal model by a kinetic equation (e.g. a linear driving force equation).	Valid for fast kinetic rates but there can be considerable model error at slow mass transfer rates.
<b>General Rate</b>	Attempts to simultaneously deal with all sources of mass transfer resistance and axial dispersion by including their contributions in a system of partial differential equations for mass conservation and transport. Two mass balance equations are written, one for the stagnant mobile phase inside the particle and one for the flowing mobile phase outside the particle.	Many variations of this model. Surface diffusion and the rate of adsorption-desorption are sometimes neglected.
<b>Lumped Pore</b>	Simplified version (an approximation model) of the general rate model.	Assumes the kinetics of adsorption-desorption is negligible. Less accurate than the general rate model but useful for moderately fast mass transfer kinetics.

### *1.5.2. Goals of Microscale Bioprocessing Techniques*

The goal in implementing a microscale bioprocess technique is to gain quantitative bioprocess information in an efficient manner and with small quantities of material. This can mean either directly mimicking some aspect of larger scale performance, often with the use of scale-down models or empirical correlation factors, or screening parameters in a relative manner to guide subsequent larger-scale development. Examples of the former are the use of a high-speed rotating-disc device to mimic the shear stresses on cell suspensions in the feed zone of an industrial centrifuge (Hutchinson et al., 2006) or the use of small-scale columns to predict large-scale elution profiles (Hutchinson et al., 2009). An example of the latter is the use of microwell screening platforms for the optimisation of mobile phase conditions in chromatographic processes (see review by Chhatre and Titchener-Hooker, 2009).

While the goal of these techniques is that they be predictive of some facet of large-scale performance, a perfect scale-down model can be difficult to achieve and validate in practice. A more modest but equally effective goal is to perform high-throughput microscale screening experiments to explore aspects of the design space and thereby inform subsequent laboratory-scale development. Then, only a small subset of focused optimisation experiments is required at the laboratory scale, where scale-up effects to pilot and manufacturing scales are well understood. Such an approach is outlined in Figure 1.6. A large amount of content about the operating space can be rapidly acquired from microscale experiments, and since only small amounts of material are required, these experiments can be done very early on in process development. A good example of this is the high-throughput evaluation of chromatographic adsorbents and mobile phase conditions in microwells (Coffman et al., 2008). Although these techniques are batch methods that differ substantially in their operation from fixed-bed chromatography, they are useful for comparing adsorbent properties and selecting mobile phase conditions. Ultimately though, it is advantageous to have validated scale-down models also within one's 'microscale toolbox'. This balance between high throughput screening methods and validated scale-down techniques is explored within this thesis, particularly as it relates to chromatography.

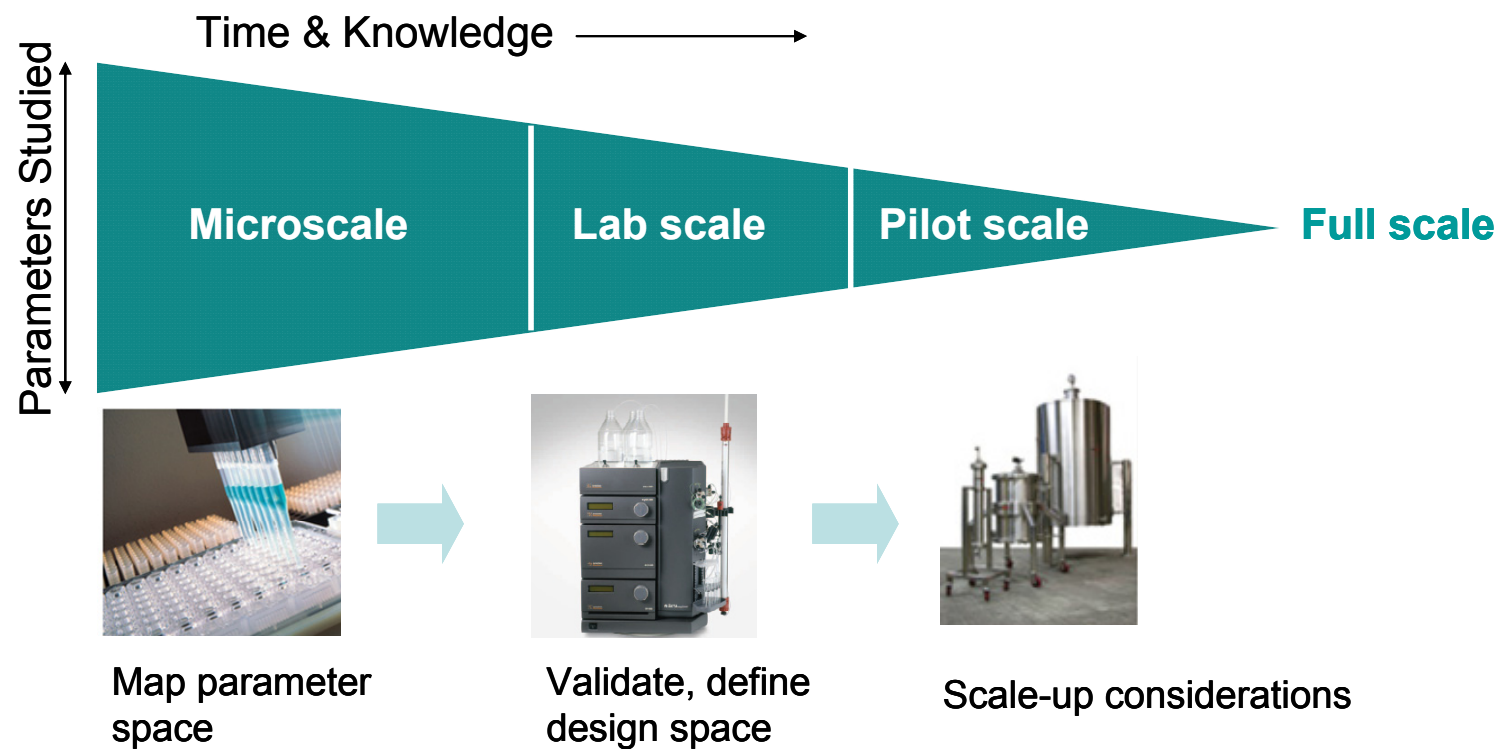


**Figure 1.6.** Integration of microscale experiments into the process development workflow. Microscale experiments can be carried out with higher throughput and therefore used to systematically map the parameter space. This increases process understanding during scale-up and reduces the number of laboratory-scale experiments that are required.

### *1.5.3. Techniques for Cell Culture and Fermentation*

Cell culture and fermentation development involves media development, strain improvement, and process optimisation of operating conditions such as mixing, oxygen transfer, pH, and temperature. Development of these processes can be time-consuming and complex, requiring the optimisation of many parameters. Therefore, microscale techniques can be advantageous for accelerating development and promoting a quality-by-design strategy. Comprehensive reviews of microwell platforms, microfluidic devices, and miniature bioreactors for cell culture and fermentation are provided by Betts and Baganz (2006), Micheletti and Lye (2006), and Marques et al. (2009).

Traditionally, cell culture and fermentation development is initially done in shaken flasks and then, later, performed in laboratory-scale bioreactors. However, the results between the two formats often are not always reproducible because of differences in mass transfer (aeration and gas exchange) and operating control. In a similar manner, microscale systems suffer from these differences in scale and format. Specific challenges with microwell systems include the addition and removal of liquids to/from the microwells, evaporation, operating control, and mixing. Mixing is especially critical for the addition of small volumes of liquid and for gas-liquid mass transfer, and it can consequently impact the overall reproducibility of the method. A number of researchers have studied the specific case of mixing in microwells, including Hermann et al. (2003) and Nealon et al. (2006). Ultimately, a complete understanding of the phenomena that occurs in shaken microwells is critical to the ability of these systems to predict larger bioreactor systems (Micheletti et al., 2006; Marques et al., 2009).

Miniature bioreactors enable a path to scale-down in which in-process monitoring, gas transfer, and control of key process variables can better match those of large-scale bioreactors. Indeed, approaches with microscale bioreactors at the millilitre scale have proven to be reasonably predictive of larger scale operation, although this has not necessarily been the case for smaller microfluidic devices, presumably because of mass transfer differences (Marques et al., 2009). Key advances contributing to the success of miniature bioreactors and microfluidic devices are: (1) the development of miniaturised sensors for dissolved oxygen, pressure, and pH; (2)

the ability to measure optical density during shaking; and (3) improvements in microfabrication techniques and robotics (Marques et al., 2009). One drawback of bioreactors is that they generally do not offer the same degree of parallelisation and automation as microwell systems and microfluidic devices, although they can potentially be interfaced with liquid-handling robots.

#### *1.5.4. Techniques for Cell Disruption*

Small-scale techniques for cell disruption may be developed with different objectives in mind. One goal for having a microscale cell disruption technique is to predict and optimise large-scale operation. Examples of this come from Varga et al. (1988) in which an ultra scale-down approach was used to obtain basic model parameters in the study of high-pressure homogenisation and from Chan et al. (2006) in which a small capillary device was used to study the effects of shear, time, and impact velocity on *E. coli* cell disruption. A second goal is for the quantitative release of intracellular protein product for subsequent assay or purification, with the final purpose being to evaluate fermentation performance and/or recover purified sample for product characterisation. Finally, a third goal is to generate small amounts of a representative feedstock for downstream process studies such as chromatographic development. For these latter two goals, the cell disruption technique need not actually mimic the large-scale operation. This was the case in this thesis, in which a microscale cell disruption technique was used to generate representative feed material for downstream microscale chromatography experiments (Chapter 7).

A number of possibilities exist for small-scale cell disruption, although many cannot match the effectiveness of large-scale mechanical methods such as high-pressure homogenisation, especially for hard-to-break cells like yeast. Bench-top homogenisers are available for 10s of millilitre-scale experiments but are generally not practical for volumes <10 mL. For microscale volumes, glass beads can be used in which the cell slurry is vortexed with multiple on-off cycles. Sonic or ultrasonic disruption can also be used (Davies, 1959; Clarke and Hill, 1970; Doulah, 1977; Feliu et al., 1998; Kapucu et al., 2000; Ho et al., 2006), although its use with yeast is somewhat limited due to the rigidity of the cell wall. In addition, a new-generation ultrasonication device known as Adaptive Focused Acoustics (Laugharn and

Garrison, 2004) has recently emerged for cell disruption. It is described further in Chapter 7.

Non-mechanical approaches may involve physical disruption, the addition of chemical agents, and/or enzymatic degradation. Physical methods include osmotic shock, in which osmotic stress is created by placing the cells in a hypotonic or hypertonic solution, and freeze-thawing, in which ice crystals that form during the freezing step mechanically disrupt the integrity of the cell wall or membrane (Garcia, 1999; Indge, 1968). However, these methods are relatively inefficient for cells having a rigid cell wall and act primarily on the cell membrane. Therefore, they often are combined with enzymatic or chemical methods. Chemical disruption methods involve adding reagents such as chelators, chaotropes, detergents, reducing agents, organic solvents, acids and/or bases (Kula and Schutte, 1987; Garcia, 1999). In addition, commercial reagents such as YeastBuster and BugBuster from Novagen (Gibbstown, NJ USA) are available for yeast and bacterial cells, respectively. Finally, enzymatic methods are sometimes used for microbial cells (Asenjo and Andrews, 1990), in which lytic enzymes act on the cell wall. These lytic enzymes may be used alone or in combination with physical or chemical methods, and they offer the advantage of providing a more selective lysis.

#### *1.5.5. Techniques for Primary Recovery*

A number of ultra scale-down methods have been developed for the study of industrial centrifugation. Hutchinson and colleagues (2006) used a high-speed rotating device to mimic the effect of shear stress on the cells in the feed zone of an industrial-scale continuous centrifuge. These data were then used in combination with laboratory-scale test tube centrifuge studies to successfully predict the performance in the large-scale centrifuge. Similar types of studies were done to define the relationship between flocculation and disc-stack centrifugation (Berrill et al., 2008), the centrifugal separation of high density cultures of *E. coli* and *S. cerevisiae* (Tustian et al., 2007), and shear damage of plasmid DNA in pump and centrifuge operations (Zhang et al., 2007). In addition to centrifugation, ultra scale-down methods have been demonstrated for expanded-bed chromatography (Willoughby et al., 2004), continuous filtration in solid-liquid separations (Reynolds et al., 2003), and microwell refolding experiments of denatured protein in inclusion

bodies (Mannall et al., 2008). Jackson and co-workers (2006) used filter plates to quantitatively study the microfiltration of *E. coli* fermentation broth, finding that custom plates showed less variability than commercially available filter plates and allowed multiple membrane types to be examined.

#### *1.5.6. Techniques for Chromatography*

Conventional small-scale and ultra scale-down approaches to preparative chromatography development have centred on using either self-packed or commercially pre-packed columns (e.g. HiTrap columns from GE Healthcare) of  $\leq 10$  mL. In one example, Hutchinson et al. (2009) used a 1-mL protein A column in combination with an empirical correction factor to predict the elution profile of an 18.3-L pilot-scale column. To automate and improve the throughput of small-scale column experiments, integrated chromatography systems have been used (Londo et al., 1998; Bhikhabhai et al., 2005; Stromberg et al., 2005; Bannister et al., 2006), as have HPLC systems (Nti-Gyabaah et al., 2009), although some chromatographic media cannot withstand the high backpressures of HPLC. Most of the off-the-shelf instruments (such as the GE Healthcare AKTA purifier system or an HPLC system) are usually operated in a serial manner or they require custom modification for parallel operation. Furthermore, even at low-millilitre column volumes, milligram quantities of sample mass may be required.

Microscale chromatographic techniques for bioprocess study often can deviate considerably in scale and format from laboratory-scale fixed-bed chromatography. Some of the more novel microscale techniques include microfluidic packed-bed systems (Shapiro et al., 2009) and the use of biochip arrays carrying chromatographic functional groups in combination with surface-enhanced laser desorption-ionisation mass spectrometry (Weinberger et al., 2002; Brenac et al., 2005). However, the more commonly used microscale chromatographic formats are those carried out in a 96-well microtitre plate format because of their high degree of experimental parallelisation and the capability for automation on liquid-handling robots. Three of these formats are reviewed by Chhatre and Titchener-Hooker (2009): (1) micro-batch adsorption, in which the sorbent is statically mixed within a microwell; (2) micro-tip columns, in which the sorbent is immobilised at the bottom of a pipette tip; and (3) miniature packed columns that are arrayed in a 96-well

format. These formats are described schematically in Figure 1.7, and a side-by-side comparison is provided in Table 1.5. Each format presents different theoretical and practical considerations for chromatographic study, as described below.

#### 1.5.6.1. Micro-Batch Adsorption

The most established of the three microtitre-plate formats is micro-batch adsorption, having been demonstrated by a number of research groups for parameter estimation and the rapid screening of process chromatographic conditions (Thiemann et al., 2004; Bensch et al., 2005; Charlton et al., 2006; Rege et al., 2006; Rios et al., 2007; Bergander et al., 2008; Coffman et al., 2008; Kelley, et al., 2008B; Kramarczyk et al., 2008; Wensel et al., 2008; Chhatre and Titchener-Hooker, 2009) as well as for the high throughput chromatographic purification of fusion proteins for functional and structural analysis (Nguyen et al., 2004; Prinz et al., 2004; Redaelli et al., 2005). Micro-batch adsorption is rooted in the well-established batch-binding methodology carried out at millilitre scales in test tubes, differing in its scale, vessel geometry, mixing mechanism, amenability to robotic automation, and throughput potential. In this format, microlitre volumes of adsorbent, typically 100  $\mu\text{L}$  or lower, are suspended in a liquid phase (feed sample or purification buffer) within the wells of a microtitre plate, thereby mimicking an agitated-tank batch system. The sample and buffer volumes depend on the specific requirements of the experiment, with the maximum volume defined by the microwell volume capacity (typically ranging from 300 – 2000  $\mu\text{L}$ /well, depending on the plate type). The liquid supernatant is then separated from the adsorbent after an experimentally defined incubation time for subsequent analysis (e.g. UV absorbance measurement, protein assay, or purity analysis). Although standard microtitre plates have been used for micro-batch adsorption (Thiemann et al., 2004; Rege et al., 2006), in which the adsorbent is sedimented and the resulting supernatant then aspirated away, filter plates are more commonly used since they allow for a highly efficient separation. With filter plates, liquid is drawn through the filter by centrifugation or vacuum and collected in a microtitre plate underneath (Fig. 1.7A), with centrifugation preferred over vacuum filtration since cross-mixing of individual well contents has been observed with vacuum filtration (Coffman et al., 2008). One disadvantage of filter plates is that there may be some leakage of solution during long incubation times, requiring the plates to be sealed on their underside (Coffman et al., 2008).

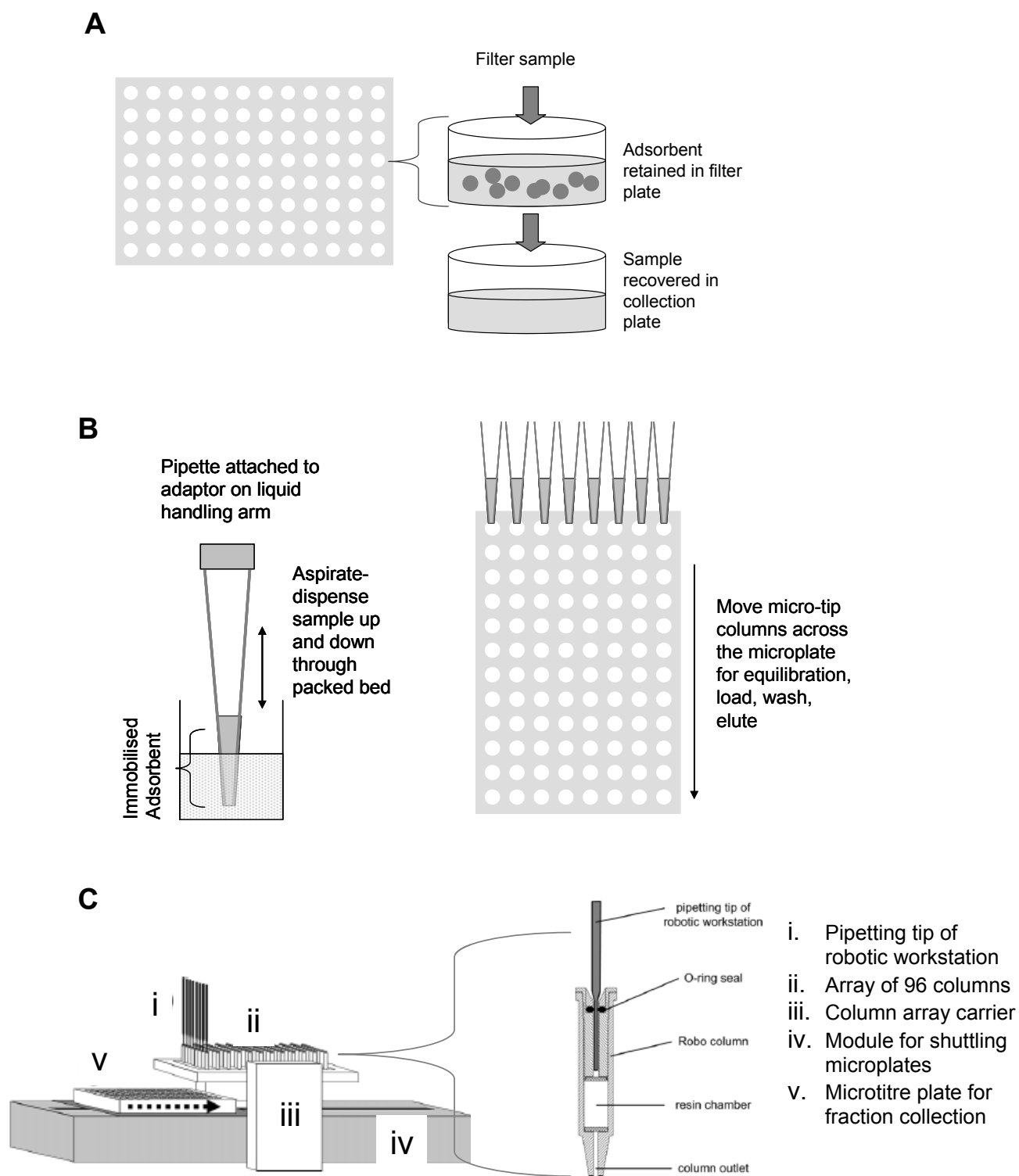


**Figure 1.7.** Schematic representation of three formats for carrying out chromatography in a microtitre plate configuration. (A) micro-batch adsorption, (B) micro-tip columns, (C) miniature columns. Schematics are not to scale. Illustrations for the miniature column format adapted from Wiendahl et al., 2008.

**Table 1.5.** Comparison of three microtitre-plate formats for microscale chromatography. Details are given for use on a Tecan robot.

	Micro-Batch Adsorption	Micro-Tip Column	Miniature Column
<b>Description</b>	Mixed suspension of media in microtitre filter plate	Immobilised adsorbent at the bottom of a pipette tip; Attaches on to liquid-handling arm	Microlitre-scale column that interfaces with the pipette tip of a liquid-handling robot
<b>Scale (adsorbent volume)</b>	2-200 $\mu$ L	5 - 80 $\mu$ L 0.5 to 1.2-cm bed heights	50 - 600 $\mu$ L 0.25 to 1.0-cm bed heights
<b>Chromatography</b>	Batch, static mixing	Batch, dynamic flow	Column, dynamic
<b>Sample presentation</b>	Batch vessel <i>Plate shaking or mixing</i>	Pressure-driven flow <i>Bi-directional flow (aspiration, dispense)</i>	Pressure-driven flow <i>Unidirectional flow</i>
<b>Elution</b>	Serial step elution	Serial step elution	Serial step elution
<b>Parallelisation</b>	96	8, 12, or 96	8
<b>Set-up</b>	User prepared or purchased (GE Healthcare)	Purchased: preparation outsourced (PhyNexus)	Purchased: preparation outsourced (Atoll)
<b>Relative Cost</b>	£-££	£££	££££
<b>Full Automation</b>	Complexity: +++++ <i>Requires adsorbent manipulation and frequent plate transfer. Well-suited for semi-automated or manual operation.</i>	Complexity: + <i>No adsorbent manipulation and minimal plate movement. Drops from system liquid (water) can be problematic.</i>	Complexity: +++ <i>No adsorbent manipulation but some plate movement required. Requires specialised carriers.</i>
<b>Key Operational Considerations</b>	Dispensing and mixing of adsorbent; Filtration efficiency; Incubation time; Evaporation; Hold-up volume	Flow rate; Incubation time (cycle number); Air bubbles; Evaporation; Hold-up volume	Flow rate (residence time); Reproducible fraction collection; Plate shuttling; Wall effects
<b>Kinetic Studies</b>	Stirred tank: finite bath adsorption	Finite bath adsorption or shallow bed	Fixed-bed column

Each stage of the chromatographic purification in micro-batch adsorption, i.e. equilibration, load, wash, and elution, is performed sequentially within a microwell, with each individual stage involving the addition of liquid (sample or buffer solution), mixing of the resin with the liquid, and then removal of the liquid, as described above. Multiple processing steps may be carried out within a particular stage, e.g. multiple additions of wash or elution buffer. Continuous linear gradient elution is not possible with this format, although the elution can be carried out as a series of incremental elution steps (a so-called 'staircase elution') creating a virtual linear gradient (see examples by Rege et al., 2006 and Kramarczyk et al., 2008).

Several key operating parameters must be considered when performing micro-batch adsorption. Among the more important are resin handling (dispensing and mixing), microwell liquid hold-up volume, kinetics of adsorption and desorption, filter membrane material type and pore size, and sample evaporation. With respect to resin handling, the accurate and precise dispensing of resin to each microwell is critical so as to minimise experimental error and variability. The most common method is to pipette a resin slurry from a reservoir to each microwell, with the accuracy and precision of the operation depending on the determination of slurry concentration, how well the slurry is suspended during aliquotting, and the pipetting accuracy. Coffman et al. (2008) evaluated the accuracy and precision of resin pipetting using a Tecan robot and found the aliquotted volume to be systematically 4% higher on average, but within the specifications of the robot, and that the standard deviation was less than 1% of the total volume. An alternative to resin pipetting is to employ a plaque-generating device (Herrmann et al., 2006), in which resin cylinders are formed by adding a resin slurry to a machined vacuum manifold and filtering the liquid away. Such devices have been commercialised for resin plaques of 8, 21, and 51  $\mu\text{L}$  by Atoll GmbH (Weingarten, Germany; MediaScout ResiQuot). Furthermore, some resin manufacturers sell pre-dispensed resin filter plates, such as GE Healthcare (Uppsala, Sweden; PreDictor plates), with resin volumes ranging from 2 - 50  $\mu\text{L}$ /well.

Once dispensed, the thorough mixing of the liquid-resin suspension in the microwell is critical for representative and reproducible adsorption/desorption processes. End-over-end rotation, which is traditionally used for tube-based methods, is not suitable

for microtitre plates and robotic automation. Therefore, orbital shaking is typically performed since it can be automated and is a low-shear method (Bensch et al., 2005), with agitation rates exceeding 1000 rpm generally required to ensure complete resin mixing (Bensch et al., 2005; Bergander et al., 2008; Coffman et al., 2008).

In addition to robust resin handling, the incubation time (resin-liquid contact time) of the processing step must be carefully considered in micro-batch adsorption experiments. While the kinetics of desorption and buffer exchange are relatively rapid, occurring on the order of minutes, protein uptake at high mass adsorbent loadings may take on the order of hours to achieve equilibrium, with the specific duration depending on the adsorbent and sample characteristics (i.e. mass transport properties). Furthermore, the exact loading times will be defined by the experimental purpose. When performing adsorption isotherm studies, longer incubation times are used to achieve equilibrium, whereas in batch uptake experiments, the incubation time is varied from a few minutes to several hours (Bensch et al., 2005; Bergander et al., 2008; Coffman et al., 2008). For a qualitative estimation of column dynamic binding capacity in high throughput screening studies, Bergander et al. (2008) suggest that the micro-batch adsorption loading time be matched on a timescale that approximates the column loading time (total time the column is exposed to feed solution) instead of the column residence time (amount of time an inert solute will spend in the column). However, these researchers caution that this rule holds only as long as intra-particle diffusion and not film mass transfer is rate determining. Coffman et al. (2008) chose an incubation time of 20 minutes in their high throughput chromatographic screening studies as a time that was sufficient to achieve > 80% of equilibrium binding and thereby provide an approximate representation of column dynamic binding capacity.

Finally, another key consideration in micro-batch adsorption is the liquid hold-up volume, especially when working at low phase ratios (ratio of liquid volume to adsorbent volume). The hold-up volume may result in carryover between processing steps and, if not accounted for, will lead to the incorrect calculation of mass balance and the inaccurate optimisation of mobile phase conditions. The resin intra-particle pore volume ( $\varepsilon_p$ ), any interstitial liquid not fully evacuated, and liquid retained on the membrane or plate all contribute to the hold-up volume. Microwell hold-up volumes

are estimated to range from 50-80% of the resin volume (Coffman et al., 2008; GE Healthcare, bulletin 28-9403-58AA).

Advantages of micro-batch adsorption are that it is relatively inexpensive and offers a high degree of experimental parallelisation and flexibility, with sorbent type and amount, sample load, and solution conditions all easily varied per well. One disadvantage, though, is that unlike the multiple stages of separation in column chromatography, each step in micro-batch adsorption represents only a single stage of equilibrium. Nevertheless, micro-batch adsorption experiments can provide a wealth of information for the development of a process chromatography step. As with conventional batch-binding methods carried out in test tubes, fundamental thermodynamic and kinetic information are acquired through adsorption isotherm and batch uptake studies, as reviewed by Bensch et al. (2005). These data can be used in batch mass transport models to determine the effective pore diffusivity ( $D_e$ ) and ultimately in column models to predict column behaviour, as described by Arve and Liapis (1987) and Bergander et al. (2008).

Even in the absence of modelling, batch-binding data can be used to inform the development of chromatography steps by indicating relative trends in adsorbent capacity, recovery, selectivity and product purity under different solution conditions and for different chromatographic media. In a series of four publications (Coffman et al., 2008; Kelley, et al., 2008B; Kramarczyk et al., 2008; Wensel et al., 2008), Coffman and colleagues describe the use of micro-batch adsorption for screening different adsorbent classes and mobile phase conditions for monoclonal antibody purification, including hydrophobic interaction chromatography (Kramarczyk et al., 2008), ceramic hydroxyapatite (Wensel et al., 2008), and ion-exchange chromatography (Kelley et al., 2008B). These researchers employed a parameter known as the partition coefficient ( $K_p$ ), derived from a low mass loading (5 mg/mL resin), to quantify antibody and/or impurity binding.  $K_p$  is defined as:

$$K_p = \frac{q}{C} \quad \text{Equation 1.20}$$

where  $q$  is the adsorbent loading (mg protein/mL of resin) at a low mass challenge and  $C$  is the concentration of unbound protein (mg/mL) remaining in the supernatant after binding. In their investigation, the value of  $K_p$  was well correlated with the

adsorbent maximum capacity ( $q_m$ ) for the hydroxyapatite and ion-exchange studies, and although the batch binding results were not identical to those of the column chromatography, it did allow for the trending of purity and recovery with adsorbent type and mobile phase condition. Similarly, Rege et al. (2006) developed a two-step chromatographic purification using micro-batch adsorption in which the microscale elution conditions trended well with the final conditions defined for the column operation.

In all of the micro-batch adsorption studies described above, the experiments were performed either manually or in a semi-automated fashion, in which many of the liquid-handling steps were automated, but not the plate manipulations (i.e. movement in and out of the centrifuge). Indeed, the format is well suited for manual and semi-automated operation; yet, full walk-away automation is ultimately desired to minimise labour and enable overnight experiments. Full walk-away automation is defined here as a method requiring no manual intervention throughout its operation except for the initial set-up and final clean-up. In principle, full automation is achievable with micro-batch adsorption since it is a plate-based format. However, in practice, this can be difficult to achieve, at least in a robust manner, because of the frequent plate manipulations in and out of the filtration device and the requirement for accurate and precise resin manipulation. As a rule of thumb, the robustness of an automated method decreases with increasing plate manipulation, since the probability of an error occurring will increase proportionally.

#### 1.5.6.2. Micro-Tip Chromatography

The micro-tip column platform (Chapman, 2005; Smith, 2005; Shukla et al, 2007B; Wenger et al., 2007; Gjerde and Hanna, 2009; Chhatre and Titchener-Hooker, 2009) is a relatively new technique, with considerably fewer literature examples than micro-batch adsorption. It is therefore the primary subject of this thesis, with a detailed description of the format given in Chapter 3. Briefly, it is a method in which the sorbent (in microlitre quantities) is immobilised at the bottom of a pipette tip. Sample or mobile phase is pipetted bi-directionally (up, down) through the column, typically with multiple aspiration and dispense cycles to increase the loading time. The micro-tip columns are picked up by the liquid-handling arm of the robot and moved across the microtitre plate, with a new microwell used for each separation

stage (i.e. equilibration, load, wash, and elution), as shown in Figure 1.7B. The extent of experimental parallelisation of this format depends on the configuration of the liquid-handling arm, with 8, 12, or 96 channels available. It was carried out eight-at-a-time on a Tecan workstation (Research Triangle, NC, USA) in this thesis.

Because micro-tip chromatography is a batch operation, there is only one theoretical plate of separation achieved per microwell stage, as with micro-batch adsorption. The principal chromatographic difference between the micro-tip and micro-batch adsorption formats has to do with the external mass transport. Extra-particle mass transport occurs by flow through a packed bed in the case of micro-tip chromatography, whereas micro-batch adsorption involves static mixing of a resin suspension. This can be particularly relevant if external mass transport is the dominant mass transport mechanism in protein uptake or for adsorbent lifetime studies where bead fouling may be influenced by the flow outside of the chromatographic bead. In addition, having hydrodynamic flow allows the micro-tip columns to be operated in a shallow-bed format (Hahn et al., 2005A and 2005B), in which sample is re-circulated through a very small chromatographic bed at high flow rates while maintaining a constant feed concentration (infinite-bath approach). Alternatively, micro-tip columns may be operated in a more conventional finite-bath format similar to micro-batch adsorption. These different modes of operation are explored in Chapter 4.

Micro-tip chromatography also affords some significant operational advantages over micro-batch adsorption, especially with respect to automation. Specifically, with micro-tip chromatography there is no concern about sorbent mixing, since there is hydrodynamic flow through a packed bed instead of static mixing of suspended resin. This is particularly beneficial for dense media, such as ceramic hydroxyapatite, which can be difficult to suspend uniformly in batch microwell experiments. In addition, there are few or no plate manipulations (i.e. movement in and out of a filtration device), greatly simplifying the automation and providing a simple path to full walk-away automation, even for groups with limited automation skill sets. These operational advantages combined with the external mass transport properties of micro-tip chromatography provided the motivation for its use in this thesis.

#### 1.5.6.3. Miniature Column Chromatography

Of the three microtitre plate formats, the miniature (mini)-column format (Wierling et al., 2007; Wiendahl et al., 2008) is the most like a fixed-bed laboratory-scale column in its geometry and operation. The supplier of mini-columns is Atoll GmbH (Weingarten, Germany), which sells pre-packed columns arrayed in a microtitre-plate footprint for use on a Tecan workstation (RoboColumn), with bed volumes of 50, 100, 200, or 600  $\mu\text{L}$  available. The column design and experimental set-up is shown in Figure 1.7C. Sample or mobile phase is pipetted through the column by inserting the fixed pipette tip of the Tecan (Research Triangle, NC, USA) robot into a needle adapter at the inlet of the column, thereby forming a primary seal around the tip. A specially designed carrier (TeChrom) holds the mini-columns, under which a microplate is positioned to collect column fractions by incrementally stepping a microplate under the mini-columns. Alternatively, this format can be performed manually using a column that accepts a manual pipette (PipetColumn) or in a centrifuge (CentriColumn).

A primary advantage of the mini-column format is that it closely mimics a conventional packed-bed format with hydrodynamic flow, and unlike the micro-tip format, it is operated with unidirectional flow and has a cylindrical geometry. This provides a better representation of column chromatography and allows column performance to be examined more directly, although column models or engineering correction factors may still be required for accurate prediction of larger scale columns. An additional benefit over the other two microwell formats is that larger sample volumes ( $> 1\text{ mL}$ ) are more easily loaded, since it means simply dispensing multiple aliquots of sample or buffer through the column. (Micro-batch adsorption is limited by the microwell volume, while micro-tip chromatography is limited by the pipette tip volume). This is particularly advantageous for low-concentration samples, where high volumetric loads are required. However, the mini-column format is not without some important challenges. One limitation is that the bed height is very short, thereby resulting in very short residence times. For example, the superficial residence time for a 200- $\mu\text{L}$  column (5 mm, *i.d.*, X 10 mm, *h*) operated at a flow rate of 3.33  $\mu\text{L/s}$  (60 cm/h) is only 60 s. Furthermore, continuous linear gradients are not feasible, at least not without custom modification of the liquid-handling workstation, as with the other microscale formats. In addition, because of

the low-volume operation, the reproducibility of fraction collection must be examined. Finally, the effects of the smaller column diameter (i.e. wall effects) must be considered in the prediction of large-scale column performance, especially with respect to dynamic binding capacity.

Wiendahl et al. (2008) used 200- $\mu$ L mini-columns on a Tecan workstation for the determination of column dynamic binding capacity and for elution experiments in the separation of protein mixtures. Breakthrough experiments were performed with 9 or 1.5 mg/mL of bovine serum albumin (BSA) on four different anion exchange adsorbents, with flow rates ranging from 0.21  $\mu$ L/s (residence time of 16 min) using a 250- $\mu$ L syringe to 1000  $\mu$ L/s (residence time of 0.2 s) using a 1000- $\mu$ L syringe. With this test system, these researchers were able to predict DBC<sub>10%</sub> and DBC<sub>50%</sub> values that differed by less than 30% of literature values, except for POROS adsorbent at the high concentration loading (>45% deviation). Despite this agreement, the breakthrough curves appear jagged by visual inspection, and a comparison of these curves to those of conventional laboratory-scale columns is not shown. Elution experiments were also performed with ion-exchange chromatography using several test protein mixtures. Again, this format displayed some promising results, with the elution profiles approximating those at the 1-mL or 2-mL scale, but with some differences observed. Although this microscale platform shows potential, more work is required, ideally with 'real-world' protein systems, to fully characterise the format and to better understand its advantages and limitations.

With respect to robotic automation, the mini-column format can be fully automated on a robotic workstation, as demonstrated by Wiendahl et al. (2008). However, full automation requires some relatively complex robotic scripts to be written, and with more plate manipulation than in micro-tip chromatography. Furthermore, several specialised equipment peripherals are required as described above, including the TeChrom carrier and a plate shuttle (TeLink) for fraction collection. However, as with micro-tip chromatography, a clear advantage is that no resin manipulation is required. One limitation of the format is that the extent of parallelisation depends on the configuration of the liquid-handling arm, currently limited to eight on the Tecan workstation.

### 1.5.7. Workflow for High-Throughput Microscale Experiments

#### 1.5.7.1. Experimental Design

High-throughput microscale techniques enable experiments to be carried out in a brute-force manner, with many conditions examined in parallel. This is useful for multivariate systems and when there is little or no *a priori* knowledge. Brute-force experimental designs have been demonstrated for adsorbent screening, parameter estimation, and mobile phase optimisation (Thiemann et al., 2004; Rege et al., 2006; Coffman et al., 2008; Kelley et al., 2008; Kramarczyk et al., 2008; Wensel et al., 2008). More sophisticated factorial and response surface designs (Mandenius and Brundin, 2008) offer a means of reducing large experimental numbers by allowing multiple variables to be examined simultaneously. However, these designs are assisted by having some *a priori* knowledge about the system in order to narrow the parameter range. In the absence of this information, iterative workflows like the one in Figure 1.8 can be used to improve the experimental efficiency, in which the design of one experimental iteration is aided by the results from the previous one. This permits a broad parameter space to be quickly narrowed and refined around an optimum. Even brute-force approaches can benefit from an iterative workflow, especially if experimental numbers become overwhelmingly large. Other more sophisticated iterative schemes for process optimisation such as simplex and genetic algorithms have also been applied for even greater experimental efficiency (Park et al., 1997; Milavec et al., 2002). In choosing a design, the intent of the experiment must be considered. If it is to fully characterise a wide operating window or for parameter estimation, then a brute-force approach may be chosen. In contrast, if it is to quickly identify a window of optimum performance, then an iterative approach may be preferred.

#### 1.5.7.2. High-Throughput Analytics

While microscale techniques are enabling tools for high throughput process development, having a well-coordinated analytical strategy is also critical so as to not risk overwhelming testing and data processing resources. The analytical strategy must be capable of handling high sample numbers and low microlitre sample volumes. One solution is to automate pre-treatment and assay steps onto a liquid-



**Figure 1.8.** Iterative experimental design for high-throughput microscale experiments.

handling robot. When implementing an automated assay strategy, though, one should consider not only the hardware but also the data processing workflow in order to avoid bottlenecks in data reduction. In addition to assay automation, a number of new analytical platforms have emerged which offer simplicity and/or higher analytical throughput for process monitoring. Examples of these include SELDI-TOF mass spectrometry (Freire et al., 2006), optical biosensors (Abdiche et al., 2008), and microfluidic separations (Ohno et al., 2008).

## **1.6. Organisation of Thesis**

This thesis seeks to fully characterise the micro-tip platform and demonstrate its use as a component of an accelerated process development strategy. The materials and methods used throughout this thesis are provided in Chapter 2. The specific details for micro-tip column operation and automation are then described in Chapter 3, with the critical operating parameters and flow properties of micro-tip chromatography defined. In Chapter 4, procedures for performing adsorption isotherms and kinetic uptake studies are demonstrated, along with two data-driven models for predicting dynamic binding capacity from micro-tip column data.

Micro-tip chromatography, as a tool for accelerated process development, is then applied to two different process development challenges. In Chapter 5, a workflow employing micro-tip chromatography is demonstrated for the rapid development of a mixed-mode chromatography step in the purification of a monoclonal antibody. In Chapter 6, a two-step chromatographic purification of virus-like particles (VLPs) is developed to provide feedback on upstream yeast fermentation development. However, with the miniaturisation of the VLP chromatographic purification then comes the need to develop a microscale cell disruption technique, since the laboratory-scale cell disruption method requires tens to hundreds of millilitres of cell slurry and is relatively low throughput. A microscale yeast cell disruption technique using Adaptive Focused Acoustics is therefore developed in Chapter 7 to enhance the throughput of the microscale VLP purification and reduce the cell weight input. Finally, in Chapter 8, the conclusions of this thesis and recommendations for future work are presented.

## **2. MATERIALS AND METHODS**

### **2.1. Materials**

#### *2.1.1. Chromatographic Separation Media*

POROS 50 HS cation exchange resin was purchased from Applied Biosystems (Foster City, CA, USA). Ceramic hydroxyapatite (CHT) and UNOsphere S were obtained from Bio-Rad (Hercules, CA, USA). SP Sepharose FF, Q Sepharose FF, MabSelect, and Capto MMC were obtained from GE Healthcare (Uppsala, Sweden). The properties of these adsorbents are described in Table 2.1. One-millilitre cartridge columns containing UNOsphere S and Capto MMC were obtained from Bio-Rad and GE Healthcare, respectively.

#### *2.1.2. Purification Reagents*

Sodium phosphate (monobasic and dibasic), sodium acetate, sodium chloride, sodium sulphate, ammonium sulphate, ammonium chloride, and methanol were purchased from Fisher Scientific (Pittsburgh, PA, USA); HEPES, MOPS, and MES buffers were obtained from Sigma-Aldrich (St. Louis, MO, USA). The nuclease Benzonase was purchased from EMD Chemicals, Inc. (Gibbstown, NJ, USA). The yeast cell wall lytic enzyme Quantazyme ylg ( $\beta$ 1,3-glucanase) was obtained from MP Biomedicals (Solon, OH, USA).

### **2.2. Protein Test Systems**

#### *2.2.1. Human Papillomavirus (HPV) Virus-like Particles (VLPs)*

Yeast cell paste containing recombinant human papillomavirus (HPV) virus-like particles (VLPs) was provided for use in this thesis by the Bioprocess R&D group at Merck & Co., Inc. (West Point, PA, USA). Specifically, the HPV VLPs were cloned and expressed in *Saccharomyces cerevisiae* as described by Hofmann et al. (1995 and 1996), Neeper et al. (1996), and Rossi et al. (2000). All fermentation processes used a common host strain that was transformed with the expression vector pGAL110. Expression was then induced by addition of galactose acting on a galactose-regulated *GALI* promoter. Experiments examining cell growth and induction conditions were carried out at a scale of  $\leq 20$  L. Fermentation cell products were then harvested by either microfiltration or centrifugation, and frozen until use.

**Table 2.1.** Properties of the chromatographic stationary phases used in this thesis (information as supplied by vendor).

<b>Separation Media</b>	<b>Class</b>	<b>Vendor</b>	<b>Base Matrix</b>	<b>Functional Group</b>	<b>Avg. Particle Size<sup>a</sup> (μm)</b>
<b>UNOsphere S</b>	Strong Cation Exchange	Bio-Rad	Cross-linked polyacryl- amide	-SO <sub>3</sub> <sup>-</sup>	80
<b>SP Sepharose FF</b>	Strong Cation Exchange	GE Healthcare	Cross-linked agarose	-O-CH <sub>2</sub> CHOHCH <sub>2</sub> O- CH <sub>2</sub> CH <sub>2</sub> CH <sub>2</sub> SO <sub>3</sub> <sup>-</sup>	90
<b>POROS 50HS</b>	Strong Cation Exchange	Applied Biosystems	Cross-linked poly(styrene- divinylbenzene)	-CH <sub>2</sub> CH <sub>2</sub> CH <sub>2</sub> SO <sub>3</sub> <sup>-</sup>	50
<b>Ceramic Hydroxy- apatite</b>	Mixed mode	Bio-Rad	(Ca <sub>5</sub> (P <sub>04</sub> ) <sub>3</sub> OH) <sub>2</sub>	Ca <sup>2+</sup> , P <sub>04</sub> <sup>3-</sup> , OH	20, 40, 80
<b>Capto MMC</b>	Mixed mode	GE Healthcare	Cross-linked agarose	MMC ligand <sup>b</sup>	75
<b>MabSelect</b>	Affinity	GE Healthcare	Cross-linked agarose	Recombinant Protein A	85

a) Average bead diameter

b) The MMC ligand has weak cation-exchange and hydrophobic-interaction functional groups (refer to Table 5.1 for the chemical structure).

A laboratory-scale chromatographic purification adapted from the procedure of Cook et al. (1999) was used for the evaluation of fermentation changes. 20% (wet cell weight/volume) cell suspensions in 200 mM MOPS, pH 7.2, with 2 mM MgCl<sub>2</sub> were lysed at the laboratory scale (0.1 –0.5 L) by high-pressure homogenisation using a Microfluidizer model 110 Y from Microfluidics, Corp. (Newton, MA, USA) at 15,000 psi with four passes. A heat exchanger maintained at 2-10° C was used to cool the lysate after each pass through the homogeniser. Benzonase was added at 50 U/mL prior to homogenisation for nucleic acid degradation. The cell disruptate was then incubated overnight at 2-8°C. Following the incubation, cellular debris was removed by batch centrifugation carried out at 10000 g for 30 minutes using a Beckman Coulter (Fullerton, CA, USA) Avanti JA20 centrifuge. Centrifugation was used in this thesis because it is amenable to parallel processing and microscale operation, although alternatives such as depth filtration would also be effective.

HPV VLPs were isolated from the clarified lysate by POROS 50HS cation exchange chromatography (CEX) operated at 2-8°C and at a pH of 7.0. At the laboratory scale, an 80-mL (2.6 cm, i.d., X 15 cm, h) column was loaded by a constant input of cell weight with a loading residence time of 3.6 minutes. HPV VLPs were recovered by step elution with 1.25 M NaCl in 50 mM MOPS. For additional purification, a polishing chromatography step employing ceramic hydroxyapatite (CHT) was carried out at room temperature (22 ± 2 °C) using a 30-mL (1.6 cm, i.d., X 15 cm, h) column with a loading residence time of 2.5 minutes. The CEX product was loaded directly onto the CHT column, followed by a wash with the CEX elution buffer. The product was then eluted by gradient elution with sodium phosphate at pH 7. In both chromatographic steps, product collection was based on UV measurements at 280 nm. Product recovery is expressed here as the amount of total protein recovered per input of wet cell weight. In some instances in this thesis, laboratory-scale data generated by the Bioprocess R&D group at Merck & Co., Inc. (West Point, PA, USA) was used in the comparison of microscale and laboratory-scale results in the purification of HPV VLPs.

### *2.2.2. Monoclonal Antibodies*

Human immunoglobulins (huIgG; monoclonal antibodies) were provided for use in this thesis by the Bioprocess R&D group at Merck & Co., Inc. (West Point, PA, USA) in a crude cell filtrate and/or as a final purified product. These huIgG were expressed in

either CHO cells by standard processes (Wurm, 2004), or in *Pichia pastoris* as described by Li et al. (2006). The antibodies were then purified from the clarified cell culture or fermentation broth by standard chromatography (protein A and ion-exchange chromatography) and filtration processes. The flowthrough fractions from the protein-A chromatographic purifications were saved and used to evaluate host-cell protein (impurity) binding in microscale experiments (as described in Chapter 5), since the antibody has been removed from this sample.

### *2.2.3. Purchased Proteins*

Polyclonal antibody from human serum ( $\geq 95\%$  purity) was purchased from Sigma-Aldrich (St. Louis, MO, USA).

## **2.3. Analytical Methods**

### *2.3.1. Protein Quantification*

#### *2.3.1.1. Ultraviolet (UV) Spectrophotometry*

Purified antibody concentrations were determined by absorbance (280 nm) using an Agilent 8453 (Santa Clara, CA, USA) spectrophotometer. Real-time absorbance (280 nm) measurements of fractions from microscale experiments were also made using UV-transparent 96-halfwell microplates purchased from Corning Lifesciences (Lowell, MA, USA) in a Tecan Ultra384 plate reader (Tecan USA, Research Triangle, NC) and calibrated against a standard curve.

#### *2.3.1.2. Total Protein by the BCA Assay*

Soluble total protein release was determined by analyzing the clarified lysate by the Bicinchoninic Acid (BCA) assay kit from Pierce (Rockford, IL, USA) in a 96-well format on a Tecan Genesis 150 workstation (Tecan USA, Research Triangle, NC). The assay was calibrated with bovine serum albumin (BSA) using a curve from 50 to 500  $\mu\text{g/mL}$ . Calibration standards and samples were diluted in 50 mM MOPS, pH 7.2, with 0.15 M NaCl. Unknown protein concentrations were then determined by interpolation from this curve (fit by linear regression).

#### 2.3.1.3. Reversed-Phase Chromatography for HPV L1 Protein Quantification

Reversed-phase chromatography was used to quantify the HPV L1 protein concentration in clarified lysate samples. HPV VLPs were first precipitated in 35% (of saturation) ammonium sulphate to remove yeast proteins and then reduced and denatured in 0.5 M dithiothreitol and 3% (w/v) sodium dodecylsulphate. After a 10-minute incubation at 75° C, 100 µL was injected on to a POROS R2/H column from Applied Biosystems (Foster City, CA, USA) heated at 60° C and equilibrated in water/0.12% (v/v) trifluoroacetic acid (TFA). The L1 protein was then eluted in a ternary gradient using acetonitrile and isopropanol with 0.1% (v/v) TFA. The assay was calibrated using a curve from 12.5 to 500 µg/mL.

#### 2.3.1.4. Immunoassay for HPV VLP Quantification

HPV VLP concentrations were quantified using a sandwich-type bead-based immunoassay with electrochemiluminescence detection carried out in a 96-well format on a Tecan Freedom EVO workstation (Tecan USA, Research Triangle, NC) with the support of the Bioprocess R&D Process Monitoring group at Merck & Co., Inc. (West Point, PA, USA). In the assay, VLPs are captured on streptavidin-coated paramagnetic beads saturated with a biotinylated serotype-specific HPV VLP monoclonal antibody. The mixture is then incubated with a second ruthenium-labelled anti-VLP monoclonal antibody and detected with a BioVeris (Gaithersburg, MD, USA) M-Series 384 analyzer. Specifically, 25 µL of the pre-coated capture beads were added to each well of the microplate, followed by the addition of 25 µL of the diluted sample or calibration standard. After a 1-hr incubation, 25 µL of the ruthenylated anti-VLP antibody solution was then added. Following a second 1-hr incubation, 175 µL of assay diluent (Tris-Buffered Saline, pH 8, with 0.1% (w/v) polysorbate-20 and 0.1% (w/v) BSA) was added to the entire plate and the plate read in the BioVeris instrument. A calibration curve ranging from 10 to 2000 ng/mL was generated using a four-parameter logistic fit, and the VLP concentration of each sample was interpolated from this standard curve.

#### 2.3.1.5. Octet Protein A Assay for IgG Quantification

Antibody concentration in crude and purified samples was analysed by bio-layer interferometry using the ForteBio (Menlo, CA, USA) Octet QK system with protein A biosensors. A 16-point calibration curve ranging from 1 to 300 µg/mL was prepared in

50 mM HEPES (pH 7.5), 150 mM NaCl, 0.05% polysorbate-20, and 1% BSA and fit with a 4-parameter logistic equation. Samples were diluted 5 to 50-fold in the HEPES assay diluent, and the unknown sample concentrations were determined by interpolation from the curve.

### 2.3.2. Purity

#### 2.3.2.1. SDS-PAGE

Crude upstream process samples and chromatographic products were analysed by SDS-PAGE for purity. Electrophoresis was carried out under denaturing (SDS sample buffer and heat) and reducing conditions, using a 4 – 12% gradient NuPAGE gel system from Invitrogen (Carlsbad, CA, USA). The electrophoresis was carried out at 150 V and room temperature using the MOPS running buffer supplied by Invitrogen. Gels were stained overnight with Sypro Ruby fluorescent protein stain from Invitrogen and scanned using a Molecular Dynamics (Sunnyvale, CA, USA) fluorescence gel imager.

#### 2.3.2.2. Residual Host-Cell Protein Immunoassay

Host cell proteins (HCP) from the CHO and *Pichia pastoris* expression systems were quantified by ELISA on a Tecan Freedom EVO workstation with the assistance of the Bioprocess R&D Process Monitoring group at Merck & Co., Inc. (West Point, PA, USA). These assays used anti-HCP polyclonal antibodies (pAbs) from Cygnus Technologies (Southport, NC, USA). Microtitre plates were coated with 5 µg/mL of the anti-HCP pAbs, followed by the addition of reference standards (solubilised clarified lysate) and samples. Following the capture step, biotinylated anti-HCP pAbs were added to the plate, forming an immune complex. This complex was detected by the addition of streptavidin-alkaline-phosphatase (AP) conjugate and the fluorogenic substrate, 4-methylumbelliferyl phosphate (4-MUP). A standard curve was generated by plotting fluorescence intensity vs. concentration. The curve was fit with a four-parameter logistic equation, and unknown sample concentrations were determined by interpolation from the curve.

#### 2.3.2.3. Quantification of Residual dsDNA with the PicoGreen Reagent

Residual dsDNA concentration was quantified in experimental samples using the Quant-iT™ PicoGreen® dsDNA Assay Kit from Invitrogen (Carlsbad, CA, USA), with all assay steps automated on a Tecan Genesis 150 workstation. The assay was

performed in Corning Costar 96-well opaque plates. The standard curve ( $\lambda$  DNA) and samples were prepared in 1X Tris-EDTA buffer with 0.1 M NaCl and 200  $\mu\text{g/mL}$  of proteinase K on a Tecan workstation at a final volume of 100  $\mu\text{L}$ . To each standard and sample, 100  $\mu\text{L}$  of 1X PicoGreen reagent was added and the plate was read at excitation 485 nm / emission 535 nm on a Tecan Ultra plate reader. The standard curve was generated by linear regression of the mean of the two replicates at each point, and the DNA concentration of each sample was interpolated from this standard curve.

### *2.3.3. Characterisation of Yeast Lysate from Cell Disruption Experiments*

#### *2.3.3.1. Optical Density*

The turbidity of the clarified lysate following cell disruption was monitored at 600 nm to characterise the extent of cell lysis. Samples were analysed in 96-well microplates from BD Biosciences (San Jose, CA, USA) using a Tecan SpectraFluor detector (Tecan USA, Research Triangle, NC).

#### *2.3.3.2. Light Microscopy*

Yeast cell breakage and debris size were assessed qualitatively by oil immersion light microscopy using an Olympus Model AX70TRF microscope (Center Valley, PA, USA). Samples were diluted to the equivalent of a 1% (w/v) cell slurry solution and examined at 1000X magnification. Images were taken digitally using a Spot 2 camera with Spot 32 software from Diagnostic Instruments (Sterling Heights, MI, USA).

## **2.4. Description of Chromatographic Methods**

### *2.4.1. Column Chromatography*

Laboratory-scale column experiments were performed on either an Applied Biosystems (Carlsbad, CA, USA) Biocad 700/Vision instrument or an AKTA Explorer system (GE Healthcare; Uppsala, Sweden). The column length and flow rate varied with the specific application. Columns were slurry packed in glass XK16 or XK26 columns from GE Healthcare or 0.5-cm diameter columns from Waters (Milford, MA, USA). Alternatively, pre-packed 1-mL cartridge columns supplied by the adsorbent vendor were used. The chromatography of HPV VLPs was performed as described in section 2.2.1. Breakthrough curves with hulgG were carried out by first equilibrating the column with  $\geq 10$  column volumes of loading buffer and then loading the protein at

varying flow rates and monitoring breakthrough by absorbance at 280 nm (refer to Chapter 4 for specific details). Prior to performing the breakthrough experiment, the hold-up volume of the system tubing was determined to compute the delay time, and breakthrough curves were corrected accordingly. Column chromatography experiments to validate microscale results were performed as described in Chapters 5 and 6.

#### *2.4.2. Micro-Tip Chromatography*

Micro-tip columns in 1-mL Tecan pipette tips were prepared by PhyNexus (San Jose, CA, USA) as a custom order as described in Chapter 3. The set-up and operation of the micro-tip chromatography platform on a Tecan workstation is discussed in detail in Chapter 3. Use of the micro-tip format for adsorbent characterisation and process development is discussed in Chapters 4-6. The specific details of each application are provided in these chapters.

#### *2.4.3. Micro-Batch Adsorption*

Micro-batch adsorption experiments using adsorbent volumes less than 100  $\mu$ L were performed either in 96-well MultiScreen filterplates (Durapore membrane; 1-micron pore size; 300  $\mu$ L well volume) from Millipore (Billerica, MA, USA) or in 1.5-mL microcentrifuge tubes from Eppendorf (Westbury, NY, USA). These experiments were carried out at ambient temperature (18-24 °C). For batch experiments carried out in a filterplate, the adsorbent slurry, sample, and purification buffers were added to each well by manually pipetting each solution or suspension. The adsorbent in the filterplates was suspended using a LabSystems Wellmix plate shaker from Thermo Scientific (Waltham, MA, USA). Liquid volume was recovered in a collection plate by centrifuging the plate at 1000 x g for one minute with a Beckman (Fullerton, CA, USA) GS-15R plate centrifuge. For experiments carried out in microcentrifuge tubes, the adsorbent was mixed by either end-over-end rotation or with gently vortexing. Liquids were recovered by careful aspiration following centrifugation at 5000 x g for 5 minutes in an Eppendorf (Eppendorf North America; Westbury, NY, USA) 5417R microcentrifuge. In many cases, to ensure the removal of resin fines, the recovered solution was then filtered through a Millipore MultiScreen filterplate as described above.

Resin suspensions as provided by the manufacturer were exchanged into the desired equilibration or storage buffer by carrying out several settle-decant steps. The percentage of adsorbent (v/v) in the slurry was then determined by filtering (by gravity) 10 mL of the resin slurry through a small 10-mL drip column. The volume of the settled resin was determined from its measured bed height and then divided by the starting slurry volume (10 mL) to calculate the % resin slurry value. The desired adsorbent volume for a particular batch experiment was calculated from this % resin slurry value. Alternatively, for very low resin volumes, small resin plaques (small cylinders of resin) were prepared using the Atoll (Weingarten, Germany) MediaScout ResiQuot vacuum manifold device. Excess adsorbent slurry was added to each well of the 96-well manifold and then a vacuum was applied to generate  $7.8 \pm 0.3$   $\mu$ L plaques. Plaques were subsequently washed by applying wash buffer to each well. The washed plaques were then transferred from the perforated manifold to a 96-well microplate, or to microcentrifuge tubes, using a pusher tool.

In addition to the experiments above, batch experiments were carried out in which adsorbent was extracted from micro-tip columns prepared by PhyNexus (refer to section 2.4.2) in order to directly compare micro-tip and micro-batch operation. This was performed by first washing the micro-tip columns in equilibration buffer as outlined in Chapter 3. Next, the micro-tip column was cut just above the micro-tip column bed and the upper frit carefully removed. A small amount of buffer was added to the resin and then the resin slurry was transferred to a vial containing the buffer or protein solution. Finally, the emptied micro-tip column was rinsed at least three times to ensure complete resin transfer.

## **2.5. Cell Disruption of Yeast**

Laboratory-scale cell disruption of yeast cells was carried out by homogenisation using a microfluidizer (Microfluidics International Corporation; Newton, MA, USA) as described above in section 2.2.1. Microscale cell disruption was performed by Adaptive Focused Acoustics using the Covaris E210 instrument (Covaris, Inc.; Woburn, MA, USA) as described in Chapter 7.

## **2.6. Statistical and Mathematical Software**

Design-of-experiment methodologies (factorial and response surface methodologies) were used to optimise cell disruption and chromatographic operations. These experiments were designed and analysed using the Design Expert statistical software from State-Ease (Minneapolis, MN, USA). Both full and fractional designs were used along with central-composite and user-defined response surfaces, the details of which are described in Chapters 5 and 7. The model that best fit the data was selected using the statistical software and verified by ANOVA and other statistical assessments.

Graphs and subsequent fitting of data to equations was performed in SigmaPlot version 10.0 (Systat Software; San Jose, CA, USA). Predictive modelling simulations of dynamic binding capacity were performed in Microsoft Excel and in Mathworks (Natick, MA, USA) MATLAB. Equations and parameters used in the modelling of dynamic binding capacity are described in Chapter 4.

### **3. OPERATION AND AUTOMATION OF MICRO-TIP CHROMATOGRAPHY**

#### **3.1. Introduction**

Micro-tip columns provide a platform for microscale chromatography that can be fully automated. Although it can be performed manually with a pipette or syringe, it is difficult to consistently control the flow rate. Consequently, it is most reliably performed on a liquid-handling robot. Full walk-away automation is accomplished with relative ease since there is no manipulation of loose adsorbent and no solid-liquid separation steps required. This capability for full automation is in contrast to other microwell methods that are often only semi-automated or which are less robust in their automation because of frequent labware manipulations. A simple path to automation enables that the method can be deployed among a wide range of users, even those with a limited skill set in robotics. An additional operational advantage of micro-tip chromatography is that there is no concern about sorbent mixing, since the external mass transport involves flow through a packed bed. This is particularly beneficial for dense media, e.g. ceramic hydroxyapatite, which can be difficult to suspend uniformly in batch microwell experiments.

This chapter describes the set-up, automation, and operation of micro-tip columns on a Tecan liquid-handling robot. Flow properties of the micro-tip columns are examined, and critical operating terms and parameters are defined. In addition, a general outline is presented for performing micro-tip chromatographic experiments. Specific procedures for carrying out adsorption isotherms, kinetic studies, mobile-phase screening experiments, and multi-step purifications are subsequently discussed in more detail in Chapters 4-6.

#### **3.2. Set-Up and Automation of Micro-Tip Chromatography**

##### *3.2.1. Micro-Tip Column Preparation*

Micro-tip columns containing 10, 40, and 80  $\mu\text{L}$  of immobilised adsorbent were supplied by PhyNexus (San Jose, CA USA) as a custom order in 1-mL clear-plastic pipette tips manufactured for the Tecan liquid-handling workstation. These micro-tip columns are marketed under the name PhyTips. Although the packed bed of the micro-tip column format resembles a laboratory column, the geometry is very

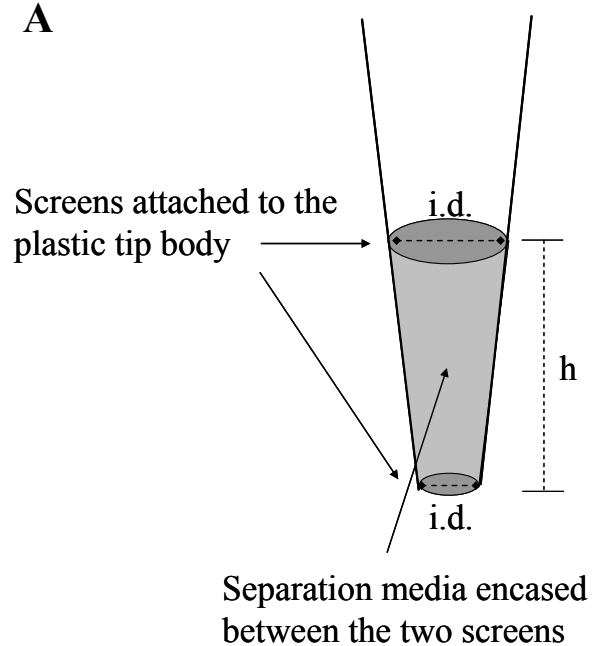
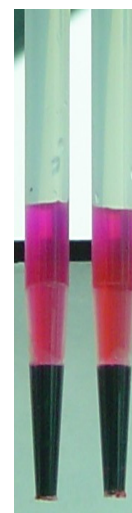
different. The bed height is significantly reduced (0.6 cm for the 10- $\mu$ L column, 0.9 cm for the 40- $\mu$ L column, and 1.2 cm for the 80- $\mu$ L column) and is tapered, giving it a conical shape. The dimensions for the three micro-tip column sizes used in this thesis are shown in Figure 3.1.

The columns are prepared by PhyNexus using a proprietary procedure in which a pre-defined volume of adsorbent slurry is drawn up for a given column volume and then situated between two hydrophilic frits which are welded to the bottom of the pipette tip. The accuracy of the bed volume is defined by the geometry of the pipette tip and the specific location of the internal frits. During manufacturing, the bed volumes of the micro-tip columns are periodically verified against a standard bed volume for that respective column size, with an allowed variation of  $\pm 10\%$ . The precision ( $n = 8$  or  $16$ ) of the micro-tip column preparation was evaluated experimentally by overloading micro-tip columns (in the nonlinear portion of the adsorption isotherm) with a human monoclonal antibody (huIgG) solution and then determining the adsorbent load. The specific details for micro-tip column operation are described later in this chapter. This assessment was carried out with 10, 40, and 80- $\mu$ L micro-tip columns containing UNOsphere S cation exchange adsorbent, loaded for 30 minutes with 0.8 mL of the protein solution at 0.8, 3.1, and 6.1 mg/mL, respectively (in 25 mM sodium phosphate, pH 6.5). The columns were then eluted with an equivalent volume of 500 mM NaCl in 25 mM sodium phosphate, pH 6.5.

The adsorbent mass loading,  $q$ , (mg protein/mL packed adsorbent) was determined by measuring the concentration of the feed and nonbound (sample remaining after loading) samples by absorbance at 280 nm and then calculated by:

$$q = \frac{C_0 V_S - C[V_S + \epsilon V_A + (1 - \epsilon)V_A \epsilon_p]}{V_A} \quad \text{Equation 3.1}$$

where  $C_0$  is the starting sample concentration (in mg/mL),  $C$  is the sample concentration after loading (in mg/mL),  $V_S$  is the sample volume (in mL),  $V_A$  is the adsorbent volume in mL,  $\epsilon_p$  is the bed porosity, and  $\epsilon$  is the bed void fraction. In this experiment,  $\epsilon$  was estimated to be 0.4, and  $\epsilon_p$  was assumed to be 0.7. (This equation assumes that most or all of the pore volume is accessible to the protein given sufficient time for pore diffusion.)

**A****B**

Column Volume (μL)	10	40	80
Column height (h), mm	6	9	12
Inner diameter (i.d.) – Top, mm	2	3	4
Inner diameter (i.d.) – Bottom, mm	1	2	2

**Figure 3.1. (A)** Schematic illustration and dimensions of the 10-, 40-, and 80-μL micro-tip columns (PhyTips) prepared by PhyNexus. Columns were prepared using 1-mL Tecan pipette tips. Approximate dimensions (measured to the nearest millimetre) for each micro-tip size are given in the associated table. **(B)** Picture showing 80-μL micro-tip columns.

Alternatively, the adsorbent loading was determined in these experiments from the mass of the eluted protein, again measured by absorbance at 280 nm, and with a recovery of 100% assumed:

$$q = \frac{C[V_E + \varepsilon V_A + (1 - \varepsilon)V_A \varepsilon_p]}{V_A}, \quad \text{Equation 3.2}$$

where C and V<sub>E</sub> are the concentration and volume of the eluted product, respectively. The precision of the loading is summarised in Table 3.1. The coefficient of variation (CV) for loading is less than 5% for all three micro-tip column sizes by both methods for determining q, implying excellent precision in the micro-tip column preparation and its operation.

**Table 3.1.** Precision study to examine the reproducibility of micro-tip column preparation and operation: loading of a huIgG onto UNOsphere S for three different micro-tip bed volumes. Columns were overloaded in each case (nonlinear portion of the adsorption isotherm). The total loading time was 30 minutes.

Bed Vol. (μL)	Replicates (n)	<i>Calculated from nonbound</i>		<i>Calculated from elution</i>	
		q *	%CV	q *	%CV
		(mg/mL)		(mg/mL)	
10	16	36.2 ± 0.4	1.9	37.6 ± 0.9	4.4
40	8	33.7 ± 0.3	1.1	39.2 ± 0.7	2.0
80	8	31.8 ± 1.3	4.9	37.8 ± 1.0	3.1

\* huIgG bound per mL of adsorbent; reported as the mean +/- 95% confidence interval

In addition to precision, information about the relative accuracy of micro-tip preparation across the three different column sizes is obtained from this experiment. The protein loading is comparable between the three micro-tip bed volumes, differing by ≤ 12% when determined from the nonbound fraction and by ≤ 4% when determined from the eluted product. The slight difference in q observed between the two methods used in its determination most likely reflects some experimental error in the micro-tip chromatography set-up, e.g. inaccuracies in the dispensed volumes, or in the absorbance measurements of the feed, nonbound, and/or eluted fractions. Absorbance measurements were made in a 96-well microtitre plate, which is prone to higher error than that of a conventional cuvette method. One other potential source of error is sample evaporation, given that the samples are not covered during the experiment. Specifically, evaporation of the nonbound fraction would result in a

slightly higher protein concentration and therefore a lower apparent adsorbent loading. Nevertheless, these errors are relatively minor, and it appears that the micro-tip preparation is reproducible across all three micro-tip column sizes.

The accuracy of micro-tip column preparation was assessed by comparing the micro-tip column loading to that of conventional batch adsorption under equilibrium conditions. The micro-tip column was again overloaded as described above. For the batch adsorption experiment, 80  $\mu$ L of a 50% adsorbent slurry were added to 800  $\mu$ L of a 3.1 mg/mL hIgG solution and mixed by end-over-end rotation. A second experiment was carried out in which the adsorbent was loaded in a high conductivity solution (0.5 M NaCl) under which the protein does not bind, with this experiment used to account for sample dilution resulting from the slurry addition. A comparison of micro-tip and batch adsorption results is shown in Table 3.2. There is good agreement between the two formats, with an observed difference of < 2%.

**Table 3.2.** Assessment of the accuracy of micro-tip column preparation by comparison of micro-tip adsorbent loading (q) to that of batch adsorption. In both experimental formats, 800  $\mu$ L of hIgG was exposed to 40  $\mu$ L of UNOsphere S adsorbent. Batch adsorption was carried out in a microcentrifuge tube with end-over-end rotation. The total loading time was 30 minutes.

Format	Replicates (n)	q * (mg/mL)	%CV	% difference from batch
Micro-tip	8	36.5 $\pm$ 0.5	1.5	-1.6
Batch	3	37.1 $\pm$ 1.8	2.0	-----

\* hIgG bound per mL of adsorbent; reported as the mean +/- 95% confidence interval

A variety of preparative chromatography media can be used with the micro-tip format. The general requirement for a new adsorbent is that its average particle size exceeds the nominal cut-off of the hydrophilic frits (about 30 microns) and that consistent flow can be achieved across the packed micro-tip column. A flow test is carried out by PhyNexus for all new adsorbents to ensure that a specified volume of fluid (water or 20% ethanol) can reproducibly flow through the micro-tip column in a defined amount of time upon applying a vacuum. In this study, preparative adsorbents from GE Healthcare (SP Sepharose FF, MabSelect, and Capto MMC),

Applied Biosystems (POROS 50HS), and Bio-Rad (UNOsphere S and ceramic hydroxyapatite) were successfully used in the micro-tip column format.

### *3.2.2. Liquid-Handling Robot*

Micro-tip chromatography was automated on a Tecan Freedom EVO 200 liquid-handling workstation (Tecan USA, Research Triangle, NC), controlled by Gemini or Evoware software. The Tecan workstation (Fig. 3.2A) was equipped with a robotic manipulation arm (RoMa) for moving microtitre plates and an eight-channel liquid handling arm (LiHa). The LiHa (Fig 3.2B) was used for transferring liquids between labware and for pipetting through the micro-tip columns. It was configured with disposable tip (DiTi) adapters for picking up the micro-tips and a 'low-DiTi-eject' accessory for setting the micro-tip columns back into their racks. Eight micro-tip columns were picked up at a time in each automated experiment. A Tecan Ultra384 plate reader (filter-based) was integrated with the system for absorbance and fluorescence measurements.

A typical Tecan deck layout for the micro-tip experiments performed in this thesis is shown in Figure 3.2C, although the layout was sometimes modified for a specific application or for higher throughput. In the set-up shown here, the Tecan deck is configured with several three- and four-position microplate carriers for holding microtitre plates, deepwell plates, partitioned-reservoir plates, and DiTi cans for holding the 200- and 1000- $\mu$ L pipette tips. In addition, there are carriers for holding 100-mL reagent troughs, sample vials, and the micro-tip columns. A Peltier rack from Gilson (Middleton, WI USA), capable of holding up to 60 sample vials, is located on the deck for temperature control (2 – 40° C).

### *3.2.3. Labware*

Micro-tip chromatography was performed in BD Falcon 96-deepwell microplates (1.0 mL/well and 2.0 mL/well) with square pyramid bottoms purchased from Fisher Scientific (Pittsburgh, PA, USA). For samples requiring temperature control, the chromatography was performed in two-mL Nalgene cryovials from Fisher Scientific on the Gilson temperature-controlled rack. Micro-tip pre-washing steps were carried out in 12-column partitioned reservoir plates from Seahorse Bioscience (Chicopee, MA USA). Eight-row or 12-column partitioned reservoir plates from

A



B

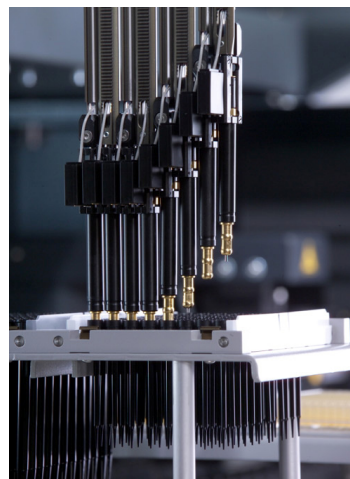
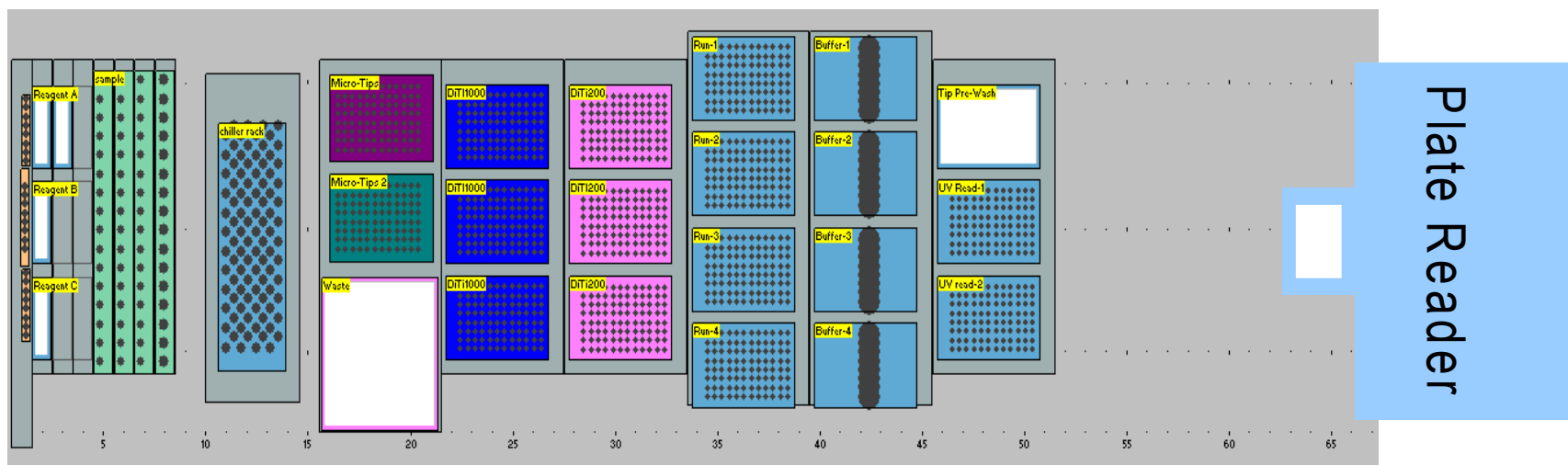


**Figure 3.2.** Tecan Freedom EVO 200 workstation used for micro-tip chromatography: **(A)** photograph of instrument; **(B)** close-up of the LiHa with DiTi adaptors (picture from Tecan); **(C)** example of a deck layout for micro-tip chromatography.

C



Seahorse Bioscience and 100-mL troughs from Tecan were used for holding buffered solutions required for the microplate chromatography. Samples were placed on the Tecan deck either in 2-mL Nalgene cryovials or in 15-mL Falcon polypropylene centrifuge tubes, also supplied by Fisher. Black liquid-sensing (non-sterile) disposable pipette tips (200 and 1000  $\mu\text{L}$ ) were purchased from Tecan, MP Biomedical (Solon, OH USA), or Axygen (Union City, CA USA). UV-transparent BD Falcon (300  $\mu\text{L}/\text{well}$ ) or Corning Costar (150  $\mu\text{L}/\text{well}$ ) 96-well microplates were purchased from Fisher Scientific for making absorbance readings at  $\lambda = 280 \text{ nm}$  in the Tecan Ultra384 plate reader.

#### 3.2.4. Liquid-Handling Parameters (*Liquid Classes*)

Liquid handling on the Tecan is defined by a set of pipetting instructions referred to as a *liquid class*. The parameters of a liquid class include aspiration and dispense speeds (volumetric flow rates given in  $\mu\text{L}/\text{s}$ ), airgaps (volumes given in  $\mu\text{L}$ ), calibration settings, pipette positioning (z height) during aspiration and dispense, liquid detection modes, and delay times. Parameters are defined separately within a liquid class for fixed and disposable pipette tips as well as for different volume ranges. The Tecan software contains some predefined liquid classes for different liquid-handling applications and liquid types, and custom liquid classes can also be developed. Having optimised liquid classes is extremely critical to the accuracy and precision of liquid handling.

Custom liquid classes were developed for micro-tip column operation to ensure accurate and reproducible flow and to operate in a flow regime that matches the typical linear velocities of laboratory-scale column chromatography. Specifically, this involved decreasing the aspiration and dispense speeds to between 2 and 20  $\mu\text{L}/\text{sec}$ , considerably lower than those normally used for pipetting fluids (100 - 600  $\mu\text{L}/\text{sec}$ ). For the aspiration and dispense positions, the micro-tip column was set to pipette 1 mm (10 steps) above the bottom of the microwell (defined here as z-max). This is a critical setting since if the micro-tip is too close to the bottom, then flow can be obstructed and becomes non-uniform. If positioned too high, then the hold-up volume in the microwell (volume that cannot be pipetted) becomes significant.

The Tecan tubing and syringes are filled with water (known as the system liquid) to ensure pipetting fidelity. However, a trade-off for this accuracy is that droplets of system liquid can sometimes fall into the micro-tips, especially after many aspiration-dispense cycles. To minimise this contamination, an air gap was positioned between the system liquid and the bottom of the DiTi adapter cone (referred to in the Tecan software as a system trailing air gap, or STAG). In the Gemini software, this air gap is drawn prior to the first aspiration following a LiHa wash and after the pipette tips have been picked up. Given that the air gap can breakdown after repeated pipetting steps, water flushes were performed periodically during micro-tip operation to replenish the air gap. One drawback of using a STAG is that there is a risk of aspirating air into chromatographic bed. Therefore, the air gap volume should be kept to a few microlitres. In the more recent Evoware software, the air gap is drawn at the end of each wash step prior to picking up the pipette tip, so this risk is eliminated. Consequently, larger air gap volumes may be evaluated ( $> 30 \mu\text{L}$ ).

### **3.3. General Procedure for Micro-Tip Chromatography**

Micro-tip chromatography is performed by pipetting sample or mobile phase up and down through the micro-tip column. Sample and purification reagents (pre-wash, equilibration, wash, and elution buffers) are presented in a 96-well microplate, and the micro-tip columns are then moved across the plate using the LiHa. No separate collection plate or plate manipulation by the RoMa is required. This differs from micro-batch adsorption where the chromatography sorbent remains in its respective microwell, and the sample and reagents are sequentially added to it, mixed, and then filtered. The micro-tip columns should be periodically set back into their rack during a purification run, and the Tecan LiHa then flushed with water to avoid dripping of system liquid into the micro-tip as discussed above. A good rule of thumb is to perform a system flush after about ten aspiration-dispense cycles and in between purification stages (i.e. equilibration, load, wash, and elution).

Figure 3.3 shows an example of a typical 96-deepwell plate layout for a protein purification having equilibration, load, wash, and elution steps. Multiple aliquots of buffer can be used within a purification stage to ensure sufficient equilibration,

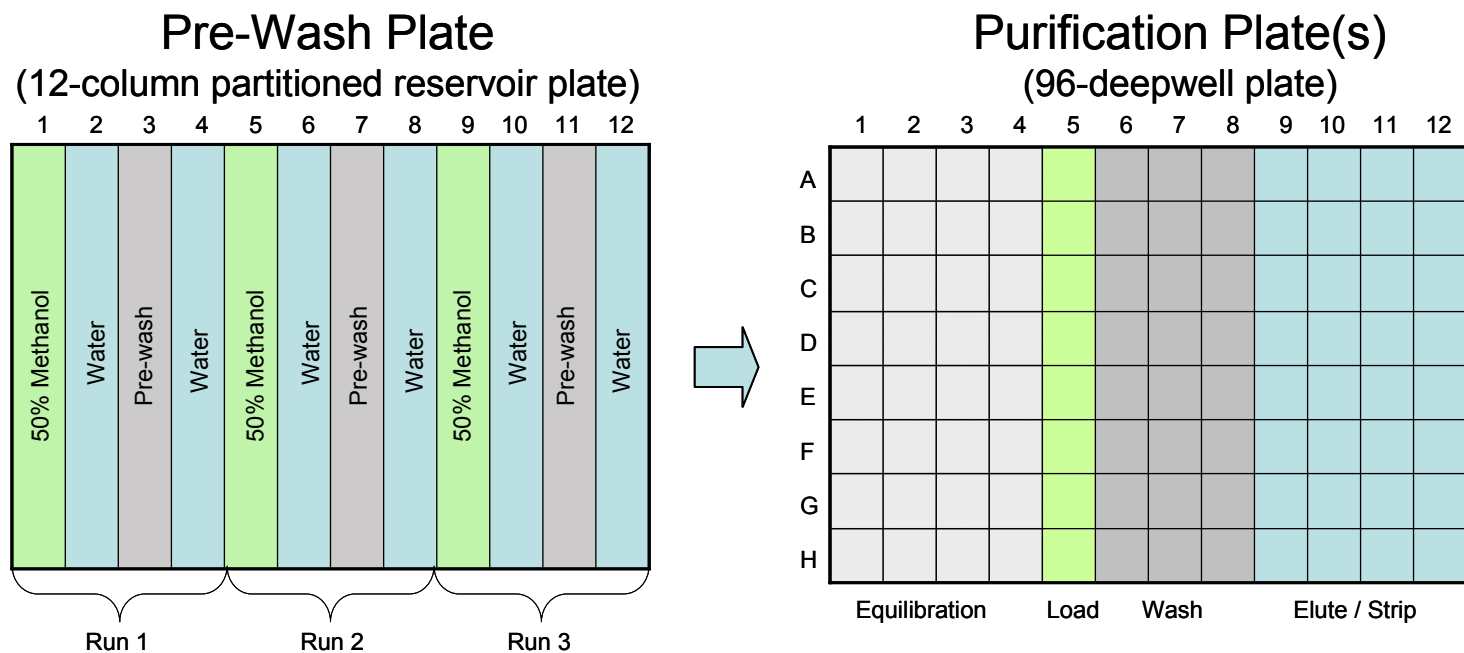


**Figure 3.3.** Example of pre-wash and purification plate layouts for a typical micro-tip column purification. Purification reagents (sample and mobile phase solutions) are transferred into the plates prior to the micro-tip chromatography. In this example, a different purification plate is used for every eight-column (micro-tip) run.

washing, and elution. Micro-tip columns may also require a series of pre-wash steps (alcohol, water, and/or pre-wash buffer) prior to equilibration, which can be carried out in a 12-column partitioned-reservoir plate or in a 100-mL trough. Purification buffers are sourced from 100-mL troughs if the same buffer is used across all eight micro-tip columns within an experimental run, or from eight-row partitioned-reservoir plates if the buffer differs with each micro-tip column. The preparation of buffers, particularly for screening experiments in which there may be many different buffer matrices, and the subsequent dispensing of these solutions into purification plates can itself be a bottleneck in high-throughput microscale experiments. Therefore, it can be advantageous to prepare batches of purification plates off-line prior to the purification experiment. Methods for preparing different buffer matrices in microtitre plates on a liquid-handling workstation from stock solutions have been developed for crystallography studies (Aguero, 2003), and such methods can potentially be applied to microscale purification experiments.

The specific volume of each aliquot is an operating parameter that is defined for a particular purification. To avoid introducing air into the micro-tip bed, the aspiration volume through the micro-tip column should always be less than or equal to the total aliquot volume minus the hold-up volume of the microwell. The hold-up volume is defined by the well geometry and the position of the micro-tip column in the well. For the BD Falcon pyramid-bottom deepwell plates used for this project, it was about 25  $\mu\text{L}$  when the micro-tip column was positioned one millimetre from the plate bottom. Evaporation of samples and purification solutions must also be considered since the microplates are uncovered during the course of an experiment. Strategies for minimising evaporation include using chilled carriers and/or placing lids on top of the microplates after completion of the purification sequence. In addition, an aliquot volume (per well) of less than 100  $\mu\text{L}$  is generally not recommended if uncovered for long periods of time.

### **3.4. Considerations for Micro-Tip Column Operation**

#### *3.4.1. Glossary of Key Operating Terms*

**Cycle number (cyc).** The total number of aspiration-dispense (up, down) cycles.

**Delay time ( $T_D$ ).** Total wait time after each aspiration and dispense step to compensate for an initial lag in fluid flow. The delay time is experimentally determined by:

$$T_D = T_{\text{actual}} - T_{\text{calc}} \quad \text{Equation 3.3}$$

where  $T_{\text{actual}}$  is defined here as the actual time taken to aspirate 97% of the target volume through the micro-tip column, and  $T_{\text{calc}}$ , is the calculated aspiration time when there is no chromatography matrix (equal to the target volume divided by the volumetric flow rate). This definition allows for a 3% inaccuracy in pipetting.

**Residence time ( $T_R$ ):** The apparent residence time during the loading of a micro-tip column is defined as the product of the total number of pipetting steps (i.e. the sum of all aspiration and dispense steps; equal to two times the cycle number) and the ratio of the adsorbent volume ( $V_A$ , in  $\mu\text{L}$ ) and the Tecan volumetric flow rate ( $Q$ , in  $\mu\text{L/s}$ ):

$$T_R = \frac{V_A}{Q} \times \text{cyc} \times 2. \quad \text{Equation 3.4}$$

Note that delay times are not accounted for in this term.

**Contact time ( $T_C$ ):** The total time that the sorbent is in contact with the liquid for a particular purification step. The contact time may also be referred to as the total loading or incubation time. It is defined here as:

$$T_C = \text{cyc} \times \left( \left( \frac{V_S}{Q} \times 2 \right) + T_{D,\text{asp}} + T_{D,\text{disp}} \right) \quad \text{Equation 3.5}$$

where  $V_S$  is the sample volume in  $\mu\text{L}$ ,  $T_{D,\text{asp}}$  and  $T_{D,\text{disp}}$  are the wait times (in s) after each aspiration step and dispense step, respectively, and  $\text{cyc}$  is the total number of aspiration-dispense cycles. If delays times are not used after each aspiration and dispense step (as in the case of batch kinetic studies), then this equation reduces to:

$$T_C = \frac{V_S}{Q} \times \text{cyc} \times 2. \quad \text{Equation 3.6}$$

**Relationship between  $T_R$  and  $T_C$ :** The relationship of  $T_R$  to  $T_C$  is defined by:

$$T_R = \frac{V_A}{V_S} \times (T_C - cyc \times (T_{D,asp} + T_{D,disp})). \quad \text{Equation 3.7}$$

Note that the  $T_R$  term does not account for delay times. Where delay times are not used, as is often the case in kinetic studies, the relationship reduces to:

$$T_R = \frac{V_A}{V_S} \times T_C. \quad \text{Equation 3.8}$$

**Average linear velocity ( $\mu_{avg}$ ):** The relationship of the Tecan volumetric flow rate to the superficial linear velocity through the micro-tip column (cm/h) is defined here as:

$$\mu_{avg} = \frac{L \times Q}{V_A} \times 3600 \quad \text{Equation 3.9}$$

where  $\mu_{avg}$  is the average linear velocity in cm/h,  $L$  and  $V_A$  are the length (cm) and adsorbent (bed) volume ( $\mu\text{L}$ ) of the micro-tip column, and  $Q$  is the volumetric flow rate ( $\mu\text{L/s}$ ). Because of the tapered shape of the micro-tip column, the linear velocity is represented here as an average since it will change across the column length.

### 3.4.2. Flow Properties of Micro-Tip Chromatography

#### 3.4.2.1. Fundamental Characterisation of Micro-Tip Flow

Micro-tip chromatography is operated optimally at pipetting speeds between 2 and 20  $\mu\text{L/sec}$  (0.12 – 1.2  $\text{mL/min}$ ). This allows superficial linear velocities that are in the range of process chromatography to be achieved and ensures a reproducible flow profile. At these flow rates,  $\mu_{avg}$  (Equation 3.9) ranges from 432-4320 cm/h for the 10- $\mu\text{L}$  column, 162-1620 cm/h for the 40- $\mu\text{L}$  column, and 108-1080 cm/h for the 80- $\mu\text{L}$  column. Although these values are expressed as average velocities, in reality the linear velocity changes down the length of the micro-tip column, being lowest at the top of the column, where the diameter is the widest, and highest at the bottom, where the diameter is the narrowest. This change in linear velocity with the axial position in the micro-tip column is shown in Figure 3.4A for the 10-, 40-, and 80- $\mu\text{L}$  columns when flowing at 5  $\mu\text{L/s}$ . Here, each column is divided into 0.3 mm slices (for a total of 20, 30, and 40 slices for the 10-, 40-, and 80- $\mu\text{L}$  columns, respectively), with  $\mu_{avg}$  calculated for each slice. The linear velocity ranges from 588 cm/h at the top of the

column to 2181 cm/h at the bottom for the 10- $\mu$ L column, 258 to 564 cm/h for the 40-  $\mu$ L column, and 145 to 559 cm/h for the 80- $\mu$ L column.

The Reynolds number (Re; Reynolds, 1883) is a dimensionless number used to characterise the nature of flow in flowing systems, providing a ratio between inertial and viscous forces. For flow in a packed chromatographic bed, Re is given by (LeVan et al., 2008):

$$\text{Re} = \frac{d_p \epsilon v}{\nu}, \quad \text{Equation 1.17}$$

where  $v$  is the interstitial linear velocity in cm/s,  $\epsilon$  is the column voidage,  $d_p$  is the average particle diameter (cm), and  $\nu$  is the kinematic viscosity of the mobile phase ( $\text{cm}^2/\text{s}$ ). Alternatively, Re can be expressed as a function of the superficial linear velocity,  $\mu$ :

$$\text{Re} = \frac{d_p \mu}{\nu}. \quad \text{Equation 3.10}$$

Because the linear velocity changes axially down the micro-tip column, the Reynolds number changes as well. This is shown in Figure 3.4B for the 10-, 40-, and 80- $\mu$ L micro-tip columns when flowing at 5  $\mu\text{L}/\text{s}$ . Here,  $d_p$  is 0.008 cm, and  $\nu$  is assumed to be the same as water, at 0.01  $\text{cm}^2/\text{s}$ . At 5  $\mu\text{L}/\text{s}$ , the Re values range from 0.13 at the top of the column to 0.48 at the bottom for the 10- $\mu$ L column, from 0.06 to 0.13 for the 40-  $\mu$ L column, and from 0.03 to 0.12 for the 80  $\mu$ L column. Flow conditions are generally considered laminar at  $\text{Re} < 10$  and fully turbulent at  $\text{Re} > 2000$  (Rhodes, 2008). Therefore, micro-tip chromatography is operated under laminar flow conditions. As shown in Figure 3.4B (refer to dashed horizontal lines), this is within the same range as a conventional cylindrical column operated between 100 and 1000 cm/h under the same conditions ( $d_p = 0.008$  cm;  $\nu = 0.01$   $\text{cm}^2/\text{s}$ ), although this range is exceeded for the 10- $\mu$ L column midway down the column.

The Biot number is another dimensionless number used to characterise mass transport properties in column chromatography. Specifically, in the case of porous adsorbents, it provides an indication of whether film mass transfer or intra-particle diffusion is rate determining. In packed bed chromatography, the Biot number (Bi) is defined by (Carta, 2005),

$$Bi = \frac{Sh}{2} \frac{D}{\varepsilon_p D_e} \quad \text{Equation 3.11}$$

Where Sh is the dimensionless Sherwood number, D is the molecular diffusivity,  $D_e$  is the effective pore diffusivity, and  $\varepsilon_p$  is the particle porosity. In adsorption beds where  $0.0015 < Re < 55$ , the Sherwood number can be calculated from the Reynolds number and Schmidt number (Sc) using the following expression (Wilson and Geankoplis, 1996),

$$Sh = \frac{1.09}{\varepsilon} Re^{0.33} Sc^{0.33} \quad \text{Equation 1.16}$$

where  $\varepsilon$  is the column voidage (assumed to be 0.4 here) and Sc is defined by,

$$Sc = \frac{v}{D} \cdot \quad \text{Equation 1.18}$$

The molecular diffusivity for a protein in water can be calculated by (Polson, 1950)

$$D = 2.74 \times 10^{-5} M^{-1/3} \quad \text{Equation 3.12}$$

where M is the molecular weight of the protein. The calculated Biot number for a huIgG (M = 150,000 Da) flowing at 5  $\mu\text{L/s}$  is shown in Figure 3.4C for the 10-, 40-, and 80- $\mu\text{L}$  micro-tip columns. In this case, a porous adsorbent with an average particle size of 80  $\mu\text{m}$  and an  $\varepsilon_p$  of 0.9 is assumed.  $D_e$  is assumed to 0.1 of the calculated molecular diffusivity ( $D = 5.1 \times 10^{-7} \text{ cm}^2/\text{s}$ ;  $D_e = 5.1 \times 10^{-8} \text{ cm}^2$ ). At a flow rate of 5  $\mu\text{L/s}$ , the Biot number ranges from 202 at the top of the column to 311 at the bottom for the 10- $\mu\text{L}$  column, from 154 to 199 for the 40- $\mu\text{L}$  column, and from 127 to 198 for the 80- $\mu\text{L}$  column. Therefore,  $Bi \gg 1$  under these conditions, indicating that pore diffusion is rate determining and that the film resistance is negligible.

#### 3.4.2.2. Volumetric Flow Profile and Determination of Delay Times

An initial resistance to flow is observed through the micro-tip column because of the back-pressure generated by the packed bed. The flow profile through a 40- $\mu\text{L}$  UNOsphere S micro-tip column is shown in Figure 3.5, in which 900  $\mu\text{L}$  of water was aspirated at 8  $\mu\text{L/s}$ . The aspirated volume was determined by gravimetric measurement of the liquid before and after aspiration at different time intervals.

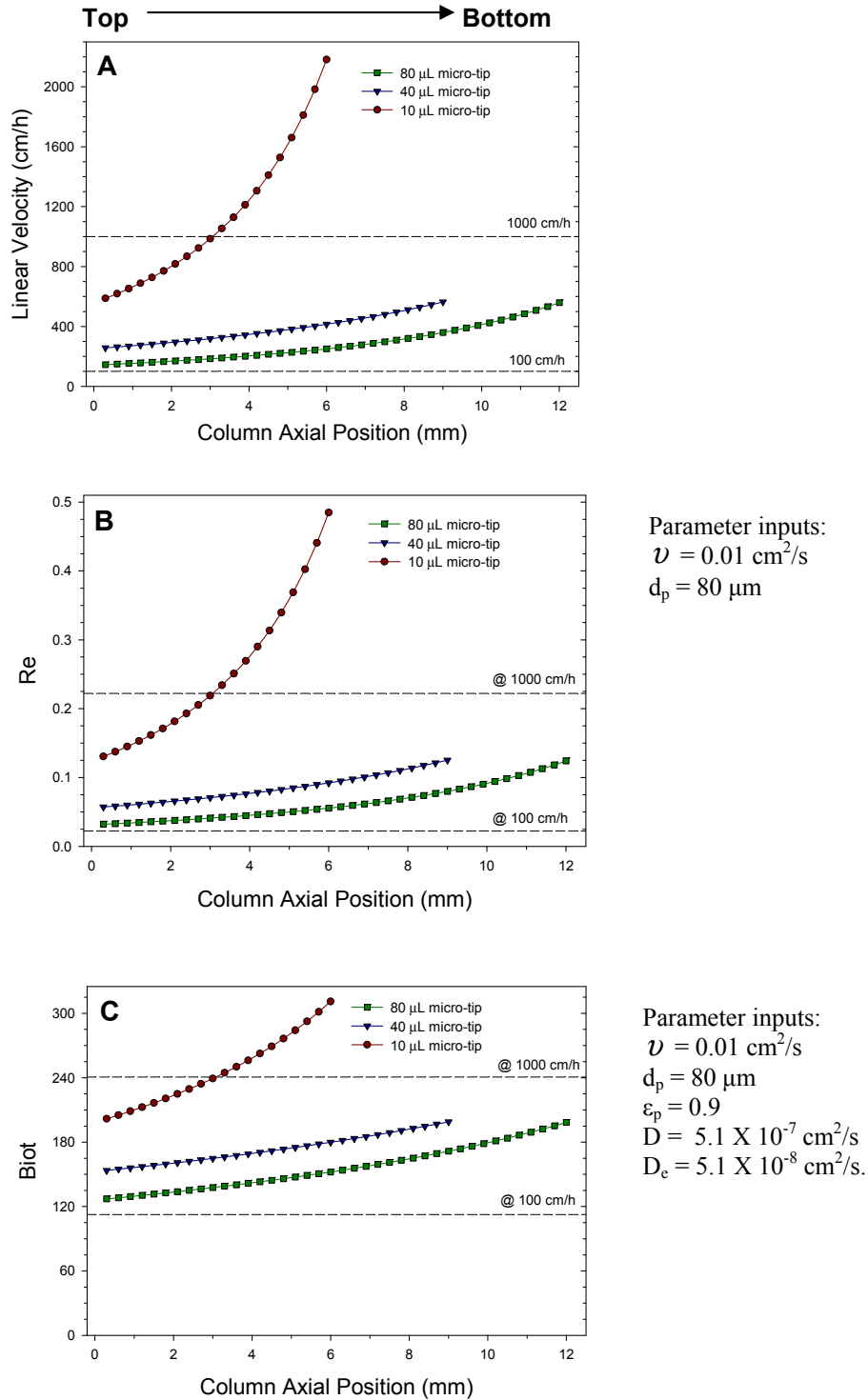


**Figure 3.4.** (A) Superficial linear velocity ( $\mu$ ), (B) Re number, and (C) Biot number as a function of column axial position for the 10- ( $\bullet$ ), 40- ( $\blacktriangledown$ ), and 80- $\mu$ L ( $\blacksquare$ ) micro-tip columns at a flow rate of 5  $\mu$ L/s. The column bed i.d. changes from 2 mm, at its top, to 1 mm, at its bottom, for the 10- $\mu$ L column, 3 to 2 mm for the 40- $\mu$ L column, and 4 to 2 mm for the 80- $\mu$ L column. Each column is divided into 0.3 mm slices, with  $\mu$ , Re, and Biot calculated for each slice. The dashed lines represent the calculated values under the same conditions for a conventional cylindrical column operated at 100 and 1000 cm/h.

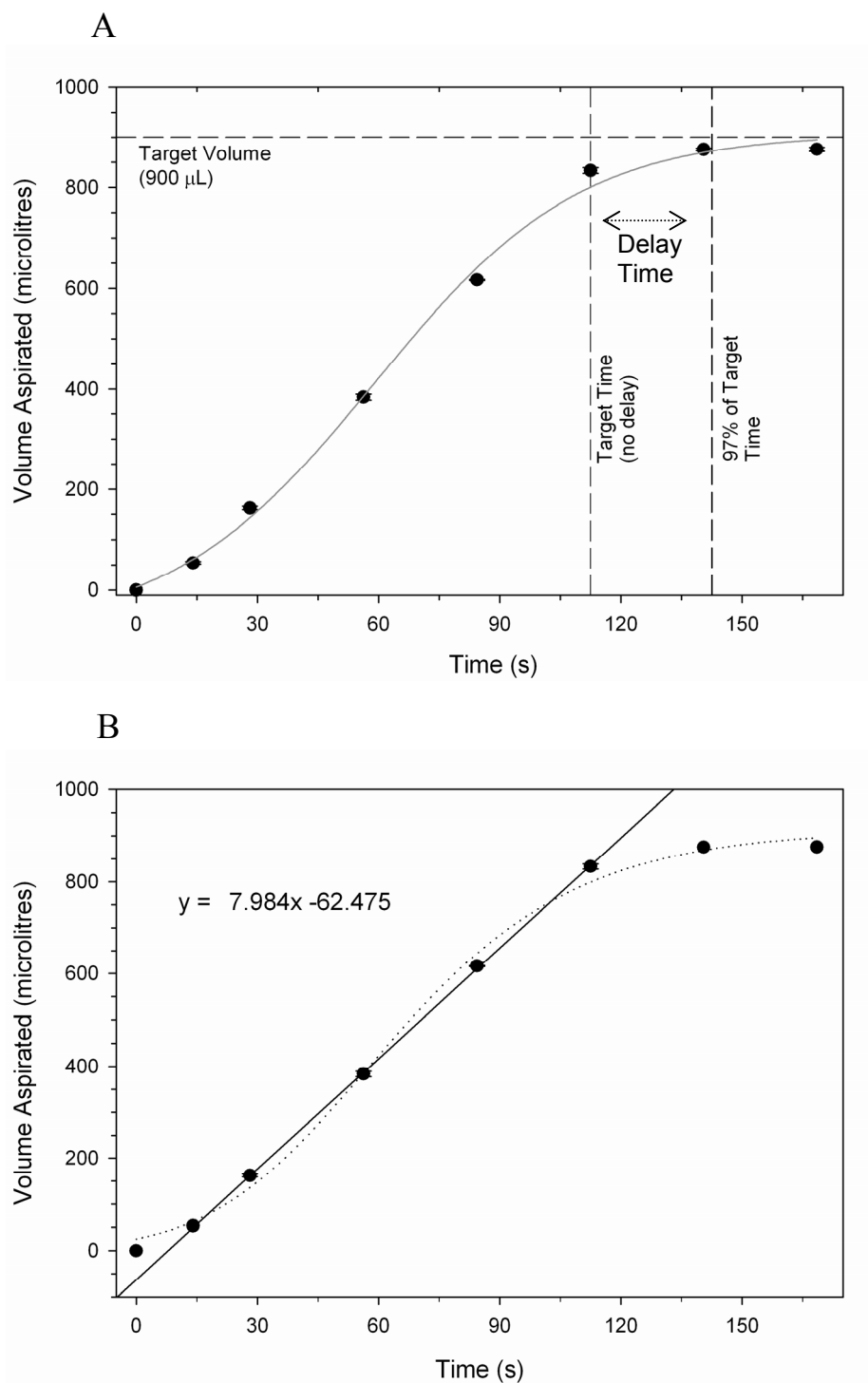


**Figure 3.5.** Volumetric flow profile through a 40- $\mu\text{L}$  UNOsphere S micro-tip column at an aspiration speed of  $8 \mu\text{L s}^{-1}$ . **(A)** Aspiration of 900  $\mu\text{L}$  of water as a function of time. The delay time was calculated as the difference between the observed time required to aspirate 97% of the target volume (143 s) and the calculated time taken to aspirate through an empty pipette tip assuming no delay (112.5 s). **(B)** The flow profile in the linear portion of the flow curve. The slope of this line is  $7.98 \mu\text{L/sec}$ , demonstrating that the flow rate is accurate.

Following the initial delay in fluid flow, the flow becomes linear and is very accurate, within 99.8% of the target flow rate. However, if the targeted aspiration volume is to be achieved, a delay time is required to compensate for the initial lag in flow and to allow the pressure to re-equilibrate across the chromatography bed. This delay time is defined by Equation 3.3 as the difference between the time taken to aspirate 97% of the target volume ( $900\ \mu\text{L} * 0.97 = 873\ \mu\text{L}$ ) through the micro-tip column and the calculated time taken to aspirate that same volume through an empty pipette tip ( $900\ \mu\text{L} / 8\ \mu\text{L s}^{-1} = 112.5\ \text{s}$ ). An aspiration volume that is within 97% of the target volume was selected to allow for any experimental error and variability (3% error is within the specifications of the Tecan robot) and to avoid extremely lengthy delay times. In the example in Figure 3.5, a delay time of 30.5 s was calculated.

Similar flow profiles were observed at 4  $\mu\text{L/s}$  and 16  $\mu\text{L/s}$ , with the flow rate in the linear portion of the profile at 102.5% and 98.8% of target, respectively. Furthermore, the experimentally determined delay time did not change significantly with flow rate: 27 sec at 4  $\mu\text{L/s}$  and 21 sec at 16  $\mu\text{L/s}$ . The delay time might be expected to vary slightly with column size and adsorbent type, depending on the extent of backpressure generated. However, the delay times for a 40- $\mu\text{L}$  ceramic hydroxyapatite column and an 80- $\mu\text{L}$  POROS 50HS column were both determined to be about 30 sec. Therefore, a delay time of 30 s at the end of each aspiration and dispense step was typically used in this thesis, and it is recommended as a default setting for most micro-tip column applications. Since the liquid-class setting of the Tecan software allows only a maximum delay time of 10 s, delay times were instead incorporated into the Tecan (Gemini) script using the timer function.

An alternative to using a delay time to compensate for the initial lag in flow is to incorporate a flow-rate correction factor. In this approach, the flow rate is multiplied by an empirically determined correction factor while the load time is based on the original (uncorrected) flow rate. For example, if a 10% correction (correction factor = 1.10) is required for aspirating 900  $\mu\text{L}$  at a flow rate of 10  $\mu\text{L/s}$ , then the flow rate would be increased to 11  $\mu\text{L/s}$  but the load time would be maintained at 90 s ( $900\ \mu\text{L} / 10\ \mu\text{L s}^{-1}$ ). In this way, the Tecan is instructed to aspirate 990  $\mu\text{L}$ , but because of the delay in fluid flow, it only aspirates 900  $\mu\text{L}$ . This approach is advantageous for

kinetics studies since continuous flow is maintained through the micro-tip column and error from delay times as a percentage of contact time is minimised. Disadvantages of this approach, however, are that the correction factor varies with load volume and flow rate and must be empirically determined. Correction factors for dispensing 800  $\mu\text{L}$  of water through a 40- $\mu\text{L}$  UNOsphere S micro-tip column at three different flow rates are given in Table 3.3.

**Table 3.3.** Flow-rate correction factors to compensate for the lag in fluid flow through a micro-tip column: Aspiration of 800  $\mu\text{L}$  of water through a 40- $\mu\text{L}$  UNOsphere S micro-tip column at three different flow rates.

Flow rate ( $\mu\text{L/s}$ )	Aspiration Time (s)	Correction Factor (X)	Corrected Flow Rate ( $\mu\text{L/s}$ )
4	200	1.038	4.15
8	100	1.062	8.50
16	50	1.106	17.7

Although a large change ( $\pm 10$  s) in delay time was not observed with flow rate, at least up to 16  $\mu\text{L/s}$ , the flow profiles do become increasingly more variable. Therefore, slower flow rates are generally preferred for uniform, reproducible flow. The lower limit for accurate flow on the Tecan Freedom EVO 200, however, is approximately 2  $\mu\text{L/s}$ . Given these constraints, an operating range between 2 and 10  $\mu\text{L/s}$  was used for the majority of experiments in this thesis.

#### 3.4.3. Micro-Tip Column Hold-Up Volume

The hold-up volume of liquid remaining in the micro-tip column after the dispense step is an important consideration since it may impact the next stage of the purification, resulting in dilution and/or sample carry-over. Specifically, this has implications for the design of the equilibration, load, and elution steps. When performing micro-tip experiments, a head volume above the column was not typically observed after the dispense step as long as there was a sufficiently long delay time. Therefore, the hold-up volume should approximate that of an evacuated (centrifugation or filtration) micro-batch experiment. Coffman et al. (2008) indicates that the liquid hold-up volume in micro-batch experiments results primarily from liquid in the adsorbent pores which cannot be removed because centrifugal forces

cannot overcome the surface tension within the pores. Accordingly, these researchers estimate that the pore hold-up volume is between 44 and 56  $\mu\text{L}$  per 100  $\mu\text{L}$  of resin, assuming a bed voidage of 0.38 and an intra-particle porosity of 0.7-0.9. Consistent with these estimates, the researchers found that the carryover volume in micro-batch adsorption experiments for eight different preparative resins ranged from 52-76  $\mu\text{L}$  per 100  $\mu\text{L}$  of resin, with the slightly higher volumes attributed to some remaining interstitial liquid.

In the case of micro-tip columns, the interstitial liquid may not necessarily evacuate as efficiently as in centrifugation. Therefore, any extra-particle fluid remaining in the column will increase the hold-up volume over those observed in the micro-batch experiments. If the full volume of extra-particle fluid is included along with the pore volume as a worst-case estimate, then the hold-up volume would be 81-94  $\mu\text{L}$  per 100  $\mu\text{L}$  of adsorbent, assuming again a bed voidage fraction of 0.38 and an intra-particle porosity of 0.7-0.9. Using the low-end of the carry-over observed in micro-batch adsorption experiments (by Coffman et al., 2008) as a best-case estimate and the high-end of the combined intra- and extra-particle volume as a worst-case estimate, then the hold-up volume resulting from the 10, 40, and 80- $\mu\text{L}$  micro-tip columns would range from 5-9, 21-38, and 42-75  $\mu\text{L}$ , respectively. However, the specific hold-up volume will depend on the adsorbent properties (i.e. adsorbent porosity) and the solution properties (i.e. viscosity and surface tension) that affect the evacuation efficiency of the extra-particle volume.

The contribution of carryover on a solute concentration can be determined for a particular equilibrium stage,  $n$ , as described by Coffman et al. (2008),

$$C_n = \frac{V_n C + V_{\text{hold-up}} C_{n-1}}{V_{\text{hold-up}} + V_n} \quad \text{Equation 3.13}$$

where  $V_n$  is the aliquot volume in microwell  $n$ ,  $C$  is the solute concentration of that aliquot volume,  $V_{\text{hold-up}}$  is the hold-up volume from the micro-tip column, and  $C_{n-1}$  is the solute concentration of the micro-tip hold-up volume (from the previous microwell,  $n-1$ ). The effect of the carry-over volume on the next equilibrium stage will then depend on the sample aliquot volume, the micro-tip bed volume, and the solute concentration in the previous  $n-1$  stage. Therefore, the effect of the hold-up

volume is minimised by using larger microwell aliquot volumes and smaller micro-tip column volumes. For example, when using an aliquot volume of 800  $\mu\text{L}$ , the worst-case errors from carry-over are  $< 1$ , 5, and 9% for the 10, 40, and 80- $\mu\text{L}$  micro-tip columns, respectively. However, these errors become much more significant, especially for the 40 and 80- $\mu\text{L}$  micro-tip columns, when using an aliquot volume of 200  $\mu\text{L}$  (5, 19, and 38%, respectively, for the 10, 40, and 80- $\mu\text{L}$  micro-tip columns).

#### 3.4.4. *Pre-Wash and Equilibration*

Micro-tip columns are typically supplied by PhyNexus in a glycerol solution, although sometimes they are supplied as a dry packed bed (as in the case of the ceramic hydroxyapatite and POROS 50HS columns used in thesis). The columns therefore need to be washed in water or in an alcohol solution, such as 50% methanol, to remove the glycerol and/or wet the chromatography adsorbent. If alcohol is used, a water wash should then be performed to remove it. In this thesis, following the water and alcohol washes, the micro-tip columns were also pre-washed with either a packing buffer, an elution buffer, or a regeneration buffer, depending on the chromatography. Generally, one aliquot of each pre-wash step (alcohol, water, pre-wash buffer) was performed, with one cycle carried out per aliquot. An aspiration volume of  $\geq 750$   $\mu\text{L}$  was generally used for the water washes, whereas volumes of 200-500  $\mu\text{L}$  were used for the other pre-wash steps.

For micro-tip column equilibration, three to four aliquots were used to ensure that the columns were fully equilibrated and that all residual wash buffer components was removed. The specific aliquot volume was determined by both the volume required for sufficient column equilibration (e.g. 10 times the column volume) and the carry-over volume between equilibration stages, with larger volumes minimising carry-over effects. Aliquot volumes  $\geq 0.5$  mL were typically used in this thesis. Since the mass transport of buffer ions is relatively rapid, one aspiration-dispense cycle (passage through the micro-tip) per equilibration aliquot was sufficient. In this thesis, the pre-wash and equilibration steps were carried out in a 12-column partitioned reservoir plate (as shown in Figure 3.3) if the solutions were the same for all eight micro-tips, or in a 96-well deepwell plate if they were different.

#### 3.4.5. Adsorption (Sample Loading)

In conventional laboratory-scale column chromatography, dynamic binding capacity is influenced by the column residence time ( $T_R$ ), with the capacity being a dynamic measure defined by a specific breakthrough point (e.g. 1, 5, or 10%) from frontal chromatography experiments. Residence times are usually between 2 and 20 min for most bioprocess chromatographic purifications, whereas the total loading times can be on the order of hours. Batch adsorption, in contrast, is typically operated with incubation times that will achieve equilibrium. In this case, total contact time with the solution ( $T_C$ ) is the critical operating parameter affecting binding capacity (Bergander et al., 2008; Coffman et al., 2008), with the specific time required to achieve equilibrium depending on the mass transport properties of the adsorbent and the associating biomolecule. Batch uptake experiments can be carried out to describe the kinetics of mass transport (e.g. with a pore diffusion model) and to model dynamic binding capacity in column chromatography (Chase, 1984; Arve and Liapis, 1987; Bergander et al., 2008). This is discussed more in Chapter 4.

Micro-tip chromatography is a batch operation like micro-batch adsorption, yet instead of static mixing, it has dynamic flow through the micro-tip column, as in conventional column chromatography. Thus, both residence time and contact time must be considered. Micro-tip residence time is affected by the column size, flow rate, and the number of aspiration-dispense cycles (equation 3.4). These residence times are generally short per aspiration-dispense cycle due to the short bed heights ( $\leq 12$  mm), even at the slowest aspiration speeds, but can be extended by increasing the aspiration-dispense cycle number. Micro-tip contact time is controlled by the sample load volume, flow rate, cycle number, and delay time, as described by Equation 3.5. The relationship between sorbent contact time and residence time is a function of the micro-tip column size and the sample load volume as described by Equations 3.8. Therefore, at fixed contact time, the residence time of the 80- $\mu$ L micro-tip column is two times greater than that of the 40- $\mu$ L column and eight times greater than that of the 10- $\mu$ L column. Conversely, at constant residence time, the contact time of the 80- $\mu$ L micro-tip column is two times less than that of the 40- $\mu$ L column and eight times less than that of the 10- $\mu$ L column.

The loading step in micro-tip chromatography is therefore optimised by a consideration of both residence and contact times, of which the contribution of each is explored further in the Chapter 4. This means that for a particular column size, the volumetric flow rate, sample volume, and number of aspiration-dispense cycles are manipulated to achieve the desired residence and contact times. Uptake experiments like those described in Chapter 4 can be conducted to optimise the loading time. In these experiments, each micro-tip column is loaded at the same flow rate and sample volume, but for a different number of cycles. Generally, 20 to 40 minutes is sufficient for a loading that approximates equilibrium binding (i.e. within 80% of equilibrium), although the exact time will vary with the adsorbent, protein, sample concentration, and mobile phase conditions. A compromise must often be made, however, between experimental throughput and the extent of adsorbent binding. For example, Coffman et al. (2008) used a 20-min incubation time in their micro-batch adsorption studies as a representation of binding time for a column operation, although binding had not always fully achieved equilibrium (i.e.  $\geq 80\%$  complete). Another example of this trade-off is shown in Chapter 6 for the hydroxyapatite chromatography in the multi-step VLP purification.

In addition to loading time, optimisation of the load step should also consider the error resulting from the micro-tip column and microwell hold-up volumes. Larger sample volumes, as discussed above, will minimise these errors. In addition to hold-up volume, the number of aspiration-dispense cycles should also be considered. For example, three aspiration-dispense cycles at 9  $\mu\text{L/s}$  is preferred over one cycle at 3  $\mu\text{L/s}$ , since more cycles will minimise the effect of the microwell hold-up volume by allowing for sample mixing.

#### *3.4.6. Wash and Elution*

In a typical purification, the sample loading step is followed by a wash step to remove any residual sample that is held up in the column and to elute weakly bound impurities. Generally, two aliquots of  $\geq 5$  column volumes were used in this thesis (or a minimum volume of 200  $\mu\text{L}$ ), with one cycle carried out per aliquot. Additional washes may sometimes be performed, depending on the chromatography, to selectively elute impurities from the column. This is an especially useful strategy for micro-tip chromatography given that a continuous linear gradient elution is not

feasible, at least not without custom modification to the liquid-handling robot. The number of aliquots, the aliquot volume, and the cycle number for these washes are experimentally optimised for impurity clearance.

As with adsorption, elution conditions are optimised by considering micro-tip contact time and residence time. An example is shown in Figure 3.6, in which a huIgG is eluted from a 40- $\mu$ L SP Sepharose FF column as a function of aspiration cycle (at constant sample volume and flow rate). The mass transport for desorption is typically much faster than for adsorption, since there is a high concentration gradient between the inside and outside of the resin pore, resulting in rapid diffusion out of the pore. This is evidenced in Figure 3.6, in which complete desorption occurs within two minutes. Therefore, short contact times ( $\leq 5$  minutes) were performed throughout this thesis and were found to be sufficient for micro-tip elution. Longer elution times, however, may be required if the mobile-phase conditions do not strongly favour desorption, or if size-exclusion effects within the pores become significant, as can be the case for polyacrylamide-based hydrogels with high intra-pore polymer concentrations (Lewus and Carta, 2001). In addition, where the desorption thermodynamics are unfavourable, additional elution aliquots can be beneficial to push the equilibrium fully towards desorption. A second elution aliquot was typically performed in this thesis to ensure complete product desorption and to recover any eluted protein that was held-up in the column following the first elution aliquot.

It has been shown by other researchers, notably by Coffman and colleagues (Kelley et al. 2008B; Kramarczyk et al., 2008), that stepwise elution procedures can be used for micro-batch adsorption to mimic a linear gradient elution. The same approach can also be applied here to micro-tip chromatography, with an example shown in Figure 3.7. This approach allows wash and elution conditions to be efficiently optimised so that impurities can be resolved from the product peak.

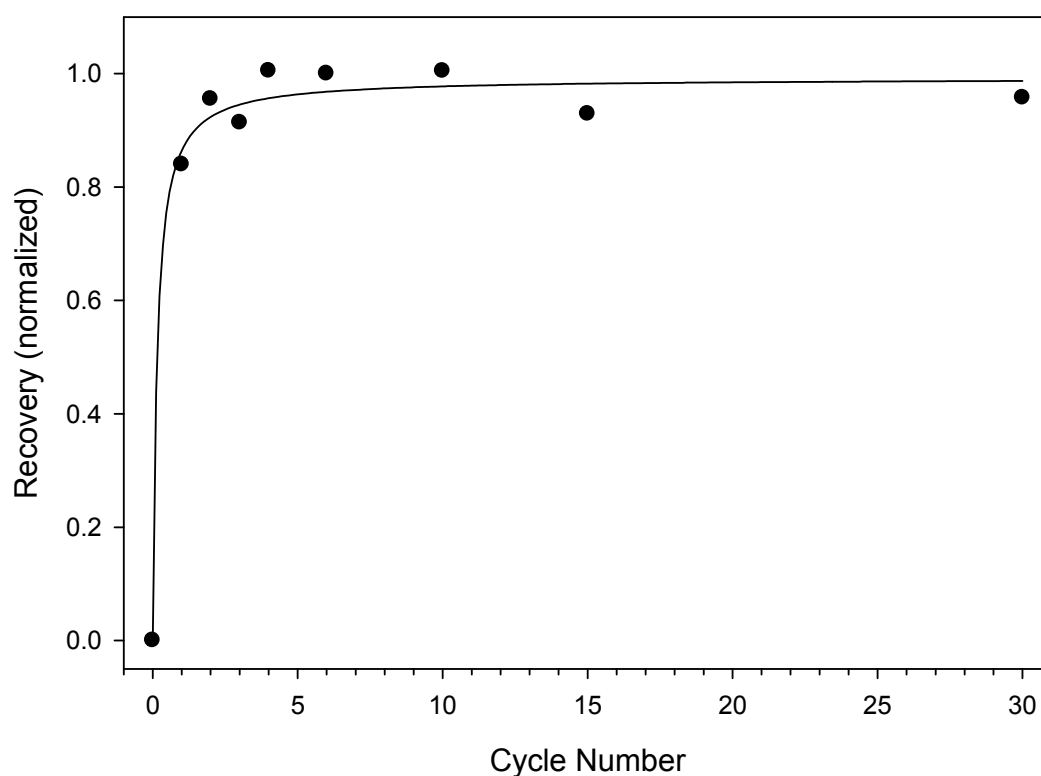


**Figure 3.6.** Desorption of a hulgG from SP Sepharose FF. Experiments were performed with 40- $\mu$ L micro-tip columns as a function of the aspiration-dispense cycle number at a constant volume (200  $\mu$ L) and flow rate (10.7  $\mu$ L/s). Recovery is normalised to that of complete desorption. One aspiration-dispense cycle = 0.625 min. In this example, desorption is complete in about two minutes.

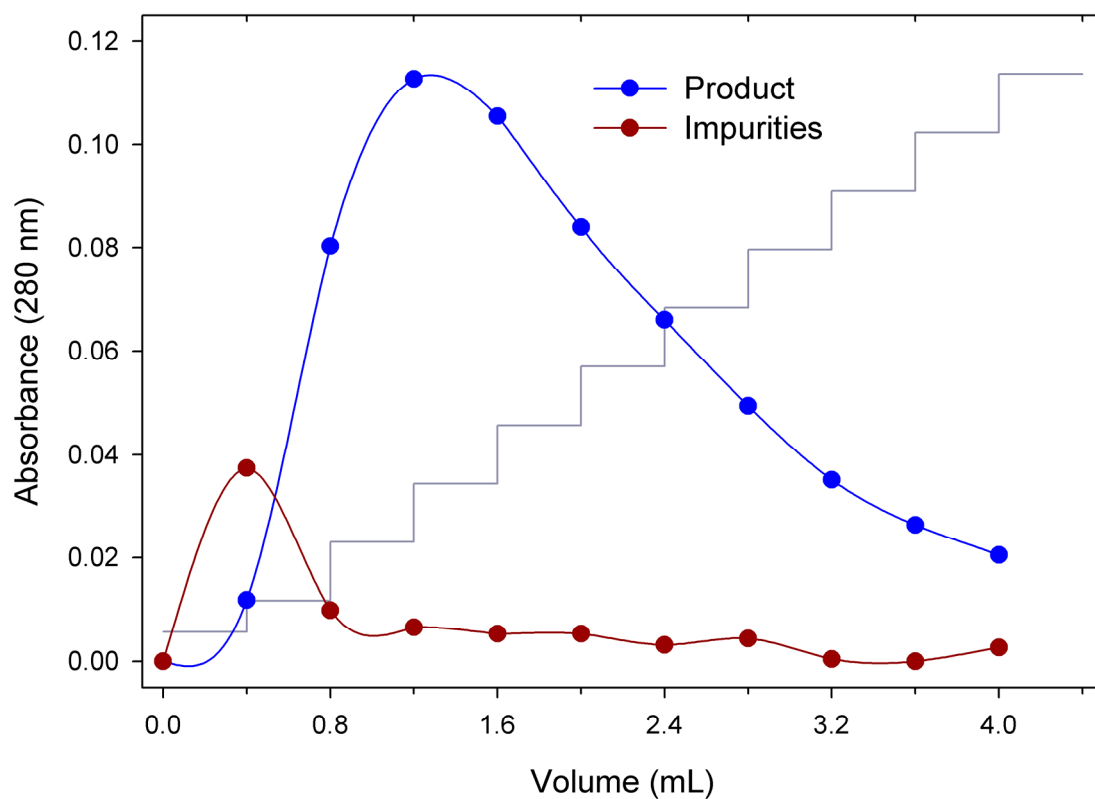


**Figure 3.7.** "Staircase" elution of a huIgG (product) and host-cell impurities from a 40- $\mu$ L Capto MMC micro-tip column. The column was eluted at pH 6.5 in 10 incremental elution steps from 0 to 1.8 M NaCl.

### 3.5. Throughput of a Micro-Tip Purification

The throughput of a micro-tip chromatographic purification depends on the time required for dispensing the purification reagents as well as the time for each stage of the separation. Table 3.4 shows the breakdown of time for each step in a typical purification sequence with pre-wash, equilibration, load, wash, and elution steps. The overall run time is 71 minutes but can be reduced if any of the stages are omitted (as in screening experiments). In addition, run times can be shortened by pre-dispensing purification buffers off-line, by decreasing the contact time of a specific stage, and/or by reducing the number of equilibration, wash, and elution aliquots performed per stage. However, these throughput enhancements may require some trade-off in performance and robustness. For example, decreasing the loading time may reduce the amount of product binding, depending on its uptake rate. A correction factor could, however, then be applied to compensate for this offset in order to predict laboratory-scale column performance. An example of this is described in Chapter 6.

**Table 3.4.** Breakdown of the run time for each step in an example eight-column micro-tip purification. In this example, the aspiration-dispense volume is 800  $\mu\text{L}$  for all steps except elution, where the aspiration-dispense volume is 400  $\mu\text{L}$ . The flow rate is 10  $\mu\text{L/s}$ , and the aspiration-dispense delay time is 30 s.

Step	Liquid-handling	Pre-Wash	Equilibration	Load	Wash	Elution	Total
Operation	Dispense aliquots <sup>a</sup>	3 aliquots x 1 cycle	4 aliquots x 1 cycle	1 aliquot x 6 cycles	2 aliquots x 1 cycle	2 aliquots x 2 cycles	-----
Time (min)	5	11	15	22	8	10	71

a) Dispensing of aliquots can be performed off-line to improve throughput.

The experiments performed in this thesis used an eight-channel Tecan LiHa, allowing eight experiments to be carried out in parallel. This is significantly less than the parallelisation possible with 96-well micro-batch adsorption. However, in practice, this difference is much lower when the analytical overhead and capability of micro-tip chromatography for full automation are considered. Significant throughput enhancements are achieved with micro-tip chromatography because no time is

required for manipulation of the chromatography media (dispensing and filtration) and because the method can be fully automated, allowing robust walk-away automation with no manual intervention. 96-channel pipetting arms are available for 200- $\mu$ L sized pipette tips, although this significantly confines microscale operating ranges. Recently, new options for 96-channel pipetting have become available that can accommodate a 1-mL pipette tip, providing the possibility of significantly higher experimental throughput. Future work should centre on the evaluation of these new pipetting arms for micro-tip chromatography while considering the impact that higher experimental throughput will have on the assay load.

### **3.6. Summary**

Micro-tip columns offer a platform for microscale chromatography that can be fully automated on a liquid-handling workstation, with little or no manual intervention required following set-up. Although the format is column-like, it is operated in batch mode, with its data output more analogous to that of micro-batch adsorption than to a laboratory-scale column. There are, however, some key operational differences between micro-tip and micro-batch adsorption. Principally, there is dynamic flow through the micro-tip columns. Parameters like residence time and contact time must therefore both be considered in its operation. Cycle number, aliquot volume (sample or mobile phase), and flow rate all contribute to the completeness of binding and desorption. In addition, an initial lag in fluid flow, the tapered geometry of the column, and the constraint on sample volume ( $< 1$  mL that can be aspirated) make this method distinct from other column-based methods. These considerations are explored further in Chapter 4 in the context of binding kinetics and the determination of binding capacity (equilibrium and dynamic).

Some suggested (default) operating ranges when setting up a new micro-tip chromatography experiment on a Tecan workstation are given in Table 3.6. Parameters should eventually be optimised for each protein and chromatographic sorbent as well as for differences in liquid-handling platforms. Examples of this optimisation are described in Chapters 5 and 6, in which the micro-tip chromatography platform is applied to two different process development challenges.

**Table 3.5.** Suggested (default) operating ranges for micro-tip chromatography (using 10-, 40-, or 80- $\mu$ L columns).

Step	Suggested Operating Values or Ranges				
	Aspiration Speed ( $\mu$ L/s)	Aliquots / Step	Cycles / Aliquot	Volume / Aliquot <sup>a</sup>	Contact time (T <sub>C</sub> ) / Aliquot
Pre-Wash	10-20	1-4	1	200 – 900 $\mu$ L <sup>b,c</sup>	$\geq$ 1 min
Equilibration	5-20	3-4	1	$\geq$ 10X CV <sup>c,d</sup>	$\geq$ 1 min
Load	2-10	1 <sup>e</sup>	$\geq$ 3	200 – 900 $\mu$ L	20-40 min <sup>f</sup>
Wash	5-10	2-3	1	$\geq$ 5X CV <sup>d</sup>	$\geq$ 1 min
Elution, Single Step	5-10	2	$\geq$ 2	$\geq$ 5X CV <sup>d</sup>	2-5 min
Elution, Staircase <sup>g</sup>	5-10	2-12	$\geq$ 2	$\geq$ 5X CV <sup>d</sup>	2-5 min

- a) Microwell hold-up volume for the BD Falcon pyramid-bottom deepwell plate is  $\sim$ 25  $\mu$ L. Maximum aspiration volume is  $\sim$ 900  $\mu$ L for a 1-mL micro-tip pipette size.
- b) For water wash,  $\geq$  750  $\mu$ L wash is recommended; for other pre-washes, volumes between 200 and 500  $\mu$ L are usually sufficient.
- c) May be carried out in a partitioned reservoir plate, with a minimum volume of 10 mL/reservoir well.
- d) CV = micro-tip column volume. Minimum recommended aliquot volume is 200  $\mu$ L; therefore, use  $\geq$  20 CV for a 10- $\mu$ L column. Maximum aspiration volume is 900  $\mu$ L.
- e) Multiple aliquots can be used if load volume exceeds 900  $\mu$ L.
- f) Refers to contact time and is optimised for sample type. 20-40 min is generally sufficient to approach equilibrium binding but will vary with protein and adsorbent.
- g) Sequential multi-step elution series of increasing elution strength.

## **4. ADSORBENT CHARACTERISATION BY MICRO-TIP CHROMATOGRAPHY**

### **4.1. Introduction**

An understanding of the retention and mass transport properties of an adsorbent facilitates the development of a robust process chromatography step. The thermodynamics of adsorption can be determined from adsorption isotherms, while the kinetics of mass transfer can be studied from batch uptake experiments. These data can then be used qualitatively in adsorbent screening or quantitatively to predict column adsorption using an appropriate adsorption model. Scale-down chromatographic methods like those reviewed in Chapter 1 (section 1.5.6) significantly increase the experimental throughput and decrease the sample volume requirement for carrying out adsorption isotherm and kinetic experiments. Performing these studies by micro-batch adsorption or with mini-column cartridges is relatively straightforward, since these formats are scaled down from well established laboratory-scale methods. Bergander et al. (2008) describes both the qualitative and quantitative determination of dynamic binding capacity (DBC) from micro-batch adsorption experiments in microtitre filter plates. Wiendahl et al. (2008) demonstrates the use of 200- $\mu$ L mini-columns on a Tecan workstation for generating breakthrough curves. In contrast to these microscale formats, micro-tip chromatography does not have an analogous laboratory-scale technique upon which to model the adsorption and kinetic experiments. This chapter examines how micro-tip columns can be operated for carrying out equilibrium adsorption and kinetic experiments. Two data-driven modelling approaches for predicting dynamic binding capacity from micro-tip data are then evaluated.

### **4.2. Equilibrium Adsorption Isotherms**

Adsorption isotherms are used to describe the thermodynamics of a chromatographic separation and are required for modelling to describe the system state at equilibrium. A conventional approach for single- and multi-component isotherm determination is to carry out static batch adsorption experiments in a mixed vessel. Alternatively, dynamic methods such as frontal analysis and pulse methods have been employed (Guiochon et al., 2006). In the batch adsorption approach, either the initial sample (adsorbate) concentration ( $C_0$ ), the sample volume ( $V_S$ ), or the adsorbent volume

( $V_A$ ) is varied, while keeping the other two parameters constant. The concentration of the adsorbate ( $C$ ) in the liquid phase is then measured following a specified incubation time with mixing (usually ranging from one hour to overnight). The amount of adsorbate associated with the adsorbent ( $q$ ) is then calculated as described in Chapter 3:

$$q = \frac{C_0 V_S - C[V_S + \epsilon V_A + (1 - \epsilon)V_A \epsilon_p]}{V_A}. \quad \text{Equation 3.1}$$

The calculation of micro-tip hold-up volume ( $\epsilon V_A + (1 - \epsilon)V_A \epsilon_p$ ) in this equation assumes that most or all of the pore volume is accessible to the protein adsorbate given sufficient time for pore diffusion (i.e. at equilibrium). It, however, was generally neglected in this thesis when it was  $\leq 5\%$  of the sample volume ( $V_S$ ).

Adsorption isotherms are performed by micro-tip chromatography in a manner that is analogous to micro-batch adsorption, although with some important distinctions. As discussed in Chapters 1 and 3, the external mass transport differs between the formats, with convective flow through a packed bed in the case of micro-tip columns and static mixing of loose adsorbent in the case of micro-batch adsorption. This difference can potentially have some effect on the film mass transfer resistance, with convective flow providing a possible benefit over static mixing in the efficiency of protein uptake. However, this potential improvement depends largely on the nature of the adsorbent and the associating protein, with an improvement more likely when adsorption occurs primarily on the adsorbent particle surface (i.e. with non-porous resins or for very large proteins which cannot access much of the adsorbent pore volume). In this case, mass transport is dictated largely by the film mass transfer rate as opposed to intra-particle diffusion. The effect of the mass transport difference between micro-tip and micro-batch adsorption, however, becomes negligible in adsorption isotherm experiments which approach equilibrium, although it does potentially have implications for kinetic studies, as discussed in the sections below.

As in batch static-mixing experiments, adsorption isotherms by micro-tip chromatography are performed by varying  $C_0$ ,  $V_S$ , or  $V_A$ . However, there are some constraints on the operating ranges imposed by the micro-tip platform, as outlined in Table 4.1. The adsorbent bed volume in this thesis was limited to 10, 40, and 80  $\mu\text{L}$ .

in a Tecan pipette tip, although other volumes such as 5, 20, 160 and 320  $\mu\text{L}$  are possible. Furthermore, the maximum sample volume that can be aspirated into the 1-mL Tecan pipette tip is about 900  $\mu\text{L}$  since the adsorbent occupies some of the pipette volume and some of the Tecan syringe volume (1 mL) is occupied by the system trailing air gap (STAG). This means that for volumes greater than 900  $\mu\text{L}$ , not all of the sample volume will be aspirated into the pipette during any one aspiration-dispense cycle. The number of aspiration-dispense cycles and the loading time in these cases must be sufficiently high to ensure complete mixing and sample contact during the loading step.

**Table 4.1.** Allowed variable ranges for carrying out adsorption isotherms with micro-tip columns (1-mL Tecan pipette format) on a Tecan workstation using the platform defined in Chapter 3. One of three parameters is varied while the other two are held constant.

Variable Parameter	Range	Notes
Sorbent Volume ( $V_A$ )	10, 40, or 80 <sup>a</sup> $\mu\text{L}$	<i>Phase ratio varied by <math>V_A</math></i> Sample volume constant $C_0$ constant Flow rate and cycle number constant
Sample Volume ( $V_S$ )	50 – 900 <sup>b</sup> $\mu\text{L}$	Sorbent volume constant <i>Phase ratio varied by <math>V_S</math></i> $C_0$ constant Flow rate and cycle number constant <sup>c</sup>
Starting Sample Conc. ( $C_0$ )	Limited only by sample solubility	Phase ratio constant ( $V_A$ and $V_S$ constant) $C_0$ varied Flow rate and cycle number constant

a) The specific adsorbent volumes available depend on the type of pipette tip being used. For the Tecan 1-mL pipette tip used in this thesis, other volumes are available such as 5, 20, 160 and 320  $\mu\text{L}$  but require further collaboration with PhyNexus.

b) 900  $\mu\text{L}$  is the upper aspiration volume for the 1-mL Tecan micro-tip format. However, sample volumes >900  $\mu\text{L}$  may be placed in the sample tube or microwell.

c) Under this approach, the time in which the sample is actually flowing through the micro-tip column will vary with sample volume.

The determination of adsorption isotherms by micro-tip chromatography is illustrated in Figure 4.1. In the shown set-up, the sample volume, flow rate, aspiration-dispense cycle number, and adsorbent bed volume are held constant, while  $C_0$  is varied across

each micro-tip column. The adsorbate concentration ( $C$ ) is measured after a specified incubation time and the respective adsorbent loading ( $q$ ) is calculated by Equation 3.1. The incubation time is controlled by the number of aspiration-dispense cycles performed. It is generally not practical to carry out overnight incubation by micro-tip chromatography due to sample evaporation; however, incubations of one to three hours are usually sufficient to achieve conditions close to equilibrium. Another consideration when using the Tecan is that the STAG may break down over time, which can lead to the formation of droplets of system liquid (water) along the sides of the pipette tip. To minimise the risk of system liquid contamination, especially during lengthy load times, it can be beneficial to set the micro-tips down and then wash the LiHa in order to re-establish the STAG (as described in Chapter 3).

Although there are sample and adsorbent volume constraints, a clear advantage of using the micro-tip format for determining adsorption isotherms is that it is highly amenable to automation on a liquid-handling workstation, with no peripheral devices for mixing or filtration required. Furthermore, there is no concern about incomplete mixing, particularly for high density adsorbents, which could otherwise decrease the rate of protein uptake (Bensch et al., 2005; Bergander et al., 2008) and, hence, the experimental efficiency. The choice of how to best carry out adsorption isotherms (i.e. which parameter to vary), depends primarily on the sample type and experimental goal. For single-component (purified) samples, varying the starting sample concentration, as shown in Figure 4.1, is the simplest approach. On the other hand, for multi-component (crude) samples, it is usually better to keep the starting sample composition the same so that the competitive interaction of the components is representative of typical feed conditions. In these cases, the sample or adsorbent volume is varied.

The micro-tip adsorption isotherm method was evaluated by examining the binding of a test human immunoglobulin (hulIgG) to the UNOsphere S cation-exchange adsorbent. The isotherm data are shown as a function of incubation time in Figure 4.1B. Also shown is an overnight incubation by micro-batch adsorption, in which equilibrium has been fully achieved. These adsorption isotherm data are fit with a Langmuir model. In this example, an approach towards equilibrium is evident, with equilibrium conditions approximated (less than a 10% difference from that of the

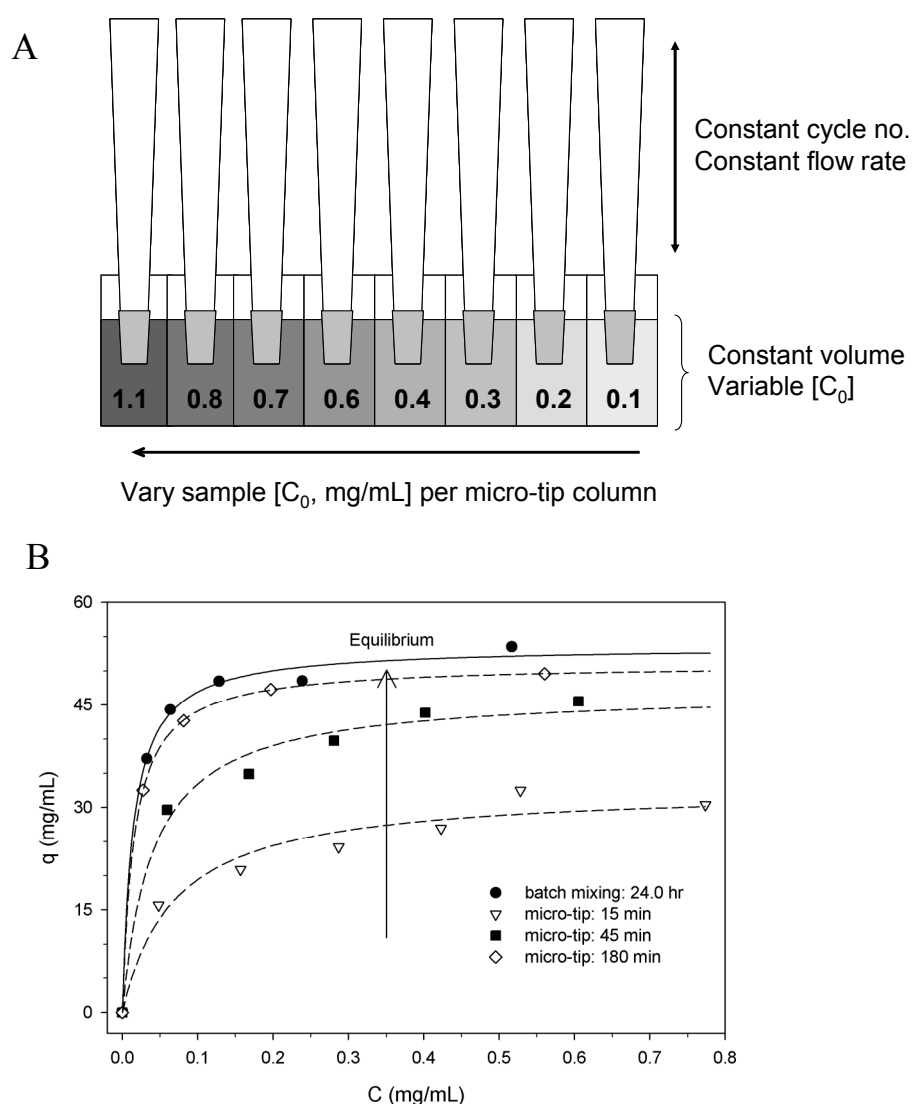


**Figure 4.1.** Determination of adsorption isotherms using micro-tip columns on a Tecan robotic workstation. **(A)** Schematic of the set-up: the micro-tip column volume, sample volume, flow rate, and aspiration-dispense cycle number are held constant as the protein concentration is varied across the eight micro-tips. **(B)** Adsorption isotherms of a test huIgG on to the UNOsphere S cation exchange adsorbent (pH 6.5; conductivity  $\leq 3$  mS/cm) as a function of contact time. Ten-microlitre micro-tip columns were used in this experiment, with 900  $\mu\text{L}$  of sample loaded onto each column ( $\mu_{\text{avg}} = 400$  cm/h). For the batch mixing experiment, 10  $\mu\text{L}$  of adsorbent was quantitatively extracted from a micro-tip column (repeated for each data point) and mixed overnight with 900  $\mu\text{L}$  of sample on an end-over-end rotator.

overnight batch incubation) in  $> 45$  min but  $\leq 180$  min. In addition to the equilibrium data, qualitative information about the adsorption kinetics can be derived from the adsorption isotherm measurements made prior to equilibrium. The use of these *pre-equilibrium*, or 'dynamic', adsorption isotherms, for the evaluation of mass transport properties is discussed later in this chapter.

The maximum adsorbent binding capacity ( $q_m$  parameter of the Langmuir model) of UNOsphere S for the test huIgG was determined by batch mixing (overnight incubation) and micro-tip chromatography at several different scales and phase ratios. These data are compared in Table 4.2. Also shown as a measurement of total adsorbent capacity is the  $DBC_{50\%}$  when loading the antibody onto a 1-mL column at 60 cm/h ( $T_R = 5$  minutes) at a concentration of 1 mg/mL. The capacities determined from the batch experiments range from 38.9 mg/mL using 8- $\mu$ L resin plaques (prepared by the Atoll ResiQuot device as described in Chapter 2) to 53.5 mg/mL using 10  $\mu$ L of adsorbent extracted from a micro-tip column. The capacity determined from the overnight batch experiment with 90  $\mu$ L of adsorbent agrees well with the column  $DBC_{50\%}$  ( $<1\%$  difference) as do the capacities determined by micro-tip adsorption ( $<16\%$  difference). It is also worth noting that the static capacity determined with the 10- $\mu$ L micro-tip column procedure is within 7 % of the micro-tip batch experiment in which the adsorbent was extracted from the 10- $\mu$ L micro-tip column and then mixed with the protein solution in a microcentrifuge tube. This suggests that despite their operating differences, the micro-tip and micro-batch formats yield comparable results given sufficient incubation time and accurate determination of adsorbent volume.

The binding capacities determined from the micro-tip experiments do, however, vary slightly with scale, trending lower with increasing micro-tip bed volume. This trend is most likely attributed to slight inaccuracies in the determination of adsorbent volumes, which may be exacerbated at very low adsorbent volumes. For example, an error of only two microlitres for a nominal bed volume of 10  $\mu$ L will translate into a 20% error. This error would be a systematic but consistent and therefore should be considered when doing microscale experiments at very low adsorbent volumes. The observed differences may also be partially explained by differences in the sample concentration and its determination as well as by differences in the phase ratio.

**Table 4.2.** Determination of the maximum equilibrium binding capacity ( $q_m$ ) for hulgG on UNOphe S by micro-tip and micro-batch adsorption methods. Also compared is the approximate maximum binding capacity ( $DBC_{50\%}$ ) as determined by column chromatography for a 1 mg/mL antibody solution flowing at 60 cm/h ( $T_R = 5$  minutes).

Method	Scale ( $\mu$ L adsorbent)	Phase Ratio ( $\mu$ L sample / $\mu$ L adsorbent)	Adsorbent Capacity (mg/mL)
Batch Mixing	7.7 <sup>a</sup>	90	$38.9 \pm 0.6$
Batch Mixing	10 <sup>b</sup>	90	$53.5 \pm 1.0$
Batch Mixing	90 <sup>c</sup>	11	$44.4 \pm 4.4$
Micro-Tip	10	90	$49.8 \pm 1.7$
Micro-Tip	40	20	$44.6 \pm 1.1$
Micro-Tip	80	10	$37.5 \pm 4.1$
$DBC_{50\%}$ <sup>d</sup> (1-mL column)	1000	N/A	44.3

a) Resin volume determined using the Atoll ResiQuot device (7.7- $\mu$ L resin plaques).

b) Adsorbent quantitatively extracted from the 10- $\mu$ L micro-tip column and used for batch adsorption.

c) 180  $\mu$ L of a 50% (v/v) slurry in loading buffer was pipetted to achieve a resin volume of 90  $\mu$ L.

d)  $DBC_{50\%}$  represents the approximate equilibrium adsorbent loading.

### 4.3. Batch Uptake Experiments

#### 4.3.1. Finite-Bath Experiments

The mass transport properties of an adsorbent are often studied by performing batch uptake experiments in a well-mixed vessel, such as a stirred tank or agitated microwell. In these experiments, a small volume of sample (generally <3% over the course of the experiment) is withdrawn at different time intervals to determine the adsorbate concentration, or a small solution stream is passed through an in-line concentration detector such as a UV spectrophotometer. Alternatively, these experiments can be carried out in parallel using a 96-well microtitre filterplate, in which a different timepoint is represented per well (Bergander et al., 2008). The ratio of adsorbent volume to sample mass in these experimental set-ups is such that the mass of sample available to bind is moderately in excess; consequently, the

sample concentration decreases over the course of the experiment. This set-up is therefore referred to as a finite-bath approach, in contrast to an infinite bath approach, where the concentration changes only negligibly throughout the experiment. The protein uptake (described as  $C/C_0$ ; or fractional approach to equilibrium,  $q/q_m$  or  $F$ ; or solid-phase concentration,  $q$ ) is then plotted as a function of time. These data can be used qualitatively for screening resins or quantitatively for studying mass transport and modelling column DBC (Chase, 1984; Arve and Liapis, 1987; Skidmore et al., 1990; Chang and Lenhoff, 1998; Hahn et al., 2005B; Bak et al., 2007; Bergander et al., 2008).

An experimental design for carrying out batch uptake experiments with micro-tip columns is illustrated in Figure 4.2. In this set-up, the sample volume, flow rate, and starting concentration are held constant, while the number of aspiration-dispense cycles for each micro-tip column is varied from high to low to generate a range of loading times. Delay times were not used when carrying out these uptake experiments so as to maintain continuous flow during loading. (The flow-rate correction strategy described in Section 3.4.2.2 was used to adjust for the initial delay in flow.) The experiment is carried out such that the micro-tip column being exposed to the longest load time (most cycles) begins first (tip one in Figure 4.2A). After a specified number of cycles (sixteen in Fig. 4.2A), the second tip begins, and then after an additional number of cycles (eight in Fig. 4.2A), tip three begins, and so on. An example of an uptake curve generated using micro-tip columns is shown in Figure 4.2B. In this example, each cycle represents a contact time ( $T_C$ ) of 0.625 min and a column residence time ( $T_R$ ) of 7.5 s.

Residence time and contact time must both be considered in micro-tip chromatography because of its packed-bed format, as discussed in Chapter 3. Micro-tip residence time, as defined by Equation 3.4, is the ratio between the micro-tip bed volume and the volumetric flow rate multiplied by the total number of pipetting steps, whereas contact time (Equation 3.5) is the total incubation time that the sorbent is in contact with the sample (total loading time). The contribution of micro-tip contact time and residence time to the overall binding kinetics can be assessed from experiments using different bed volumes since the ratio of  $T_C:T_R$  will vary as

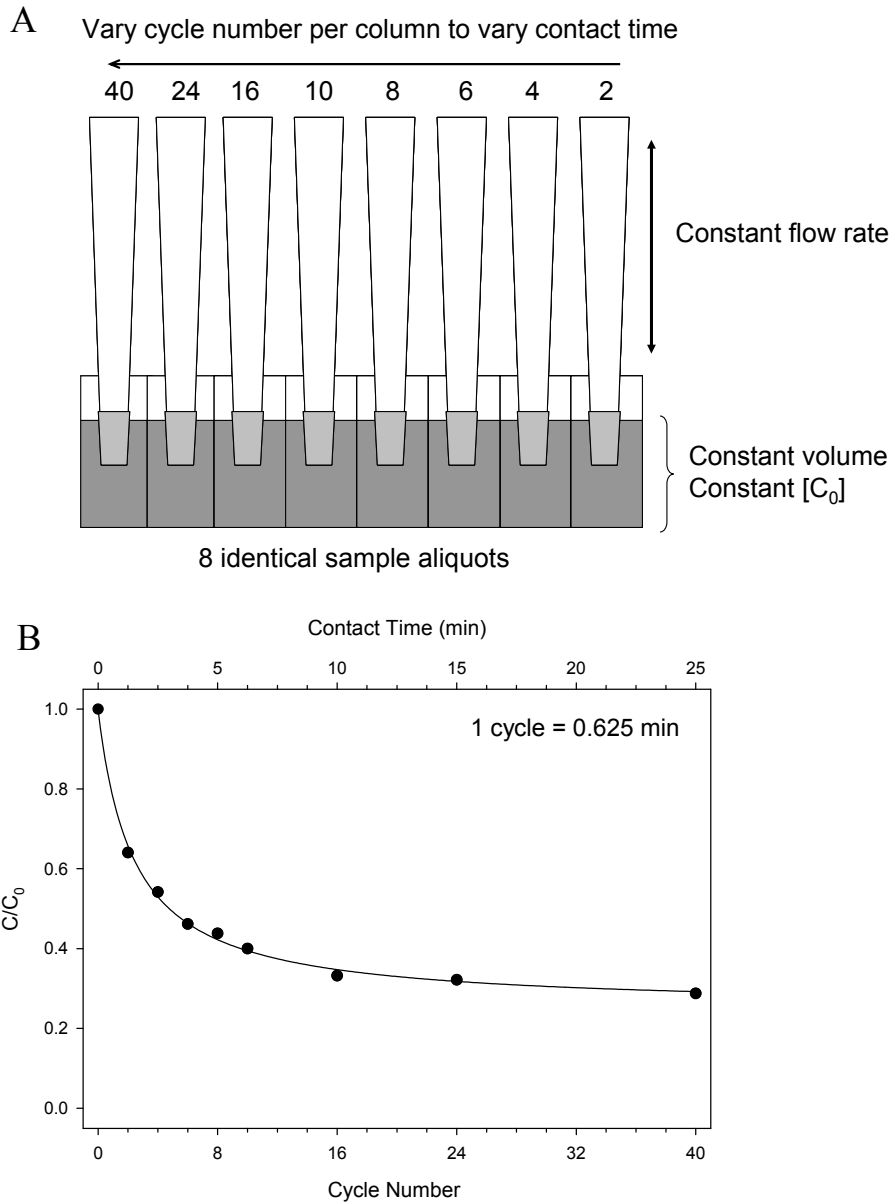


**Figure 4.2.** Micro-tip method for performing batch uptake experiments (carried out on a Tecan workstation). **(A)** Schematic of set-up. The micro-tip column volume, sample volume, sample concentration, and pipetting flow rate are held constant, while the number of aspiration-dispense cycle is varied across the eight tips. **(B)** Uptake curve of a 10 mg/mL huIgG solution (volume = 0.2 mL) onto the Sepharose FF cation exchange adsorbent. Forty-microlitre columns were used in this experiment, flowing at an average linear velocity of 864 cm/h (0.64 mL/min). The contact time (load time) per cycle is 0.625 minute, while the residence time is 7.5 s. The uptake curve is fit with an empirical equation (3-parameter hyperbolic decay equation):

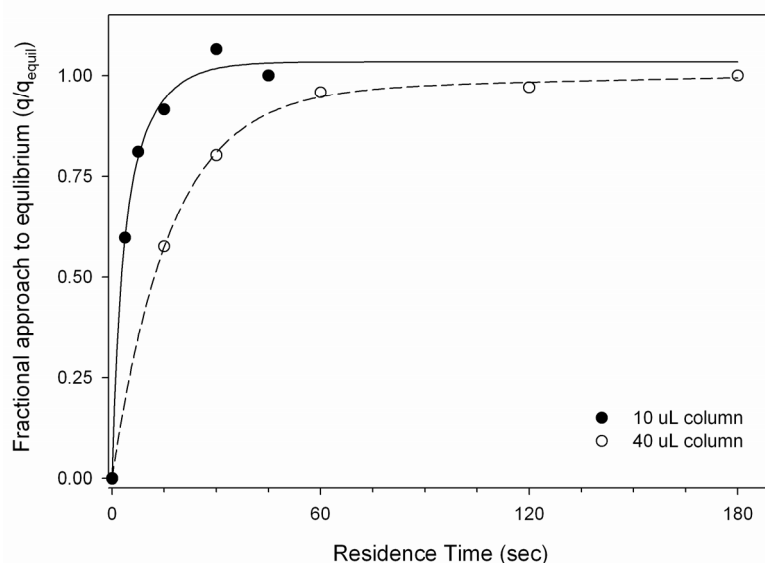
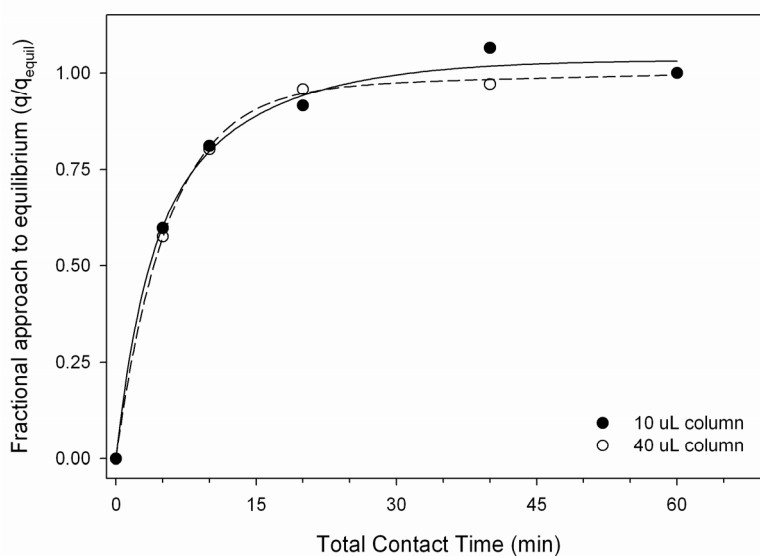
$$\frac{C}{C_0} = y_0 + \frac{ab}{b+x}$$

defined by Equation 3.8:

$$T_R = \frac{V_A}{V_S} \times T_C . \quad \text{Equation 3.8}$$

For example, at a fixed contact time, flow rate, and sample volume, the residence time of the 40-μL column is four times longer than that of the 10-μL column. In Figure 4.3, the fractional approach to equilibrium ( $q/q_{\text{equil}}$ ) for the test huIgG onto UNOsphere S is shown as a function of residence time (Fig. 4.3A) and of contact time (Fig. 4.3B) at both the 10- and 40-μL scales. Here,  $q$  is the binding capacity at each pre-equilibrium time point (i.e. derived from the *pre-equilibrium* adsorption isotherm), whereas  $q_{\text{equil}}$  is the capacity determined from the adsorption isotherm at 60 minutes (contact time). As observed in Figure 4.3, when uptake is plotted as a function of residence time, the uptake curves differ significantly between the 10- and 40-μL scales, with the uptake seemingly faster at the 10-μL scale. However, the expectation is that the fractional approach to equilibrium should be comparable between the two scales given that the selected binding conditions for each are in the nonlinear portion of the adsorption isotherm. In contrast, when plotted as a function of contact time, the curves overlay closely, despite the four-fold difference in residence time.

These data imply that contact time, not residence time, is the more critical parameter for carrying out kinetic experiments by micro-tip chromatography, at least in the case of a globular protein such as an immunoglobulin binding to a porous cation-exchange adsorbent. This agrees with the observations by Bergander et al. (2008) in their batch adsorption studies in microwells, where equating the batch incubation time to the total column loading time was found to be critical for predicting column dynamic binding capacity. Furthermore, this is consistent with many quantitative studies of protein transport in porous ion-exchange adsorbents in which protein uptake is best described by diffusive theories (Helfferrich, 1965; Ruthven, 2000; Dziennik et al, 2003 and 2005), with the most commonly employed being the pore diffusion and homogeneous diffusion (solid diffusion) models (Lenhoff, 1987; Skidmore et al., 1990; Fernandez et al., 1996; Chang and Lenhoff, 1998; Carta et al., 2005; Dziennik et al, 2005).

**A****B**

**Figure 4.3.** Binding of a hulgG on UNOsphere S as a function of **(A)** residence time and **(B)** contact time using 10- and 40- $\mu\text{L}$  micro-tip columns. The ratio of residence time ( $T_R$ ) to contact time ( $T_c$ ) between the 10- and 40-  $\mu\text{L}$  columns varies by 4-fold:  $0.75 \text{ s } T_R / \text{min } T_c$  for the 10- $\mu\text{L}$  column and  $3.0 \text{ s } T_R / \text{min } T_c$  for the 40- $\mu\text{L}$  column. Here,  $q$  is the capacity at each pre-equilibrium timepoint, whereas  $q_{\text{equil}}$  is the capacity of the equilibrium adsorption isotherm (estimated from 60-min timepoint). Data is fit with an empirical equation (bi-exponential equation, exponential rise to maximum):  $F = A_1(1 - e^{-bx}) + A_2(1 - e^{-dx})$ .

Given a diffusive mechanism, the rate of intra-particle mass transport should be proportional to the effective pore diffusivity ( $D_e$ ) of the protein within the adsorbent pore network as defined in Equation 1.19:

$$D_e = k_p \frac{\varepsilon_p D}{\tau}, \quad \text{Equation 1.19}$$

where  $k_p$  is the pore hindrance parameter ( $<1$ ),  $\varepsilon_p$  is the intra-particle void fraction,  $D$  is the protein diffusivity, and  $\tau$  is the tortuosity factor ( $>1$ ). The pore hindrance parameter depends on the ratio of protein size to pore size, generally decreasing with increasing molecular size due to steric hindrance and viscous drag. Therefore, it should be lower for the ~150 kDa hIgG protein than for smaller globular proteins like lysozyme or ribonuclease, resulting in a lower value of  $D_e$ . For even a larger protein macromolecule such a virus-like particle (VLP), the hindrance parameter may be such that much of the pore volume becomes essentially inaccessible, especially since most commercial resins are optimised for proteins having diameters less than 5 nm. As a rule of thumb, resins with a pore size ten times larger than the biomolecule adsorbate are recommended for fast mass transfer (Muller, 2005). DePhillips and Lenhoff (2000) investigated the mean pore diameters of 14 cation exchange resins by inverse size exclusion chromatography and found that they ranged from 20-150 nm. Therefore, for VLPs, much of the adsorption presumably occurs only on the external surface of the adsorbent bead, potentially making micro-tip residence time a more significant factor in protein uptake than is the case for the test hIgG shown in Figure 4.3.

For the majority of monomeric and comparatively smaller multimeric proteins such as immunoglobulin, mass transfer rates are, however, primarily driven by intra-pore diffusive mechanisms when binding to porous preparative adsorbents. Therefore, batch uptake curves generated by micro-tip chromatography would be expected to approximate those of micro-batch adsorption even though the external mass transport properties differ. This indeed appears to be the case for the test hIgG used in this thesis, as observed in Figure 4.4. Although a slight difference (10.6%) in the maximum equilibrium adsorbent concentration ( $q_m$ ) is observed between the two formats, this is attributed more to experimental error in the determination of resin volume than to any operational differences. As stated before, an advantage of the

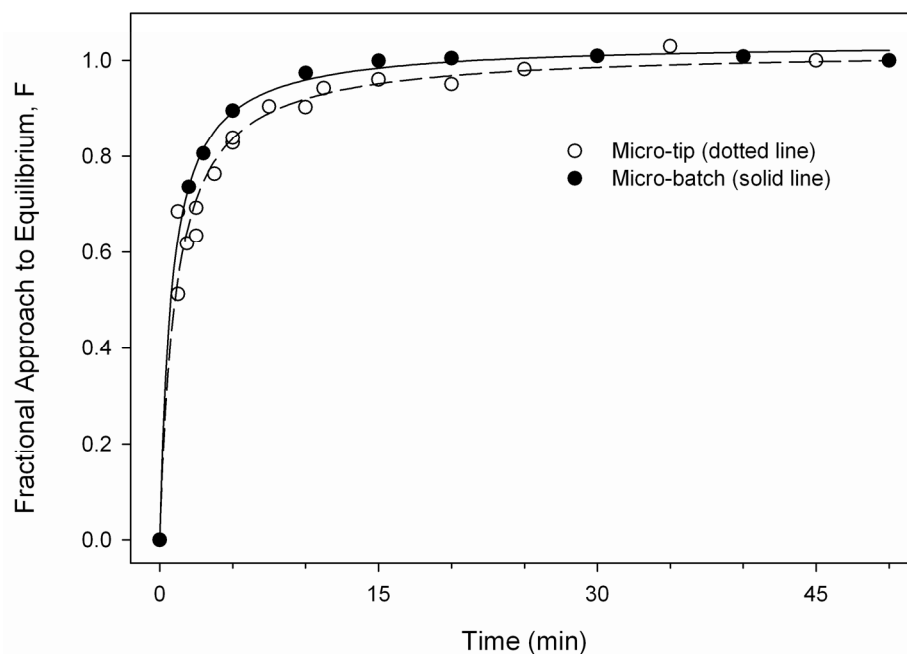


**Figure 4.4.** Comparison of batch uptake curves generated by micro-batch adsorption and micro-tip chromatography. In this experiment, 200  $\mu\text{L}$  of a 10 mg/mL solution of huIgG was applied to 40  $\mu\text{L}$  of UNOsphere S. The average flow rate of the micro-tip column was 864 cm/h (0.640 mL/min), with the duration (contact time) of one aspiration-dispense cycle equal to 37.5 s. A slight difference (10.6%) in the maximum equilibrium adsorbent concentration,  $q_m$ , was observed between the two formats. This is attributed to experimental error in the determination of adsorbent volume. Data is fit with an empirical equation of best fit (2-parameter, single rectangular hyperbolic function):

$$F = \frac{ax}{b+x}.$$

micro-tip column format is that mixing concerns are alleviated. This is particularly important for kinetic studies using dense adsorbents. The effects of agitation intensity on uptake rates in microwell adsorption experiments have been noted by a number of research groups (Bensch et al., 2005; Bergander et al., 2008; Kramarczyk et al., 2008), with the optimal intensity depending on well geometry, sample volume and viscosity, adsorbent particle density, and orbital amplitude. Incomplete adsorbent mixing can confound uptake measurements since the transfer from the bulk liquid to the chromatographic particles may become rate limiting when mixing is inadequate. This problem is avoided with micro-tip columns so long as the flow is evenly distributed through the packed bed.

Another potential advantage of micro-tip chromatography is that the effect of flow rate can be assessed independently of contact and residence time since the number of aspiration-dispense cycles can be adjusted with changing flow rate so as to keep  $T_C$  and  $T_R$  constant. The effect of a four-fold difference in linear velocity on the batch uptake kinetics of the test hIgG onto three different cation exchange adsorbents is shown in Figure 4.5. The uptake rate does appear to increase slightly at the higher flow rate for each adsorbent, most noticeably with SP Sepharose FF. This may be explained by the fact that the thickness of the laminar sublayer ( $\delta$ ) around the stationary phase particle should decrease with increasing flow rate, thereby reducing the external film mass transfer resistance. In addition, in the case of the POROS adsorbent, which has a bimodal pore distribution (Regnier, 1991), convective flow through the transecting macropores (600-800 nm in size) is promoted at higher superficial flow velocities, although some researchers have challenged this claim (Weaver and Carta, 1996). In the examples shown in Figure 4.5, the overall difference in uptake kinetics is minor, presumably because mass transfer in the network of diffusive pores is rate limiting.

An important caveat, however, to the observations above is that differences in microwell mixing and cycle number might also explain the observed differences with flow rate, and these effects would be most significant at very short contact times where the differences are their greatest. For the example shown in Figure 4.5, only two cycles are performed to obtain a contact time of five minutes (residence time of 1 minute) at the slower flow rate, whereas eight cycles are performed at the faster

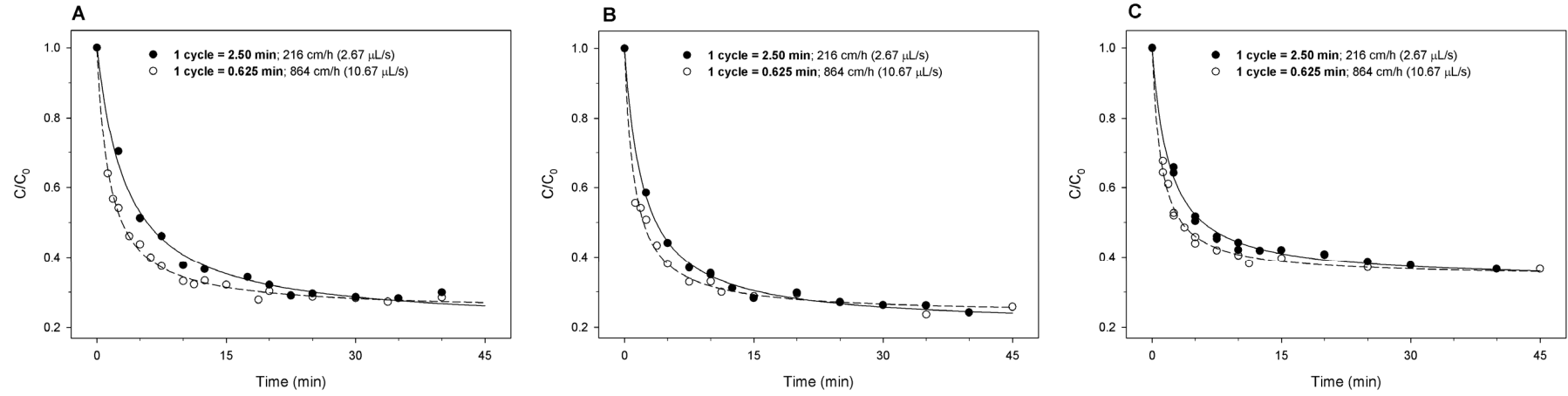


**Figure 4.5.** The effect of a four-fold difference in flow rate ( $\mu_{\text{avg}} = 216$  cm/h, solid circles; and 864 cm/h, open circles) on protein uptake for three different cation-exchange adsorbents: **(A)** SP Sepharose FF, **(B)** UNOsphere S, **(C)** POROS 50 HS. In these experiments, 200  $\mu\text{L}$  of a 10 mg/mL huIgG solution (pH 6.5 and conductivity  $\leq 3$  mS/cm) was loaded onto 40- $\mu\text{L}$  micro-tip columns. The aspiration-dispense cycle number is four times greater at the faster flow rate to maintain an equivalent contact time to that of the slower flow rate. The uptake curves are fit with an empirical equation (3-parameter hyperbolic decay equation):

$$\frac{C}{C_0} = y_0 + \frac{ab}{b+x}.$$

flow rate. The error from the microwell hold-up volume (volume not aspirated) contributes more significantly when only two cycles are performed as opposed to eight. Furthermore, mixing should be more efficient at faster flow rates since flow is more turbulent and because more cycles are performed per unit time. Whether or not these differences in uptake rates are attributable to operating conditions such as well mixing or due to difference in mass transfer resistance is not clear. However, given that pore diffusion appears to be the dominant mass transport resistance, it seems preferable to perform uptake experiments at higher flow rates than those recommended in Chapter 3 (i.e. perform at  $\geq 10 \mu\text{L/s}$ ). Although the flow may be more variable from column-to-column, higher flow rates allow for shorter time intervals to be studied, provide better microwell mixing, and ensure that fresh sample is continuously delivered to the chromatographic bead surface.

Batch uptake curves like the ones shown in Figure 4.6 are useful for making qualitative comparisons about the mass transport properties of adsorbents during resin screening. For the huIgG test system used in this thesis, the uptake onto the three CEX adsorbents is comparable when normalised for mass uptake (Fig. 4.6B), although the adsorbent capacities vary slightly (Fig. 4.6A). However, differences might be more apparent for other adsorbents or proteins. Quantitative approaches for modelling micro-tip batch uptake data for the prediction of DBC are described later in this chapter.

#### *4.3.2. Pre-Equilibrium Adsorption Isotherms*

The micro-tip method for adsorption isotherms allows data to be easily obtained as a function of time ( $T_C$  or  $T_R$ ), thereby providing an alternative perspective on mass transport in which uptake is examined across the entire concentration range of the isotherm. A modelling approach for predicting DBC from these pre-equilibrium data is discussed later in this chapter. These results can also be used qualitatively to compare adsorbent or mobile phase conditions, as shown in Figure 4.7. In this example, the binding of the test huIgG protein to UNOsphere S and POROS 50HS is examined. By visual assessment, the uptake rate appears to be slightly higher for the POROS adsorbent, as evidenced by the earliest timepoint. The average linear velocity is 3600 cm/h in these micro-tip experiments, which is well within the perfusive regime of the adsorbent and considerably higher than that used in Figure

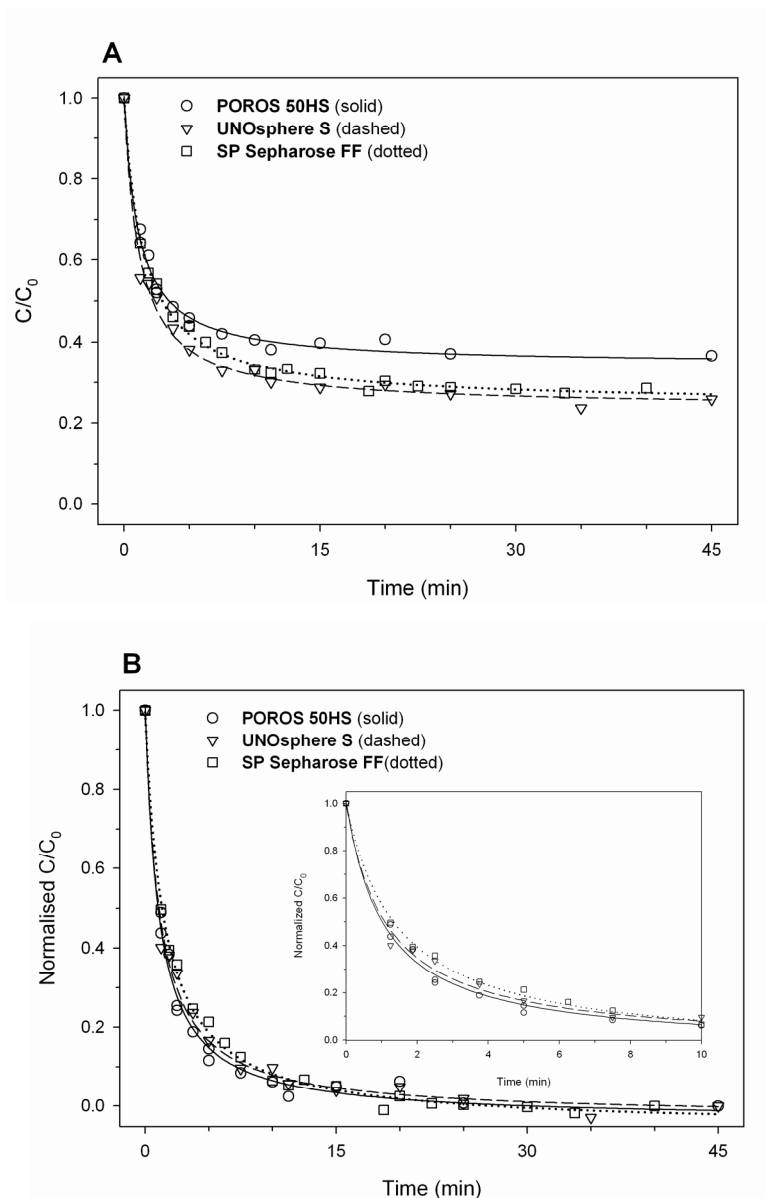


**Figure 4.6. (A)** Uptake ( $C/C_0$ ) of the huIgG test protein onto three different cation exchange adsorbents as a function of contact time ( $T_C$ ) using 40- $\mu$ L micro-tip columns. One aspiration-dispense cycle = 0.62 minutes; flow rate = 864 cm/h (0.64 mL/min). The uptake curves are fit with an empirical equation (3-parameter hyperbolic decay equation):

$$\frac{C}{C_0} = y_0 + \frac{ab}{b+x}.$$

**(B)** Normalised uptake curves (normalised to the uptake at final timepoint, 45 min, for each adsorbent). Inset provides a close-up view of the first ten minutes of uptake.

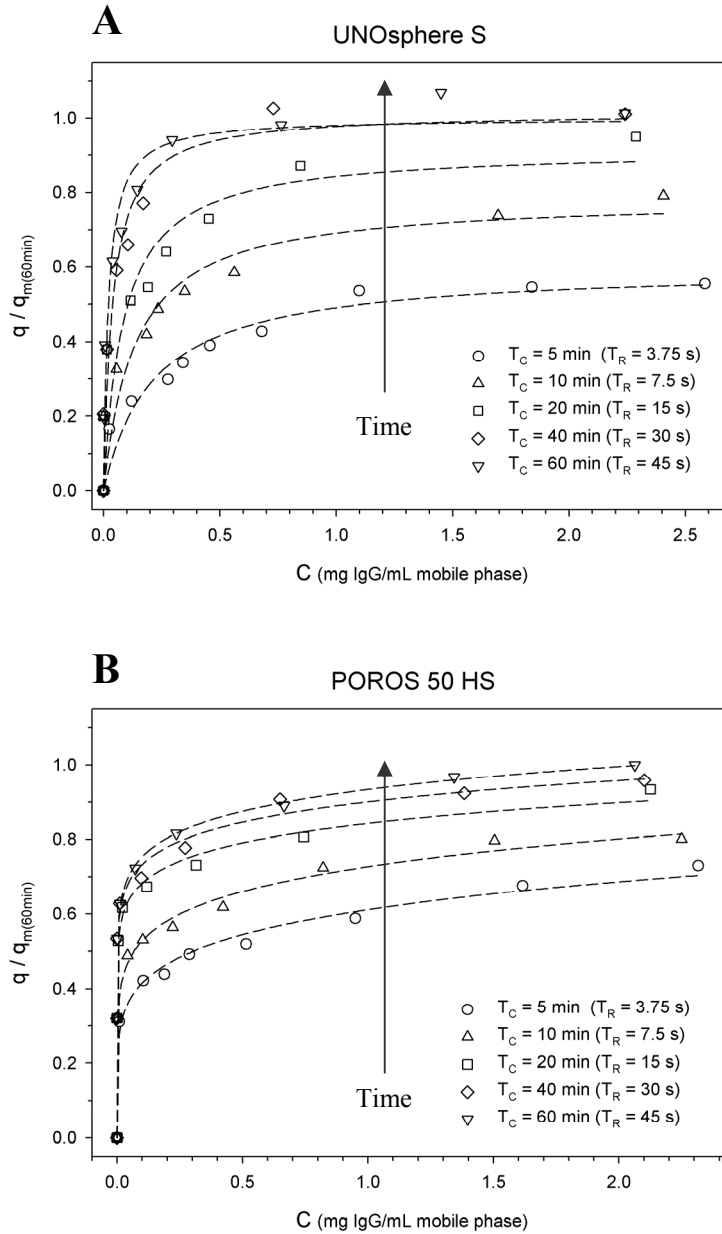


**Figure 4.7.** Pre-equilibrium ('dynamic') adsorption isotherms of the binding of the test huIgG to **(A)** UNOsphere S and **(B)** POROS 50HS strong cation exchange adsorbents. Ten-microlitre micro-tip columns were used in these experiments, loaded with 800  $\mu$ L of sample at varying starting concentrations ( $C_0$ ) and flowing at 18  $\mu$ L/s (3600 cm/h). The adsorption isotherms for the UNOsphere S adsorbent are best fit with a Langmuir model (Equation 1.3), while those for POROS 50HS are best fit with a Freundlich model (Equation 1.2). The data are normalised to the maximum adsorbent capacity ( $q_m$ ) determined from the 60-min timepoint.

4.6. It is interesting to note that the UNOsphere S isotherms are fit well with a Langmuir model, while those of the POROS 50HS are better fit with a Freundlich model. This presumably reflects differences in the binding mechanism and/or the uptake kinetics, and could perhaps be related to the bimodal pore distribution of the POROS adsorbent.

Pre-equilibrium adsorption isotherms can be graphed as either a function of contact time or residence time. However, as demonstrated in the batch uptake experiments in the previous section, the more relevant parameter is contact time, at least for the test system used in this thesis (huIgG binding to porous cation-exchange adsorbents). This finding is evident from the pre-equilibrium adsorption isotherm data shown in Figure 4.8. In these experiments, the micro-tip columns were operated at two different scales, 10- $\mu$ L and 40- $\mu$ L, such that the ratio of residence-time-to-contact-time varies by four-fold at constant load volume, flow rate, and cycle number. When controlling for residence time (30 s), the apparent protein uptake is considerably higher for the 10- $\mu$ L column (40 min contact time) than for the 40- $\mu$ L column (10 min contact time). However, when controlling for contact time (10 min), the dynamic adsorption isotherms overlay almost exactly despite a four-fold difference in residence time (7.5 s and 30 s, respectively).

#### *4.3.3. Shallow-Bed Adsorption*

An alternative to the finite-bath set-up described above is shallow-bed adsorption (Hahn et al., 2005A) in which the sample is re-circulated through a very small packed-bed column, usually of  $\leq 10 \mu\text{L}$ . Shallow-bed chromatography is operated in an infinite-bath format, which means that the feed sample is of a sufficiently high volume or concentration so that the sample concentration changes negligibly during protein uptake onto the adsorbent (i.e.  $C \approx C_0$  throughout the experiment). Specifically, according to Carta et al. (2005), the outlet concentration should be no less than 80% of the inlet concentration.

In a conventional shallow-bed experimental set-up, as shown in Figure 4.9A, a 10- $\mu$ L packed bed is connected to a pump which re-circulates the sample or buffer solution through the bed. Two valves are positioned in the flow circuit. One switches (nearly instantaneously) between the sample and equilibration, wash, and elution buffers, and

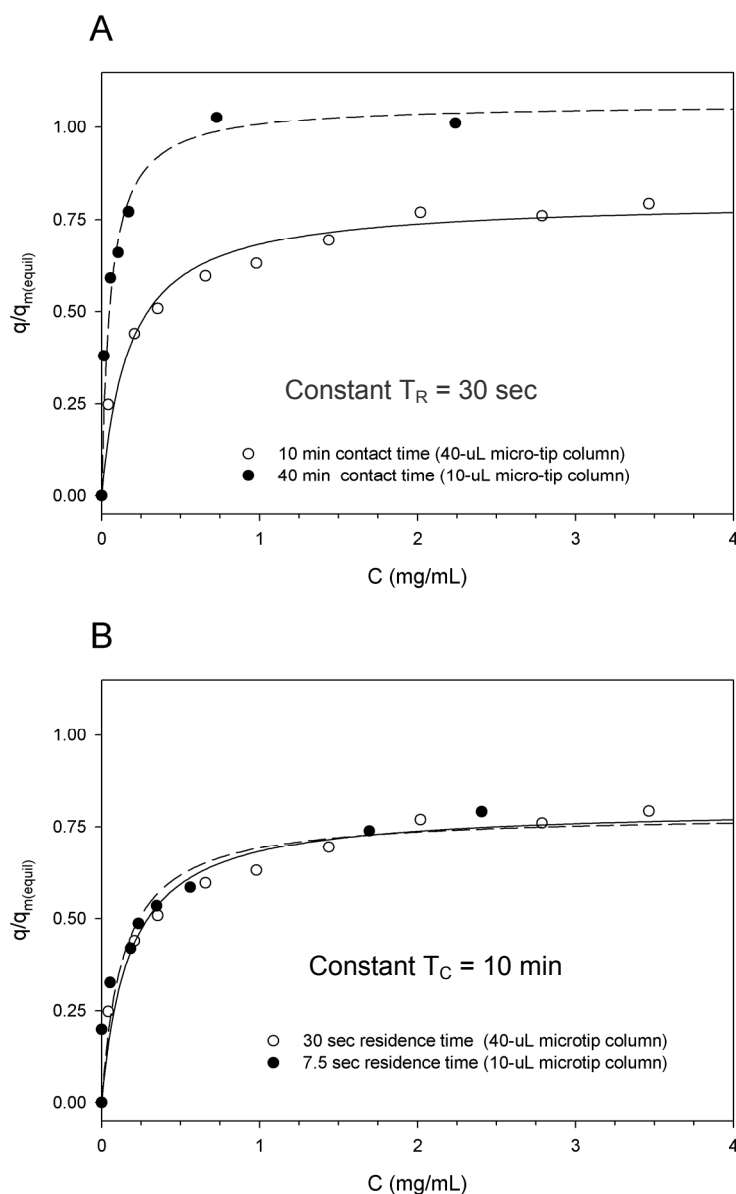
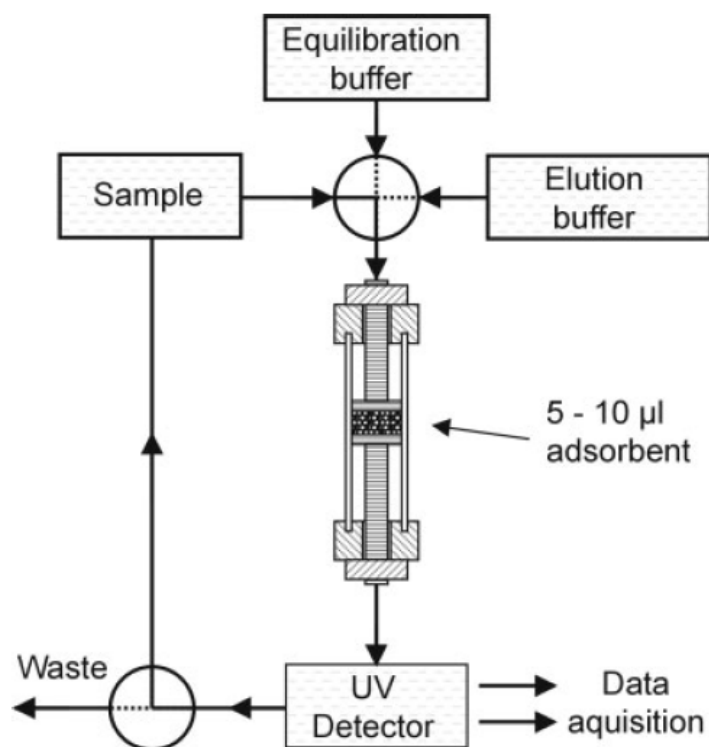


**Figure 4.8.** Pre-equilibrium adsorption isotherms (hulgG adsorption to UNOsphere S) using 10- and 40-μL columns as a function of **(A)** constant residence time ( $T_R$ ) = 30 s and **(B)** constant contact time ( $T_C$ ) = 10 min. The ratio of  $T_R$ :  $T_C$  is 4-fold higher for the 40-μL micro-tip column than for the 10-μL column, when loading at constant sample volume and flow rate. Data is fit with an empirical equation (2-parameter, single rectangular hyperbolic function):

$$\frac{q}{q_{m(equil)}} = \frac{ax}{b + x}.$$

**A**



**B**

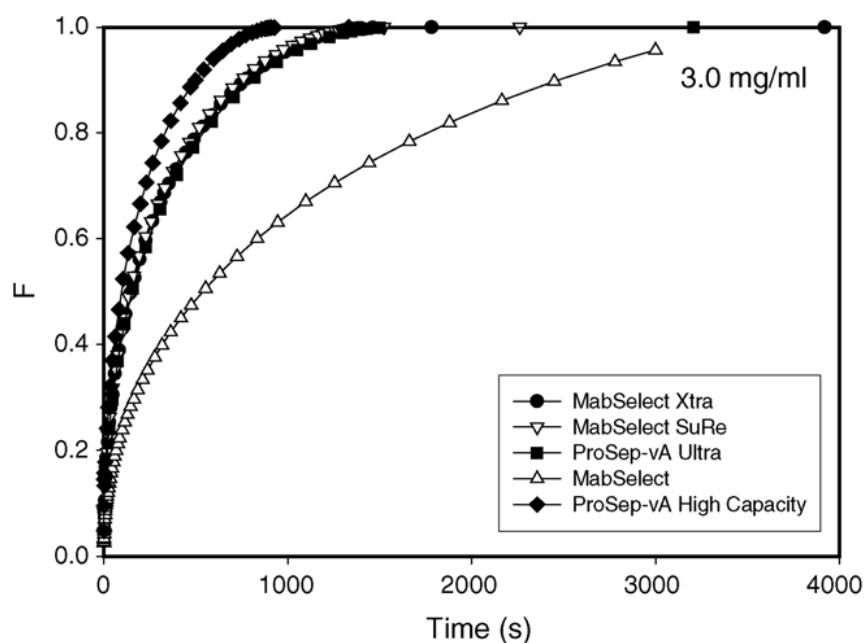


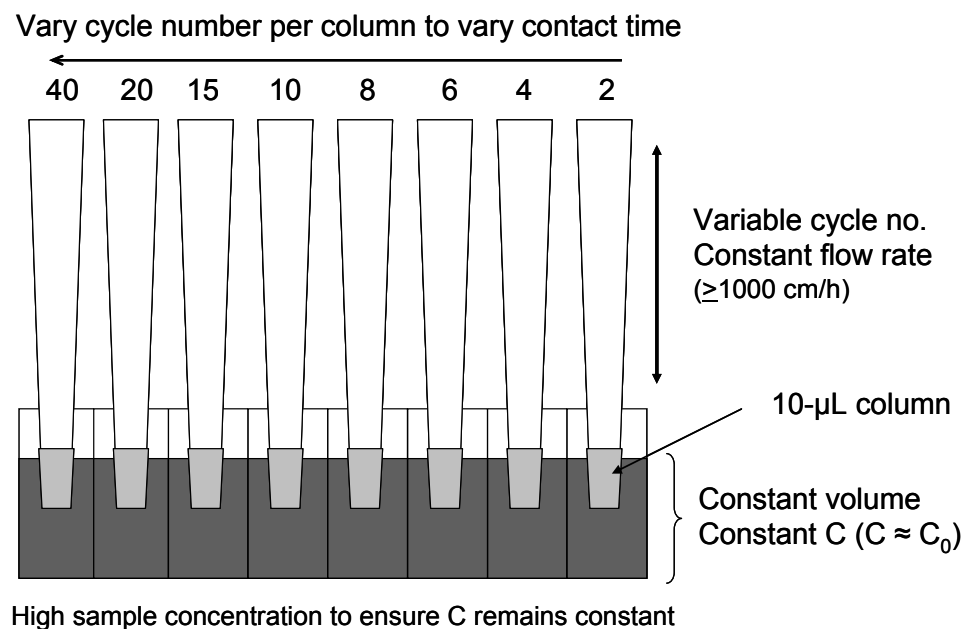
**Figure 4.9.** Conventional shallow-bed set-up and uptake curves: **(A)** Schematic of the shallow-bed set-up (figure from Hahn et al., 2005A); **(B)** Uptake curves of polyclonal IgG on Protein A affinity media from Hahn et al. (2005B).  $F$  is the fractional uptake to equilibrium ( $q/q_m$ ).

a second alternates between a UV detector and a waste outlet. The shallow-bed column is first equilibrated in loading buffer and then loaded with sample, which is re-circulated at a high flow rate for a specified amount of time. The high flow rate ensures that the feed concentration in the mobile phase remains constant throughout the run ( $C \approx C_0$ ). Carta (2005) indicates that under typical shallow-bed conditions, this usually requires flow velocities of  $\geq 600$  cm/h. Hahn et al. (2005B) used flow velocities of 1224 cm/h, and Fernandez et al. (1996) used flow velocities from 2250 to 5940 cm/h. After the specified loading time, the sample is washed out and then the column is eluted with an appropriate elution buffer. The amount of bound sample determined from elution is then plotted as a function of loading time to construct uptake curves and adsorption isotherms. Some examples from the literature (Hahn et al., 2005B) of uptake curves derived from shallow-bed experiments are shown in Figure 4.9B.

The micro-tip format appears to meet the critical conditions of shallow-bed chromatography. First, the 10- $\mu$ L micro-tip column is suitably sized for these experiments, and the protein concentration can be held constant during loading ( $C \approx C_0$ ) if a sufficiently high concentration is used. Second, the high linear velocities required for shallow-bed chromatography are well within the operating range of the micro-tip format (400 – 4000 cm/h for the 10- $\mu$ L column). Third, micro-tip chromatography also allows for rapid switching between column feeds by moving the pipette tip from one microwell to another, much like that of an in-line valve, although it may take a fraction of a second longer.

A schematic of the experimental set-up for carrying out shallow-bed adsorption with micro-tip columns is shown in Figure 4.10. Movement of the micro-tip columns between the microwells (containing equilibration buffer, sample, wash buffer, and elution buffer) serves essentially as a virtual valve in this set-up. Experiments can be carried out in parallel (eight-at-a-time), with a different loading time examined per micro-tip column. The contact times for the equilibration, wash, and elution steps are the same between micro-tip columns. The shallow-bed experiment is in many ways performed analogously to a finite-bath batch uptake experiment with the key distinction being that a higher sample concentration is required to ensure that the

### A) Micro-Tip Operation:



### B) Plate Layout:

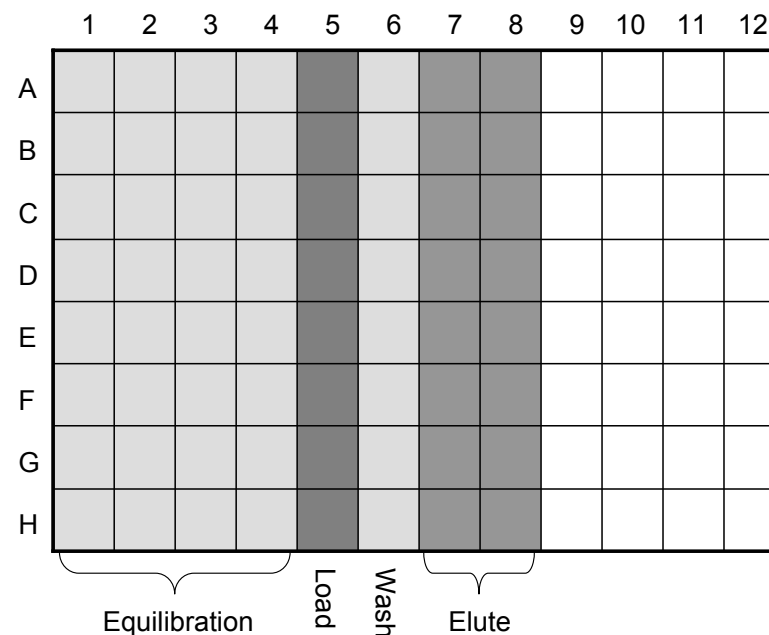


**Figure 4.10.** Scheme for performing shallow-bed adsorption (infinite-bath format) by micro-tip chromatography. **(A)** A constant volume is aspirated and dispensed rapidly through a 10- $\mu$ L column at  $\mu_{\text{avg}} \geq 1000$  cm/h. Contact time is varied by varying the aspiration-dispense cycle number. The starting sample concentration (mass challenge) must be sufficiently high so that it remains approximately constant throughout adsorption (<20% decrease). **(B)** The micro-tip columns can be rapidly switched between the equilibration (columns 1-4), load (column 5), wash (column 6) and elution (columns 7-8) by moving into a new microwell. The amount of adsorbed product is then determined by quantifying the amount of eluted product.

starting concentration does not change significantly (<20%) during adsorption. In addition, it is the eluted product, not the nonbound fraction that is assayed to determine the amount of protein uptake per unit time.

A limitation, however, of the micro-tip format for shallow-bed chromatography is that only a maximum of 0.9 mL can be aspirated into the micro-tip column. This in turn limits the low end of the sample concentration range that can be evaluated. In a conventional shallow-bed set-up, lower sample concentrations can be examined by increasing the re-circulating volume through the column, so that the total mass challenge to the adsorbent remains high. The high flow rate ensures that the local sample concentration around the chromatographic beads does not decrease significantly during loading. Although volumes greater than 0.9 mL can be placed in the microwell in micro-tip chromatography, only 0.9 mL can be aspirated through the pipette tip. Consequently, the full volume is not effectively re-circulated, since the sample, whose concentration may decrease across the aspiration step, must pass through the column again a second time during the dispense step before being returned to the remaining volume in the microwell.

Results from a micro-tip shallow-bed experiment examining the uptake of a polyclonal antibody from human serum onto a 10- $\mu$ L protein A (MabSelect) column is shown in Figure 4.11. The experiment was carried out with an antibody concentration of 10 mg/mL and a volume in the microwell of 1.0 mL (total mass = 10 mg). The flow rate was 1.2 mL/min ( $\mu_{\text{avg}} = 3960$  cm/h). The  $q_m$  of the adsorbent for this huIgG is about 65 mg/mL under these conditions. As a result, the feed concentration cannot theoretically decrease by more than 7%, even at the longest timepoint. The shape of the micro-tip uptake curve resembles those of the literature reference shown in Figure 4.9B (Hahn et al., 2005B). However, the literature example for MabSelect could not be reproduced identically because of several experimental constraints. First, the antibody concentration is more than three-fold higher in the micro-tip experiment (10 mg/mL) than in the literature example (3 mg/mL) because of the volume limitation of the micro-tip format (maximum aspiration volume of 0.9 mL requires a higher concentration to ensure that the sample concentration changes only minimally throughout the experiment). Second, the exact human polyclonal antibody sample used in the literature example could not

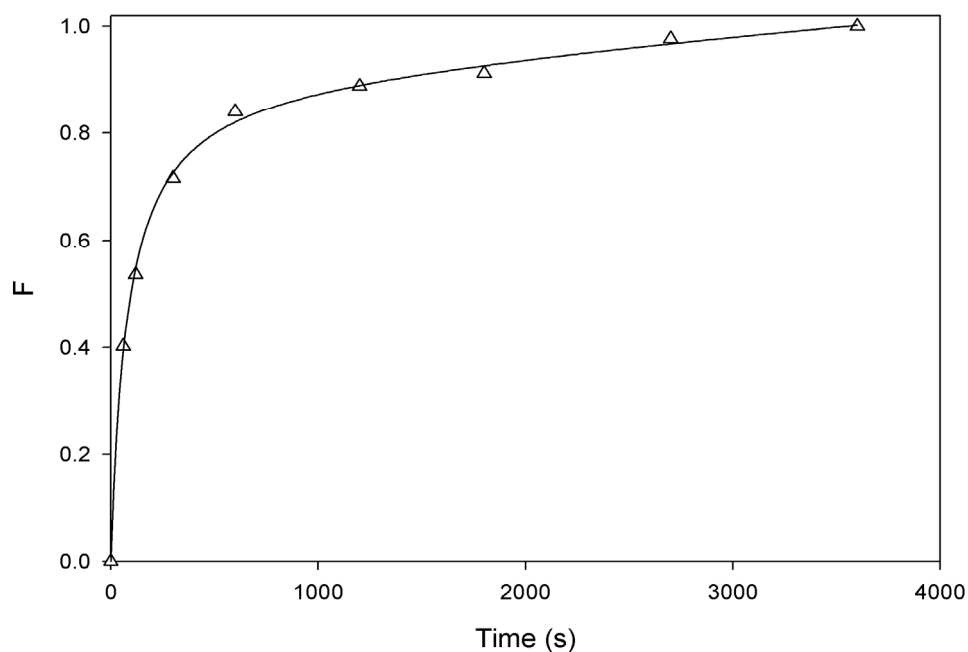


**Figure 4.11.** Uptake curve from a shallow-bed experiment using micro-tip columns. 10 mg/mL of polyclonal antibody from human serum (1.0 mL in well; 0.9 mL aspirated) was re-circulated through a 10- $\mu$ L MabSelect Protein A column at a flow rate of 20  $\mu$ L/s (average linear velocity of 3960 cm/h). Uptake data (F, fractional uptake to equilibrium capacity, equal to  $q/q_m$ ) fit with an empirical equation (3-parameter hyperbola):

$$F = \frac{ax}{b+x} + cx .$$

be obtained for the micro-tip experiment. The antibody was sourced from Sigma-Aldrich (St. Louis, MO, USA) in the micro-tip experiment and from Octapharma Pharmazeutische Produkte (Vienna, Austria) in the literature example. Consequently, these samples display somewhat different binding behaviour.

Shallow-bed operation appears to be a feasible format for use with micro-tip chromatography, although there are limitations with respect to sample concentration and volume. A key advantage in using micro-tip chromatography is its ability to be carried out in parallel on a robotic workstation. Acquiring shallow-bed experimental data then provides a path to predict DBC, using the appropriate models as reviewed by Hahn et al. (2005A). The shallow-bed approach, however, was not pursued further in this thesis, principally because of the constraint on sample concentration. Instead, two modelling approaches using finite-bath micro-tip data were examined for the prediction of column DBC. These are discussed in the sections below.

#### **4.4. Prediction of Dynamic Binding Capacity from Micro-Tip Column Data**

Predictive modelling of column adsorption offers the potential for reducing the sample amounts and experimental numbers that are required for the determination of dynamic binding capacity (DBC). Column breakthrough experiments, even when using small laboratory-scale columns, can consume gram quantities of product. The determination of DBC and its relationship to mobile phase composition, feed concentration, and flow rate is critical to characterising the productivity and economics of the chromatographic unit operation. A multitude of models have been applied to the prediction of DBC, ranging from simple staged equilibrium models to complex general rate models. Non-dispersive models such as those employed by Chase (1984), using the Thomas solution (Thomas, 1944), and Arnold et al. (1985), using the solutions by Hall et al. (1966), have been applied to predict adsorption processes for affinity chromatography. These models assume that a single rate-limiting step is driving the overall mass transport, such as the reaction kinetics of binding or pore diffusion. In contrast, multi-component general rate models, such as those by Arve and Liapis (1987), Gu et al (1993), and Kempe et al. (1999), attempt to account for multiple mass transfer resistances including film diffusion, pore diffusion, and reaction kinetics.

The rigorous evaluation and development of models for predicting column adsorption processes is outside the scope of this thesis. However, two data-driven approaches are examined below to demonstrate how micro-tip data might be applied to the prediction of DBC. The goal here is a pragmatic one, that being to predict laboratory-scale column DBC upon scale-up from micro-tip columns, rather than to elucidate mass transport mechanisms or predict the full shape of the breakthrough curve. The first model applies an approach used by Bergander et al. (2008), in which model parameters are estimated from batch uptake experiments using a shrinking-core pore diffusion model (Helfferich, 1965; Teo and Ruthven, 1986; Helfferich, 1990; Weaver and Carta, 1996; 2005; Dziennik et al., 2005). In this approach, the external mass transfer resistance is considered negligible in comparison to pore diffusion. The second modelling approach employs a simple staged-reaction model, in which adsorption is described by a series of batch adsorption stages, with the parameters from the *pre-equilibrium* Langmuir adsorption isotherms ( $q_m$  and  $K_D$  as a function of contact time) used to account for the adsorption kinetics.

#### 4.4.1. Modelling Data from Batch Uptake Experiments

##### 4.4.1.1. Modelling Approach

Bergander et al. (2008) were able to predict the DBC of a human polyclonal IgG on a MabSelect SuRe column (1-mL HiTrap) from microwell batch uptake data with good agreement. By doing so, the micro-batch adsorption format yielded a ten-fold savings in time and a fifty-fold savings in sample consumption. In their approach, they used a shrinking core model to approximate intra-particle mass transfer by pore diffusion, while external mass transfer resistances were assumed to be negligible. The shrinking core model assumes a favourable rectangular adsorption isotherm, and therefore pore binding occurs with a sharp uptake front, with this front moving inward with increasing load. Uptake ( $q/q_m$ ) is then modelled by (Teo and Ruthven, 1986; Weaver and Carta, 1996):

$$\frac{D_e C_0}{R_p^2 q_m} t = \left(1 - \frac{1}{Bi}\right) I_2 - I_1, \quad \text{Equation 4.1}$$

where

$$I_1 = \frac{1}{6\lambda\Lambda} \ln \left[ \frac{\lambda^3 + \eta^3}{\lambda^3 + 1} \left( \frac{\lambda + 1}{\lambda + \eta} \right)^3 \right] + \frac{1}{\lambda\Lambda\sqrt{3}} \left[ \tan^{-1} \left( \frac{2\eta - \lambda}{\lambda\sqrt{3}} \right) - \tan^{-1} \left( \frac{2 - \lambda}{\lambda\sqrt{3}} \right) \right] \quad \text{Equation 4.1a}$$

$$I_2 = \frac{1}{3\Lambda} \ln \left( \frac{\lambda^3 + \eta^3}{\lambda^3 + 1} \right) \quad \text{Equation 4.1b}$$

$$\Lambda = \frac{V_M q_m}{V_S C_0} \quad \text{Equation 4.1c}$$

$$\eta = \left( 1 - \frac{\bar{q}}{q_m} \right)^{1/3} \quad \text{Equation 4.1d}$$

$$\lambda = \left( \frac{1}{\Lambda} - 1 \right)^{1/3} \quad \text{Equation 4.1e}$$

$$Bi = \frac{k_f R_p}{D_e} \quad \text{Equation 4.1f}$$

In these equations,  $D_e$  is the effective pore diffusivity,  $R_p$  is the particle radius,  $k_f$  is the film mass transfer coefficient,  $V_M$  is the volume of the matrix particles,  $V_S$  is the volume of the supernatant (mobile phase),  $q_m$  is the maximum adsorption capacity (equilibrium adsorption capacity),  $q$  is the concentration of the bound protein, and  $C_0$  is the feed concentration.

The column DBC using this approach is then predicted using the following equation (Carta et al., 2005; LeVan et al., 2008):

$$DBC_{10\%} = \frac{q_m C_0}{K_D + C_0} \times \begin{cases} 0.364N - 0.0612N^2 + 0.0042N^3 & \text{for } N < 2.75 \\ 1 - 1.03N^{-1} & \text{for } N \geq 2.75 \end{cases} \quad \text{Equation 4.2}$$

where  $DBC_{10\%}$  is the dynamic binding capacity at 10% breakthrough and  $K_D$  is the equilibrium dissociation constant, respectively.  $N$  is the number of pore transfer units as defined by:

$$N = \frac{15(1 - \varepsilon) D_e T_R}{R_p^2} \quad \text{Equation 4.2a}$$

where  $\varepsilon$  is the bed void fraction, and  $T_R$  is the apparent residence time in a column defined as the ratio between the column length and superficial velocity of the mobile phase.

#### 4.4.1.2. Application of Model to Micro-Tip Data

The modelling approach of Bergander et al. (2008) described above was applied to data from finite-bath micro-tip experiments for the prediction of  $DBC_{10\%}$  in the test

case of the binding of hulgG to a 1-mL UNOsphere S column. Micro-tip adsorption isotherm and batch uptake experiments like those shown in Figures 4.1 and 4.2 were performed. The adsorption isotherm was favourable under the conditions of loading (pH 6.5 and conductivity  $\leq 3$  mS/cm) and, as recommended by Bergander et al. (2008), the phase ratio and initial protein concentration in the batch uptake experiments were such that the decrease in bulk protein concentration was  $\leq 80\%$ . The effective pore diffusivity was approximated at different feed concentrations and flow rates using the shrinking core model as described above, and the  $DBC_{10\%}$  was then predicted. The key model inputs are given in Table 4.3. MATLAB version 7 (The Math Works Inc., MA, USA) was used for the model computations. The feed concentration in the experimental column experiments was 1.0 mg/mL, and the column was run at five different flow rates. No correction was made for column bed compression given the rigidity of the UNOsphere resin.

**Table 4.3.** Key model parameter inputs to predict  $DBC_{10\%}$  from micro-tip data using the approach outlined by Bergander et al. (2008).

Input Parameter	Definition	Value	Source
$q_m$	Equilibrium binding capacity	46.1 mg/mL	Adsorption isotherm from micro-tip chromatography
$K_D$	Isotherm dissociation constant	0.058 mg/mL	Adsorption isotherm from micro-tip chromatography
$R_p$	Particle radius	0.004 cm	Vendor (Bio-Rad) literature
$\epsilon$	Bed voidage fraction	0.4	Standard assumption from literature
$V_S$	Supernatant feed volume	0.8 cm <sup>3</sup>	Original data set
$V_m$	Volume of matrix particles	0.01333 cm <sup>3</sup>	Original data set
$MW$	Molecular weight	150,000	Assumed for IgG
$\mu_{avg}$	Micro-tip superficial average linear velocity	0.82 cm/s	Original data set
$\nu$	Kinematic viscosity	0.01 cm <sup>2</sup> /s	Assumed to be the same as water

In Table 4.4, the predicted values are compared to the experimentally generated breakthrough data from a 1-mL column having a 0.5 cm internal diameter (i.d.) and a 5.0 cm height (h). These results are also depicted graphically in a parity plot, shown in Figure 4.12. The prediction of DBC is adequate across the range examined, with the slope of the line almost equal to one, although the parity appears to diverge most at the limits of this range. This suggests some inaccuracies in the assumptions used in the model. The error is highest at conditions of low binding capacity (29% at  $T_R = 0.5$  min, but is <20% across the remainder of the capacity range). If the data is not fit through the origin, a good empirical correlation is observed (dashed line in Fig. 4.12;  $R^2 = 0.95$ ). However, the use of an empirical correction factor would require one or more column breakthrough experiments to be carried out to establish this relationship.

**Table 4.4.** Comparison of predicted  $DBC_{10\%}$  modelled from micro-tip data to that of the experimental column data (1-mL column; 0.5 cm, *i.d.*, x 5.0 cm, *h*;  $C_0 = 1$  mg/mL) for binding of hulgG to UNOsphere S. The modelling approach used by Bergander et al. (2008) for micro-batch adsorption was applied here. Model parameters are given in Table 4.3. Using the shrinking core model<sup>a</sup>,  $D_e = 5 \times 10^{-8}$  cm<sup>2</sup>/s.

<b>Flow Rate</b>	<b>Linear Velocity</b>	<b><math>T_R</math></b>	<b>Predicted <math>DBC_{10\%}</math></b>	<b>Experimental <math>DBC_{10\%}</math></b>	<b><math>\Delta</math></b>
mL/min	cm/h	min	mg/mL	mg/mL	
2.0	600	0.5	10.9	15.4	-29%
1.0	300	1.0	18.7	23.1	-19%
0.67	200	1.5	24.0	27.3	-12%
0.50	150	2.0	30.3	28.9	5%
0.20	60	5.0	38.3	33.1	16%

a)  $D_e$  was determined using a shrinking core model described by Carta and Weaver (1996) by iterating upon its value in the simulated uptake curve across a range of  $10^{-8}$  to  $10^{-4}$ . The final  $D_e$  value selected was that which minimised the root mean square between the experimental (micro-tip batch data) and modelled values.

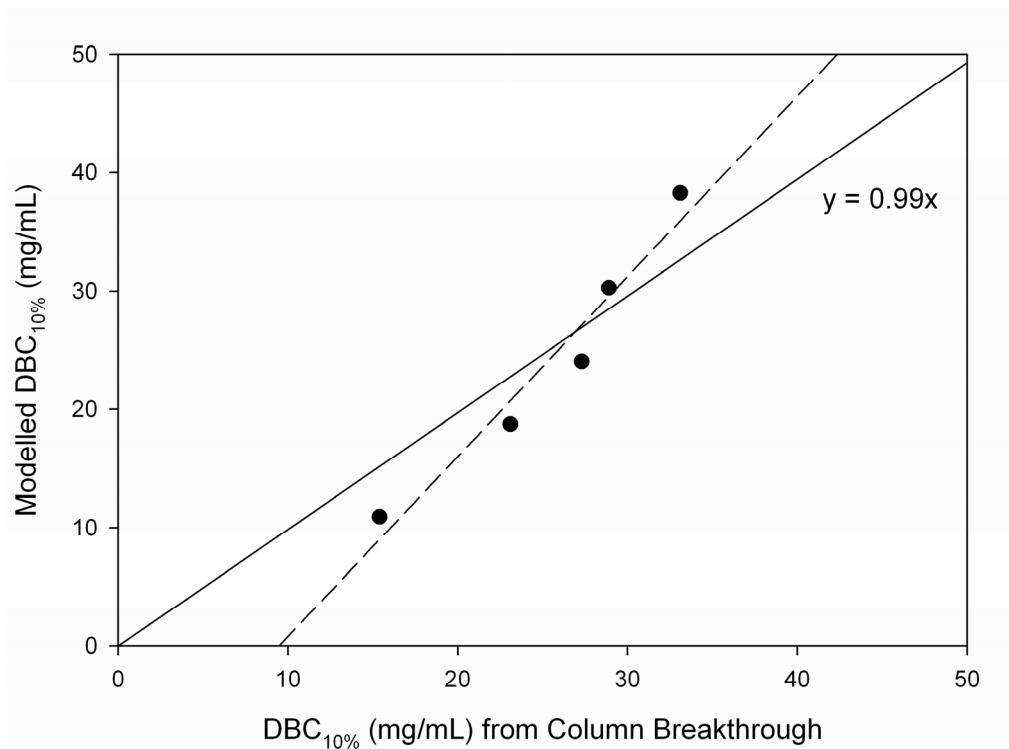


**Figure 4.12.** Parity plot comparing the predicted DBC<sub>10%</sub> of huIgG on UNOsphere S to experimental column breakthrough data (from data shown in Table 4.4). Modelling was performed using the approach by Bergander et al., 2008. The experimental DBC<sub>10%</sub> was generated using a 1-mL column (0.5 cm, i.d., x 5 cm, h) with a huIgG concentration of 1 mg/mL. The effective pore diffusivity ( $D_e = 5 \times 10^{-8}$ ) was determined from micro-tip batch uptake data using the shrinking-core model. The solid line is the linear fit constrained through the origin, yielding a slope of 0.99. The dashed line is the linear fit with no constraints:  $y = 1.52x - 14.43$  ( $R^2 = 0.95$ ).

There are some important limitations to this approach because of the simplifying assumptions of the model. The shrinking core model implies a highly favourable rectangular isotherm. This requirement appears to be met for the binding of huIgG on UNOsphere S in the mobile phase conditions examined (Fig. 4.1B). This may not always be the case though for varying mobile phase compositions, i.e. higher salt concentration, or different proteins. Ruthven (2000), however, suggests that a rectangular model may still provide a useful approximation for many situations, even when the form of the actual isotherm is not rectangular. The modelling approach here is also less useful at low protein concentration and/or low phase ratios (as discussed by Bergander et al., 2008), since some of the terms of the model breakdown. Specifically, the model requires that the numerator in the following term used in the shrinking core model match or exceed the value of the denominator:

$$\frac{1}{\Lambda} = \frac{V_s C_0}{V_m q_m} \geq 1 .$$

In other words, this means that the total amount that could ever bind under saturation in the prevailing buffer conditions should be exceeded or equalled by the quantity initially present in the bulk phase. In the test system examined here, where  $V$  was  $0.8 \text{ cm}^3$  and  $V_m$  was  $0.01333 \text{ cm}^3$ , this condition was not met when  $C_0$  was  $<0.8 \text{ mg/mL}$ . Despite these limitations, this modelling approach shows a reasonable agreement to the experimental data across the flow rate ranges examined.

#### 4.4.2. Modelling Data from Pre-Equilibrium Adsorption Isotherms

##### 4.4.2.1. Modelling Approach

A staged reaction model was evaluated as a second approach for predicting DBC from micro-tip data, using the Langmuir parameters of  $q_m$  and  $K_D$  from *pre-equilibrium* isotherm data to account for the kinetics of adsorption. A staged reaction model simplistically relates a chromatographic column to a series of stirred tank reactors (STRs), in which the column is divided into  $n$  batch adsorption stages. The column feed is then treated incrementally in stages, with each element equivalent to the flow velocity multiplied by the STR residence time. The residence time of each STR is calculated from the vessel height, bed voidage, and linear velocity. The mass balance equation and the adsorption isotherm relationship are

then used to calculate the bound adsorbate concentration for the residence time of each stage.

For example, as was done in this thesis, the model can be used to treat a 1-mL packed column as four 0.25-mL STRs having Langmuir adsorption behaviour. Increasing the number of stages beyond four did not significantly change the shape of the modelled breakthrough curve for the test system (hulIgG binding to UNOsphere S) used in this thesis. The sample concentration,  $C$ , is obtained by treating each STR as a batch adsorption with  $C_0$  being the concentration of the starting material for the first stage and then of the preceding stage for all subsequent stages. The adsorbent loading,  $q$ , is also obtained for each STR by mass balance. Each 0.25-mL addition of starting material to the first STR then takes into account the material already adsorbed and is iterated accordingly. A modified version of the batch adsorption equation is used for each sample volume addition as follows,

$$C = \frac{\left( -b + \sqrt{b^2 + 4 \left( \frac{V_A}{V_T} q^o + C_0 \right) K_D} \right)}{2} \quad \text{Equation 4.3}$$

$$b = \left( K_D + \frac{V_A}{V_T} (q_m - q^o) - C_0 \right), \quad \text{Equation 4.3a}$$

where  $q^o = q$  from the previous iteration (sample volume addition),  $C_0 = C$  from the previous STR,  $K_D$  and  $q_m$  are derived from the Langmuir adsorption isotherm,  $V_A$  is the volume of adsorbent used, and  $V_T$  is the total tank volume (liquid + adsorbent). In this thesis, since a packed bed system using a highly porous adsorbent is being modelled,  $V_A/V_T$  was assumed to be one. The breakthrough curve is then plotted as the protein concentration leaving the final STR (y-axis) against the loading volume (x-axis). An example of this is shown in Figure 4.13, in which  $K_D$  is varied.

A somewhat similar approach was taken by Howard Chase (1984) in the prediction of packed column adsorption for preparative affinity chromatography (adsorption of lysozyme to Cibacron Blue-Sepharose and  $\beta$ -galactosidase to an immobilised antibody column). To model column adsorption rates and account for mass

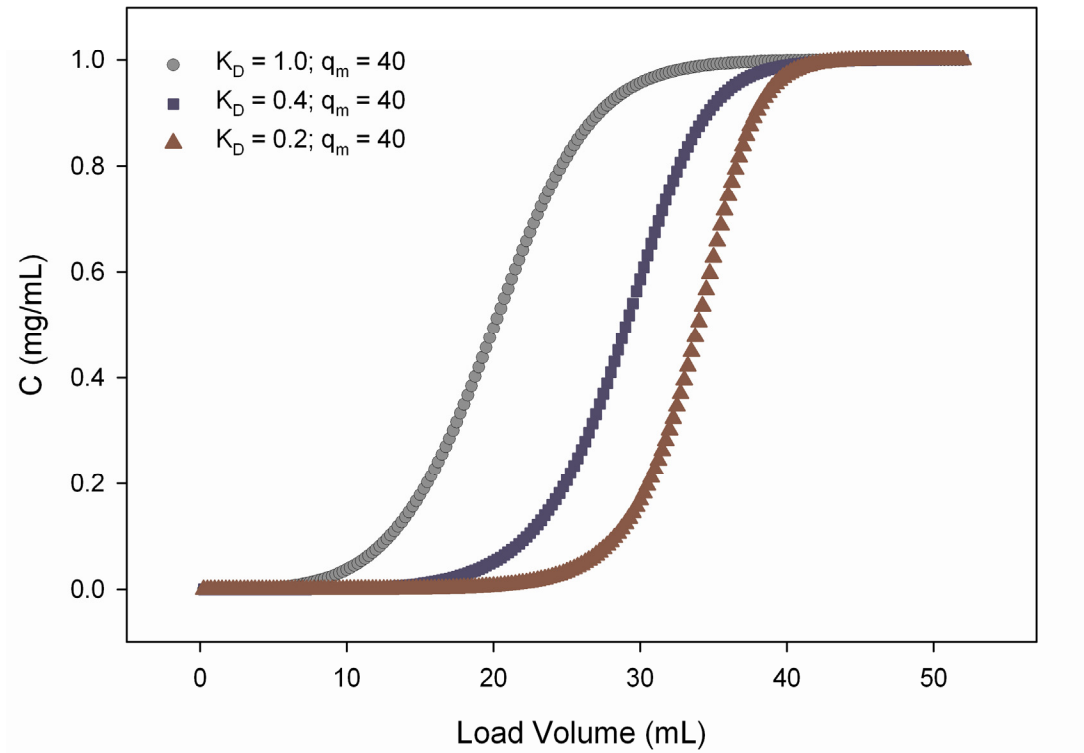


**Figure 4.13.** Example of data output when modelling column breakthrough with a staged reaction model. In this example, the effect of varying the Langmuir constant of  $K_D$  (mg adsorbate/mL mobile phase) is examined while  $q_m$  (mg adsorbate/mL adsorbent) remains constant. The feed concentration is 1.0 mg/mL and the column volume is 1.0 mL. The column is treated as four 0.25-mL stirred tank reactors (STR) having Langmuir adsorption behaviour.

resistances, Chase used a lumped kinetic approach in which the adsorption and desorption processes are described by second-order Langmuir kinetics:

$$R = k_1 C(q_m - q) - k_2 q, \quad \text{Equation 4.4}$$

where  $R$  is the rate of interface mass transfer,  $k_1$  is the forward rate constant and  $k_2$  is the reverse rate constant. The rate constant  $k_1$  is then determined from experimental batch uptake data, while  $K_D$  and  $q_m$  are derived from batch adsorption isotherms. In this model, axial dispersion is assumed to be negligible (ideal model). Thomas (1944) provides an analytical solution to the differential mass balance and rate equations used in this modelling approach. Chase was able to predict the column performance of his test systems with reasonable success despite the fact that this modelling approach does not treat all potential sources of mass transfer resistance.

The modelling approach applied in this thesis accounts for the adsorption kinetics in a different manner. Here, the parameters of  $K_D$  and  $q_m$  from the pre-equilibrium adsorption isotherms are inputted into the model to account for the non-equilibrium behaviour from mass transfer resistances during column adsorption. As shown previously, the uptake of the test huIgG protein on UNOsphere S in micro-tip chromatography is primarily a function of contact time. However, micro-tip contact time is not necessarily an equivalent term to either contact or residence time in conventional column chromatography, since column operation is dynamic with unidirectional flow while micro-tip chromatography is a batch operation. Hence, the relationship between the contact time of the micro-tip data and the residence time and/or contact time of the column chromatography must be established.

The result of matching the micro-tip contact time ( $T_{C\text{-microtip}}$ ) to the column residence time ( $T_{R\text{-column}}$ ) and then using the  $K_D$  and  $q_m$  parameters of that contact time in the staged reaction model is shown in Figure 4.14A. As expected, this approach does not adequately predict the column DBC since the two terms do not reflect equivalent operations. In the micro-tip experiment, the adsorbent is exposed to the entire sample for a short contact time (five minutes in the example in Figure 4.14A). In the column experiment, although the residence time is only 5 min, the entire loading (contact) time of the column to the feed is much longer (>20 min until breakthrough

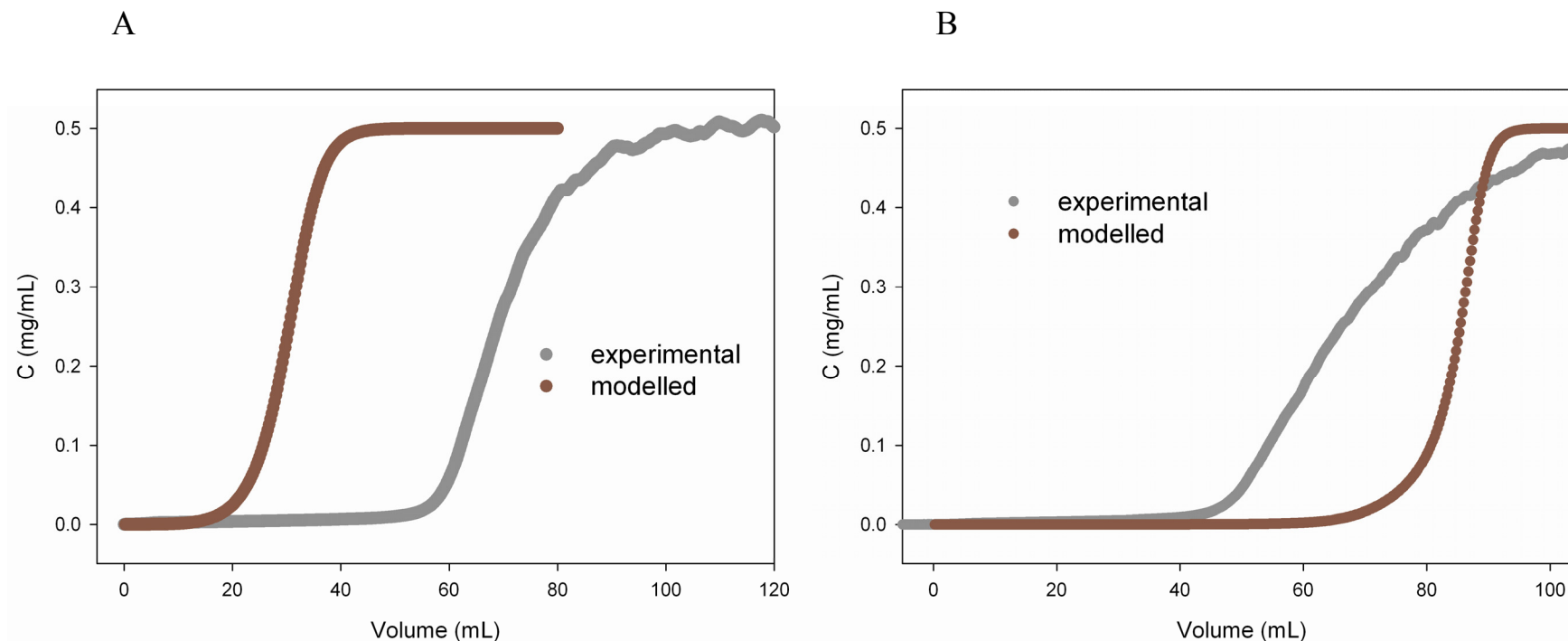


**Figure 4.14.** Breakthrough curves modelled from micro-tip pre-equilibrium adsorption isotherm data using a staged reaction model. The experimental breakthrough curves were generated by loading 0.5 mg/mL huIgG onto a 1-mL (0.56 cm, i.d., X 4 cm, h) UNOsphere S column at a buffer pH of 6.5 and a conductivity of  $\leq 3$  mS/cm. **(A)** Breakthrough curve derived from matching the residence time of the experimental column ( $T_{R\text{-column}}$ ; in this case, 2 min) to the micro-tip contact time ( $T_{C\text{-microtip}}$ ) of the pre-equilibrium adsorption isotherm used for determination of  $K_D$  and  $q_m$  in the staged reaction model. **(B)** Breakthrough curve derived from matching the column contact time ( $T_{C\text{-column}}$ , as defined by Equation 4.5; in this case, 88.6 min) to the micro-tip contact time ( $T_{C\text{-microtip}}$ ) of the pre-equilibrium adsorption isotherm used for determination of  $K_D$  and  $q_m$  in the staged reaction model.

and >60 min until adsorbent saturation), allowing sufficiently more time for pore diffusion and protein uptake. Likewise, matching the micro-tip contact time ( $T_{C\text{-microtip}}$ ) to the column contact time ( $T_{C\text{-column}}$ ) does not adequately predict the column DBC (Fig. 4.14B).  $T_{C\text{-column}}$  is defined here as the time required to challenge the column with a mass loading equivalent to the maximum adsorbent capacity ( $q_m$  determined from the *equilibrium* adsorption isotherm):

$$T_{C\text{-column}} = \frac{(q_m * V_A)}{Q * C_0}, \quad \text{Equation 4.5}$$

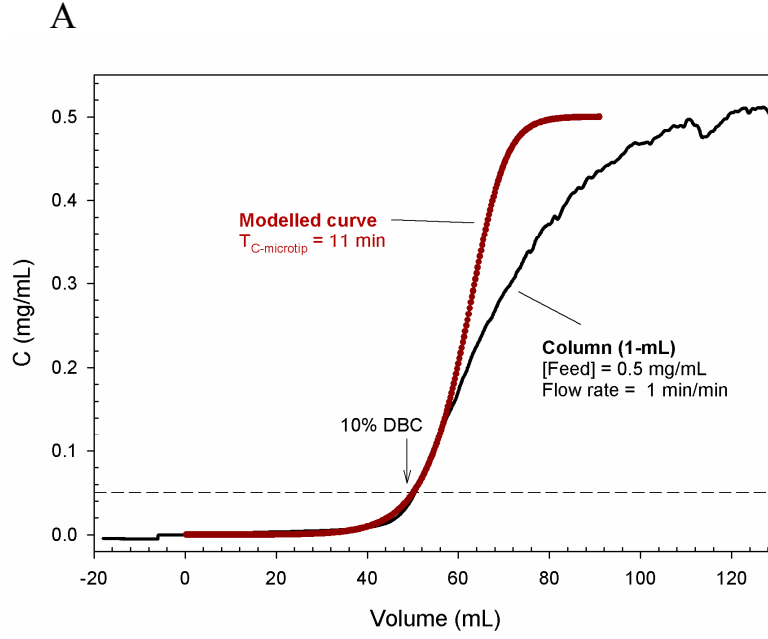
where  $q_m$  is the equilibrium adsorbent capacity in mg/mL,  $V_A$  is the adsorbent (column) volume in mL,  $Q$  is the volumetric flow rate in mL/min, and  $C_0$  is the feed concentration in mg/mL. Again, the lack of agreement here is presumably because these two times ( $T_{C\text{-microtip}}$  and  $T_{C\text{-column}}$ ) do not reflect equivalent operations.

If a calibration experiment, however, is first performed to determine an empirical correction factor ( $\alpha_{10\%}$ ) which relates  $T_{C\text{-microtip}}$  to  $T_{C\text{-column}}$ , the  $DBC_{10\%}$  can be predicted with high accuracy for different loading conditions (flow rate, feed concentration, and slight changes in column geometry) as demonstrated below. Although this approach requires a column experiment to be performed, a single column breakthrough experiment is sufficient for predicting changes in feed concentration and flow rate. In this way, the number of breakthrough experiments is significantly reduced. The correction factor  $\alpha_{10\%}$  is determined by:

$$\alpha_{10\%} = \frac{T_{C\text{-microtip}}}{T_{C\text{-column}}}, \quad \text{Equation 4.6}$$

where  $T_{C\text{-microtip}}$  is the pre-equilibrium adsorption isotherm contact time used (to determine  $K_D$  and  $q_m$ ) to model a breakthrough curve which produces a  $DBC_{10\%}$  that is equal to that of the calibration run. An example of this determination is shown in Figure 4.15. After determining  $\alpha_{10\%}$ , a corrected column contact time,  $T'_{C\text{-column}}$ , can be used to model changes in feed concentration and flow rate.  $T'_{C\text{-column}}$  is determined by:

$$T'_{C\text{-column}} = \alpha_{10\%} * T_{C\text{-column}} \quad \text{Equation 4.7}$$



B

$$T_{C\text{-column}} = \frac{(q_m * V_{\text{column}})}{(Q * C_0)}$$

$$= \frac{44.3 \text{ mg/mL} * 1 \text{ mL}}{1 \text{ mL/min} * 0.5 \text{ mg/mL}} = 88.6 \text{ min}$$

$$\alpha_{10\%} = \frac{T_{C\text{-microtip}}}{T_{C\text{-column}}}$$

$$= \frac{11.0 \text{ min}}{88.6 \text{ min}} = 0.124$$

**Figure 4.15.** Example of a calibration experiment used to relate micro-tip contact time ( $T_{C\text{-microtip}}$ ) to column contact time ( $T_{C\text{-column}}$ ). **(A)** Experimental breakthrough curve from the calibration run, in which 0.5 mg/mL hulgG was loaded onto a 1-mL UNOsphere S column (pH 6.5, conductivity  $\leq 3$  mS/cm) at 1 mL/min. Also shown is the modelled curve which yielded an equivalent  $\text{DBC}_{10\%}$  to that of the column experiment.  $T_{C\text{-microtip}}$  represents the micro-tip batch contact time used for modelling (i.e. the contact time of the pre-equilibrium adsorption isotherm used to determine  $K_D$  and  $q_m$  for the model). **(B)** Calculation of the correction factor,  $\alpha_{10\%}$ , which relates micro-tip contact time to column contact time.  $T_{C\text{-column}}$  is the time required to challenge the column with a mass loading equivalent to  $q_m$ .

#### 4.4.2.2. Application of Model to Micro-Tip Data

The modelling approach described above is summarised in Figure 4.16. This approach was demonstrated in this thesis with the test huIgG protein binding to UNOsphere S (pH 6.5 and conductivity  $\leq 3$  mS/cm). The  $K_D$  and  $q_m$  parameters were determined as a function of contact time from pre-equilibrium adsorption isotherm experiments, with the data fit with an empirical equation of best fit (Fig. 4.17). These terms were then used in the staged reaction model as described above. The calibration run and determination of  $\alpha_{10\%}$  were performed (Figure 4.15) to relate  $T_{C\text{-microtip}}$  to  $T_{C\text{-column}}$ . The prediction of column dynamic binding capacity at different loading concentrations (0.5 and 1.0 mg/mL) and flow rates (from 0.2 to 4.0 mL/min) is given in Table 4.5 for two 1-mL columns having slightly different geometries (pre-packed cartridge column and in-lab packed column).

**Table 4.5.** Prediction of column  $DBC_{10\%}$  using a staged reaction model and micro-tip pre-equilibrium adsorption isotherm data for the binding of huIgG to UNOsphere S.  $T_R$  = column retention time;  $T'_C$  = corrected column contact time used for modelling column  $DBC_{10\%}$ . The correction factor,  $\alpha_{10\%}$ , is 0.124 in this test case.

Column Size i.d. x h cm	[Feed] mg/mL	Flow Rate mL/min	Linear Velocity cm/h	$T_R$ min	$T'_C$ min	Predicted $DBC_{10\%}$ mg/mL	Column $DBC_{10\%}$ mg/mL	$\Delta$
0.5 X 5	1.0	2.00	600	0.5	2.75	14.5	15.4	-5.8%
0.5 X 5	1.0	1.00	300	1.0	5.50	22.5	23.1	-2.6%
0.5 X 5	1.0	0.67	200	1.5	8.20	27.0	27.3	-1.1%
0.5 X 5	1.0	0.50	150	2.0	11.0	30.0	28.9	3.8%
0.5 X 5	1.0	0.20	60	5.0	27.5	37.2	33.1	12.4%
0.56 X 4	0.5	4.00	960	0.25	2.75	9.90	11.0	-10.0%
0.56 X 4	0.5	2.00	480	0.5	5.50	17.1	17.5	-2.3%
<b>0.56 X 4<sup>a</sup></b>	<b>0.5</b>	<b>1.00</b>	<b>240</b>	<b>1.0</b>	<b>11.0</b>	<b>25.0</b>	<b>25.2</b>	<b>-0.8%</b>
0.56 X 4	0.5	0.50	120	2.0	22.0	31.8	29.5	7.8%

a) calibration experiment (shown in bold)

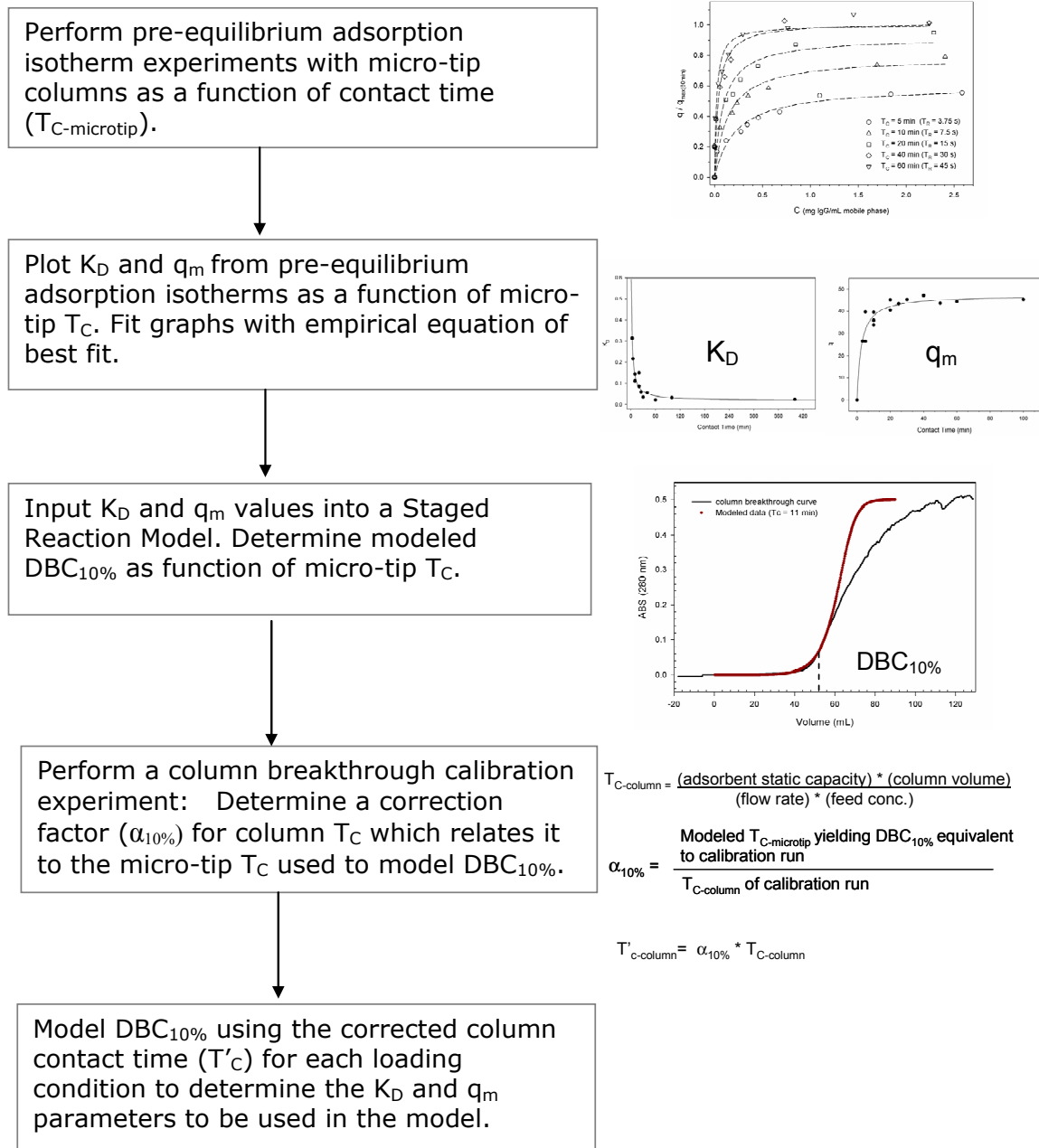


**Figure 4.16.** Outline of the staged-reaction modelling approach for the prediction of column  $DBC_{10\%}$  from micro-tip pre-equilibrium adsorption isotherm data.

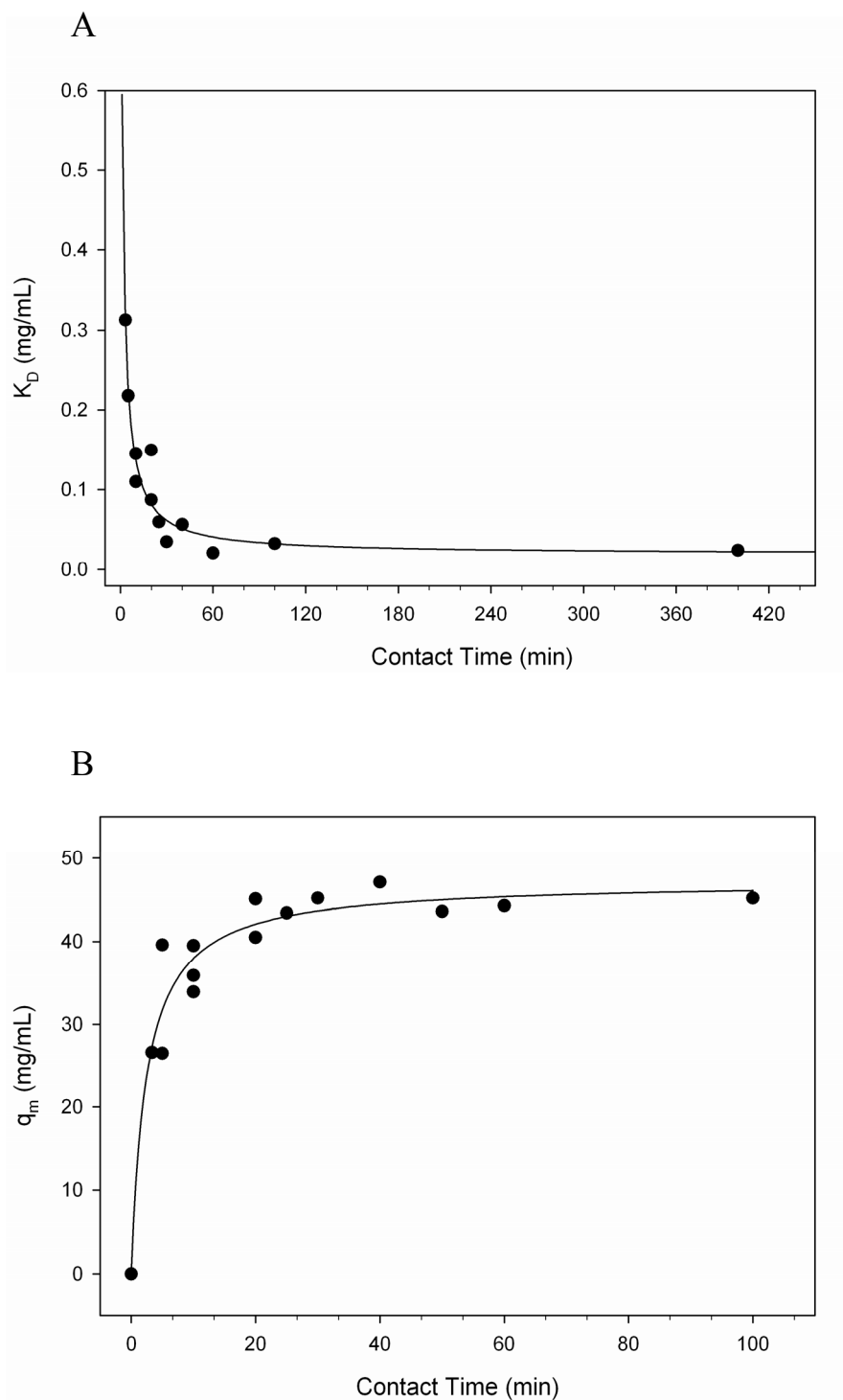


**Figure 4.17.** (A)  $K_D$  (mg huIgG/mL mobile phase) and (B)  $q_m$  (mg huIgG/mL adsorbent) constants as a function of micro-tip contact time derived from micro-tip pre-equilibrium adsorption isotherms (Langmuir model) in the binding of huIgG to UNOsphere S (pH 6.5;  $\leq 3$  mS/cm conductivity). The data are fit empirically with an inverse third order polynomial ( $R^2 = 0.86$ ) in (A) and with a two-parameter, single rectangular hyperbolic function ( $R^2 = 0.73$ ) in (B).

Agreement between the predicted  $DBC_{10\%}$  value and the experimental data is observed, with differences  $\leq 12\%$  across the range of conditions examined. This close agreement is also evident in the parity plot shown in Figure 4.18B, with the slope of the linear regression line equal to 0.97. The  $DBC_{10\%}$  is also shown as a function of flow rate in Figure 4.18A. Interestingly, the  $DBC_{10\%}$  values for the column loaded at 0.5 mg/mL are slightly higher at any given flow rate than for the 1.0 mg/mL loading, even though the adsorption equilibrium should be favoured at higher concentrations. However, this may be explained by the fact that the column contact time doubles when decreasing the feed concentration from 1.0 mg/mL to 0.5 mg/mL. This, in turn, improves the mass transfer by allowing for more contact time for intra-particle diffusion. This may also potentially allow for a more favourable concentration gradient to be established across the particle surface and within its pores.

A key advantage of this modelling approach is that it is primarily data driven and requires very few assumptions of model parameters.  $DBC_{10\%}$  was predicted with high accuracy for the test system examined here. An area of future work would be to evaluate this modelling approach with other adsorbents and proteins. A disadvantage of this approach is that it requires a calibration experiment and therefore does not fully eliminate the need to carry out a column breakthrough experiment. Yet, assuming this approach is transferable to other adsorbents and protein systems, it does reduce the laboratory-scale experimental numbers to a single breakthrough experiment. It could be argued that a single breakthrough curve is sufficient in and of itself (i.e. in the absence of micro-tip data) to estimate the effect of residence time on DBC. However, having micro-tip data in combination with this data should allow this prediction to be done with higher fidelity, as evidenced by the very accurate predictions in Table 4.5.

For future work, it would be interesting to examine if a single calibration run is still sufficient when examining a range of different mobile phase conditions (e.g. salt and pH) since this was not examined here. An additional consideration is that of scale. In the work presented here, both the calibration run and dynamic column experiments were performed at the same scale (1 mL). It is not clear whether or not this approach would be predictive of the DBC for say a 10-mL or 1-L column, if a 1-

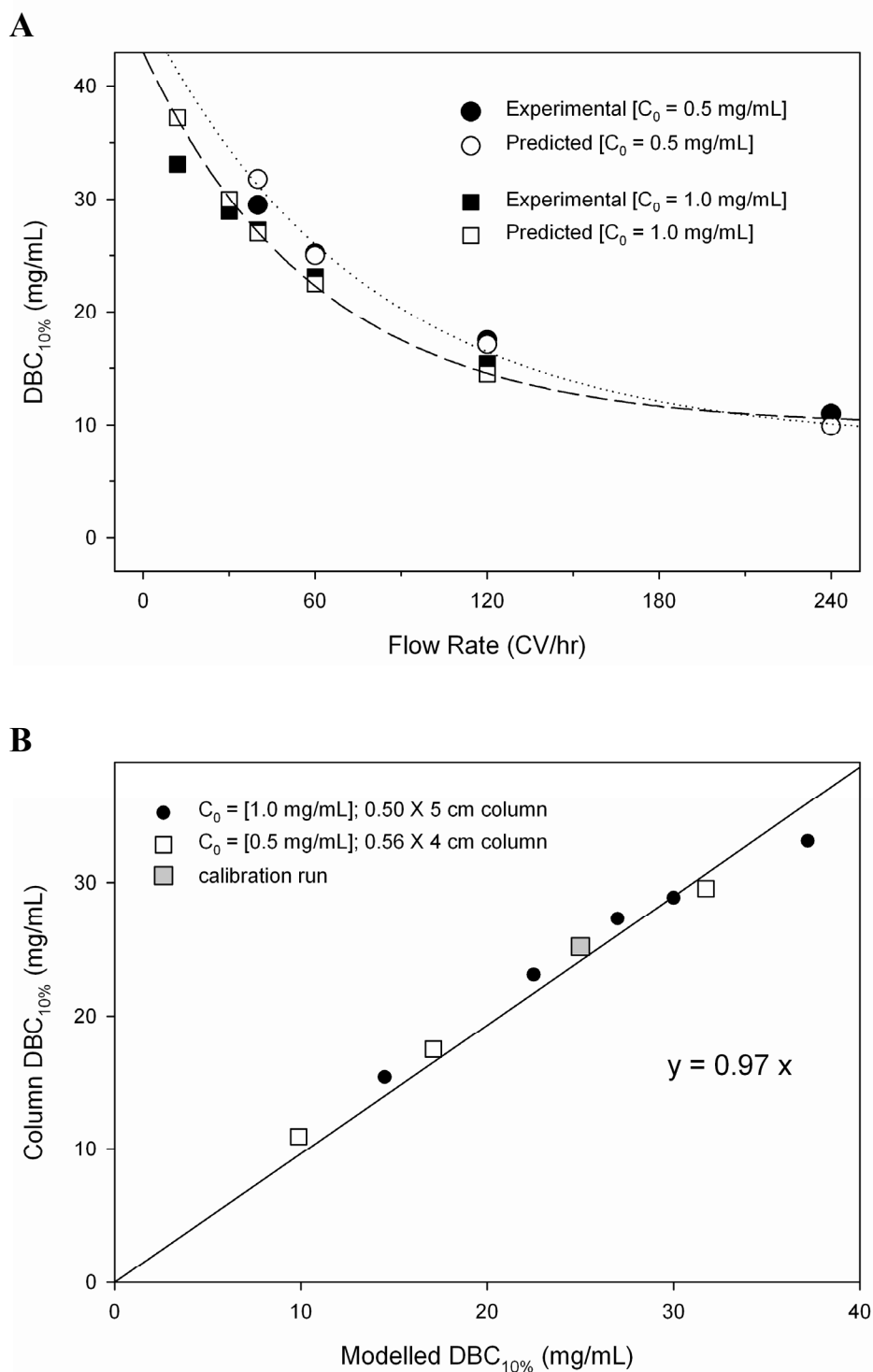


**Figure 4.18.** Comparison of predicted dynamic binding capacities (at 10% breakthrough) from micro-tip experiments using a staged reaction model to those of the experimental column. **(A)**  $DBC_{10\%}$  as a function of flow rate (CV/h). The modelled data is fit with an empirical equation of best fit (3-parameter exponential decay). **(B)** Correlation between column and predicted values (linear regression, fit through origin).

mL column was used for the calibration experiment. However, changes in DBC with scale are always a key consideration, even for conventional DBC determination by frontal analysis. These differences are associated more with differences in wall effects, packing efficiency, and column geometry, which are not considered in the staged reaction model.

Although not surprising, it is worth noting that the modelling approach applied here does not accurately predict the full shape of the breakthrough curve, as evidenced in Figure 4.15A. Here, the experimental curve is significantly more distended than the modelled curve, deviating most significantly in the latter half of the curve. This observation reveals some of the shortcomings of the model; specifically, it oversimplifies the adsorption process. Even though the model attempts to account for the deviation from equilibrium in column operation by using pre-equilibrium adsorption isotherm parameters, it does not account for axial dispersion nor does it rigorously deal with the multiple components of mass transfer resistance. More complex, multi-component general rate models (Arve and Liapis, 1987; Gu et al., 1993; Kempe et al., 1999) are better suited for this purpose. The error, then, of this model in predicting the full breakthrough curve has more to do with its simplifying assumptions than in the quality of the data generated by the micro-tip columns. However, the goal in this thesis was not to predict the full breakthrough curve or elucidate the underlying mechanisms of mass transfer. Rather, it was a practical one, that being to have a simple, data-driven model for efficiently predicting column DBC from micro-tip data for the purpose of process development.

#### **4.5. Summary**

The results presented here demonstrate the utility of the micro-tip format for adsorbent characterisation. Furthermore, they provide insight into the mass transport properties of micro-tip chromatography and how this format compares with other microwell formats. Although micro-tip chromatography is unique in its operation, it is, in many ways, similar to micro-batch adsorption and can often be used analogously in the characterisation of a chromatographic step. However, micro-tip columns offers the advantage of not requiring an adsorbent mixing step, thereby ensuring efficient mass transport even for very dense adsorbents. In this thesis, the

adsorption isotherms that were carried out by micro-tip chromatography were in good agreement with those by conventional batch methods, although slight differences were observed between micro-tip column scales. These differences are presumed to be due to slight inaccuracies in the adsorbent bed volume from column preparation. Micro-tip methods for studying adsorption kinetics were also demonstrated using both finite-bath and infinite-bath (shallow bed) formats. Although shallow-bed chromatography appears to be a valid option for micro-tip chromatography, it was not chosen for further study because of the constraint on sample concentration. In addition to these conventional formats, *pre-equilibrium* adsorption isotherms were generated as an alternative approach for examining mass transport properties. In all of these formats for kinetic study, it was the sorbent contact (incubation) time and not the residence time that most influenced protein uptake onto the adsorbent. This is consistent with intra-particle diffusive mechanisms being rate-determining for uptake of a globular protein such as hIgG onto a porous resin.

Batch uptake data can be used qualitatively when screening different adsorbents and mobile phase conditions, or quantitatively for the prediction of column DBC. Many models have been developed for describing the adsorption process and the prediction of DBC, ranging from nondispersive reaction models to general rate ones. Two data-driven models were evaluated here for predicting initial breakthrough ( $DBC_{10\%}$ ) from micro-tip experimental data. The first applied a shrinking core model to batch adsorption data and assumed that external mass transfer is negligible. The second employed a staged reaction model, but instead of determining reaction kinetics it used pre-equilibrium adsorption isotherm data to account for the adsorption kinetics. Each showed reasonable agreement to the experimental data in the prediction of DBC but did not necessarily predict the full shape of the breakthrough curve.

## **5. CAPTURING THE POTENTIAL OF MIXED-MODE LIGANDS WITH MICRO-TIP CHROMATOGRAPHY**

### **5.1. Introduction**

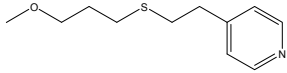
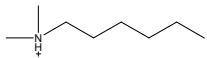
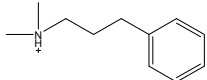
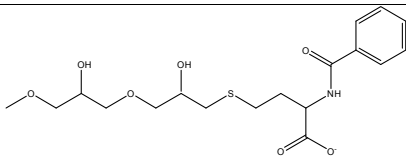
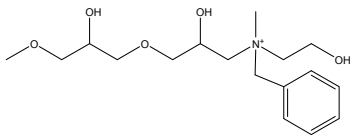
New multi-modal chromatography ligands offer the potential for a next generation of protein purification processes. However, the development of mixed mode chromatography steps imposes a heavy burden on process development since multi-parameter screening is required for their optimisation. High-throughput methods such as micro-tip chromatography offer a solution to this problem by allowing a thorough, yet timely, exploration of the parameter space. A microscale workflow using micro-tip chromatography is demonstrated in this chapter for the development of a multimodal weak cation-exchange (Capto MMC) chromatography step in the purification of a monoclonal antibody from *Pichia pastoris* cell filtrate. This workflow allowed the chromatography step to be developed with less time and labour. The final optimised conditions predicted by the microscale development were subsequently confirmed with a small laboratory-scale column. This approach is potentially adaptable to other chromatography types beyond mixed-mode, providing a path for the logical development of process chromatography steps.

### **5.2. Mixed Mode Chromatography: New Opportunities and Challenges**

Mixed mode chromatography presents the opportunity of replacing a more costly affinity capture step with a mixed-mode one, consolidating two chromatography steps (e.g. intermediate and polishing) into one, providing a strategy for purifying away difficult-to-remove impurities, and/or carrying out ion-exchange chromatography at higher ionic strength. Advances in bioinformatic and combinatorial tools (Roque et al., 2005; Clonis, 2006) have enabled the rapid and cost-effective design of new ligands, increasing the options for mixed-mode chromatography. A list of some commercially available mixed-mode adsorbents is given in Table 5.1.

Ceramic hydroxyapatite is a classically used mixed-mode chromatography, in which protein retention is driven by a cation-exchange mechanism between phosphate groups on the adsorbent and amino groups on the protein, and by metal affinity, between calcium sites on the adsorbent and protein carboxyl groups (Ng et

**Table 5.1.** Some commercially available mixed-mode chromatographic media.

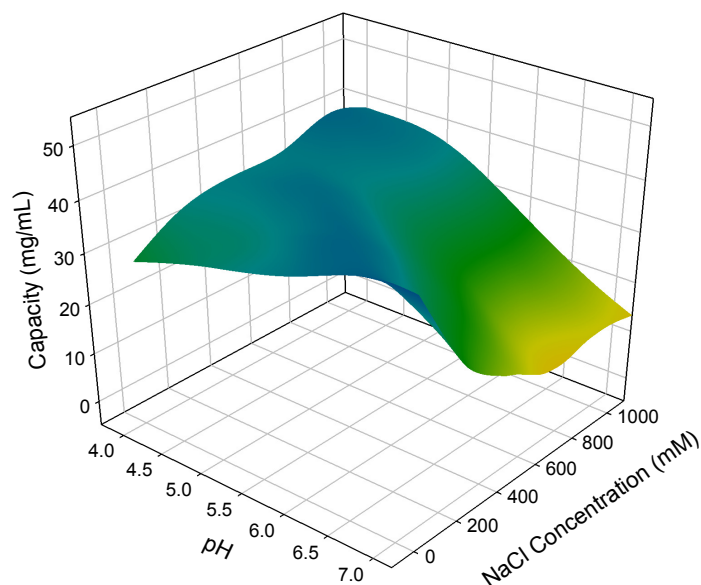
Adsorbent Name	Proposed Binding Mechanism	Base Matrix	Ligand Chemistry
Bio-Rad Ceramic Hydroxyapatite	Cation-exchange and coordination bonds	Hydroxy-apatite	$\text{Ca}_{10}(\text{PO}_4)_6(\text{OH})_2$
Pall MEP Hypercel	Hydrophobic charge induction (pKa = 4.8, antibody selective ligand)	Cellulose	 4-mercapto-ethyl-pyridine
Pall HEA HyperCel	Hydrophobic charge induction (pKa = 8.0, aliphatic substituent)	Cellulose	 Hexylamine
Pall PPA HyperCel	Hydrophobic charge induction (pKa = 8.0, aromatic substituent)	Cellulose	 Phenylpropylamine
GE Healthcare Capto MMC	Weak cation-exchange and hydrophobic interaction	Agarose	 2-benzamido-4-mercaptobutanoic acid
GE Healthcare Capto Adhere	Strong anion-exchange and hydrophobic interaction	Agarose	 N-benzyl-N-methyl ethanolamine
BakerBond ABx	Weak cation exchange with weak anion exchange	Silica or polymeric	-COOH and polyethylene imine (-C <sub>2</sub> H <sub>5</sub> N)

al., 2007). Recently, several new multimodal ligands have been developed that combine hydrophobic and ion-exchange mechanisms (Table 5.1). The MEP, HEA, and PPA Hypercel adsorbents from Pall (Port Washington, NY, USA) utilise a hydrophobic charge induction mechanism, in which a pH shift is used during elution to weaken hydrophobic interactions via electrostatic repulsion (Burton and Harding, 1998; Chen et al., 2008A). Prototypes of anion and cation-exchange multimodal

ligands were prepared on an agarose-based porous resin (Sephacrose 6 Fast Flow) by Johansson et al. (2003A and 2003B) and evaluated for their ability to capture proteins at high ionic strength (28 mS/cm). It was found that the multimodal anion-exchange ligands that were optimal for protein capture at high salt concentration were non-aromatic and based on a primary and/or secondary amine with a nearby hydrogen donor. For multimodal cation exchange, aromatic ligands with a carboxylic acid group worked best, particularly when there was a hydrogen acceptor close to the carboxylic group. Two multimodal ion exchange adsorbents on highly cross-linked agarose media are now commercially available from GE Healthcare (Table 5.1), employing the N-benzyl-N-methyl-ethanolamine ligand (Capto Adhere) for multimodal strong anion exchange and the MMC ligand (Capto MMC) for multimodal weak cation exchange. In contrast to the findings of Johansson et al. (2003A), the Adhere ligand does have an aromatic group, but it is recommended as an intermediate or polishing step to be operated in a flow-through mode rather than as a capture step. Another adsorbent, BakerBond ABx sold by Mallinckrodt Baker (Phillipsburg, NJ, USA; Table 5.1), combines a carboxyl group with a polyethylene imine, thereby providing weak anion exchange with weak cation exchange.

Although mixed mode adsorbents offer the potential for increased selectivity and more salt-tolerant loading conditions, their design spaces are considerably more complex and the conditions for optimal operation less intuitive. This is evidenced in Figure 5.1, in which the binding capacity of two different purified monoclonal antibodies (referred hereafter as mAb-1 and mAb-2) on Capto MMC is shown as a function of pH and NaCl concentration (derived from screening experiments as described in the sections below). Although the test antibodies used here are both human IgG1 antibodies having an isoelectric point (pI) of 9, their binding behaviour is comparatively different. For mAb-1, the binding profile is relatively flat, with a shallow decline in capacity observed with increasing pH ( $\geq 6$ ) and NaCl concentration. Meanwhile, for mAb-2, this decline in capacity is significantly steeper and begins at around pH 5, with clear binding optima at pH 4 and 7. For both mAbs, binding is tolerant of higher salt concentrations at low pH ( $\leq 5$ ). The observed differences in binding behaviour are presumably due to differences in the

**A**



**B**

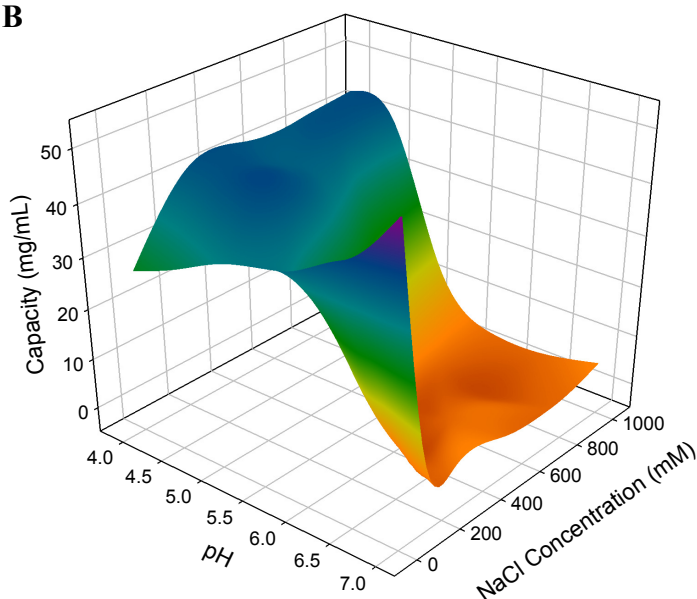


**Figure 5.1.** Binding capacity of two human monoclonal antibodies (huIgG) to Captopril (Capto MMC) as a function of sodium chloride (0 to 1 M) and pH (4 to 7): (A) mAb-1 and (B) mAb-2. Experiments were carried out by micro-tip chromatography using the screening methods as outlined in sections 5.3 and 5.4. The isoelectric point (pI) of both antibodies is 9.

hydrophobic properties of the antibodies and/or differences in their charge distribution (i.e. local patches of charge), since their pIs are approximately the same.

### **5.3. High-Throughput Development of Mixed Mode Chromatography**

Mixed mode chromatography is usually optimised empirically because of the complexity of the adsorption mechanism. Consequently, this development must be repeated for each new, unique biomolecule. A large component of such development centres on the screening of mobile phase conditions, including pH, ionic strength, and salt/buffer type and concentration. To obtain a comprehensive characterisation of the design space requires many experiments to be performed, a number that is usually not feasible at the laboratory scale because of material and resources constraints. Microscale methods like micro-tip chromatography are well suited for this development because of their high degree of experimental parallelisation and low volume requirements.

#### *5.3.1. Developmental Workflow Using Micro-tip Chromatography*

A high-throughput workflow using micro-tip chromatography is described in Figure 5.2 for the development of mixed mode chromatography. This workflow employs a sequence which is analogous to that of high-throughput drug discovery. A primary evaluation of mobile phase parameters affecting adsorption (capture) of the target protein and its impurities is first carried out. In Figure 5.2, this includes pH, salt type, and salt concentration but may include additional parameters, if necessary. When there is little or no prior experimental knowledge, a range-finding study may first be required to estimate parameter ranges and eliminate parameters that are not critical. Response maps of adsorbent capacity, recovery, and impurity binding obtained from the primary evaluation are then used to select the operating mode (flow through or bind-and-elute), the process function (capture, intermediate, or polishing step), and the optimal mobile phase conditions. A secondary evaluation is then performed to define and optimise each stage (loading, wash, and elution) of the chromatographic purification in order to predict process-scale column performance. The microscale results are subsequently verified at the laboratory scale, as scale-up from this point is well established.

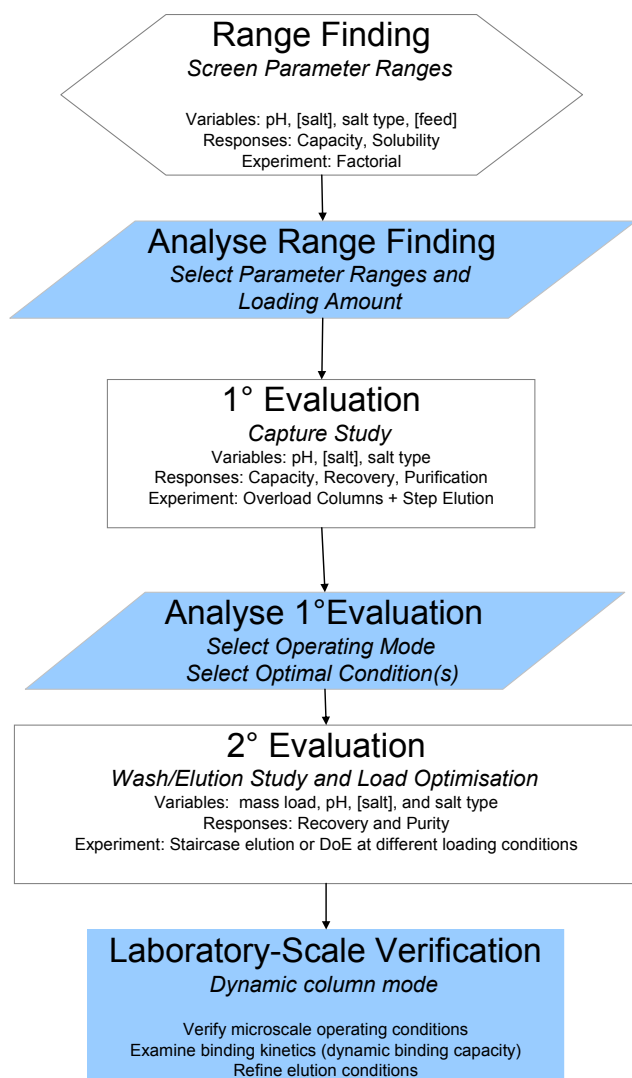
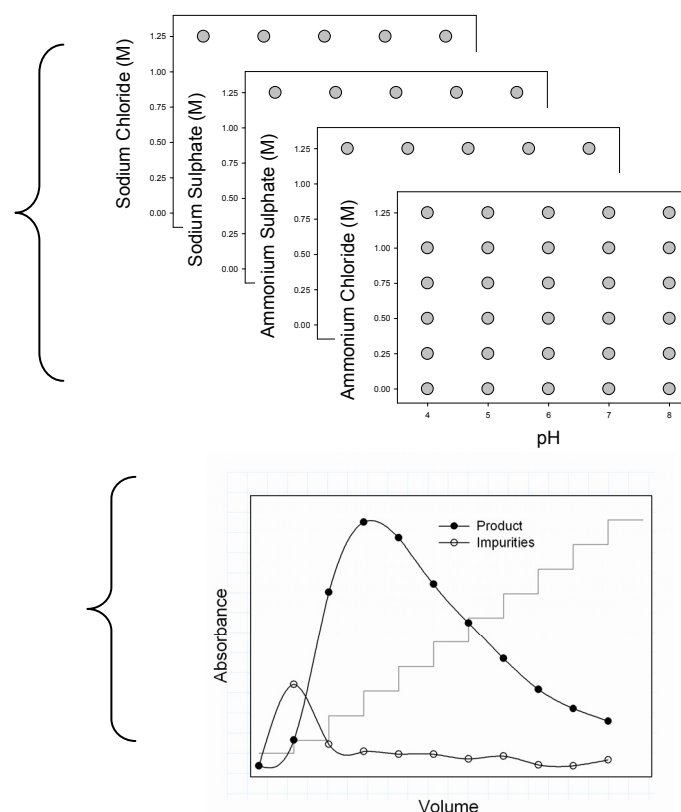


**Figure 5.2.** High-throughput workflow using microscale chromatography for the development of a mixed-mode chromatography process step.



### 5.3.2. Design of High-Throughput Experiments

Despite their high throughput, the design and implementation of microscale chromatographic experiments must still be strategic so as to not overwhelm analytical testing and data processing resources. A well-designed workflow, therefore, considers experimental efficiency and the concomitant analytical strategy. For the workflow used in this thesis, high-throughput analytical platforms were applied, including absorbance measurements in microtitre plates, product mass quantitation with a parallel biosensor technique (ForteBio Octet), and impurity detection (host-cell protein ELISA and a dye-binding DNA method) using fully automated 96-well microplate-based assays. The details of these analytical techniques are described in Chapter 2.

With respect to the experimental design of the microscale workflow, a brute-force design is proposed for the primary evaluation when the variable number is such that the microscale experiments can be completed with high throughput and reasonable experimental numbers. This was the case in this study, in which three parameters (pH, salt type, and salt concentration) were studied. More efficient response surface methodologies, such as central composite, Box-Behnken, and D-optimal designs, or iterative methods, such as simplex or genetic algorithms, become more advantageous when the number of parameters is such that it will overwhelm experimental and analytical resources. However, a caveat with using these more sophisticated designs is that they may not provide the resolution necessary to fully characterise a complex and broad operating space like mixed mode chromatography. Consequently, a follow-up examination focusing on areas of interest may be required. No matter which design is selected, a factorial design is usually advantageous as a pre-screen prior to a response-surface or brute-force design to identify main effects, eliminate those parameters which are less critical, and establish approximate parameter ranges. Such a pre-screen was performed in this study to establish parameter ranges.

## 5.4. Demonstration of the High-Throughput Developmental Workflow

The microscale workflow outlined in Figure 5.2 was demonstrated with multimodal weak cation-exchange chromatography (Capto MMC) for the capture of mAb-1 from a crude clarified *Pichia pastoris* filtrate. The Capto MMC adsorbent consists of a

highly cross-linked agarose base matrix with a multi-modal ligand as shown in Table 5.1, having cation-exchange, hydrophobic interaction, and hydrogen-bonding properties. Typically in monoclonal antibody purifications, Protein A chromatography is used as the capture step because of its very high purification efficiency. Protein A is a 42 kDa cell wall protein from *Staphylococcus aureus* which binds with high affinity to the Fc region of most antibodies. However, there are some disadvantages associated with its use. Firstly, protein A chromatography is relatively expensive; therefore, it must be capable of being re-used for many cycles to make it cost-effective. However, it usually cannot be cleaned with sodium hydroxide, a standard cleaning agent in preparative scale chromatography, thereby adding to the associated cost of the step. A second potential disadvantage of protein A chromatography is that it requires elution at low pH, which can result in product aggregation and/or precipitation. Finally, for antibodies produced in yeast host cells, the protein A ligand itself is susceptible to yeast proteases, resulting in potentially higher levels of leached protein A and column deterioration.

For the primary evaluation with Capto MMC, three mobile phase parameters were examined for their effect on binding: pH, salt concentration, and salt type. Because of the hydrophobic properties of the MMC ligand (see Table 5.1), four different salt types were evaluated by varying two cations,  $\text{NH}_4^+$  and  $\text{Na}^+$ , with two anions,  $\text{SO}_4^{2-}$  and  $\text{Cl}^-$ . These ion pairs were selected based on their location in the Hofmeister series (Hofmeister, 1888; Zhang and Cremer, 2006), with  $\text{NH}_4^+$  being more lyotropic than  $\text{Na}^+$ , and  $\text{SO}_4^{2-}$  being more lyotropic than  $\text{Cl}^-$ . The contribution of the buffer (used for pH control) on the chromatography was neglected to minimise the number of experiments. This was done by using an universal buffer mixture of 10 mM sodium acetate, 10 mM sodium phosphate, and 10 mM HEPES, spanning a broad pH range from 4 to 8. If necessary, buffer effects can be subsequently explored upon defining a narrower pH range. Using the response maps of mAb-1 capacity and impurity binding from the primary evaluation as a guide, the secondary evaluation then centred on optimising the full chromatographic sequence that included the loading, wash, and elution steps. For the development of wash and elution strategies, a 'staircase' method was employed, in which small incremental steps of increasing elution strength were made by moving the micro-tip columns across the microplate

into wells of varying eluent concentration (or pH). The optimised micro-tip purification was then verified with a 1-mL HiTrap Capto MMC column experiment.

#### 5.4.1. Experimental Details of Micro-Tip Chromatography

Micro-tip chromatographic experiments were performed with 10- $\mu$ L Capto MMC columns on a Tecan workstation as described in Chapter 3. Prior to their use, the Capto MMC columns were pre-washed in 12-column reservoir plates using the following sequence: (1) 0.5 mL of 50% methanol, (2) 0.8 mL of water, (3) 0.2 mL of 50 mM HEPES, pH 8.5, with 0.5 M NaCl (elution buffer), and (4) 0.8 mL of water. The micro-tips columns were then equilibrated with four 0.85-mL aliquots of loading buffer. Experiments were performed at flow rates between 2 and 20  $\mu$ L/s and delay times between 10 and 30 s, with a flow rate of 5  $\mu$ L/s ( $\mu_{\text{avg}} = 990$  cm/h) used for the loading, wash, and elution steps. These conditions are within the recommended ranges as defined in Chapters 3 and 4. For the pre-wash, equilibration, and post-loading wash steps, a single aspiration-dispense cycle was performed per well (aliquot). For the loading and elution steps, multiple aspiration-dispense cycles were carried out per well (aliquot) to increase the contact time at a fixed linear velocity. A loading (contact) time of 40 minutes was used in this study to ensure semi-equilibrium binding ( $\geq 80\%$  of equilibrium binding), while allowing for sufficient experimental throughput. Elution times were  $\geq 5$  minutes per elution step (of increasing elution strength) to ensure complete desorption, with 2-3 elution steps performed for the capture studies and 9 steps (staircase elution) performed for the elution studies. Samples from micro-tip chromatography experiments were then assayed by optical measurements in microtitre plates ( $\lambda = 280$  nm or 600 nm), Octet protein-A biosensors for antibody detection, the PicoGreen DNA assay, SDS-PAGE, and an anti-*Pichia pastoris* host-cell protein (HCP) ELISA (see Chapter 2 for details). The specific experimental details for each stage of the experimental workflow are discussed below.

#### 5.4.2. Range-Finding Study

Although it was known that mAb-1 is an IgG1 with a pI of around 9, this information was insufficient to predict *a priori* its binding behaviour on the multimodal weak cation-exchange adsorbent (Capto MMC). Therefore, range-finding experiments

were carried out with protein-A purified material ( $\geq 90\%$  purity) to establish the approximate parameter ranges, ensure product solubility under these conditions, estimate adsorbent capacity, and identify preliminary conditions for product elution (i.e. a 'strip' elution buffer to examine recovery). Specifically, a  $2^2$  factorial design examining pH (5, 7) and salt concentration (0, 1M) with two categorical factors (sodium chloride, ammonium sulphate) was performed to establish the appropriate parameter ranges for the primary evaluation (capture study) and estimate the maximum adsorbent binding capacity. The results from these two salts were considered to be approximately representative of the other two salts to be used in the capture study (ammonium chloride and sodium sulphate). Purified mAb-1 was exchanged into each mobile phase condition (buffered with 12.5 mM sodium acetate and 12.5 mM sodium phosphate at the desired pH) by performing a 10-fold dilution from a concentrated feedstock. Each column was then challenged with 65 mg of purified mAb-1 per mL of Capto MMC. Adsorbent capacity ( $q$ ) was determined by measuring the concentration of the starting feed sample and the nonbound fraction after loading (by absorbance at 280 nm) and calculated by:

$$q = \frac{C_0 V_s - C V_s}{V_A} \quad \text{Equation 5.1}$$

where  $C_0$  is the starting sample concentration (mg/mL),  $C$  is the concentration of the nonbound fraction after loading (mg/mL),  $V_s$  is the sample volume (in mL), and  $V_A$  is the adsorbent volume in mL. In these experiments, the micro-tip column hold-up volume ( $\varepsilon V_A + (1 - \varepsilon) V_A \varepsilon_p$ ; see equation 3.1) was assumed to be negligible since  $V_A$  is 10  $\mu\text{L}$  while  $V_s$  is 800  $\mu\text{L}$  (micro-tip hold-up is  $\leq 1\%$  of  $V_s$ ).

The results of the factorial experiments are shown in Figure 5.3. The maximum adsorbent capacity observed under these mobile phase conditions was 51 mg of mAb-1 per mL of adsorbent. From these results, a wider pH range (4-8) and salt concentration (0-2 M) was selected for further examination in the primary evaluation. However, to ensure that mAb-1 was soluble at these higher salt concentrations, particularly in the case of ammonium sulphate, a solubility screen was performed by diluting the mAb-1 feedstock ten-fold to 0.8 mg/mL (the concentration at which the primary evaluation was to be carried out) into solutions

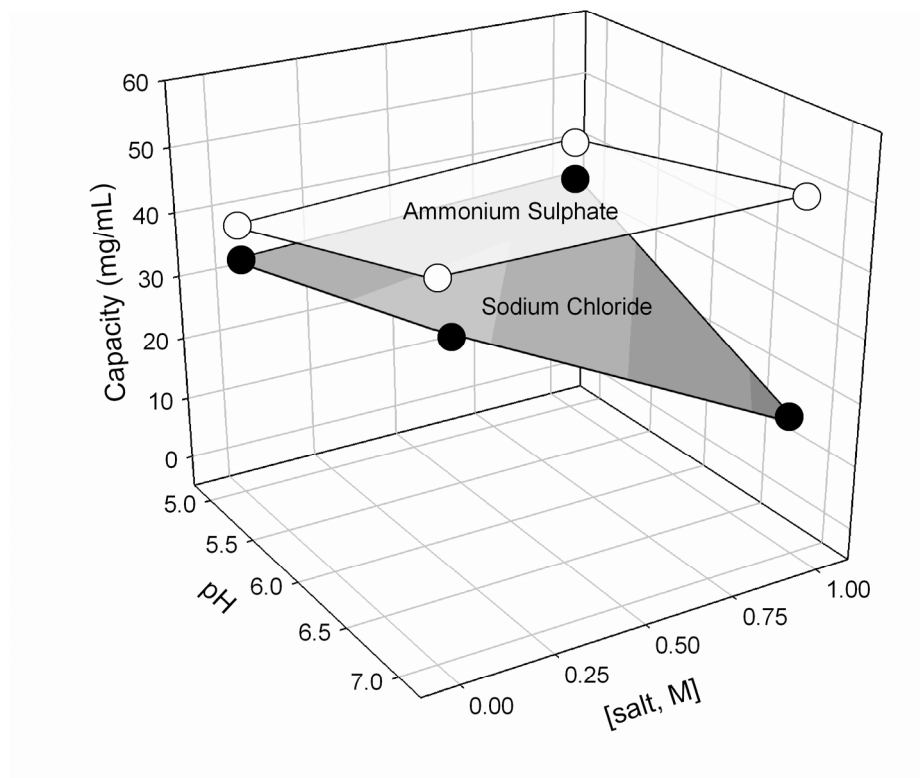


**Figure 5.3.** Factorial design ( $2^2$ ) to establish parameter ranges (pH, salt concentration) for the examination of mAb-1 (purified) binding to the multimodal weak cation-exchange adsorbent (Capto MMC) in sodium chloride and ammonium sulphate salts. Binding capacity ( $q$ ) is shown as a function of salt concentration (0, 1 M) and pH (5, 7).

buffered at pH 5 or pH 7 and at salt concentrations up to 2.0 M. Solubility was then assessed by monitoring each sample at 600 nm, with signals three times above background ( $\geq 0.04$  absorbance units) considered to be indicative of aggregation and/or precipitation. The solubility screen showed that mAb-1 does begin to aggregate and/or precipitate at ammonium sulphate concentrations  $\geq 1.5$  M (Table 5.2), and this occurs with a slight pH dependency. Therefore, the upper salt concentration was constrained to 1.25 M for the subsequent primary evaluation to ensure mAb-1 solubility across the pH range examined.

**Table 5.2.** Examination of mAb-1 solubility across a salt range from 0 to 2 M for multimodal weak cation-exchange (Capto MMC) chromatography development. Absorbance at  $\lambda = 600$  nm was measured in microtitre plates. Concentration of mAb-1 after dilution into the salt solution is 0.8 mg/mL. Absorbance values  $\geq 0.04$  (3 times above background; shown in bold) were considered indicative of aggregation and/or precipitation.

[Salt], M	0.00	0.50	1.00	1.25	1.50	2.00
NaCl, pH 5	0.0213	0.0138	0.0121	0.0111	-----	-----
NaCl, pH 7	0.0185	0.0166	0.0130	0.0129	-----	-----
(NH <sub>4</sub> ) <sub>2</sub> SO <sub>4</sub> , pH 5	0.0169	0.0113	0.0136	0.0162	0.0207	<b>1.2765</b>
(NH <sub>4</sub> ) <sub>2</sub> SO <sub>4</sub> , pH 7	0.0177	0.0112	0.0129	0.0175	<b>0.0938</b>	<b>1.2936</b>

In addition to defining the parameter ranges for loading, the results from the factorial experiment also indicate that mAb-1 binding decreases with increasing pH and ionic strength. From these data, a strip elution solution consisting of 0.5 M NaCl in 50 mM HEPES, pH 8.5, was subsequently tested and shown to be sufficient ( $\geq 80\%$  recovery) for the elution of mAb-1 from Capto MMC. This strip buffer was used during the primary evaluation to examine the reversibility of binding under different loading conditions.

### 5.4.3. Primary Evaluation: Capture Study

#### 5.4.3.1. Experimental Layout

A primary evaluation was subsequently carried out using the ranges determined from the range-finding study to evaluate the adsorption capacity and selectivity of the multimodal weak cation-exchange adsorbent (Capto MMC) for mAb-1 and the host cell protein impurities. Thirty-two chromatography experiments (4 runs X 8 experiments/run) were carried out for each salt type in a single fully automated method, in which pH and salt concentration were varied. The pH was studied at five points (4.0, 5.0, 6.0, 7.0, and 8.0) and the salt concentration at six points (0, 0.25, 0.50, 0.75, 1.0, and 1.25), with one point (pH 7.0, 0 M NaCl) replicated three times to estimate the experimental precision. As indicated above, a universal buffer mixture of 10 mM sodium acetate, 10 mM sodium phosphate, and 10 mM HEPES was used, spanning the entire pH range. The column feed was exchanged into each loading mobile-phase condition by dilution (10-fold or higher) from a concentrated feedstock. In each experiment, the adsorbent was overloaded with mAb-1, at 73 mg per mL of adsorbent, to provide an estimate of binding capacity under each condition. Adsorbent capacity for mAb-1 was then determined as in the range-finding study and calculated using equation 5.1. Product recovery was evaluated by carrying out a strip elution with 0.5 M NaCl in 50 mM HEPES, pH 8.5, for the purpose of ensuring that binding was reversible. The recovery was calculated by:

$$\%recovery = \frac{m_{eluted}}{m_{captured}} \times 100, \quad \text{Equation 5.2}$$

in which  $m_{eluted}$  is the mass eluted from the column with the strip elution buffer and  $m_{captured}$  is the mass that bound to the micro-tip column (as calculated by equation 5.1).

The 96-deepwell plate used in these experiments was configured as shown in Figure 5.4, with columns 1-4 for equilibration, column 5 for dilution of the feedstock, column 6 for loading the desired volume of diluted sample, columns 7-8 for washing the column post-loading, and columns 9-10 for elution. The micro-tip columns (at positions A-H) were moved across the plate from left to right to complete the experiment, as described in section 5.4.1. Absorbance measurements at 280 nm were

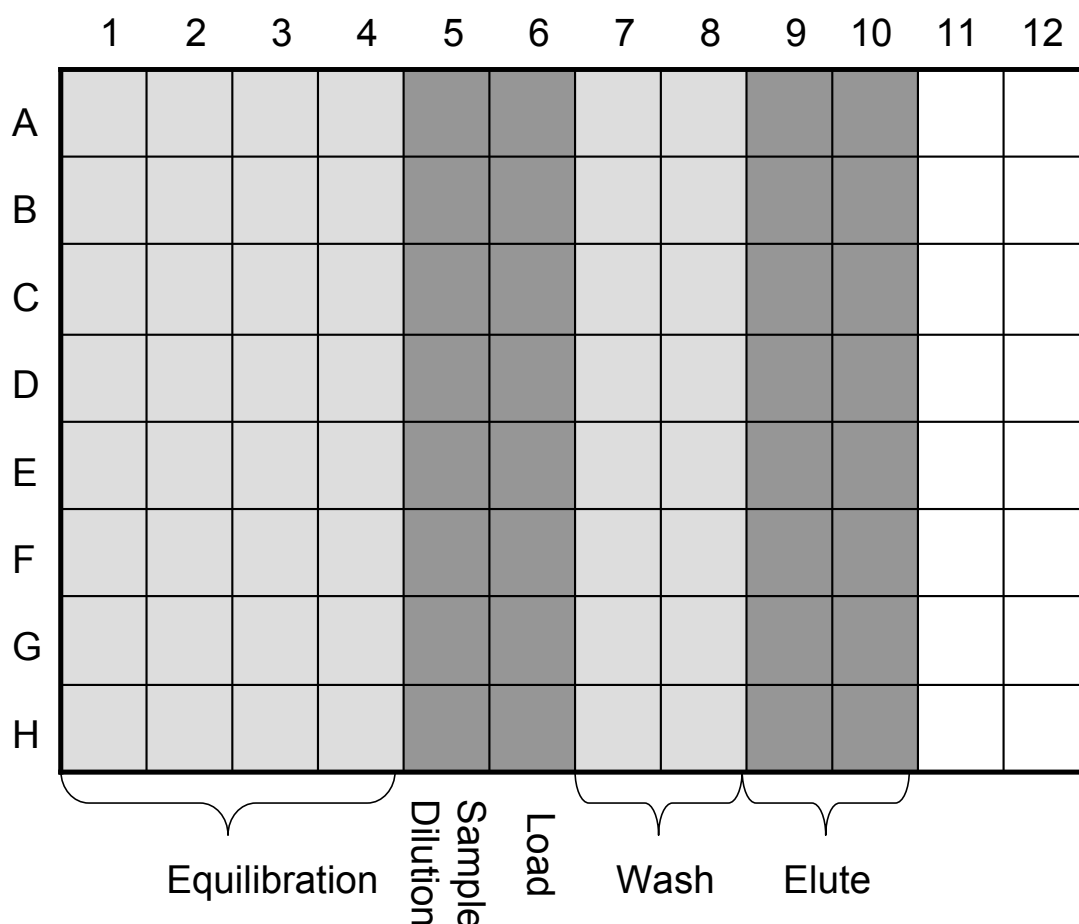


**Figure 5.4.** Plate layout (2-mL deepwell microtitre plate) for the primary evaluation of product (mAb-1) and host-cell impurity binding. Prior to the micro-tip chromatography, the purification solutions are pre-dispensed into the 96-well plate by the Tecan robot using standard disposable pipette tips, and the sample is pre-diluted into the desired mobile phase in Column 5 (with excess volume prepared for analytical testing). The desired volume of diluted sample for loading is then transferred to Column 6 for the micro-tip experiment. For the micro-tip chromatography, the micro-tip columns were first pre-washed in separate microplates (not shown), and then the micro-tip experiment was performed, with Columns 1-4 for equilibration, Column 6 for loading the sample (transferred from Column 5), Columns 7-8 for washing the micro-tip columns post-loading, and columns 9-10 for elution.

made in a 96-halfwell UV transparent microtitre plate for the determination of adsorbent binding ( $q$ ) and recovery.

In this study, experiments were performed first with purified mAb-1 and then, for a subset of conditions, with a sample containing representative host-cell contaminants in order to assess the binding behaviour of these impurities. Two strategies are available for assessing impurity binding. As was done for the test case used in this thesis, if purified product and a representative impurity sample are available, then their binding can each be screened separately and their response surfaces overlaid. Specifically, purified mAb-1 ( $\geq 90\%$  purity) was obtained in this study by an alternative purification with protein A chromatography. Meanwhile, the flow-through fraction from this same protein A chromatography served as a representative impurity sample, given that most of the antibody binds to the protein A column and is therefore removed from the flow-through fraction. This approach has the advantage of greatly simplifying both the experimental design and the analytical testing. Instead of examining multiple loading amounts, the micro-tip columns are overloaded with either purified antibody or an impurity sample at a single point on the asymptotic (nonlinear) portion of the adsorption isotherm, providing an estimate of maximum equilibrium capacity ( $q_m$ ). This may also serve as a qualitative surrogate for retention in cases where adsorbent capacity trends with binding affinity. Such a trend was observed in some of the work performed in this thesis with cation exchange chromatography and was noted by Kelley et al. (2008) in their high throughput micro-batch adsorption studies. An additional advantage is that absorbance (at 280 nm) can be used as a rapid measure of product and impurity binding instead of requiring separate analyses that are specific for both, significantly reducing the analytical burden. The disadvantage though is that it increases the number of micro-tip experiments. Moreover, no direct information about the competition between the product and impurities is obtained, which could alter the conclusions, especially in the case of strongly competing impurities. However, at this initial stage of development, the primary goal is to rapidly identify the best local region in the design space for maximising product binding and minimising impurity binding, so some error can be tolerated. The impact of competitive binding between the antibody and its impurities can be examined later during the secondary evaluation.

Separate samples of purified product and representative impurities are not always available, however, especially early in a program, or if an alternative purification procedure like protein A is not available. Furthermore, sometimes it may be critical to examine the competitive binding between product and impurities early on. In these cases, a representative feed stream is loaded, preferably at two (high, low) or more loading amounts to better understand the competitive binding behaviour. Coffman and co-workers (2008), studying the binding of monoclonal antibodies onto hydroxyapatite, ion-exchange, and hydrophobic-interaction adsorbents, performed a low challenge at 5 mg/mL of adsorbent, in the linear portion of the adsorption isotherm, and a high challenge at 30 mg/mL (or higher), which is more typical of an overloaded process operation. However, two points may not always be sufficient to fully characterise the binding interaction and competition between impurities. In this approach, assays for the specific detection of product and host cell impurities are required since absorbance at 280 nm cannot distinguish between them.

#### 5.4.3.2. Results of the Capture Study

Three-dimensional response maps of Capto MMC adsorbent capacity (estimate of  $q_m$ ) for purified mAb-1 in each of the four salts are shown in Figure 5.5. The shape of these response maps are affected most by the anion type, with the map of sodium sulphate resembling ammonium sulphate and that of sodium chloride resembling ammonium chloride. This is consistent with the observation that the Hofmeister effect is more pronounced with anions (Zhang and Cremer, 2006). The small deviations in the response surfaces are presumed to be from experimental variability. An estimation of the experimental variability was determined from the data points replicated across each experimental set (pH 4, 5, 6, 7, and 8 with no added salt), with the CV < 9% ( $n = 4$  to 10) in all cases. For the chloride salts, binding is weakened by increasing salt concentration at higher pH (> 6), suggesting that electrostatic interactions dominate in this pH range. However, at lower pH (< 6), binding is less affected by salt concentration, implying that hydrophobic interactions also play a role. In contrast to the chloride salts, increasing the salt concentration for the sulphate ions at higher pH weakens binding only to a certain point (approximately 0.5 M of the cation). Then, binding increases again, forming a valley in the response surface. This suggests that hydrophobic interactions are overwhelming electrostatic effects at higher salt concentrations. Binding capacity is the same or increases at

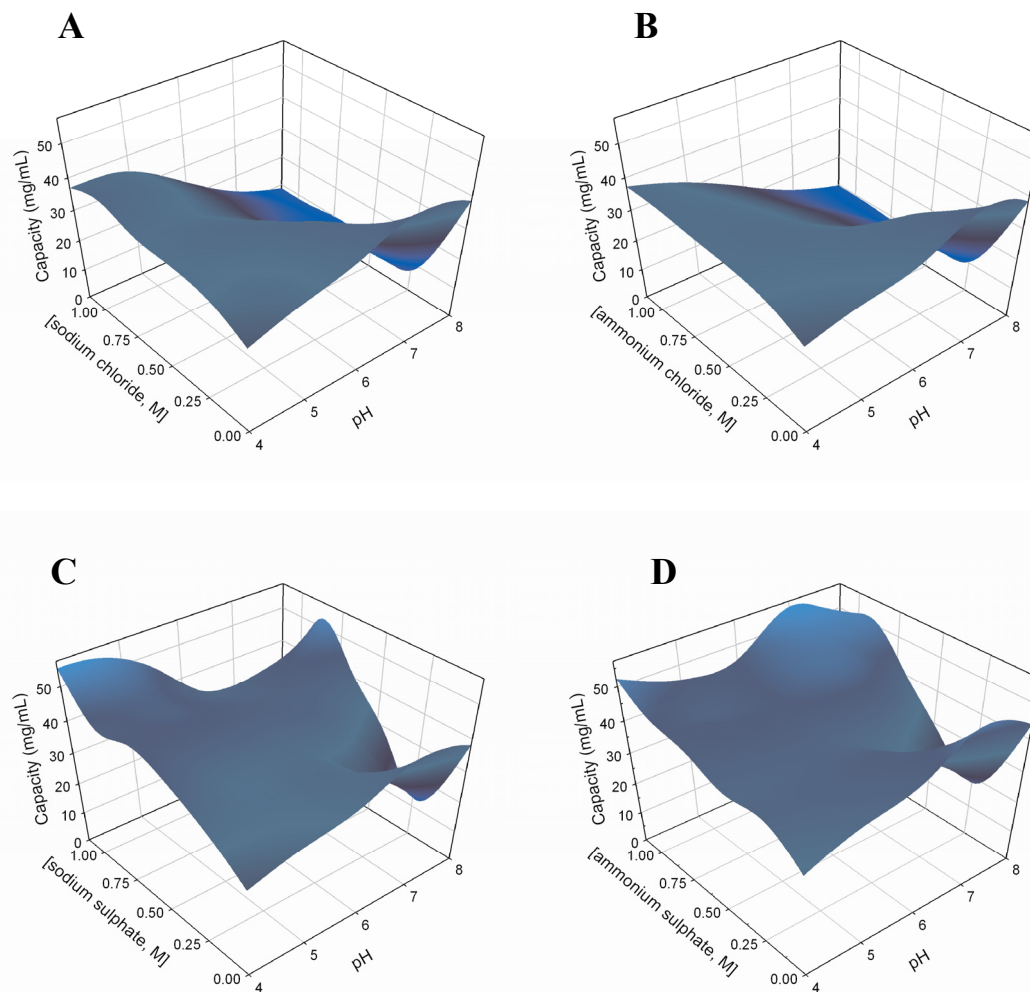


**Figure 5.5.** Response surface graphs of capacity (q) of the multimodal weak cation-exchange adsorbent (Capto MMC) for purified mAb-1 in four salt types as a function of salt concentration and pH: (A) sodium chloride, (B) ammonium chloride, (C) sodium sulphate, (D) ammonium sulphate.

lower pH, similar to the chloride ions, with one exception. A second valley is observed at pH 6 and high salt concentration, being more prominent for sodium sulphate, which indicates that the cation type has some influence on binding at this pH. Another difference between the chloride and sulphate salts is that the sulphate salts approach a binding capacity of 55 mg/mL whereas the chloride salts approach 40 mg/mL.

Only the ammonium sulphate and sodium chloride salts were carried forward for the evaluation of host cell protein binding because of the similarity between the anion pairs. In this case, a representative impurity sample containing no mAb-1 (protein A chromatography flow-through fraction) was used to evaluate host-cell protein binding. The contour plots of impurity binding (HCP ELISA) are compared with those of mAb-1 binding in Figure 5.6. Here, the impurity binding is represented as a fraction of the maximum impurity binding observed. Four lead mobile-phase conditions were identified for mAb-1 capture: (1) pH  $6.6 \pm 0.2$  and no added salt; (2) pH  $7.1 \pm 0.2$  and no added salt; (3) pH  $5.5 \pm 0.2$  and 0.25 M ammonium sulphate; and (4) pH  $7.0 \pm 0.2$  and 0.9 M ammonium sulphate). These conditions were selected because they provided sufficiently high mAb-1 capacity ( $\geq 40$  mg/mL) and low impurity binding ( $\leq 0.2$  relative host cell protein binding). Of these, the condition yielding the highest capacity was the pH 7.0, 0.9 M ammonium sulphate point (51 mg/mL adsorbent). An additional criterion that was considered was the robustness of the operating range around each point (i.e. insensitivity to small changes in pH or salt concentration). Specifically, the pH 5.5, 0.25 M ammonium sulphate condition was chosen because of its very robust operating window (wide range of insensitivity to changes in pH and salt concentration). Overall, given the potential for very high impurity clearance, the Capto MMC adsorbent appears to be well suited for use as a capture step in the purification of mAb-1 from *Pichia Pastoris* cell filtrate, when operated in a bind-and-elute mode.

#### 5.4.3.3. Use of Statistical Software for Selecting Lead Conditions

A statistical DoE software package can greatly facilitate data analysis, even if it is not used for the experimental design, by enabling multiple variables and response factors to be evaluated simultaneously, particularly in cases where the evaluation

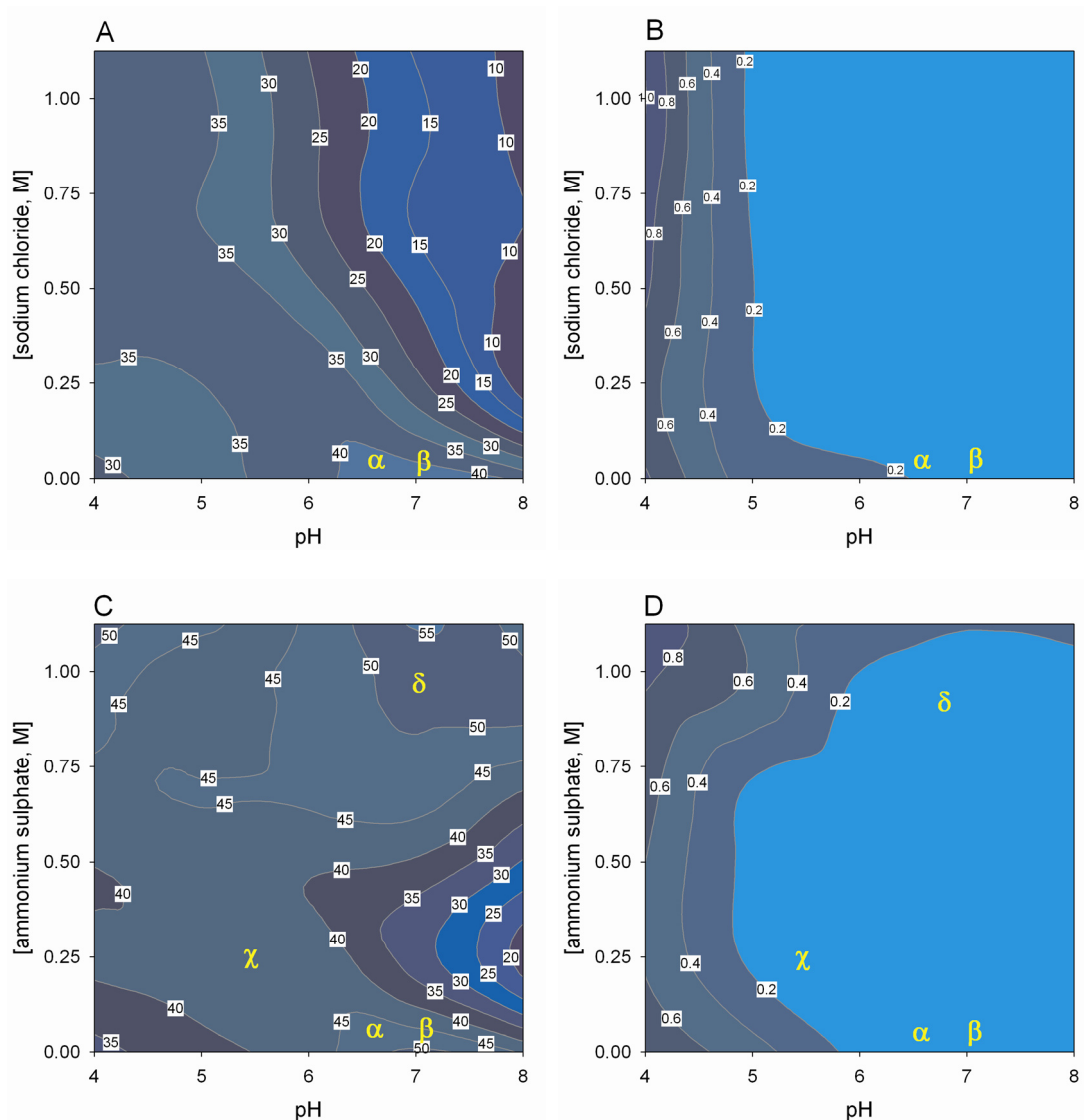


**Figure 5.6.** Contour plots showing the capacity (q) of the multimodal weak cation-exchange adsorbent (Capto MMC) for purified mAb-1 and host cell proteins (HCP) as a function of pH and salt concentration: (A) purified mAb-1 capacity (mg/mL adsorbent) in sodium chloride; (B) impurity sample in sodium chloride (fraction of maximum impurity binding); (C) purified mAb-1 capacity (mg/mL adsorbent) in ammonium sulphate; (D) impurity sample in ammonium sulphate (fraction of maximum impurity binding). Binding optima selected for examination in secondary experiments:  $\alpha$ , pH  $6.6 \pm 0.2$  and no added salt;  $\beta$ , pH  $7.1 \pm 0.2$  and no added salt;  $\chi$ , pH  $5.5 \pm 0.2$  with 0.25 M ammonium sulphate; and  $\delta$ , pH  $7.0 \pm 0.2$  with 0.90 M ammonium sulphate.

cannot be done easily by visual inspection. In addition, these software packages typically allow specifications to be placed on the data, such as limiting the parameters used or their range, requiring a result to be between a minimum or maximum value, and weighting the responses (e.g. capacity, purification factor, and recovery) according to their importance to the purification (process function).

In this study, Design Expert software (version 7.1.3) from Stat-Ease (Minneapolis, MN, USA) was used to analyse the data from the sodium-chloride and ammonium-sulphate capture study. These data, because of their complex response surface, were fit with a cubic polynomial model (the highest order model available in the software). The responses of mAb-1 capacity (set to maximise this response), impurity binding (set to minimise this response), and recovery (set to exceed a minimum threshold of 65%) were evaluated in the statistical analysis. The capacity and impurity binding responses were equally weighted with high importance. No constraints were placed on the parameter input ranges (pH 4 to 8; salt concentration 0 to 1.25 M). A 'desirability' plot for optimal loading, which balances capacity with the extent of purification, is shown in Figure 5.7, with 0 being the least desirable condition, and 1, the most desirable. The most favourable loading regions from this statistical evaluation agree well with the visual assessment made in Figure 5.6.

#### 5.4.4. Secondary Evaluation: Elution Study and Loading Optimisation

The purpose of the primary capture study is not only to maximise the binding capacity but also to attempt to achieve some selectivity on the adsorption side of the chromatographic separation. This is particularly desirable for a capture chromatography step in order to reduce the burden of separation during elution and on the purification in subsequent process steps. In the study here, binding conditions were identified for the multimodal weak cation-exchange adsorbent (Capto MMC) that showed very good selectivity for mAb-1, in which many of the *Pichia pastoris* host-cell protein impurities were not retained. A secondary evaluation was then performed to optimise the lead loading conditions and define the wash and elution strategies, with the ultimate goal being to have a purification sequence that is predictive of laboratory- and process-scale operation. The response maps from the primary evaluation were used to guide the selection of ranges for elution pH and salt concentration.

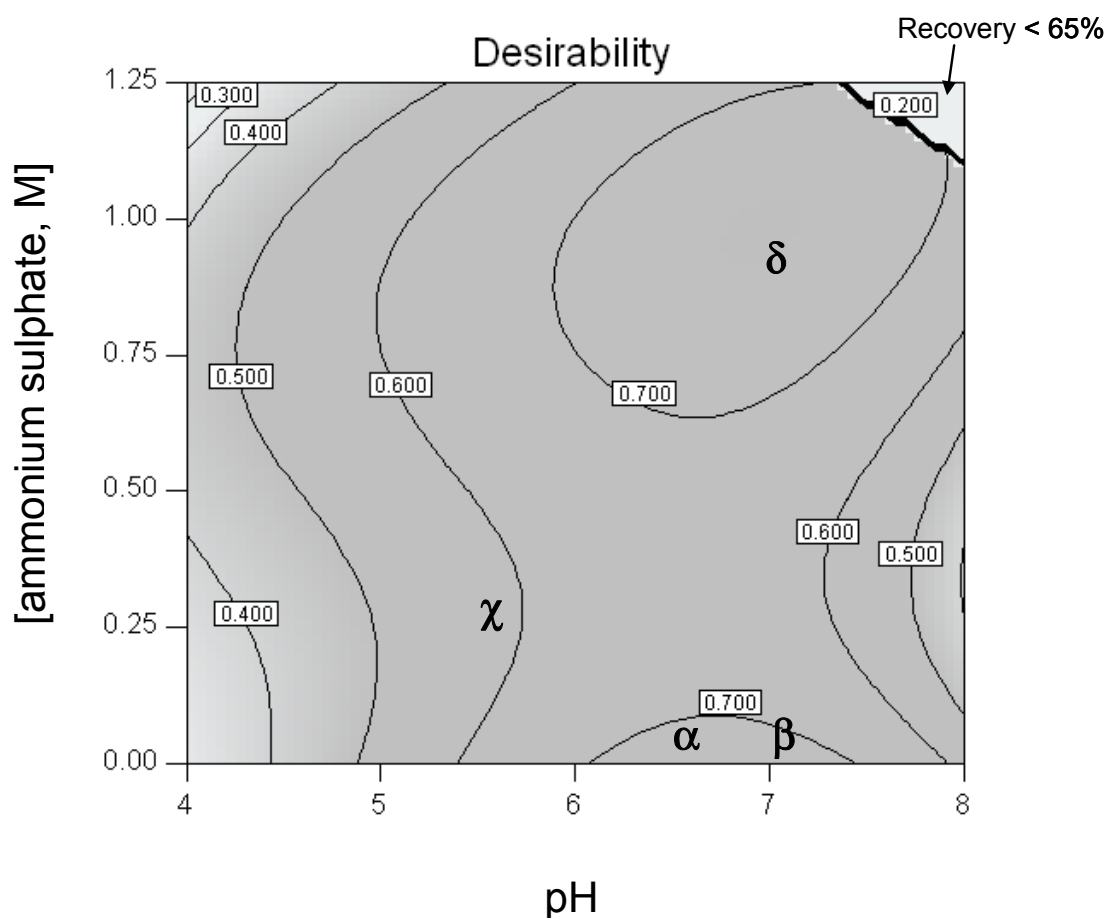


**Figure 5.7.** Determination of desirable loading conditions from the ammonium sulphate screen using statistical software (Design-Expert from Stat-Ease). Contour lines represent the desirability of the load conditions, with 1 be most optimal and 0 being the least optimal. Capacity and purification factor were weighted with equal importance, and a minimum recovery of 65% was required. Response surfaces for capacity and purification factor are fit with a cubic polynomial model. The optimal conditions chosen by visual inspection from the contour plots (Fig. 5.6) are designated on this graph by  $\alpha$ ,  $\beta$ ,  $\chi$ , and  $\delta$ .

#### 5.4.4.1. Experimental Layout

The experimental methods used here for the secondary evaluation were also fully automated, having loading, wash, and elution steps. In contrast to the primary capture study, the micro-tip columns were loaded with crude sample (clarified cell supernatant) and generally were not overloaded, except to estimate binding capacity under the optimised conditions. Feed samples were exchanged into different mobile phase conditions by either membrane dialysis or dilution of a concentrated feedstock. A staircase elution method was used as a means to efficiently develop the product elution, in which incremental steps of increasing eluent strength were made. The layout of the 96-deepwell purification plate for the secondary evaluation experiments is shown in Figure 5.8. For each experiment (micro-tip columns A-H), the sample was diluted into the loading buffer in column 1 (if necessary), loaded with the desired volume in column 2, washed in column 3, and then eluted in columns 4-12. Sodium phosphate was used as a buffer for solutions with a pH of 6.2-7.8, and HEPES buffer was used for all solutions above this range (up to pH 8.5).

#### 5.4.4.2. Results of the Elution Study

As observed from the response maps shown in Figure 5.5 and 5.6, mAb-1 adsorption is weakened at higher pH and ionic strength, although binding strength begins to increase again for the sulphate salts at concentrations greater than 0.25 M (cation concentration of 0.5M). Figure 5.9 shows the effect of elution buffer pH (6.5 – 8), salt type, and cation concentration (0 to 1.6 M  $\text{NH}_4^+$  or  $\text{Na}^+$ ) on mAb-1 elution. In these experiments, the columns were loaded with cell filtrate to 30 mg mAb-1 per mL of Capto MMC adsorbent at  $\text{pH } 7.1 \pm 0.2$  and no added salt. Higher elution pH resulted in a more efficient elution, presumably because of increased charge repulsion and disruption of electrostatic interactions. In addition, the sodium salts yielded a slightly higher recovery, most likely because sodium does not promote as much hydrophobic interaction as ammonium. Furthermore, sodium chloride is preferred over sodium sulphate since hydrophobic interactions at higher concentrations are not favoured. Therefore, sodium chloride was used as the eluent for the remainder of the secondary evaluation.

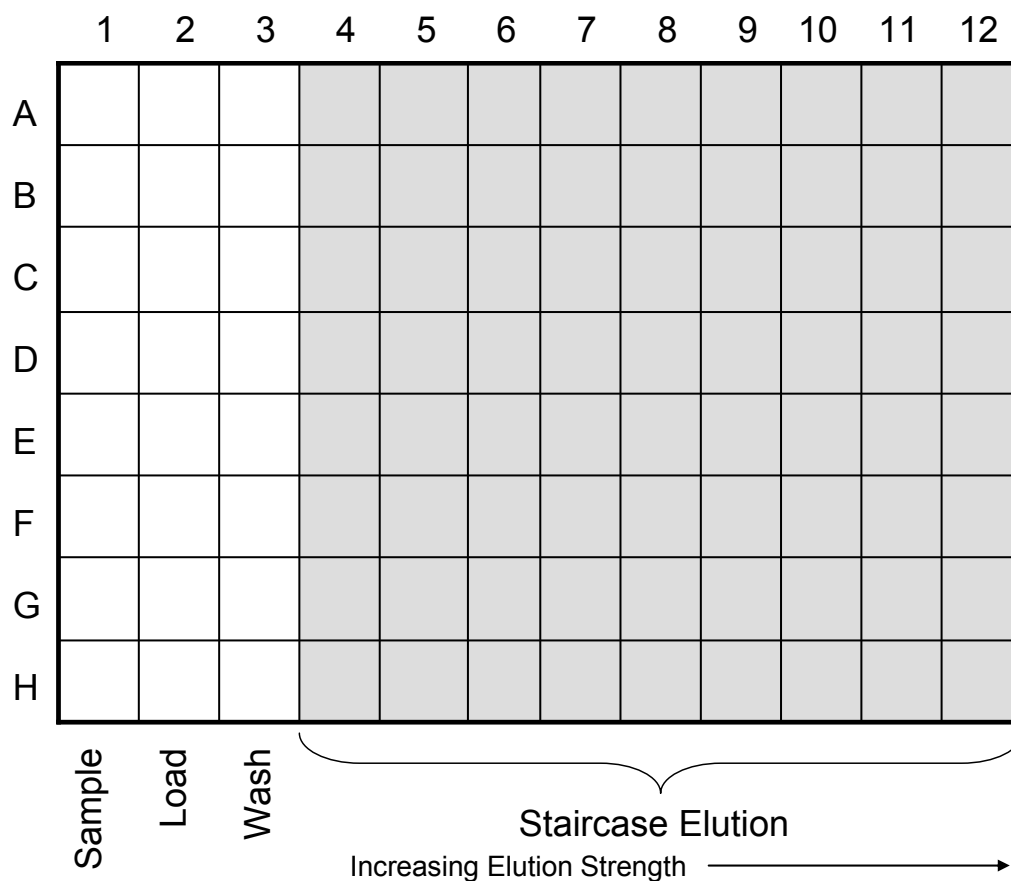


**Figure 5.8.** Plate layout (2-mL deepwell microtitre plate) for the secondary evaluation study (elution and loading optimisation) in the development of a mixed-mode chromatography step. Micro-tips were pre-washed and equilibrated in separate microplates. The sample and purification solutions were pre-dispensed into the 96-well plate by the Tecan workstation from troughs and/or reservoir plates prior to the micro-tip column chromatography. For each experiment (micro-tip columns A-H), the feed sample was diluted into the loading buffer in column 1 (if necessary), allowing for excess volume for analytical testing, then loaded with the desired feed volume in column 2, washed in column 3, and eluted in columns 4-12.

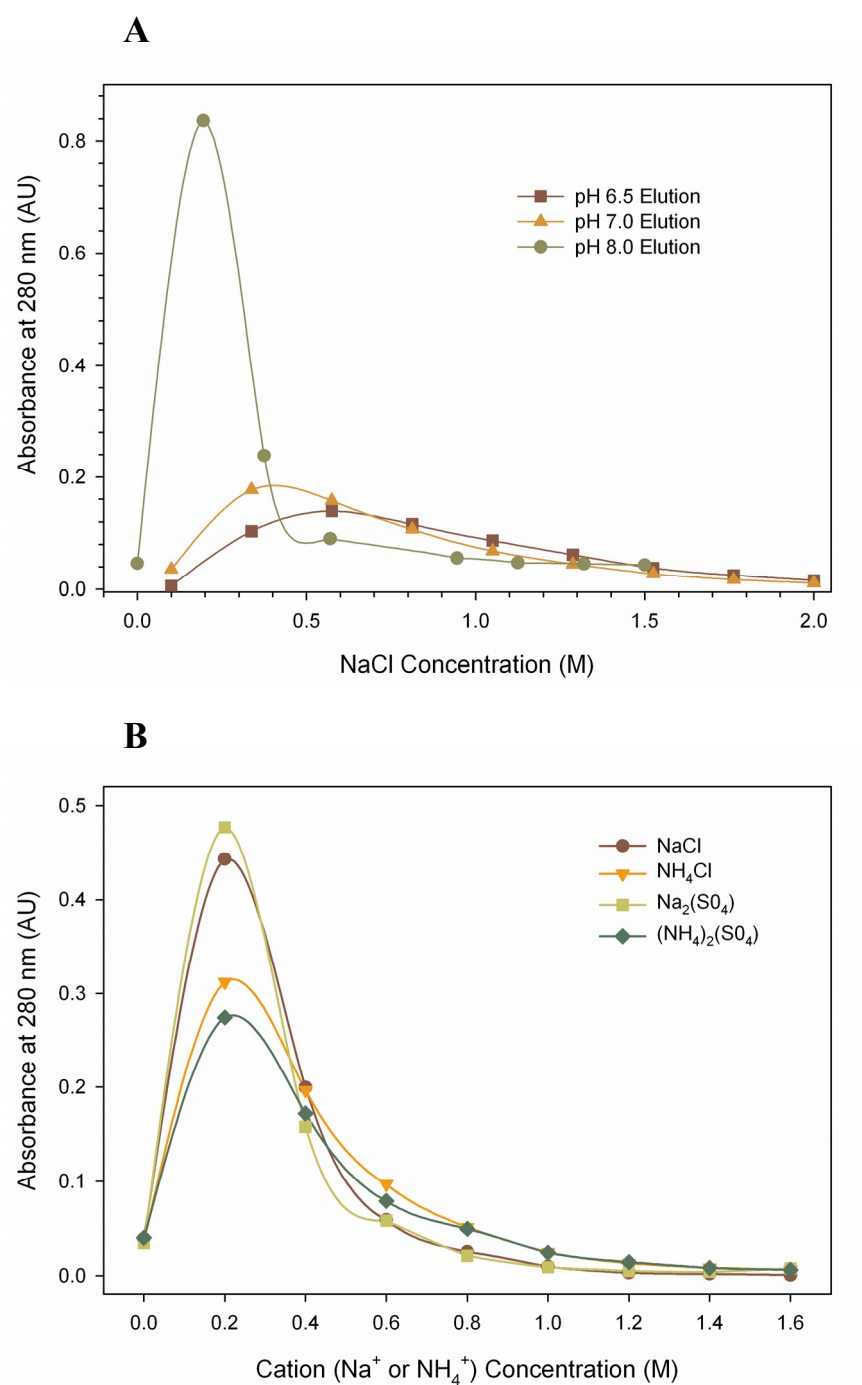


**Figure 5.9.** Evaluation of mobile phase conditions for the elution of mAb-1 from the multimodal weak cation-exchange adsorbent (Capto MMC): **(A)** effect of pH (elution with NaCl); **(B)** effect of salt concentration and salt type at pH 8. The micro-tip columns were loaded with diluted cell filtrate (loading = 30 mg mAb-1/mL adsorbent) at pH  $7.1 \pm 0.2$  and low ionic strength (no added salt).

#### 5.4.4.3. Definition of the Final Purification Sequence

The four optimal loading conditions shown in Figures 5.6 and 5.7 were compared by carrying out a staircase elution (0.25 M increments) with sodium chloride at pH 8. A direct load of the clarified cell filtrate (pH 7.2, conductivity  $\leq 10$  ms/cm) was carried out in lieu of the pH 7.1 condition (no salt added), whereas for the other conditions, the clarified cell filtrate was exchanged into the desired solution condition by dialysis. In these experiments, the columns were loaded at 20 mg mAb-1 per mL of adsorbent. The elution profiles from these purifications are shown in Figure 5.10A, along with the yield as measured by the Octet protein-A biosensor assay. Interestingly, for the condition loaded at 0.9 M ammonium sulphate (pH 7.0), the product begins to elute with decreasing salt concentration (0.9 to 0 M) and a concomitant increase in the pH from 7 to 8. In contrast, elution for the other three conditions does not begin until the salt concentration is increased to 0.25 M NaCl at pH 8.0. This suggests that adsorption in 0.9 M ammonium sulphate is driven primarily by hydrophobic interactions, whereas the interaction in the other three loading conditions is predominantly electrostatic, or a combination of the two.

While the recovery is comparable for the four loading conditions (83-88%), the extent of purification differs, as observed in Figure 10B. Several protein contaminants as well as free antibody light chain elute at pH 8 (0 M NaCl). As a result, some of the product co-elutes with these impurities for the feed loaded in 0.9 M ammonium sulphate. The purity of each of the products from the other three loading conditions is comparable, with a purity of ~90% by SDS-PAGE. Since the direct loading of the clarified cell filtrate is the most convenient of the three conditions, with no buffer exchange required, it was chosen as the winning condition for verification in a dynamic laboratory-scale column chromatography experiment. The adsorbent capacity for mAb-1 (when loading the clarified cell filtrate) as determined by the micro-tip chromatography experiments is about 35 mg/mL. At this loading, the product recovery was ~80%, and over a 5000-fold reduction in host cell protein levels was achieved (as determined by HCP ELISA).

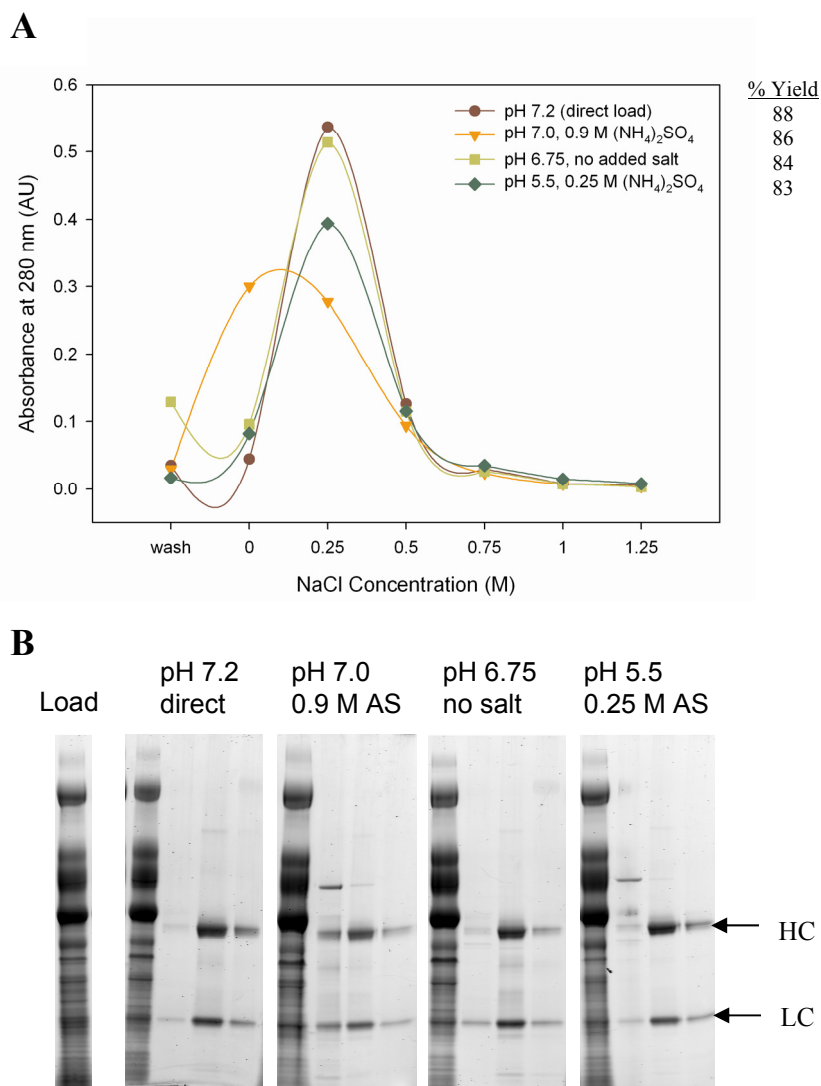


**Figure 5.10.** Secondary evaluation of four loading conditions in the purification of mAb-1 from clarified cell filtrate by multimodal weak cation-exchange (Capto MMC) chromatography. **(A)** Incremental step elution with increasing sodium chloride concentration (0.25 M/step), with the % yield of the mAb shown in the legend: (●) direct load of cell filtrate at pH 7.2 (conductivity  $\leq 10$  mS/cm); (▼) load at pH 7.0 in 0.9 M ammonium sulphate (AS; dialyzed); (■) load at pH 6.75 (dialyzed, no added salt); and (◆) load at pH 5.5 in 0.25 M ammonium sulphate (dialyzed). Each micro-tip column was underloaded at 20 mg/mL and eluted with sodium chloride at pH 8. **(B)** SDS-PAGE (reducing conditions; Sypro Ruby protein stain) of each microscale purification. The first lane is the clarified cell filtrate. Within each loading condition, lane 1 is the nonbound fraction, and lanes 2-4 are the eluted fractions (pH 8) at 0 M NaCl, 0.25 M NaCl, and 0.5 M NaCl, respectively. HC = heavy chain of the mAb; LC = light chain of the mAb.

#### *5.4.5. Laboratory-Scale Column Verification of the Microscale Results*

The optimised purification determined by micro-tip chromatography (direct load of the clarified filtrate and elution with sodium chloride at pH 8.0) was verified with a laboratory-scale column experiment using a 1-mL Hi-Trap Capto MMC column. The crude cell filtrate (pH  $7.2 \pm 0.2$ ; conductivity  $\leq 10$  mS/cm) was loaded directly onto the column at a residence time of four minutes (37.5 cm/h; total load time of 145 minutes) and a loading challenge of 36 mg of mAb-1 per mL of adsorbent. The product was eluted with sodium chloride at pH 8.0 in a twenty column-volume (CV) linear gradient from 0 to 1 M.

The UV chromatogram and purity (by HCP ELISA and gel electrophoresis) results from the column experiment are shown in Figure 5.11. Most of the host-cell protein impurities do not bind to the column and are recovered in the column flow-through fractions, as was the case in the microscale purification. The dynamic binding capacity at 2% breakthrough was determined from this column experiment to be approximately 34 mg/mL adsorbent, in line with the semi-equilibrium capacity of 35 mg/mL observed in the micro-tip experiments. The product elutes from the column at about 0.36 M NaCl, also consistent with the micro-tip chromatography (elution between 0.25 and 0.5 M NaCl elution steps, as shown in Figure 5.10). For those host-cell proteins that do bind to the column, the majority of them appear to elute following the mAb-1 elution, at around 0.7 M NaCl. It therefore may be possible to achieve additional HCP clearance by modifying the elution gradient. The product purity is 88% by SDS-PAGE, comparable to a protein-A purified product.

The laboratory-scale column results are compared to the microscale results in Table 5.3. The microscale purification is predictive of the column performance with respect to column capacity, yield, and purity. Although the step yield is below 90%, it is still an acceptable step recovery given the significant clearance of host cell proteins (99.99%) and DNA (97.99) that is achieved. The remaining HCP contaminants are about 3-fold lower in the laboratory-column product than in the micro-tip column. This is presumably due to the increased resolution gained in carrying out column chromatography with linear gradient elution. However, given the reasonable separation achieved between the mAb-1 product and the HCPs in

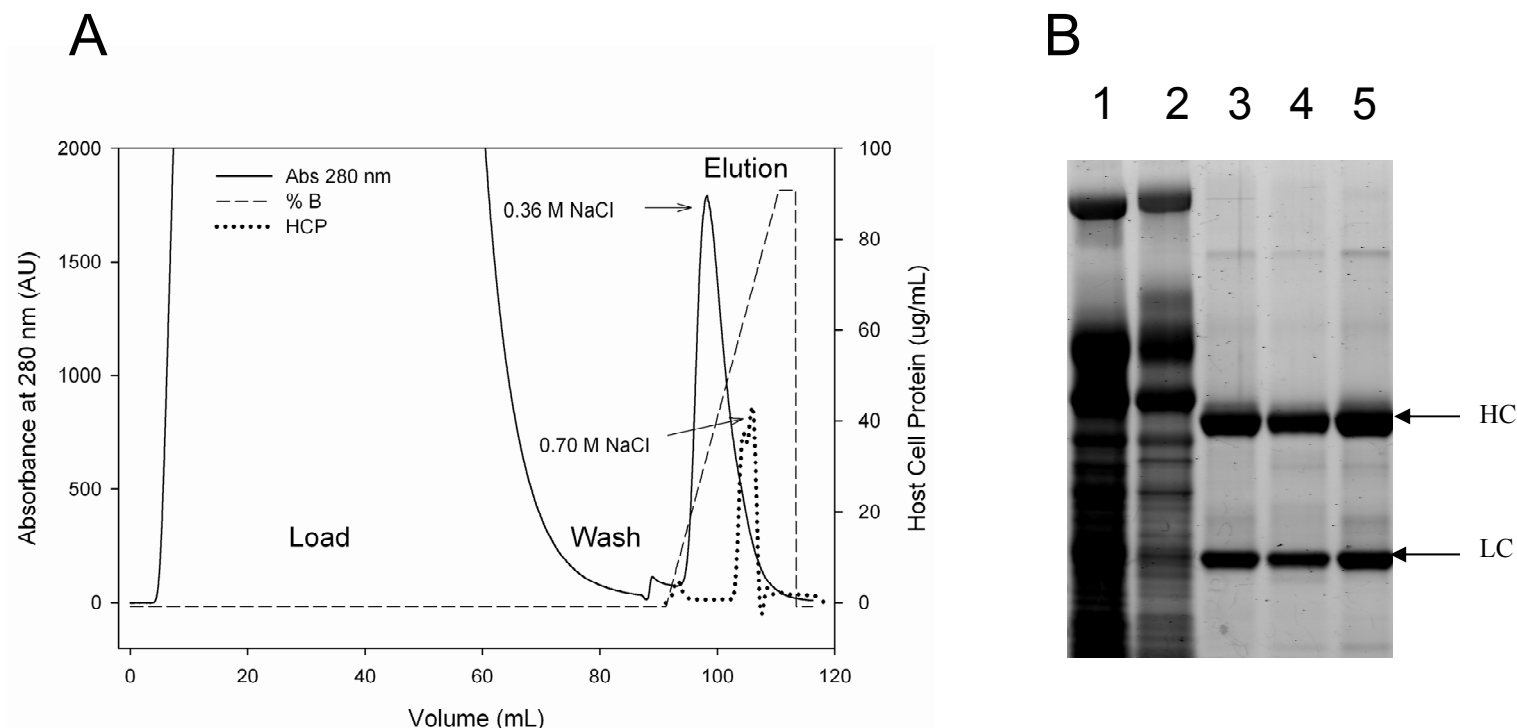


**Figure 5.11.** Verification of the microscale results for the multimodal weak cation-exchange (Capto MMC) chromatography at the laboratory column scale (1-mL Hi-trap column). **(A)** Column chromatogram in which the clarified cell filtrate was loaded directly on the column at a residence time of four minutes. The product (mAb-1) was eluted at pH 8.0 with NaCl in a 20-CV linear gradient from 0 to 1.0 M. The dotted line represents host-cell protein (HCP) elution as measured by ELISA. **(B)** SDS-PAGE (under denaturing and reducing conditions; Sypro Ruby protein stain) to examine the extent of purification: **lane 1**, column feed (clarified cell filtrate); **lane 2**, nonbound fraction; **lane 3**, column product; **lane 4**, microscale chromatography product; **lane 5**, purified product from protein A chromatography (for comparison). HC = heavy chain; LC = light chain.

Figures 5.10 and 5.11, a step gradient yielding similar results seems achievable with careful optimisation of the NaCl concentration.

**Table 5.3.** Comparison of results between micro- and laboratory-scales<sup>a</sup> for the purification of mAb-1 from cell filtrate using multimodal weak cation-exchange (Capto MMC) chromatography.

	<b>Capto MMC</b> Micro-Tip Column (10 µL; Batch)	<b>Capto MMC</b> Lab-Scale Column (1 mL; Dynamic)
Step Recovery (%)	77	82
Purity, by SDS-PAGE (%)	88	88
Purity, by HCP <sup>b</sup> ELISA (ppm)	5346	1624
HCP Clearance (%)	99.98	99.99
DNA clearance (%)	not assayed	97.99

a) Adsorbent loading at each scale was approximately 35 mg mAb/mL adsorbent.

b) HCP = *Pichia pastoris* host cell proteins

### 5.5. Experimental Throughput

The microscale workflow demonstrated here allowed the mixed mode chromatographic purification to be developed in under 2-3 weeks. This time accounts for not only the purification experiments but also the analytical testing and sample preparation. With one Tecan robot and one trained full-time equivalent (FTE), the range-finding study and primary evaluation can be completed in approximately 5-7 days, assuming 1 day for the initial range finding experiment and 1-1.5 days per salt condition (accounts for evaluation of both the purified and impurity samples). If more parameters are examined (e.g. buffer concentration), then this would increase this time or require a more sophisticated DoE strategy, as opposed to the brute-force one applied here. Alternatively, use of a 96-channel liquid handling arm would increase the throughput by a factor of 12 over the 8-channel arm used in these experiments. The secondary evaluation can be completed in about 2-5 days, depending on the experimental outcomes, but this time does not account for any associated analytical testing or sample preparation. If these are taken into account, then the evaluation could take double this time. The column

verification then requires 1-2 days. In contrast to the throughput of the microscale experiments, a comparable set of conventional laboratory-scale columns experiments might conservatively take about 2-3 months. Most likely though, fewer experiments would be done and, consequently, the parameter space would not be as thoroughly characterised.

## **5.6. Summary**

A high-throughput, automated workflow using batch microscale chromatography has been designed for the rapid and comprehensive development of mixed mode chromatography steps. Such a workflow allows development to be completed in days rather than weeks and is amenable to chromatography types beyond that of mixed mode. This workflow was successfully demonstrated here in the development of a capture step using multimodal weak cation-exchange (Capto MMC) chromatography for the purification of a monoclonal antibody from crude cell filtrate. One hundred and twenty solution conditions were evaluated in the primary screen for their effect on binding capacity, enabling a thorough exploration of the design space and helping to guide development of loading and elution conditions. Four lead conditions for loading were then further evaluated, and elution conditions were defined for maximum product yield and purity. The final selected conditions revealed that mixed mode chromatography provides a potential alternative to protein A chromatography for the purification of mAb-1 from crude yeast cell filtrate. The optimised microscale purification was then scaled up to the laboratory scale (1-mL column), with the results from the dynamic column experiment consistent with the batch 10- $\mu$ L micro-tip experiments in terms of yield, purification, and adsorbent capacity. This agreement between scales is consistent with the results of Chhatre and colleagues (2009), in which the data from 20- $\mu$ L micro-tip screening experiments trended well with those from 10-mL column experiments.

Having a high-throughput microscale workflow like the one outlined here is a first step in implementing a quality by design (QbD) process development paradigm. High-throughput, parallel experimentation allows the 'knowledge space' and critical operating boundaries of a chromatography step to be thoroughly mapped. Although not all aspects of microscale chromatography will scale linearly to the laboratory or

process scale, fundamental knowledge about the chromatography can be learned and, in turn, used to define the design space. Furthermore, the use of appropriate modelling techniques like those described in Chapter 4 may offer a route to scale-up prediction using these data. In these ways, the use of microscale methods not only accelerates process development but also leads to more robust, better understood bioprocesses.

## **6. A MULTI-STEP CHROMATOGRAPHIC SCALE-DOWN WITH MICRO-TIP CHROMATOGRAPHY**

### **6.1. Introduction**

The optimisation of yeast fermentation processes requires balancing expression titres with product quality. Changes to cell fermentation conditions are typically evaluated following cell disruption, with expression levels quantified by immunoassay (Cruz et al., 1998; Sun et al., 2002; Maranga et al. 2003; Zhang and Lynd, 2003), HPLC (Amari and Mazsaroff, 1996), enzyme activity (Fisher and Woods, 2000), flow cytometry (Soriano et al., 2002), optical biosensors (Bracewell et al., 2004), or fluorescence polarization (Sun et al., 2002). However, these titres do not always predict the effects that intracellular aggregation, proteolysis, post-translational modifications, and differences in relative impurity levels can have on purification yield and product purity. Furthermore, for recombinant subunit vaccines, heterogeneity in the size and surface properties inherent in virus-like particles (VLPs) makes unit operations such as chromatography less predictable. Experiments which optimise fermentation conditions should therefore consider more than mass expression, but also the quality of the material and its effect on the downstream purification.

Such an example was encountered in the production of recombinant human papillomavirus (HPV) VLPs. The VLPs are produced by expression of the major capsid L1 protein of HPV in *Saccharomyces cerevisiae* (Hofmann et al., 1995; Hofmann et al., 1996; Neeper et al., 1996; Rossi et al., 2000), which assembles into icosahedral particles whose structure resembles the native capsid (Baker et al., 1991). Here, the most informative feedback on fermentation changes was obtained by completing a two-step chromatographic purification and then evaluating process yield and product purity (Wenger et al., 2007). This chapter addresses the development of a mimic of this purification using micro-tip columns. The performance of the micro-tip chromatography is compared to the laboratory-scale column chromatography with respect to yield, purity, and experimental throughput. The successful miniaturisation of the chromatography subsequently necessitated a microscale method for yeast cell disruption in order to eliminate this resulting bottleneck and obtain a fully microscale purification. The development of a microscale cell disruption technique for yeast is discussed in Chapter 7.

## 6.2. Chromatography of Viral Particles

The majority of preparative chromatographic adsorbents for protein purification are optimised for proteins having diameters less than 5 nm. DePhillips and Lenhoff (2000) investigated the mean pore diameters of 14 cation exchange resins by inverse size-exclusion chromatography and found that they ranged from 20-150 nm, consistent with the average pore sizes given by the manufacturers of these adsorbents. Because viral particles can range in size from about 10 to 100 nm in diameter, their capture by standard chromatographic methods is inefficient due to low particle diffusivity and inaccessibility to much of the pore volume (Lyddiatt and O'Sullivan, 1998; Zhang et al., 2001; Lyddiatt, 2002). The chromatography of viral particles is further complicated by aggregation and variable particle morphology, which have been observed for HPV VLPs produced in eukaryotic cells (McCarthy et al., 1998; Shi et al., 2005; Mach et al., 2006). In particular, Mach and co-workers (2006) observed that the expression of HPV types 6, 11, and 16 VLPs in yeast yielded particles that were irregularly shaped, broadly distributed, and smaller than the native virus particles. Transmission electron micrographs showing the distribution of VLPs expressed in yeast are provided in Figure 6.1. VLPs that were disassembled and then reassembled *in vitro* are also shown in Figure 6.1 in comparison to the those that were not treated.

Because aggregation and heterogeneity in the particle size and morphology of VLPs would be expected to impact the performance of chromatographic steps, developing fermentation processes which are consistent for these product attributes is important to obtaining downstream process consistency. As shown in Figure 6.2, analysis of post-fermentation HPV VLP titres by immunoassay does not adequately predict final purification yields, presumably because of differences in these attributes, so that a laboratory-scale purification is needed to assess fermentation performance. The purification involves first disrupting the yeast cells by homogenisation and removing the cellular debris by centrifugation. The VLPs are then captured from the clarified lysate by strong cation exchange chromatography (CEX; 80-mL POROS 50HS column) and additionally purified by ceramic hydroxyapatite chromatography (CHT; 30-mL column). Each fermentation paste is then evaluated on its final product yield and purity through the purification. The specific details of the laboratory-scale purification are given in Chapter 2.

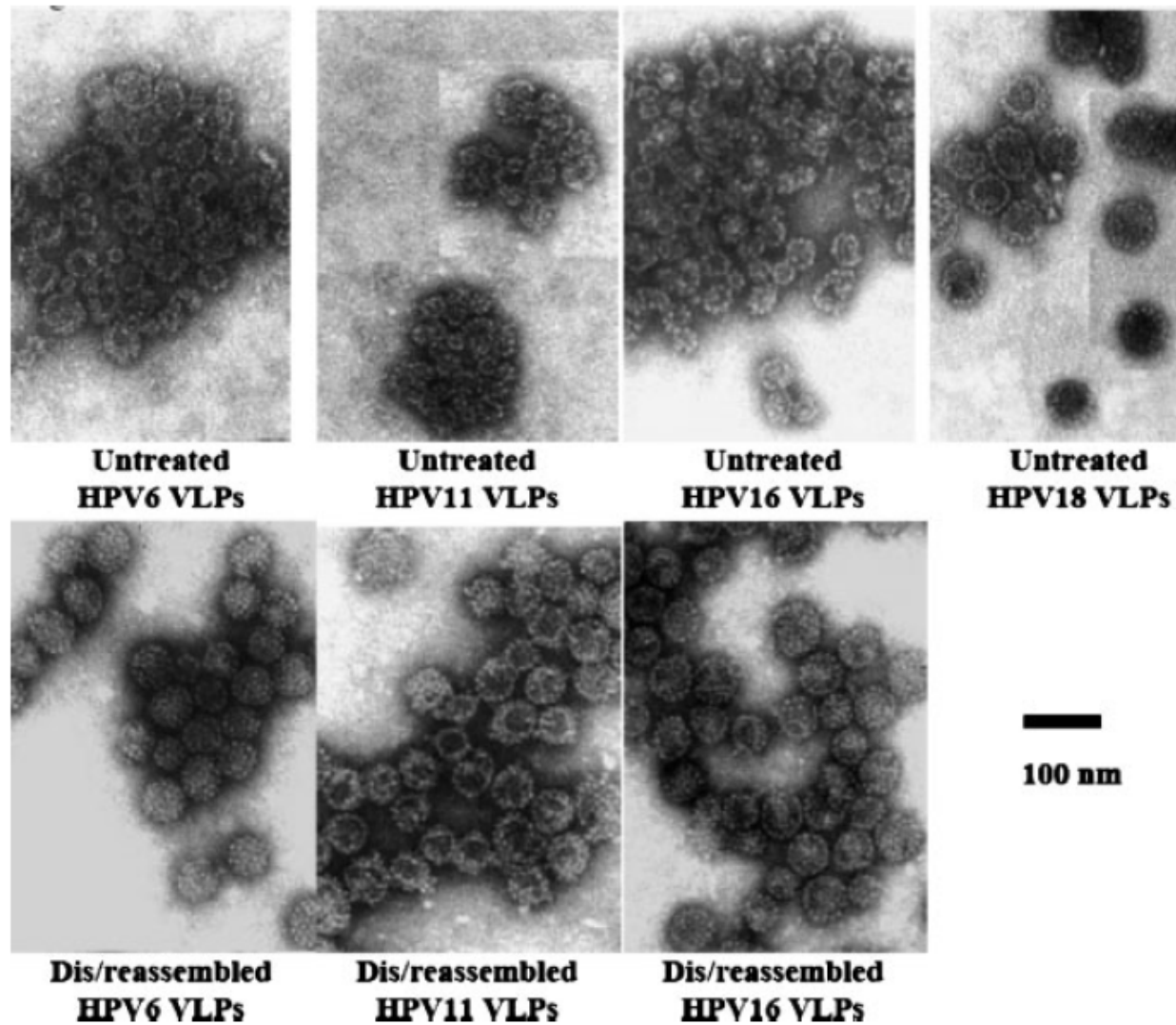


**Figure 6.1.** Transmission electron micrographs of HPV 6, 11, 16, and 18 VLPs, from the publication by Mach et al. (2006). Untreated VLPs, as expressed and purified from yeast, are compared to VLPs that were disassembled and then reassembled *in vitro*.

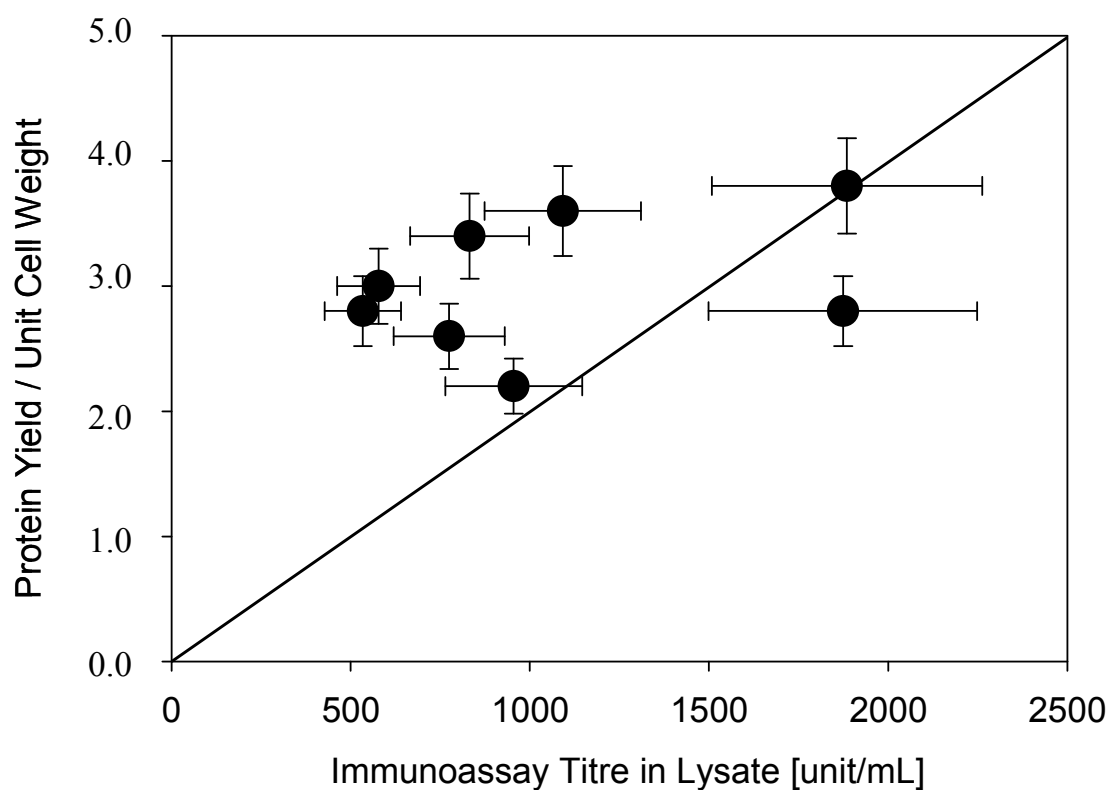


**Figure 6.2.** Correlation of the VLP titre in lysate by immunoassay to the total protein recovery through a multi-step chromatographic purification. The protein recovery is normalised to cell weight input.

### **6.3. Miniaturisation of the VLP Chromatographic Purification**

The thorough optimisation of fermentation conditions for a multivalent vaccine requires that many hundreds of fermentations be carried. Given that a purification is needed to best evaluate the impact of these fermentation changes on the downstream chromatography, this means hundreds of small-scale purifications must be performed. Miniaturising and automating these development experiments allows them to be carried out in the numbers necessary to rigorously optimise and validate the fermentation process, while simultaneously decreasing the time, materials, and labour required. Therefore, in the case of HPV VLPs, a chromatographic mimic of the laboratory-scale column purification was developed using micro-tip chromatography (Wenger et al., 2007), as outlined in the flow diagram in Figure 6.3. The micro-tip chromatography was performed using an 80- $\mu$ L CEX column and a 40- $\mu$ L CHT column. In doing so, the purification was miniaturised by about three orders of magnitude and automated on the Tecan workstation.

Micro-tip chromatography was carried out as described in Chapter 3, with pre-wash, equilibration, loading, wash, and elution steps. The chromatographic sequence was the same as that performed for the laboratory-scale purification (Chapter 2), with one primary exception. The linear sodium-phosphate gradient elution of the laboratory-scale CHT polishing chromatography was converted to a single step elution. The specific parameters of micro-tip column operation are given in Table 6.1, along with the run times. Eight micro-tip columns were picked up in each automated run, with the product pool of two CEX columns loaded onto one CHT column. This allowed for a sufficient loading of the CHT column, while providing excess material for analytical testing of the CEX process intermediate. Flow rates used throughout the VLP purification ranged from 5-20  $\mu$ L/sec, equivalent to an average linear velocity of 270-1080 cm/hr for the 80- $\mu$ L CEX column and 405-1620 cm/hr for the 40- $\mu$ L CHT column. Prior to the CEX purification, the micro-tip columns were wetted with 50% methanol (200  $\mu$ L), followed by washes with water (650  $\mu$ L), elution buffer (160  $\mu$ L), and equilibration buffer (3 X 500  $\mu$ L). For the CHT chromatography, tips were washed with 0.4 M sodium phosphate (pH 6.8) and the elution buffer (150-300  $\mu$ L) prior to washes with equilibration buffer (4 X 600  $\mu$ L). Pre-treatment and equilibration steps were carried out using a 12-column reservoir plate.

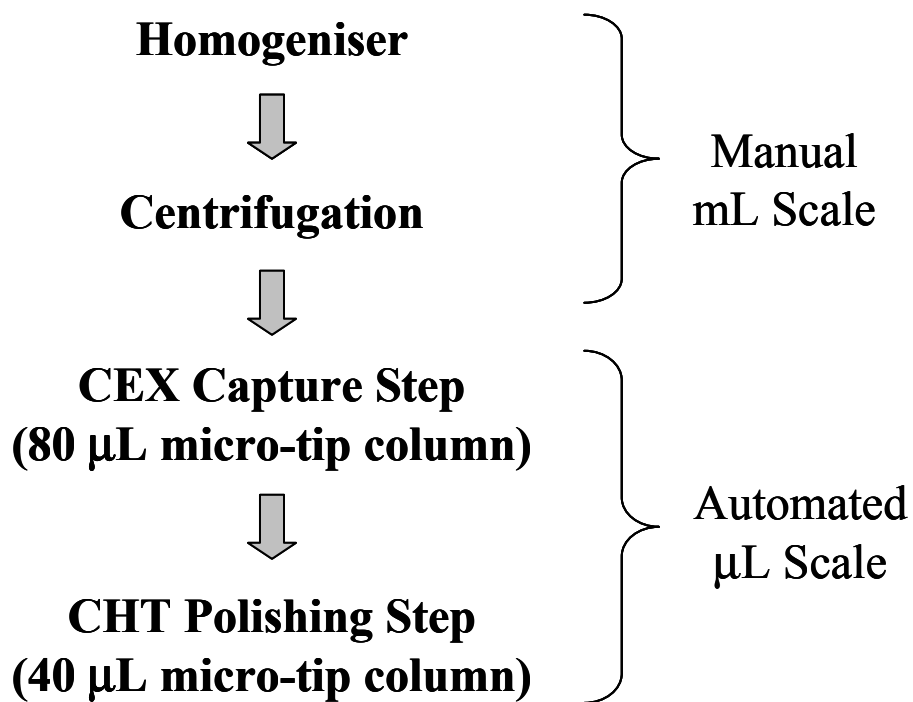


**Figure 6.3.** Purification scheme of HPV VLPs using micro-tip chromatography to provide feedback on fermentation performance.

**Table 6.1.** Run parameters for the CEX and CHT micro-tip chromatography for the purification of HPV VLPs.

		Reagent Dispensing	Pre-Washes	Equilibration	Loading	Wash	Elution #1	Elution #2	
<b>CEX</b>	Volume (μL)	N/A	160-650	500	410	400	300	100	
	Aliquots/Step	N/A	3	3	1	3	1	1	
	Cycles/Aliquot	N/A	1	1	3 - 4	1	3	2	
	Flow rate (μL/s)	N/A	5-20	10	20	10	10	10	
	Delay Time/Cycle (s) <sup>a</sup>	N/A	60-90	75	90	120	80	80	
	Time/Stage (min)	10	8	9	9	10	7	4	<b>Total = 57 min</b>
<b>CHT</b>	Volume (μL)	N/A	160-300	600	533	300	120	100	
	Aliquots/Step	N/A	3	4	1	2	1	1	
	Cycles/Aliquot	N/A	1	1	4	1	4	2	
	Flow rate (μL/s)	N/A	5-10	20	20	10	10	10	
	Delay Time/Cycle (s) <sup>a</sup>	N/A	75-150	90	100	100	100	80	
	Time/Stage (min)	10	9	10	11	6	8	4	<b>Total = 58 min</b>

a) Delays times greater than 30 s (60 s per cycle) were used to increase the contact time with the mobile phase and/or to account for higher sample viscosity.

The clarified lysate was applied to each CEX column at a volumetric loading of 410  $\mu\text{L}$ , and 533  $\mu\text{L}$  of the CEX product was loaded onto each CHT column. The loading flow rate for both chromatography steps was 20  $\mu\text{L/s}$ , and the delay time was 45 s after each aspiration and dispense step. This delay time is longer than the 30 s recommended in Chapter 3 but was used to ensure a complete volumetric loading, particularly for the more viscous clarified lysate. As discussed in Chapter 3, although the average linear velocities used in the micro-tip column format are within the range of typical laboratory column operation, the residence and contact times per aspiration-dispense cycle are much lower due to the short bed height. The principal strategy for increasing total residence time is to perform multiple aspiration-dispense cycles. The protein uptake of each column feed onto the CEX and CHT micro-tip columns was examined as a function of cycle number (Figure 6.4). These uptake experiments were carried out as described in Chapter 4, with each micro-tip column having a different cycle number and hence a different contact and residence time. The loading times are also shown in Figure 6.4. The loading of the column feed was monitored by absorbance at 280 nm ( $\text{ABS}_{280}$ ) and total protein concentration (BCA assay). For the CHT feed, the  $\text{ABS}_{280}$  and BCA measurements represent the approximate VLP concentration since the CEX product is >75% purified. However, for the CEX feed, they represent both impurity and VLP binding. Therefore, an immunoassay was used to determine VLP binding to the CEX column.

Four aspiration-dispense cycles were used for sample loading in both the CEX and CHT chromatography steps (represented by the dotted vertical lines in Fig. 6.4). This cycle number achieved a compromise between experimental throughput and completeness of binding, with the goal being to having a total run time for each chromatography step of less than one hour. For the CEX chromatography (Fig. 6.4A), VLP and total protein binding is nearly complete (>95%) after about three cycles (contact time,  $T_C$ , of 6.6 min; residence time,  $T_R$ , of 24 sec); however, four cycles ( $T_C$  of 8.7 min;  $T_R$  of 32 sec) were performed in the final method to ensure method robustness. This rapid uptake is presumably because the column is underloaded to allow for variations in VLP titres under different fermentation conditions. It is also consistent with the favourable mass transport properties of the POROS 50HS adsorbent.

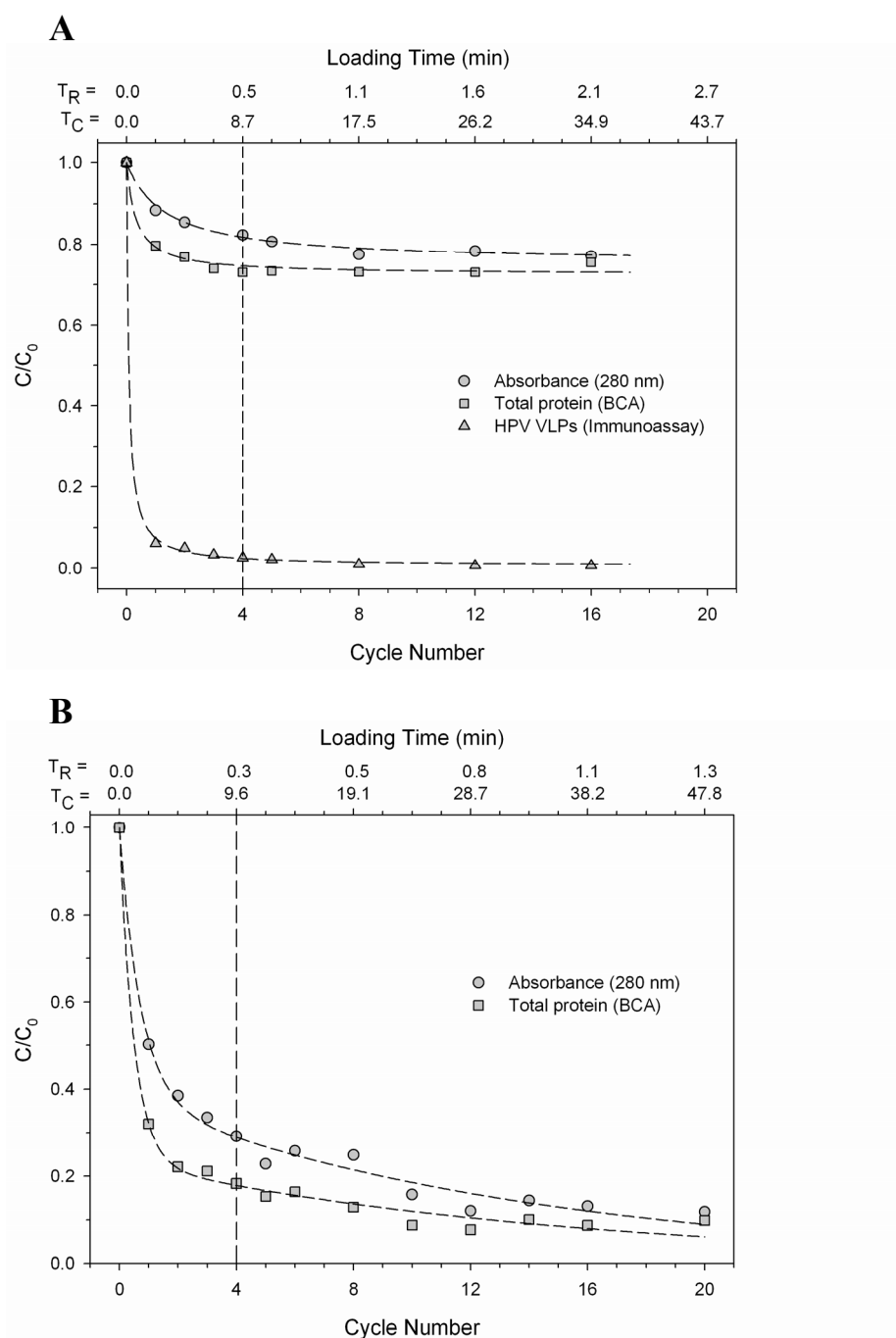


**Figure 6.4.** Binding of the column feed sample to **(A)** the 80- $\mu$ L CEX and **(B)** the 40- $\mu$ L CHT micro-tip columns as a function of cycle number and loading time (contact time,  $T_C$ ; and residence time,  $T_R$ ). For the CEX chromatography, 410  $\mu$ L of clarified lysate was loaded at 20  $\mu$ L/s. For the CHT chromatography, 533  $\mu$ L of the CEX product was loaded at 20  $\mu$ L/s. The post-aspiration and -dispense delay times (45 s) are included in the calculation of  $T_C$ , but not  $T_R$ . The dotted vertical lines in each graph represent the number of cycles chosen for the final method, providing a compromise between throughput and completeness of adsorption.

In contrast to the CEX step, protein uptake is only 70-80% complete for the CHT chromatography after four cycles (Fig. 6.4B). This may be because of differences in the mass transport properties of the adsorbents (i.e. pore size), because the column is loaded closer to saturation, or because the residence time is shorter (16 s vs. 32 s for CEX) even though the contact time is about the same (9.6 min vs. 8.7 min for CEX). Compared to the antibodies studied in Chapters 3-5, micro-tip residence time is expected to contribute more to the overall uptake rate of VLPs because much of the pore volume is inaccessible, as indicated by the low adsorbent capacities for VLPs. Yet, residence time does not fully explain the difference in uptake between the two chromatography steps, since binding remains incomplete (<90%) for the CHT step even when operated with the same residence time as the CEX step (32 s). Therefore, the difference also probably has to do with the higher mass loading of the CHT column and differences between the mass transport properties of the two adsorbents. With the CHT chromatography, there is an initial phase of rapid uptake of about 70-80% of the protein, presumably from binding onto the adsorbent particle surface. This is followed by a second phase of much slower uptake of the remaining protein. This slower uptake likely represents adsorption within the accessible pore volume. However, here the effective pore diffusivity would be relatively low for VLPs, and therefore uptake would be slower.

There is almost no protein breakthrough (< 5%) observed in the laboratory-scale column operation ( $T_R$  of 2.5 min; total load time of  $\geq 15$  min). This difference may be due to the longer loading time of the column, but it also reflects the operational differences between micro-tip (bi-directional flow; batch operation) and conventional column (uni-directional flow; dynamic operation) chromatography, as discussed throughout this thesis. However, even though binding is incomplete for the CHT micro-tip chromatography after four cycles, it was selected for the final method for the purpose of higher experimental throughput. As described later in the chapter, because the offset in recovery was consistent, it could be accounted for by using an empirical correction factor when predicting laboratory-scale column performance.

In the final optimised method, the micro-tips columns for each chromatography step are washed after the loading step and then eluted as described in Table 6.1. The CEX column is eluted with 1.25 M sodium chloride (buffered at pH 7), and the CHT

column, with a single step elution with sodium phosphate (buffered at pH 7). The final selected elution volume is a balance between having a volume large enough to ensure robust micro-tip operation yet small enough to yield a concentration sufficient for analysis. Multiple aspiration cycles are performed to ensure sufficient contact and residence time for reproducible and quantitative desorption. In each chromatography, a second elution with a smaller aliquot of buffer is carried out to recover the column hold-up volume from the first elution and maximise recovery.

Overall, the CEX chromatographic sequence required no significant modification at the microscale since the laboratory-scale chromatography is operated in an on-off mode. For the CHT chromatography, although the linear gradient elution was converted to a single step elution, this change does not significantly affect the final product purity as demonstrated in the section below. One reason for this close agreement is that neither chromatographic step requires resolution from closely eluting protein impurities due to the strong retention of VLPs. Therefore, these steps can be operated in a simple step-gradient mode for miniaturisation, with load, wash, and elution steps. Additional wash and elution steps would be required in cases where the retention properties of the product and impurities are very similar.

#### **6.4. Performance of the Microscale Chromatography**

VLP recovery and purity through the micro-tip chromatographic purification are comparable to what is obtained with the laboratory-scale columns. The results from a purification carried out with multiple replicates are summarised in Table 6.2. The SDS-PAGE results are shown in Figure 6.5, with the corresponding purity values reported in Table 6.2. Since the feed to the CEX column is impure, the total protein recovery at this step is normalised to the input of cell weight. The protein recovery at the CEX step is slightly lower for the microscale format, although when adjusted for purity, the difference in recovery is < 5%. The step yield across the CHT column is also lower for the micro-tip chromatography when compared to the laboratory scale (~11% in this example), even when accounting for purity. It should be noted, however, that the CHT step yield is very low even at the laboratory scale for this particular fermentation paste, providing an example of how the upstream process can impact the downstream chromatography. In addition to the acceptable accuracy of

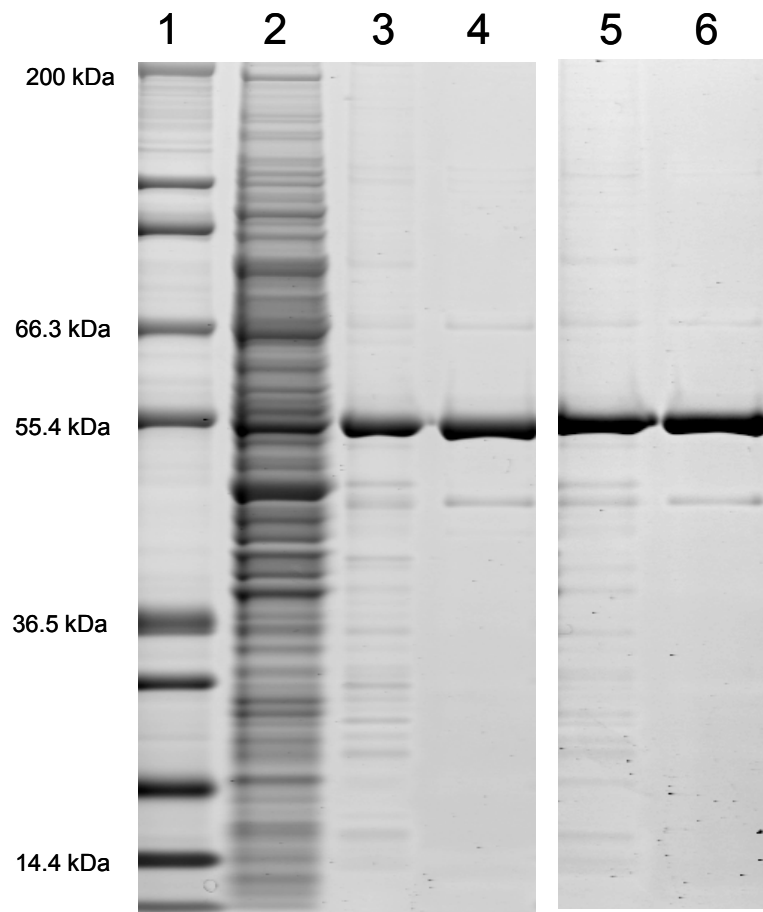


**Figure 6.5.** SDS-PAGE analysis (4-12% NuPage gel; reducing conditions; Sypro Ruby protein stain) of the HPV VLP multi-step chromatographic purification comparing the laboratory and micro-tip column scales. **Lane 1**, molecular weight standard; **Lane 2**, clarified lysate (CEX column feed); **Lane 3**, laboratory-scale column CEX product; **Lane 4**, laboratory-scale column CHT product; **Lane 5**, micro-tip column CEX product; **Lane 6**, micro-tip column CHT product. The HPV L1 capsid protein migrates at ~55 kDa. The corresponding purity of the laboratory-scale and microscale CHT products is 94 and 96%, respectively, within the error of the assay.

**Table 6.2.** Comparison of the micro-tip and laboratory column purifications of HPV VLPs for the assessment of fermentation performance.

	<b>n</b>	<b>Recovery</b>	<b>% Purity<sup>b</sup></b>
		<i>mg total protein recovered per unit cell weight input<sup>a</sup></i>	
<b>CEX Chromatography</b>			
Micro-Tip Column (80 µL)	8	7.7 ± 0.2	83
Laboratory Column (80 mL)	2	8.7 ± 0.2	77
<b>CHT Chromatography</b>		<i>% protein step yield</i>	
Micro-Tip Column (40 µL)	8	24 ± 1	96
Laboratory Column (30 mL)	2	27 ± 1	94

a) Recovery of the CEX chromatography is expressed as the milligrams of total protein recovered per input of wet cell weight since column feed is a crude lysate.

b) Purity was determined by SDS-PAGE (reducing conditions; Sypro Ruby stain) densitometry, as described in Chapter 2, using the product pool of replicate purifications. Assay variability is estimated to be <5%.

the micro-tip purification, the precision of the method is very high, an essential requirement for chromatographic miniaturisation. In this example, the coefficient of variation (CV) was less than 5% for eight replicate purifications.

The correlation of the automated microscale chromatographic purification to the laboratory-scale column purification was examined by comparing the VLP recovery under a wide range of fermentation cell induction and growth conditions for multiple HPV types. Fermentation productivity is expressed here as the total protein recovered after each chromatographic step per input of cell weight. This value generally reflects the recovery of VLPs since the chromatographic product purity is relatively high (>75% for the CEX product and >95% for the CHT product). Figure 6.6 shows the correlation between the two formats following the CEX and CHT steps. In both cases, the data is fit by linear regression through the origin.

A very good correlation in productivity is observed between the two scales through both chromatography steps, and this correlation might improve even further with more replicates of the laboratory-scale purifications (n=1 per condition in fermentation paste). While there is more scatter observed in the CEX recovery data (Fig 6.6A;  $R^2 = 0.73$ ) than in the CHT recovery data (Fig 6.6B;  $R^2 = 0.92$ ), the agreement between scales for the CEX step is very close to one ( $y = 0.98x$ ). The observed scatter is not entirely unexpected for a capture step, where an impure feed

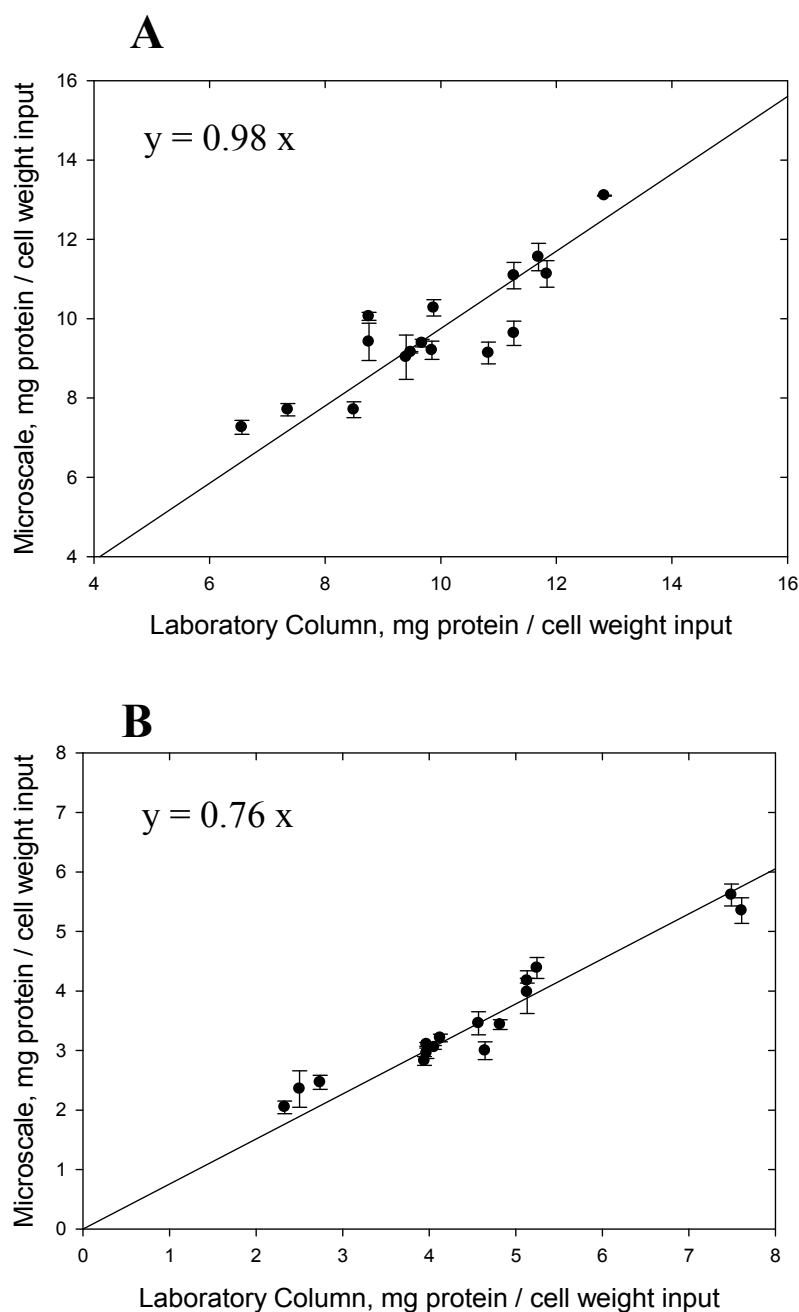


**Figure 6.6.** Correlation between the automated microscale purification and the laboratory-scale column purification in the assessment of fermentation productivity (mg protein recovered / cell weight input) across a wide range of cell growth and induction conditions: **(A)** recovery following the CEX chromatography; **(B)** recovery following the CHT chromatography. Only one replicate was carried out for each of the laboratory-scale purifications, whereas two to eight replicates were performed in each microscale assessment. The variability (CV) of the laboratory-scale purification is estimated to be  $\leq 10\%$ .

is loaded (leading to more operational and assay variability). Increasing the number of loading cycles might reduce the scatter of the data, but the results here demonstrate a reasonable compromise between throughput and binding. In contrast, the overall recovery following the CHT chromatography is considerably less variable. However, it is consistently lower for the microscale purification ( $y = 0.76x$ ), implying a lower step yield through the CHT microscale purification.

The lower step yield of the CHT chromatography is predicted by the data shown in Figure 6.4, in which binding is about 70-80% complete after four cycles ( $T_C$  of 9.6 min;  $T_R$  of 16 sec). In the laboratory-scale column chromatography, the total protein recovered in the flow-through of the laboratory-column purification was typically <5%, whereas  $25\% \pm 8\%$  of the total protein was recovered in the flow-through of the micro-tip columns. As discussed above, this incomplete binding was accepted as a trade-off for higher throughput. Another minor contribution to the lower recovery of the micro-tip columns may also involve differences in desorption between it and conventional column chromatography. Elution is carried out in batch mode with the micro-tip format, with two stages (two microwell aliquots) of elution, as opposed to the multistage operation of laboratory chromatography, where the buffer is continuously being replenished and pushing the equilibrium toward desorption. Despite these effects, the offset in overall yield of 24% is very consistent across all the purifications, allowing the correlation to be used as an empirical correction factor in order to obtain higher throughput.

### **6.5. Throughput and Resource Benefits Using the Microscale Purification**

The microscale purification increases throughput by 8- to 16-fold over the laboratory column purification depending on whether or not replicate purifications are performed, while the materials requirement is lowered by two to three orders of magnitude. In addition, the labour is reduced by 50%. These calculations assume that the Tecan is operated continuously over a full 24 hours. The other assumptions used in these calculations are described in Table 6.3. The time of each micro-tip chromatography step conservatively incorporates an additional half hour in these calculations, yielding a final time of 1.5 hr per chromatography step. Therefore, the total time to process eight data points through the multi-step microscale purification

is 4.5 hr, since two CEX purifications are carried out for every one CHT purification. An additional two hours is allotted per day for the set-up of each Tecan and for sample preparation (centrifugation of cell lysate and dilution to the target feed concentration). If overnight runs are performed, then about four runs can be completed within a 24-hour period, for a total of 32 purifications per Tecan system. Overnight runs require that the pre- and post-run samples be chilled to ensure their stability and that the plates be covered to avoid evaporation. The calculations in Table 6.3 make the assumption that two Tecans are available to be operated per day. This allows for a total of 64 purifications to be performed, so that 32 fermentation pastes can be evaluated in duplicate, or 64 with one replicate.

In contrast, only four pastes can be evaluated per day at the laboratory-column scale by one person operating two chromatography systems. This assumes that overnight operation is not possible because some manual operation between the CEX and CHT chromatography steps is required (which was the case for the laboratory-scale method compared here). In principle, full automation is possible with a more sophisticated chromatography system, and hence, throughput would double. The laboratory-scale purification also requires more manual labour for packing and cleaning columns, setting up the chromatography systems, and preparing purification reagents, totalling to about six hours of labour per day. Therefore, the productivity of the laboratory-scale purification, defined here as the number of pastes processed per hour of labour required, is about 0.67 pastes/hr, while the productivity of the microscale purification is 8 pastes/hr when duplicate purifications are performed, or 16 pastes/hr if only a single replicate is carried out. This translates into a 12- to 24-fold improvement in overall productivity. In addition to these gains, over 200 times less sample volume is required.

## **6.6. Summary**

A laboratory-scale chromatographic purification of HPV VLPs was miniaturised by three orders of magnitude using micro-tip chromatography and automated on a robotic workstation. Overall, the automated purification is concordant with the laboratory-scale purification in the assessment of VLP recovery and purity, while the productivity (pastes evaluated/hour of labour) of the purification is improved by

more than 10-fold, even when duplicate purifications are carried out at the microscale. The miniaturisation and automation of the chromatography also significantly decreases the amount of sample needed to evaluate yeast fermentations, requiring low millilitre quantities. Successfully eliminating the chromatographic purification as a bottleneck affords the possibility of scaling down the fermentation and cell disruption steps, thereby enabling whole microscale process development strategies. The scale-down of the cell disruption step is discussed in Chapter 7.

**Table 6.3.** Comparison of the experimental throughput, labour, and resources required for the microscale and laboratory-scale chromatographic purifications.

		Microscale	Laboratory Scale
<b>Throughput</b>	Run time (hr)	4.5 <sup>a</sup>	4.5
	Systems	2	2
	Data points/run	8	1
	Overnight runs	yes	no
	Runs/day/system	4	2
	<b>Throughput / 24hr (single replicate)</b>	<b>64</b>	<b>4</b>
	<b>Throughput / 24hr (two replicates)</b>	<b>32</b>	<b>2</b>
<b>Labour</b>	Column packing/day	0 <sup>b</sup>	2 <sup>c</sup>
	Manual operation/day	4	4
	<b>Total Labour (hr)</b>	<b>4</b>	<b>6</b>
<b>Material/ Purification</b>	Sample (mL)	<1	200
	CEX Adsorbent (mL)	0.16 <sup>d</sup>	80
	CHT (mL)	0.04	30
	Buffers (mL)	<100	2000-3000

a) One total microscale run includes two CEX purifications and one CHT purification.

b) Micro-tip column preparation is outsourced to PhyNexus.

c) The CEX column was re-used but the CHT column was not.

d) Two CEX columns X 0.08 mL = 0.16 mL.

## **7. A CELL DISRUPTION METHOD FOR INTEGRATED MICROSCALE BIOPROCESSING**

### **7.1. Introduction**

Recombinant proteins that are not secreted extracellularly require a cell disruption method for their release and subsequent purification. For the VLP purification described in Chapter 6, the cell disruption method (microfluidizer) used at the laboratory scale is relatively low throughput and requires tens to hundreds of millilitres of cell slurry. A small-scale disruption method for *Saccharomyces cerevisiae* was therefore needed to fully realise the throughput and low-volume benefits of the micro scale-down process. However, developing a microscale disruption method for yeast is challenging because of its mechanically rigid cell wall.

In this chapter, the use of a newly developed technology known as Adaptive Focused Acoustics (AFA; Laugharn and Garrison, 2004) is examined to enable a reduction in scale into the low millilitres to hundreds of microlitres range while matching the contaminant profile of homogenisation, with the goal being to assess the suitability of the method as an element of a microscale process. AFA operates by delivering highly focused, computer-controlled acoustic radiation at frequencies significantly higher than those used in conventional ultrasonication. In this study, key instrument parameters and operating conditions were optimised for yeast cell disruption with the aid of design-of-experiment (DoE) methodologies. The addition of a yeast lytic enzyme was also examined to decrease treatment times and further improve the comparability to the laboratory-scale homogenate. The effectiveness of the AFA technique was evaluated by total protein release, product-specific protein release, optical density, and light microscopy. In addition, the micro-tip chromatographic purification described in Chapter 6 was used to assess the effect that the AFA cell disruption has on the downstream chromatography, since the chromatography is known to be sensitive to upstream changes, including those from aggregation and changes in VLP morphology.

### **7.2. The Yeast Cell Wall**

*Saccharomyces cerevisiae* is commonly used as an expression system for the commercial production of non-glycosylated proteins. It can be grown to high cell densities in chemically defined media, yields high levels of protein expression, is

scalable, and has no bacterial endotoxins (Hatti-Kaul and Mattiasson, 2003; Gerngross, 2004). The yeast cell wall is a highly dynamic structure which serves to stabilise the cell against changes in osmotic potential, protect against physical stress, maintain cell shape, and limit permeability, especially of macromolecules (Klis et al., 2006). As shown in Figure 7.1, the cell wall of *Saccharomyces cerevisiae* is comprised of an inner layer of cross-linked glucan ( $\beta$ 1,3 linkage with some  $\beta$ 1,6 branches) and chitin, with a thickness of 70-100 nm, and an outer layer of heavily glycosylated mannoproteins (Kollar et al., 1997; Klis et al., 2002; Lesage and Bussey, 2006). However, the exact composition and mechanical properties of the cell wall will vary with growth conditions and genetic modifications (Firon et al., 2004; Klis et al., 2006). The three dimensional network of  $\beta$ 1,3-glucan comprises about 30-55% of the cell wall mass (Klis et al., 2006) and provides much of its mechanical strength, shape, and elasticity. Young's moduli of  $112 \pm 6$  MPa and  $107 \pm 6$  MPa have been determined for exponential and stationary phase yeast cells, respectively (Smith et al., 2000). At least 20 different glycoproteins are present in the external mannoprotein layer of the cell, comprising 30-50% of the wall mass. One potential function of this glycoprotein layer is to protect the inner glycan layer from enzymatic attack.

### **7.3. Small-Scale Disruption of Yeast Cells**

Yeast cell lysis requires a method that can disrupt the highly rigid cell wall. A summary of some commonly employed laboratory-scale methods is provided in Table 7.1, using either mechanical or non-mechanical mechanisms. While mechanical methods such as high-pressure homogenisation or glass-bead mills are most often used at the laboratory and industrial scales (Follows et al., 1971; Kula and Schutte, 1987; Hopkins, 1991; Garcia, 1999; Hatti-Kaul and Mattiasson, 2003), these methods generally require tens to hundreds of millilitres at a minimum. Volumes less than ten millilitres are generally not practical.

Glass beads have been used for processing microlitre volumes in high throughput purifications, often in combination with a lysis buffer containing Triton X-100 (Holz et al., 2003; Prinz et al., 2004). In these experiments, the cells are vortexed with

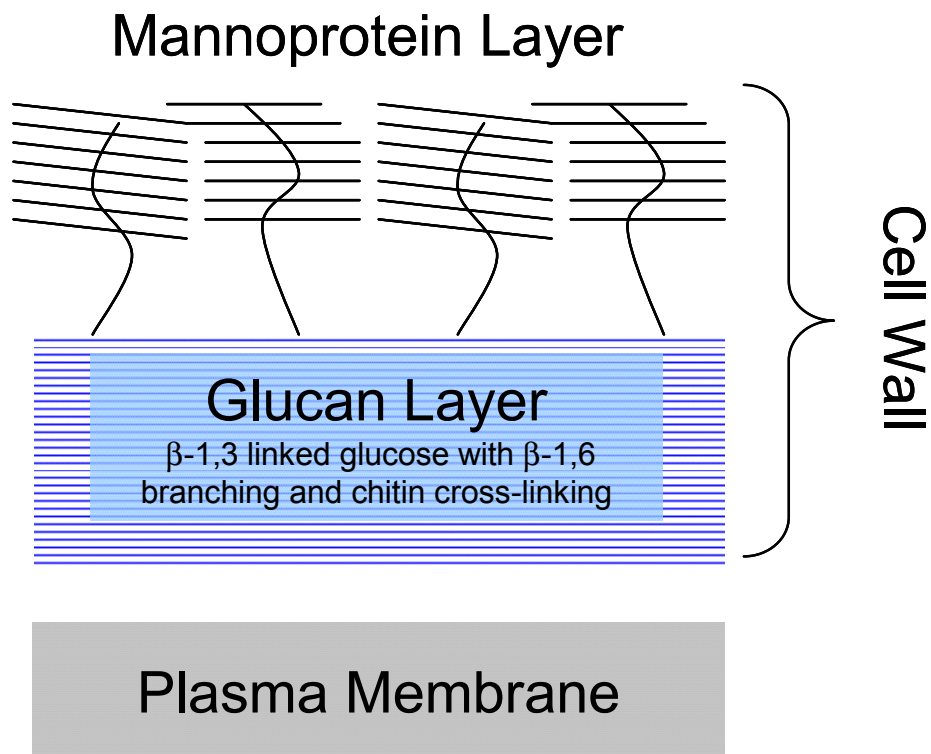


**Figure 7.1.** Architecture of the yeast cell wall. Chains of  $\beta$ -1,3-linked glucose residues are connected with  $\beta$ -1,6 branching to form a glucan backbone which provides much of the mechanical rigidity of the cell wall. Chitin,  $\beta$ -1,6 glucan, and mannoproteins are anchored to this glucan layer. The outer layer is comprised of heavily glycosylated mannoproteins, which provides protection against degradation of the glucan layer by enzymes.

**Table 7.1.** Overview of laboratory-scale methods for yeast cell disruption.

Method	Principle	Scale			Advantages	Disadvantages
		μL	mL	L		
<b><i>Mechanical</i></b>						
High-pressure homogenisation	Fluid shear from valve unit and cavitation in impingement zone		✓	✓	Efficient and effective for yeast; Scale-able to production scale	Requires 10's of millilitre volumes; Usually requires multiple passes
Glass beads (batch) + Vortex	Solid-shear from glass beads	✓	✓		Efficient and effective for yeast; Scale-able to production scale (bead mill)	Harsh conditions (product damage); Can be difficult to control and optimise
Ultrasonication (≥ 20 kHz)	Liquid shear from cavitation	✓	✓		Works well at microlitre volumes; Independent of cell concentration	Inefficient and often incomplete; Sample heating; Free radicals; May not be representative of homogenisation
<b><i>Non-Mechanical</i></b>						
Chemical/Physical Treatment	Permeabilisation by detergent (e.g. Triton X-100) or solvent (e.g. DMSO), often combined with physical method such as freeze/thaw or osmotic shock	✓	✓		Works well at microlitre volumes; Solution-based lysis	Permeabilisation or incomplete lysis -therefore, not representative of homogenisation
Lytic Enzymes	Enzymatic degradation of cell wall, with disruption of cell membrane using a chemical agent (e.g. Triton X-100) or with osmotic shock	✓	✓		Works well at microlitre volumes; Simple; Solution-based lysis; Selective product recovery	Permeabilisation or incomplete lysis - therefore, not representative of homogenisation; Proteolysis of product can be a concern; Expensive at larger scales

multiple on-off cycles. Hummel and Kula (1989) used glass beads in combination with a mixer-mill device to disrupt bacteria and yeast cells. Volumes as low as 100  $\mu$ L were disrupted, with eight samples treated in parallel. A treatment time of six minutes was sufficient to release greater than 90% of the total protein for cell concentrations  $\leq 40\%$ , therefore making it possible to disrupt about eighty samples per hour. Kim et al. (2004) used glass beads within a microfluidic compact disc (CD) chamber, in which the yeast cells were disrupted by the forward and backward movement of the CD over the course of five to seven minutes. The efficiency of this method was about 65% of the laboratory method. In general, a critical disadvantage of glass-bead methods is that they can be difficult to control, thereby resulting in higher variability and potential damage to the product.

Sonication has also been used for yeast cell disruption (James, et al., 1972; Ciccolini et al., 1997; Garcia, 1999; Agrawal and Pandit, 2003) but is often inefficient due to the rigidity of the yeast cell wall. Long treatment times are typically required, which lead to sample heating and the accumulation of free radicals. This, in turn, can result in damage to the protein product. Furthermore, non-uniformity in the distribution of energy resulting from interference and scattering in small treatment vessels and from the complex nature of the sample can diminish the effectiveness of cell disruption and lead to poor reproducibility.

Non-mechanical approaches to yeast cell disruption involve the use of physical methods, chemical agents, and/or lytic enzymes. A chemical procedure using 0.05% Triton X-100 or 40% DMSO in combination with a freeze-thaw step was demonstrated by Miozzari and co-researchers (1978) for the permeabilisation of *Saccharomyces cerevisiae*. However, the most effective non-mechanical methods typically use a lytic enzyme (Hunter and Asenjo, 1988; Asenjo and Andrews, 1990; Garcia, 1999; Salazar and Asenjo, 2007), either alone or in combination with osmotic shock or a chemical agent. An enzyme cocktail comprised of a cell wall lytic protease, acting on the mannoprotein layer, and a  $\beta$ -1,3 glucanase, acting on the glucan layer, is often used for *Saccharomyces cerevisiae*. Other enzymes such as a  $\beta$ -1,6 glucanase, mannanase, or chitinase may also be beneficial. One disadvantage of enzymatic techniques is that proteolysis of the product can occur from contaminants in the enzyme reagents and/or from intracellular proteases when the

cell breakage is not sufficiently fast (Salazar and Asenjo, 2007). An advantage of enzymatic techniques, though, is that they can provide for differential or selective product release with only a fraction of the contaminating proteins (Huang et al., 1991; Asenjo et al., 1993). Yet, this is not necessarily desirable if the goal is to have a feedstock for downstream chromatography that is representative of the laboratory-scale homogenate with respect to both product and contaminant profile, as was the case in this thesis for the VLP purification to evaluate fermentation changes.

#### **7.4. Adaptive Focused Acoustics**

Adaptive Focused Acoustics (AFA; Laugharn and Garrison, 2004) offers an alternative to the small-scale cell disruption methods discussed above. It is an acoustic process similar to ultrasonication, with the primary difference being that it is operated at significantly higher frequencies, ranging from about 100 kHz to 100 MHz (Fig. 7.2). This provides several key advantages. First, working in this higher frequency range allows the delivery of highly focused acoustic radiation for more efficient disruption. The AFA instrument (Covaris E210; Woburn, MA, USA) used in this work has a focal zone that is ellipsoidal shaped, with a diameter of approximately 2 mm and a length of approximately 7 mm. This small focal zone allows the method to be scaled to low-millilitre-to-microlitre vessel sizes. Second, the high-frequency acoustic energy is able to transverse through a liquid water bath and the sample vessel (glass or plastic), with no direct contact with a probe required. As a result, the procedure is entirely non-contact, with sealed tubes placed into a de-gassed water bath above the acoustic transducer of the instrument. Third, the interference and scattering of the acoustic energy field that is commonly associated with ultrasonication is minimised in AFA because the operating wavelengths are in the millimetre-to-micron range, similar to the pathlength through the treatment vessel. This reduces sample heating and improves the overall efficiency of disruption. Another advantage of AFA process is that it is computer-controlled, facilitating walk-away automation and improving reproducibility.

The operating principle of AFA for the disruption of cells is similar to that of conventional sonication (Davies, 1959; Clarke and Hill, 1970; Doulah, 1977), with the key difference being the higher operating frequency. Pressure waves generated

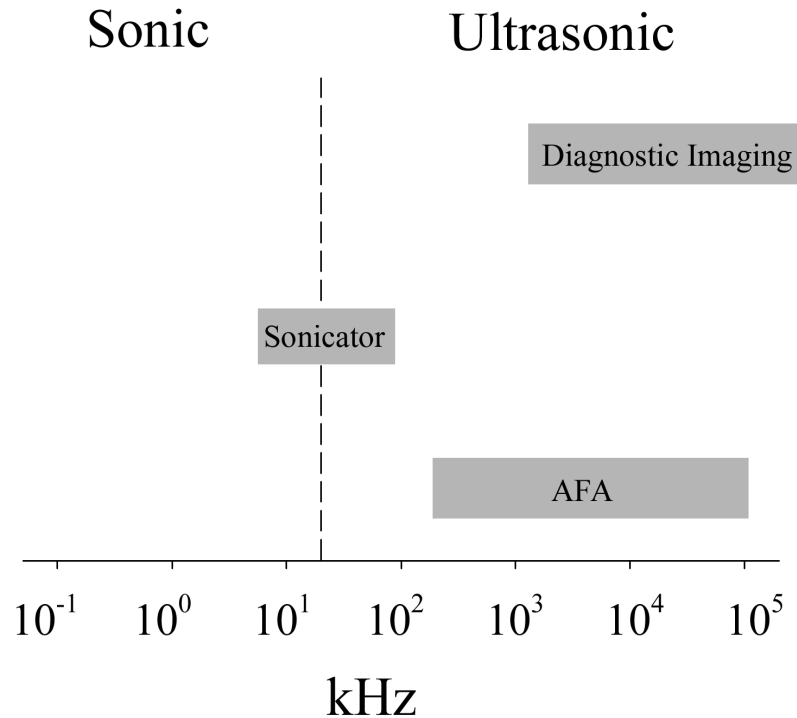


**Figure 7.2.** Frequency range of the Adaptive Focused Acoustics (AFA) device from Covaris (Woburn, MA, USA). The ranges for conventional sonicators and diagnostic imaging devices are shown for comparison. The instrument is typically operated in the megahertz range (similar to diagnostic imaging techniques), which results in shorter wavelengths\* and therefore enables the process to be scaled down to lower sample volumes.

\* Relationship of wavelength and frequency:  $\lambda = c/f$ , where  $\lambda$  is the wavelength (m) of the ultrasound wave,  $f$  is the frequency (Hz), and  $c$  is the velocity of the sound wave ( $\sim 1500$  m/s in distilled water at  $25^\circ\text{C}$ ). The energy imparted to the fluid (intensity) is proportional to the pressure amplitude of the sound wave.

from the acoustic vibrations lead to non-linear sub-micron bubble growth. When the energy dissipates, these cavitation bubbles then collapse, resulting in elastic waves that generate intense local shear gradients and eddying. Because millions of cavitation events are created in very short intervals of time (microseconds), the disruption power can be quite significant and ultimately will lead to cell rupture. In this way, the cells are disrupted mechanically, essentially with high velocity jets of solute. Parameters affecting sonication efficiency include temperature, the amplitude of the sound wave vibrations, sample volume and viscosity, cell concentration, and vessel properties (Hopkins, 1991; Garcia, 1999; Hatti-Kaul and Mattiasson, 2003).

#### *7.4.1. Experimental Details*

Recombinant human papillomavirus (HPV) virus-like particles (VLPs) were cloned and expressed in *Saccharomyces cerevisiae* as described in Chapter 2. Fermentation product was provided frozen for purification as a centrifuged cell pellet. Twenty percent (wet cell weight/volume) cell suspensions buffered at pH 7.2 were lysed at the laboratory scale using a Microfluidizer model 110 Y from Microfluidics International Corporation (Newton, MA, USA), as described in Chapter 2.

Cell disruption experiments by AFA were performed with a Covaris E210 instrument (Fig. 7.3). A list of instrument parameters and their operating ranges is provided in Table 7.2. Each experiment was performed with 1.5 mL of cell suspension (buffered at pH 7.2) ranging from 10 to 20% (wet cell weight/volume) in capped 16 x 100 mm (diameter x height) borosilicate glass tubes supplied by Covaris. A 3 x 4 rack containing the sample tubes was placed into the de-gassed water bath of the instrument maintained at  $8 \pm 4^\circ \text{C}$  in which the acoustic transducer was also submerged (Fig. 7.3B). The disruption experiments were carried out serially, with each tube sequentially moved over the transducer. The ellipsoidal-shaped focal zone (diameter of ~2 mm and an axial length of ~7 mm) is focused to a geometric point approximately 70 mm from the face of the transducer. Acoustic power delivered to the sample vessel is monitored by an RF power meter, which measures the electrical power that the RF amplifier supplies to the transducer. The instrument can be operated in one of three modes to optimise the mechanical reflux and ensure the precise transfer of ultrasonic energy (refer to section 7.5.3 for a discussion of these modalities).

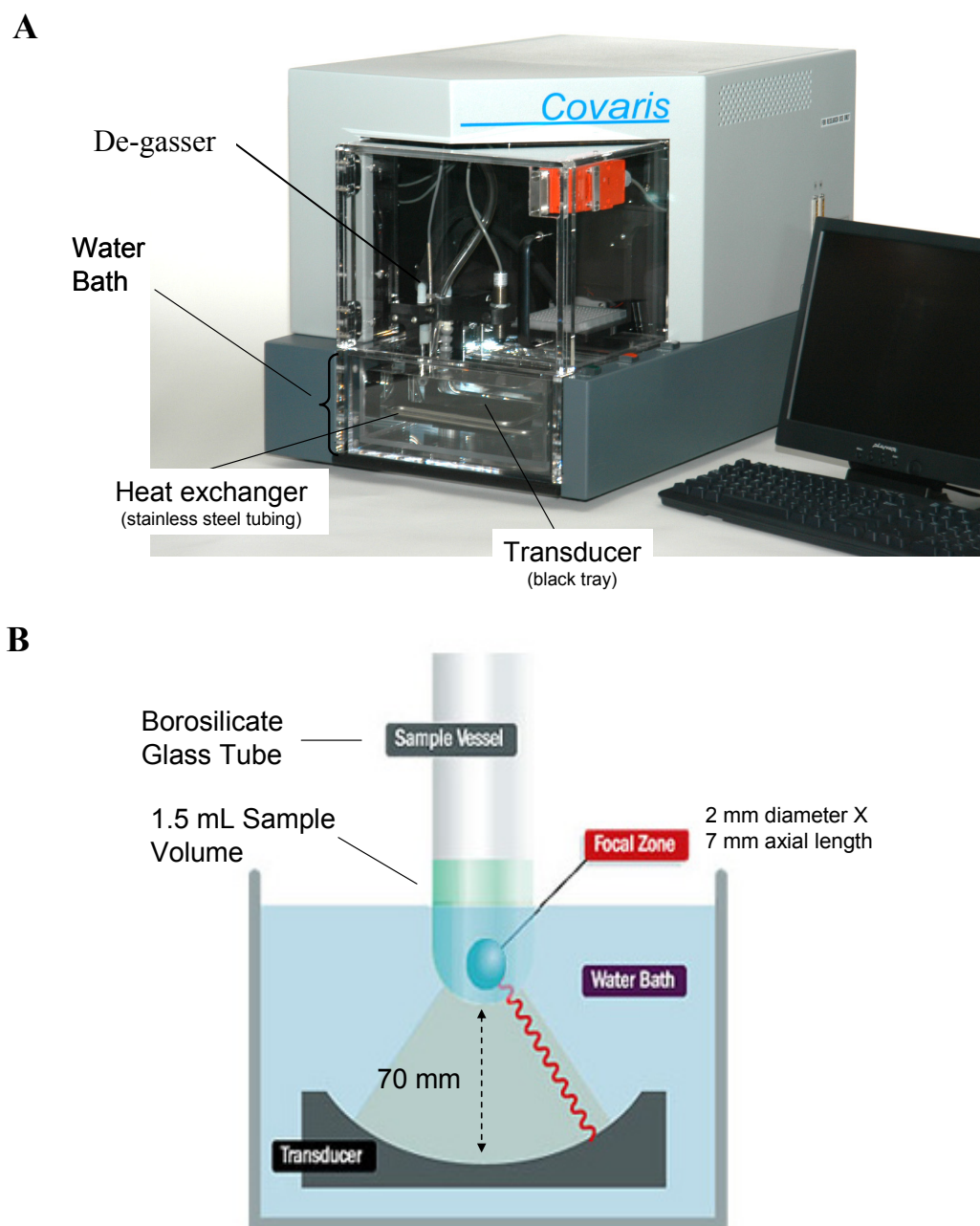


**Figure 7.3.** The Covaris E210 instrument (Woburn, MA, USA) for Adaptive Focused Acoustics: **(A)** Photograph of the Covaris E210; and **(B)** Schematic showing the instrument configuration. Acoustic energy radiates from a dish-shaped transducer that converges on a small focal zone, enabling a high degree of control without directly contacting the sample. Figures are adapted from Covaris, Inc. ([www.covarisinc.com](http://www.covarisinc.com)).

**Table 7.2.** Instrument parameters for the Covaris E210 (Adaptive Focused Acoustics)

Parameter	Definition	Operating Range	Range Evaluated
<b>Vessel Type/Rack Configuration</b>	Vessel (tube) type and rack used for AFA treatment	Racks <sup>a</sup> exist for glass and plastic tubes of varying size, 96-well microtitre plates, and microcentrifuge tubes	6 X 4 rack for 13 x 65 mm (d x h) borosilicate glass tubes 3 X 4 rack for 16 x 100 mm (d x h) borosilicate glass tubes
<b>Duty cycle (dc)</b>	Percent of time that the transducer is generating acoustic waves (on-off cycle)	0.1 - 20% (0.1, 0.5, 1, 2, 5, 10, and 20%)	5, 10, and 20%
<b>Intensity</b>	Proportional to the amplitude of the pressure wave	5 – 500 mV <sup>b</sup>	25 -500 mV
<b>Cycles per burst (cpb)</b>	Number of waveforms created by the transducer in an "on" cycle	50 – 1000 (50, 100, 200, 500, and 1000)	50 - 1000
<b>Dithering</b>	The controlled horizontal movement of the treatment vessel around a centre point for sample mixing	Vary radius (in mm) and rate (in rpm) of the circular motion and dwell time (s) between motions	Not evaluated (All settings at 0)
<b>Mode of Operation</b>	Modality for delivering acoustic energy (frequency tuning)	Vertical sweeping, frequency sweeping, power tracking	Vertical sweeping, frequency sweeping, power tracking

a) Number of vessels per rack depends on the specific configuration.

b) In more recent versions of the software, intensity is expressed as a scale from 0.1 to 10.

Cellular debris was separated from the lysate by batch microcentrifugation (1.5 mL/microcentrifuge tube) at 10,000 x g for 5 minutes using an Eppendorf (North America; Westbury, NY, USA) 5417R microcentrifuge. One millilitre of this supernatant was then aspirated for subsequent analysis or purification by micro-tip chromatography. The micro-tip chromatographic purification was performed as described in Chapter 6. Analyses of the lysate and purification samples were carried out by the methods described in Chapter 2. These included the measurement of total protein release by the BCA assay, product release by either RP-HPLC or immunoassay, optical density at 660 nm, light microscopy, and SDS-PAGE.

#### *7.4.2. Characterisation of Instrument Parameters*

The overall intent of this work was to demonstrate the application of AFA as a suitable method for small-scale yeast cell disruption and additionally to define conditions that produce lysate that is representative of the laboratory-scale homogenate for downstream chromatographic study. However, before optimising toward these goals, several key AFA instrument parameters were first characterised in order to understand their effect on the delivery of acoustic power and on changes in sample temperature. The acoustic power delivered to the sample vessel during cell disruption was monitored as a function of two instrument settings, duty cycle (dc; percentage of time that the transducer is generating acoustic waves) and intensity (proportional to the amplitude of the pressure wave). Refer to Table 7.2 for a detailed description of the instrument parameters. One and a half millilitres of a 12% (w/v) cell suspension were used in this study since this volume and concentration are suitable for both microscale cell disruption and subsequent downstream micro-tip chromatography. Duty cycle was varied at 5, 10 or 20%, while the intensity was examined over a range from 25 to 500 mV. The cycles-per-burst (cpb) setting was held constant at 50 in these experiments, and the instrument was operated in the power tracking modality. The impact of duty cycle and intensity on acoustic power is shown in Figure 7.4A. The effect of duty cycle is generally linear, whereas that of intensity is nonlinear across the range examined. The maximum power input into this system approaches 120 W and is achieved at the maximum instrument settings of 20% dc and 500 mV.

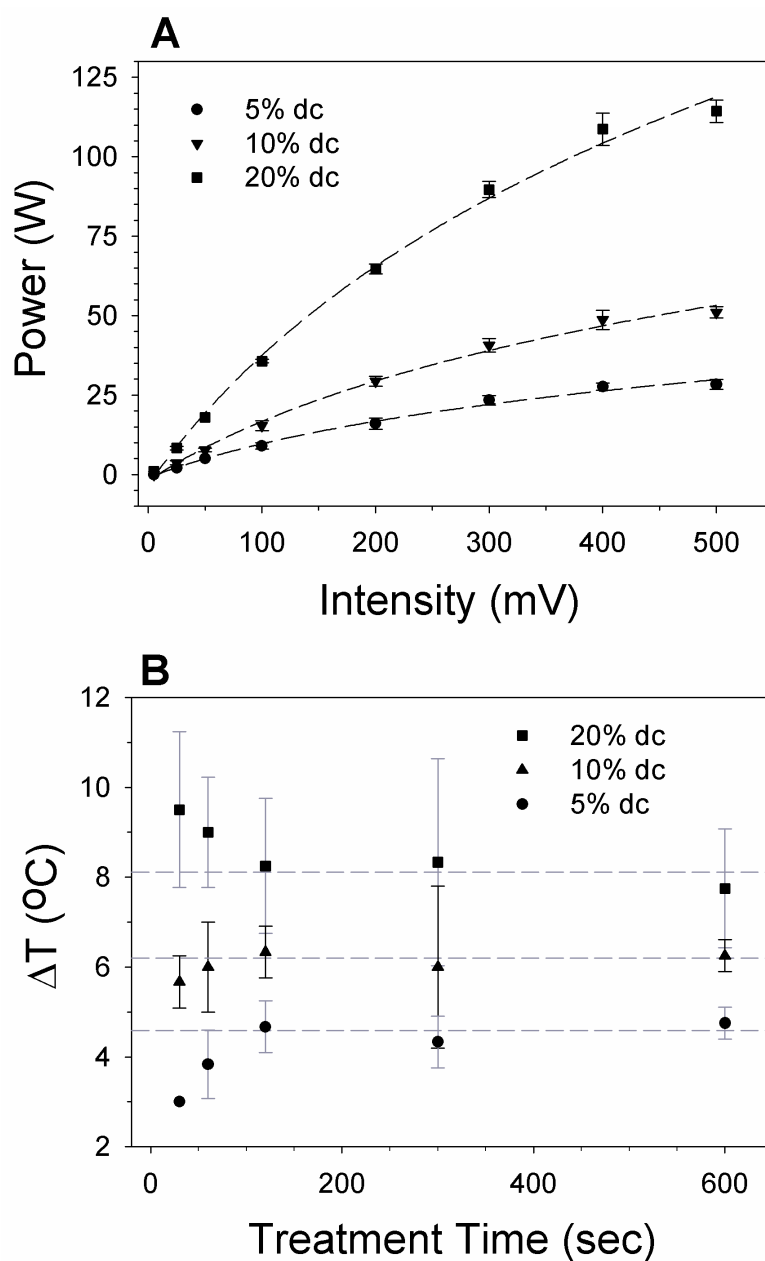


**Figure 7.4.** Characterisation of instrument parameters in the disruption of yeast cells by Adaptive Focused Acoustics (Covaris E210). 1.5-mL cell suspensions at 12% (w/v) were used in these experiments. **(A)** Acoustic power as a function of intensity at duty cycles of 5, 10, and 20% (power tracking modality). **(B)** Change in temperature ( $\Delta T = T - T_0$ ) over time at duty cycles of 5, 10, and 20% (power tracking modality; intensity of 500 mV; 50 cbp). The starting temperature is  $8 \pm 4$   $^{\circ}\text{C}$ . The dotted lines represent the mean temperature change of the last three timepoints (120, 300, and 600 sec) at each duty cycle.

The material type (glass or plastic), thickness, and size of the sample vessel can affect the transfer of acoustic power. Borosilicate glass tubes were used in these experiments to ensure the most efficient energy transfer. The geometry of the sample vessel can also affect the cell disruption by impacting the mechanical reflux. In this investigation, two tube diameters were examined, 13 and 16 mm. While both were equally effective for use in yeast cell disruption, the 13-mm tube was prone to breaking on occasion, especially at high acoustic power. This is presumably because its diameter is closer to the size of the focal zone, thereby putting more stress on the tube. Consequently, 16-mm tubes were used for all subsequent experiments.

Sonication methods often lead to sample heating during cell disruption. However, because AFA operates at significantly shorter wavelengths, there should be less interference and scattering of the acoustic energy field in microscale sample vessels (low-millilitre-to-microlitre volumes). This reduces the potential for sample heating. To evaluate the thermal stability of the system, the temperature change of the 1.5-mL 12% cell suspension was measured as a function of time (30 – 600 s) at 5, 10, and 20% dc (intensity of 500 mV and cpb of 50). In these experiments, the samples were first allowed to equilibrate in the water bath of the instrument maintained at  $8 \pm 4$  °C and then temperature measurements were made immediately before and after AFA treatment using a Fisher Scientific (Pittsburgh, PA, USA) traceable double thermometer. At least two experiments were carried out for each timepoint.

The change in temperature at each treatment time is shown in Figure 7.4B. The increase in temperature is highest at a 20% dc, consistent with a higher input of acoustic power. Most of the temperature increase occurs in the initial minute of lysis, with little additional change thereafter. As observed from Figure 7.4B, the average temperature increase (mean of the 120, 300, and 600-sec timepoints) is 4.6 °C at 5% dc, 6.2 °C at 10% dc, and 8.1 °C at 20% dc, all of which is below the 20-25 °C increase observed for homogenisation. This relatively modest increase in temperature minimises the risk of thermal damage to biological samples.

## 7.5. Optimisation of AFA for Yeast Cell Disruption

Although power is an important parameter in optimising cell breakage, higher power is not necessarily optimal. For example, the mechanical reflux of the sample must be optimised so that as much of the sample as possible remains in contact with the focal zone and does not move up the sides of the tube. Furthermore, conditions for maximal cell breakage must be balanced with product stability. Therefore, design-of-experiment (DoE) approaches were used to empirically optimise the yeast cell disruption by AFA for the various operating conditions. Initially, a fractional factorial was used to rapidly screen five operating parameters to determine which have the most significant effect on yeast cell disruption. A limitation of a fractional factorial, however, is that parameter interactions cannot be estimated. These were examined in a subsequent response-surface analysis, with product stability then evaluated under these optimised conditions.

### 7.5.1. Fractional Factorial to Identify Critical Operating Parameters

The three primary instrument parameters of duty cycle, intensity, and cycles-per-burst were examined. While duty cycle and intensity directly contribute to acoustic power and, hence, the mechanical reflux of the cell lysis, cycles-per-burst is optimised empirically for different sample viscosities on the basis of cavitation and mixing. In this investigation, duty cycle was varied at 5 or 20%, the intensity at 250 or 500 mV, and the cycles per burst at 50 or 500. In addition, the cell concentration was varied at 10% or 20% and the time, at 60 or 300 sec. Sample volume was held constant in this evaluation at a quantity that is sufficient for the downstream microscale purification (1.5 mL), but is another variable for consideration if larger volumes are required (Feliu et al., 1998).

The extent of cell disruption was quantified by the total soluble protein released during cell disruption. Parameters significant to cell disruption were identified by evaluation of a half-normal probability plot. The % contribution of each parameter as shown in Table 7.3 was then calculated from the partial (Type III) sum of squares for each individual term divided by the total sum of squares for all terms. The % contribution was used here as a measure of parameter significance since the degrees of freedom is the same for all terms. Treatment time, duty cycle, and intensity each have a significant effect on cell disruption, consistent with an increase in acoustic

power and time, as described above. An increase in the disruption of microbial cells and protein release kinetics with increasing acoustic power has been demonstrated previously for ultrasonication (James et al., 1972; Feliu et al., 1998; Kapucu et al., 2000). The effects of the cycles-per-burst and cell concentration factors are negligible.

**Table 7.3.** Two-level fractional factorial to screen parameters affecting cell disruption by Adaptive Focused Acoustics.

Factor	Duty Cycle <sup>b</sup>	Intensity <sup>c</sup>	Cycles/burst <sup>d</sup>	Time	Cell Density <sup>e</sup>
% Contribution <sup>a</sup>	28.8	35.9	0.8	34.0	0.5

a) The % contribution is calculated from the partial (Type III) sum of squares for each individual term divided by the total sum of squares for all terms. The degrees of freedom is the same for all terms.

b) Duty cycle is defined as the percentage of time that the transducer is creating acoustic waves (5, 20%).

c) Intensity is proportional to the amplitude of the pressure wave generated by the AFA transducer (250, 500 mV).

d) Cycles per burst are the number of waveforms generated by the transducer in a burst (50, 500).

e) Cell density was varied at 10 and 20% (wet cell weight per volume).

### 7.5.2. Response Surface for the Optimisation of AFA Operating Conditions

A central composite response surface design was subsequently carried out to define the empirical optimum for yeast cell disruption by adjusting duty cycle, intensity, and time. In this study, the time was varied over five levels: plus and minus the axial points (4, 386 s), plus and minus the factorial points (60, 330 s), and the midpoint (195 s). The intensity was varied at four levels instead of five because the upper instrument limit was exceeded for the higher axial point: plus and minus the axial points (100, 500 mV), plus and minus the factorial points (250, 500 s), and the midpoint (400 s). The midpoint (195 s, 400 mV) was replicated five times, while all other points were carried out once. In addition, the response surface design was repeated over two levels of duty cycle (categorical factor), 10 and 20%. The amounts of total soluble protein (measured by the BCA assay) and product (HPV L1 protein measured by RP-HPLC) released under each of these conditions were analysed to quantify the extent of cell disruption. All data were normalised to disruption by the homogeniser. The response surface was best fit with a two-factor interaction model.

Under the conditions examined here, a duty cycle of 20% outperformed that of 10%. The response map showing the release of soluble protein and product (HPV) as a function of time and intensity at a duty cycle of 20% is given in Figure 7.5. To guide

subsequent optimisation experiments, the results were extrapolated to identify treatment times where the AFA disruption method is representative of homogenisation. This model predicts that a treatment time of about ten minutes is required at an acoustic power  $\geq 100$  W (maximum instrument settings of 20% dc and 500 mV intensity) to achieve total protein and product release that are comparable to that of homogenisation.

### *7.5.3. Evaluation of Instrument Operating Modality*

In addition to the parameters evaluated in the response surface, the operating modality of the instrument was examined for its impact on cell breakage. Three modalities are available for the purpose of maximising the efficiency of the ultrasonic energy transfer and, hence, the mechanical reflux. In the first modality, known as vertical sweeping, the treatment vessel is mechanically moved up and down very slightly to vary the position of the focal zone (in this study, by 0.5 mm at 10 cycles per minute). In the second modality, referred to as frequency sweeping, the transducer electronically sweeps through a range of acoustic frequencies, thereby altering the position of the focal zone. This is the default modality for many biological applications. Finally, in the third modality, called power tracking, the instrument optimises the operating frequency using an electrical feedback loop to deliver peak power to the sample vessel. The impact of these three operating modalities on yeast cell disruption is shown in Figure 7.6. Here, soluble total protein release (measured by the BCA assay) is shown as a function of time. Also compared in this figure is the VLP release (measured by immunoassay) for vertical sweeping and power tracking. The choice of instrument modality has only a minor effect on cell disruption at these optimised instrument settings, with power tracking offering a slight advantage. In general, about 8-10 minutes is required for soluble protein release that is equivalent to that of homogenisation, with the trend suggesting that additional protein release may occur beyond ten minutes. The extent of VLP release appears to level off at about 80% of that obtained from homogenisation in this same time interval, although the product recovery through the microscale chromatographic purification is closer to 90%, as discussed below (Figure 7.7D).

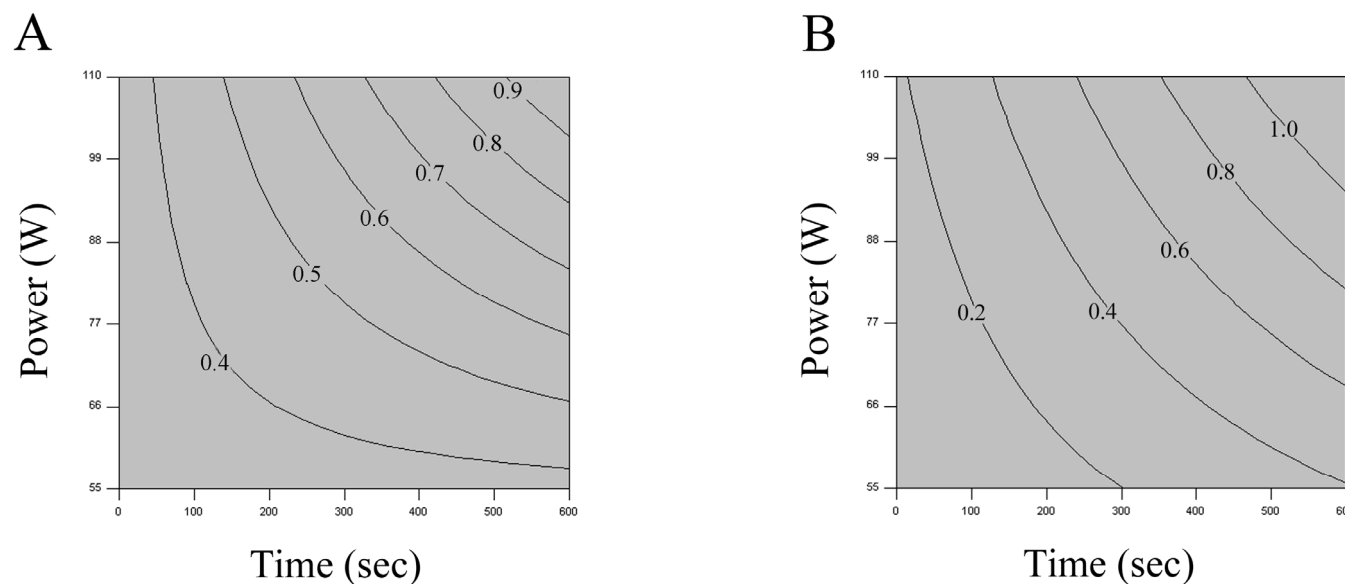


**Figure 7.5.** Response surface contour plots of yeast cell disruption by Adaptive Focused Acoustics (central composite design, fit with a two-factor interaction model): **(A)** total soluble protein (measured by the BCA assay) and **(B)** product release (HPV L1 protein measured by RP-HPLC) as a function of treatment time and acoustic power at a duty cycle of 20% (1.5 mL of a 12% w/v cell suspension). Each contour line represents the iso-response (z-value) of the fraction of cell disruption normalised to disruption by homogenisation. The curvature of the lines indicates that there is a parameter interaction. These data reveal that the system output power should be maximised (20% duty cycle and 500 mV intensity) to achieve levels of cell disruption comparable to the homogeniser in a reasonable treatment time.

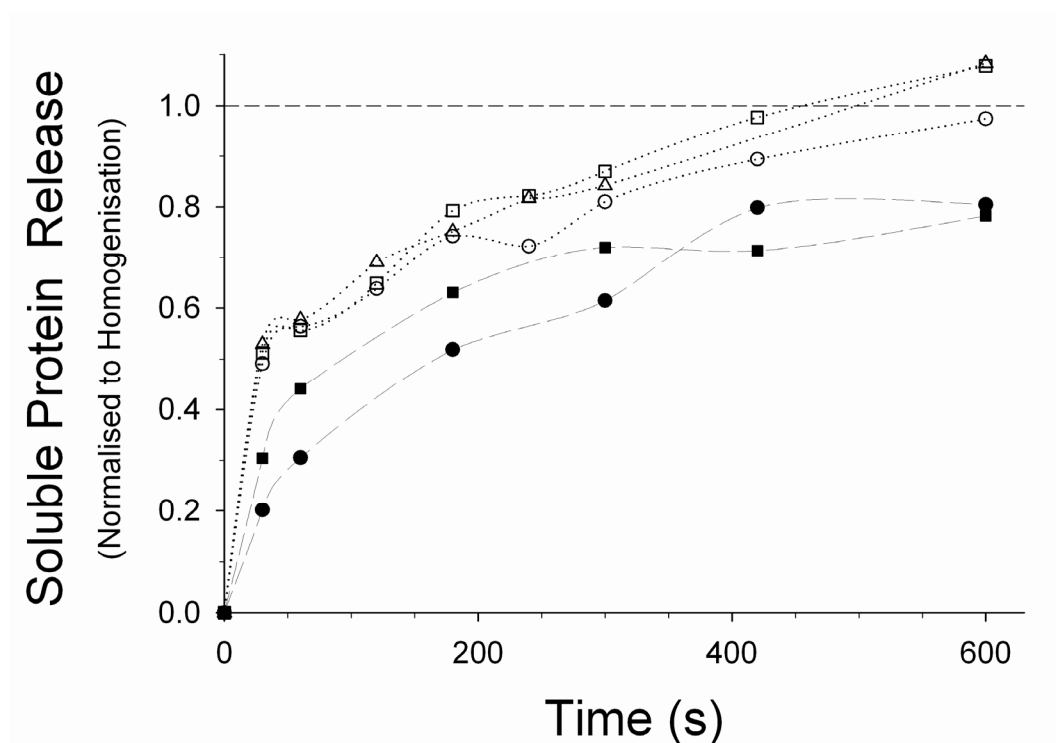


**Figure 7.6.** Effect of the AFA operating modality on total soluble protein release: vertical sweeping (○), frequency sweeping (Δ), and power tracking (□). A 1.5-mL cell suspension (12% w/v) was disrupted at an intensity of 500 mV and a duty cycle of 20%. Also shown is the HPV VLP release (measured by immunoassay) for vertical sweeping (●) and power tracking (■). All results are normalised to cell disruption by homogenisation.

#### *7.5.4. Addition of a Lytic Enzyme to Improve AFA Cell Disruption Efficiency*

The addition of a lytic enzyme,  $\beta$ 1,3-glucanase (acting on the  $\beta$ 1,3-glucan layer of the yeast cell wall), was examined in combination with the optimised AFA operating conditions for its ability to reduce exposure time and improve the comparability of the AFA method to homogenisation. In these experiments, cells were treated with one unit of  $\beta$ 1,3-glucanase per mg (wet cell weight) for 2 hr (with end-over-end rotation) at 18-22 °C prior to disruption by AFA. Timecourse studies of varying AFA treatment time over a range of 30 to 600 s were then carried out with enzyme-treated and untreated cells.

The effect of the enzyme pre-treatment was assessed by measuring the release of soluble protein (BCA assay) and VLPs (immunoassay), monitoring the turbidity of the clarified lysate (OD 600nm), and determining the recovery of VLPs through the micro-tip chromatographic purification described in Chapter 6. These results are shown in Figure 7.7 plotted against AFA exposure time. Although pre-treatment with enzyme is not absolutely required given a sufficient AFA exposure time, enzymatic pre-treatment does significantly improve the overall efficiency. The soluble protein concentration is equivalent to or exceeds that for homogenisation after only one minute (Fig. 7.7A), and equivalent VLP release is achieved in 2-3 minutes (Fig. 7.7B). The longer time required for product release is presumably because VLP assembly occurs in the nucleus (Rose et al., 1993; Wang et al., 2003) and therefore requires additional time for the disruption of the nuclear envelope. The turbidity of the clarified lysate from the microscale disruption does not quite achieve that of homogenisation, even with enzyme present (Fig. 7.7C). These results most likely derive from the differences in the lysis mechanism between the two methods, with more cell membrane disruption occurring in the homogeniser, which is also reflected in the light microscopy differences discussed below (Fig. 7.8).

For the yeast strain and growth conditions used here for VLP production, no lytic protease was required. The  $\beta$ 1,3-glucanase alone was sufficient to decrease exposure time and improve the efficiency of cell disruption. This may not always be the case, however, since the yeast cell wall architecture can vary with yeast strain and growth conditions (Firon et al., 2004; Klis et al., 2006). For example, the composition of the

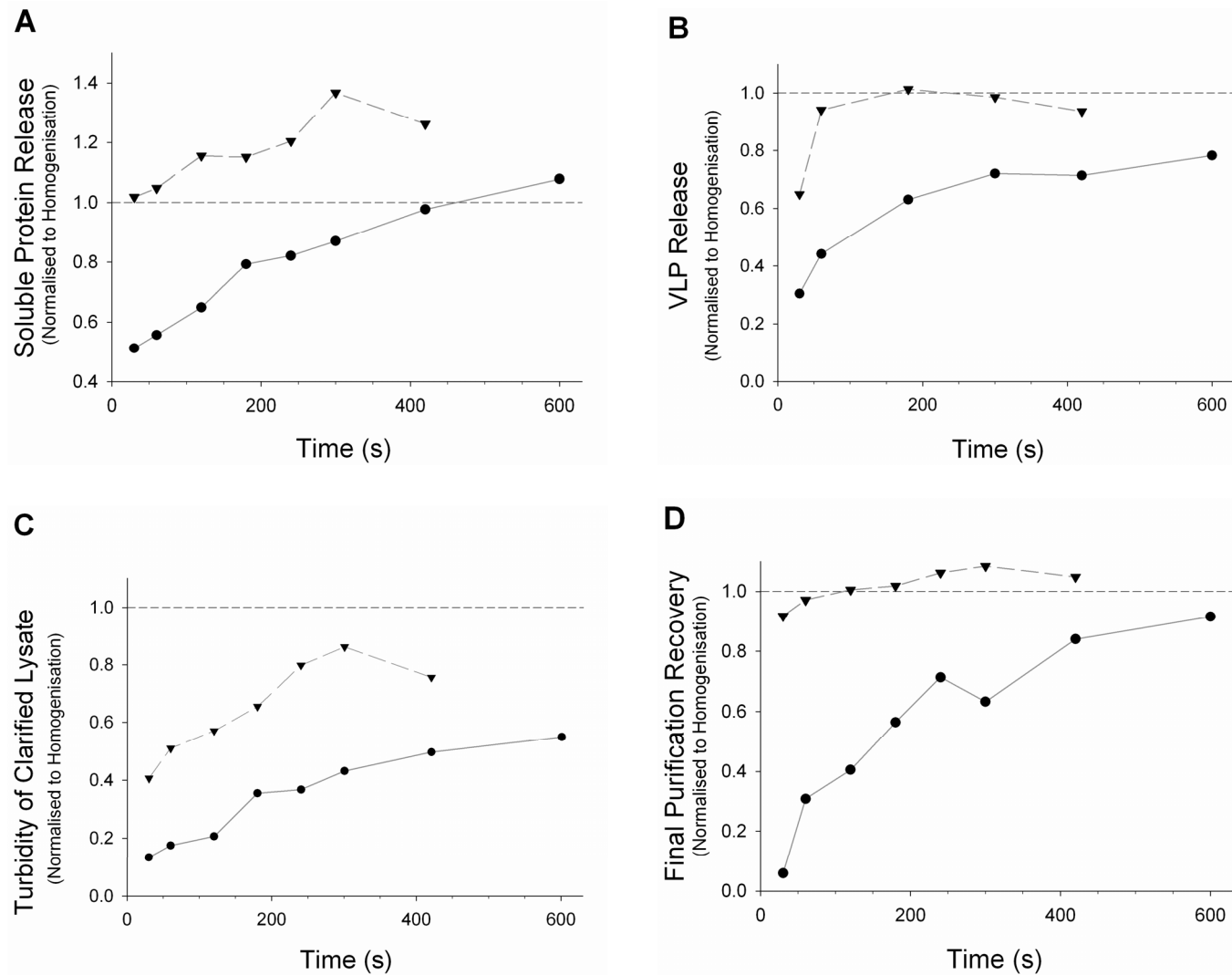


**Figure 7.7.** Timecourse of cell disruption by Adaptive Focused Acoustics with (▼) and without (●)  $\beta$ 1,3-glucanase pretreatment. **(A)** Total soluble protein release (BCA assay); **(B)** release of HPV VLPs (immunoassay); **(C)** turbidity (OD600 nm) of the clarified lysate; **(D)** final product recovery through the two-step micro-tip chromatographic purification. All data are normalised to that obtained by homogenisation.

outer layer may be such that it hinders the accessibility of the  $\beta$ 1,3-glucanase to the inner glucan layer, thereby requiring the use of a lytic protease or mannanase. In some cases,  $\beta$ 1,6-glucanase or chitinase may also be required. One potential alternative to a lytic protease is to use  $\beta$ -mercaptoethanol (Salazar and Asenjo, 2007), which reduces the disulfide bridges that bind mannoproteins and thereby improves the accessibility of  $\beta$ 1,3-glucanase to the glucan layer. One drawback of using an enzymatic pre-treatment is the risk of product degradation, such as proteolysis from residual protease activity in the enzyme mixture. Consequently, when selecting a lytic enzyme, it is critical to establish that it causes no modifications to the product.

#### 7.5.5. VLP Stability During AFA Cell Disruption

The stability of the HPV VLPs during AFA cell disruption was monitored by the immunoassay for VLPs (refer to Chapter 2), which is specific for a conformational epitope. In this experiment, purified VLPs were spiked into a cell slurry solution and their recovery determined by immunoassay following AFA treatment for ten minutes. This result was compared to a control in which the purified VLPs were spiked into the lysate after cell disruption (to determine the analytical spike recovery in the crude cell lysate). As shown in Table 7.4, the spike recovery of the sample undergoing AFA treatment is identical to that of the control, indicating that the VLPs are not significantly affected under these conditions.

**Table 7.4.** Recovery of purified VLPs spiked into the yeast cell suspension prior to disruption and also into the yeast lysate after disruption (control) to assess product stability during AFA disruption (exposure time of ten minutes). The VLP concentration was measured by the immunoassay described in Chapter 2.

Sample	Measured Concentration ( $\mu$ g/mL)	% Recovery
Spike Concentration	447	-----
Spiked prior to disruption	383	86
Spiked after disruption (control)	385	86

A second measure of stability is drawn from the analysis of the chromatographically purified VLPs from the AFA lysate and the homogenate, as described in section 7.6 below. No additional protein degradation is observed by SDS-PAGE relative to homogenisation, even in the presence of the lytic enzyme (Figs. 7.9B and 7.9C). However, this enzyme addition may be less suitable for other product types, particularly for those containing carbohydrates. It should also be noted that HPV VLPs demonstrate relatively good thermostability (Shank-Retzlaff et al., 2006).

#### *7.5.6. Evaluation of Cell Disruption by Light Microscopy*

Oil-immersion light microscopy was carried out to visually assess the nature of cell breakage. Figure 7.8 shows images of the initial cell slurry and the lysates following homogenisation and AFA lysis. Cell disruption is clearly evident in all three lysate samples, although some qualitative differences are observed. The lysate from the homogeniser shows extensive fragmentation of cells, with large particles of aggregated cellular debris visible. In general, fewer cell ghosts are observed in the homogenate than in the lysate from the AFA disruption, in which cell ghosts and large membrane fragments are more evident. Of the two AFA lysates, the cell breakage appears to be more extensive for the enzymatically treated cells, consistent with the observations in Figure 7.7.

### **7.6. AFA Cell Disruption as a Component of a Fully Microscale Purification**

The final developed AFA method for yeast cell disruption involves operating the instrument at 20% dc, 500 mV intensity and 50 cpb, and using the power tracking modality, although the choice of modality is less critical. Cell concentration is also less critical and may be varied, at least between the range of 10 and 20% (w/v) that was examined here. Treatment time will depend on whether or not the cells are pre-treated with a lytic enzyme and may also vary with sample volume (not examined in this study). Without a lytic enzyme, AFA treatment times of  $\geq 7$  minutes are generally required. With a lytic enzyme pre-treatment, these times are reduced to about 3 minutes, and the overall comparability of the AFA disruptate to the laboratory-scale homogenate is improved because of a greater degree of cell disruption.

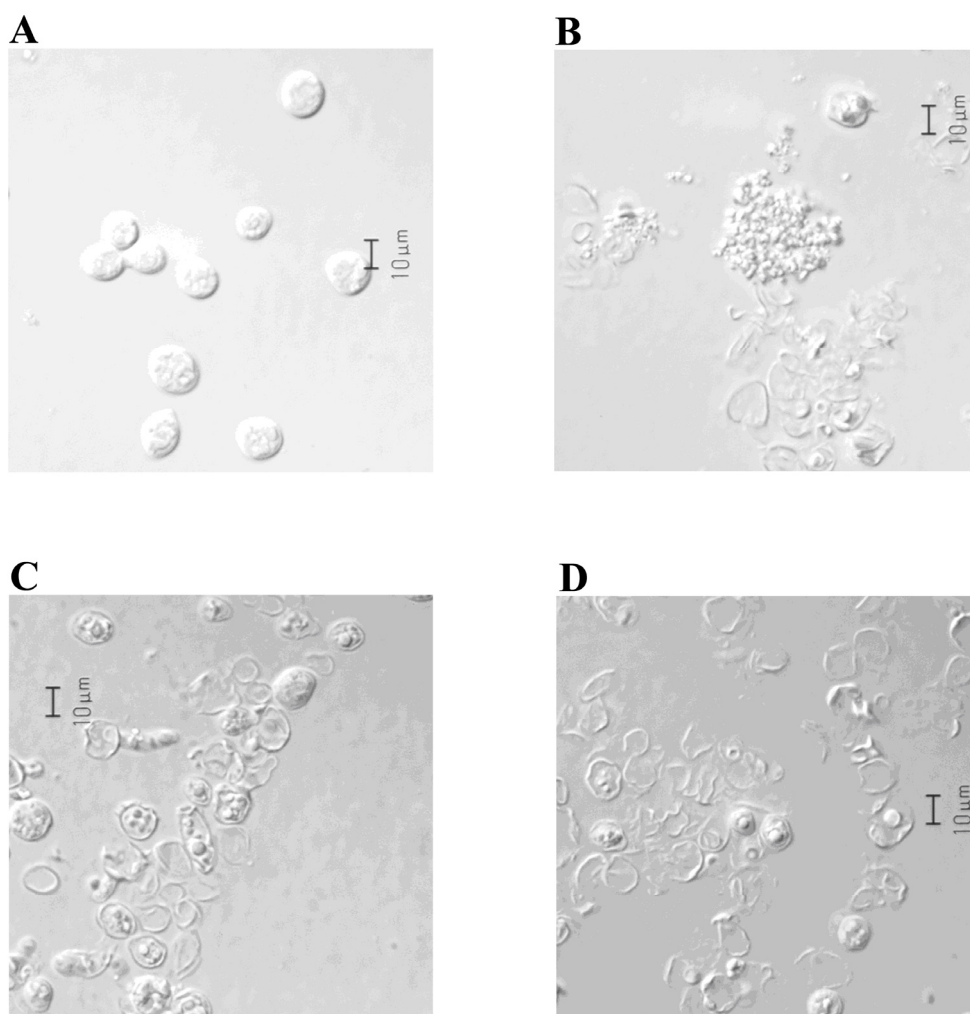


**Figure 7.8.** Light microscopy of yeast cells before and after cell disruption: **(A)** initial cell slurry; **(B)** after homogenisation; **(C)** after AFA cell disruption (treatment time of 10 min); **(D)** after  $\beta$ 1,3-glucanase pre-treatment and AFA cell disruption (treatment time of 7 min).

#### *7.6.1. Performance of the AFA Lysate Through the Chromatographic Purification*

Differences in cell breakage such as the ones observed above by light microscopy can potentially impact the debris clarification stage, as described by Clarkson et al. (1993). Hence, the AFA method developed here will be less useful as a mimic of homogenisation for developmental experiments focusing on solid-liquid separations. However, by incorporating a small-scale batch centrifugation for solid debris removal, the technique is useful for providing representative feed material for chromatography experiments since the soluble protein contaminant profile of the clarified lysate is very similar to that from homogenisation, as evidenced by SDS-PAGE (Fig. 7.9A).

To demonstrate this point, the micro-tip chromatographic purification described in Chapter 6 was performed to assess whether the AFA cell disruption method impacted upon the downstream multi-step chromatography. Overall, the microscale disruption exerted no significant effects on the downstream chromatography relative to the laboratory-scale homogenisation. Recovery of VLPs through the microscale purification using AFA cell disruption is equivalent ( $\leq 10\%$  difference) to homogenisation after three minutes of AFA treatment in combination with enzymatic pre-treatment (Fig. 7.7D). Without enzymatic pre-treatment, the recovery is somewhat less but is 80% of that of the homogenisation after 7 minutes and about 90% after ten minutes. The robustness of the AFA disruption was further evaluated with three different fermentation pastes (Table 7.5). In this assessment, the difference in chromatographic product recovery between the AFA method and homogenisation ranged from 0 to 13%, even though the AFA exposure time was only seven minutes and there was no enzyme pre-treatment. Comparability should improve even further with the inclusion of the  $\beta$ 1,3-glucanase pre-treatment step. In addition to VLP recovery, product purity after each chromatographic step is comparable, as shown in Figures 7.9B and 7.9C. Furthermore, the addition of the lytic enzyme does result in any additional proteolytic degradation.

#### *7.6.2. Sample Requirement, Experimental Throughput, and Labour Savings*

The AFA cell disruption supports a fully microscale purification in which to characterise the impact of fermentation changes on the downstream VLP purification and ultimately enables the subsequent scale-down of yeast fermentation experiments.

The amount of cell weight input (milligram quantities) required for the microscale purification is about 100-fold less than that needed for the standard laboratory-scale purification. Because of this reduced sample requirement, the microscale purification enables fermentation timepoints to be evaluated in order to provide feedback throughout the fermentation process rather than for just a single end-point evaluation. Consequently, parameters such as the harvest time window can be more rapidly and easily defined. An example of this is shown in Figure 7.10, with the product recovery through the multi-step chromatography shown as a function of harvest time. In this example fermentation, an induction phase is observed, followed by an optimal time for cell harvest at the penultimate timepoint, prior to an observed decline in productivity at the final timepoint.

**Table 7.5.** Performance of the AFA cell lysate through the micro-tip chromatographic purification for three different fermentation pastes. The AFA cell disruption (7-min treatment time; without  $\beta$ 1,3-glucanase addition) is compared to homogenisation with respect to final chromatographic product recovery.

<b>Final Chromatographic Recovery (mg protein / cell weight input)</b>			
<b>Fermentation Paste</b>	<b>AFA</b>	<b>Homogenisation</b>	<b>% difference</b>
1	4.3 $\pm$ 0.1	4.5 $\pm$ 0.1	-4%
2	3.4 $\pm$ 0.6	3.4 $\pm$ 0.2	0%
3	5.4 $\pm$ 0.4	6.2 $\pm$ 0.4	-13%

In addition to needing considerably less sample input, the AFA cell disruption improves the throughput and reduces the labour required of the fermentation-feedback purification. The projected throughput and labour costs are given in Table 7.6 relative to the laboratory-scale cell disruption with the microfluidizer. If a lytic enzyme is used, the throughput is increased by over four-fold while the labour is reduced in half. This translates into greater than an eight-fold improvement in productivity, defined here as the number of pastes processed per hour of labour.

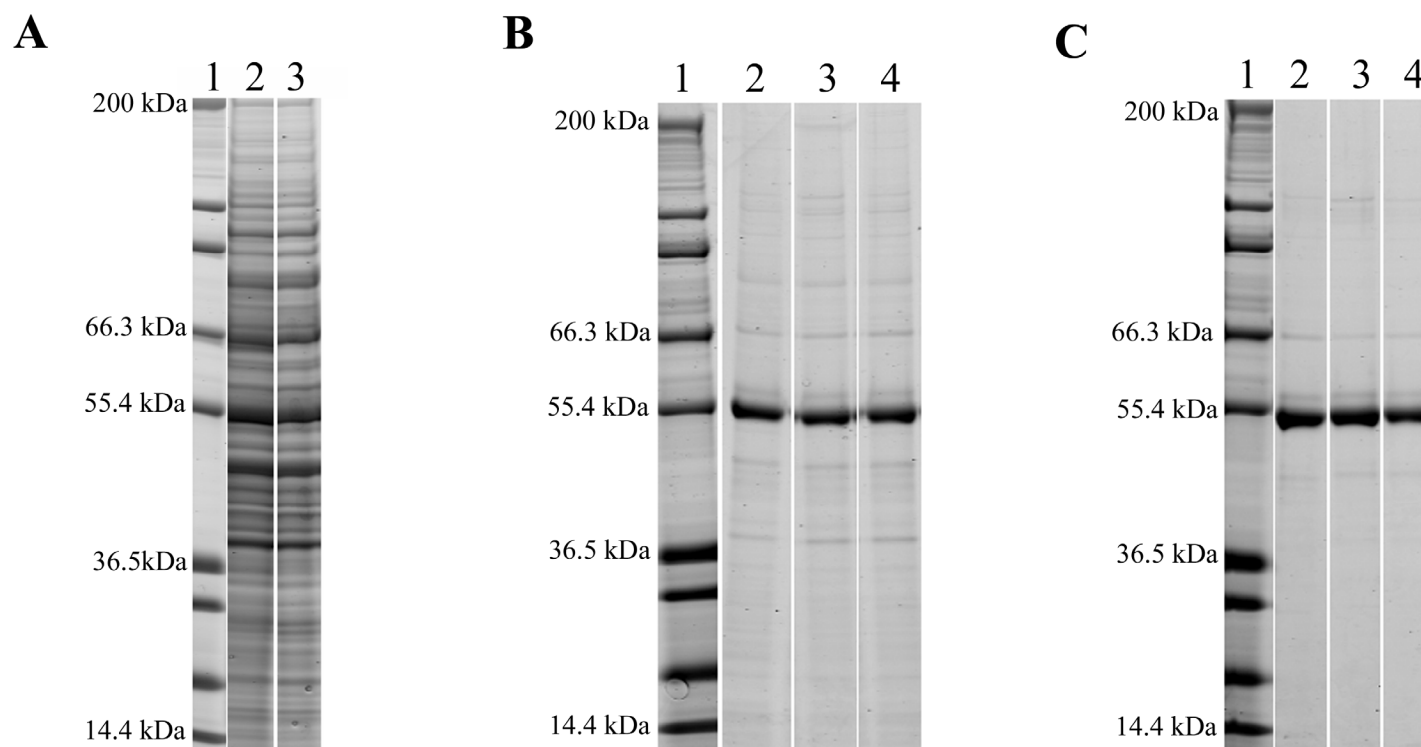


**Figure 7.9.** SDS-PAGE (4-12% gel; reducing conditions; Sypro Ruby protein stain) of (A) the clarified yeast lysate following cell disruption and of the (B) cation exchange and (C) hydroxyapatite chromatographic products following the microscale purification. (A) **Lane 1**, molecular weight standard; **Lane 2**, lysate from homogenisation; **Lane 3**, lysate from AFA method (no  $\beta$ 1,3-glucanase pre-treatment). (B) and (C), **Lane 1**, molecular weight standard; **Lane 2**, chromatographic product from homogenisation; **Lane 3**, chromatographic product from AFA lysis; **Lane 4**, chromatographic product from AFA lysis and  $\beta$ 1,3-glucanase pre-treatment. The HPV L1 protein migrates at  $\sim$  55 kDa.

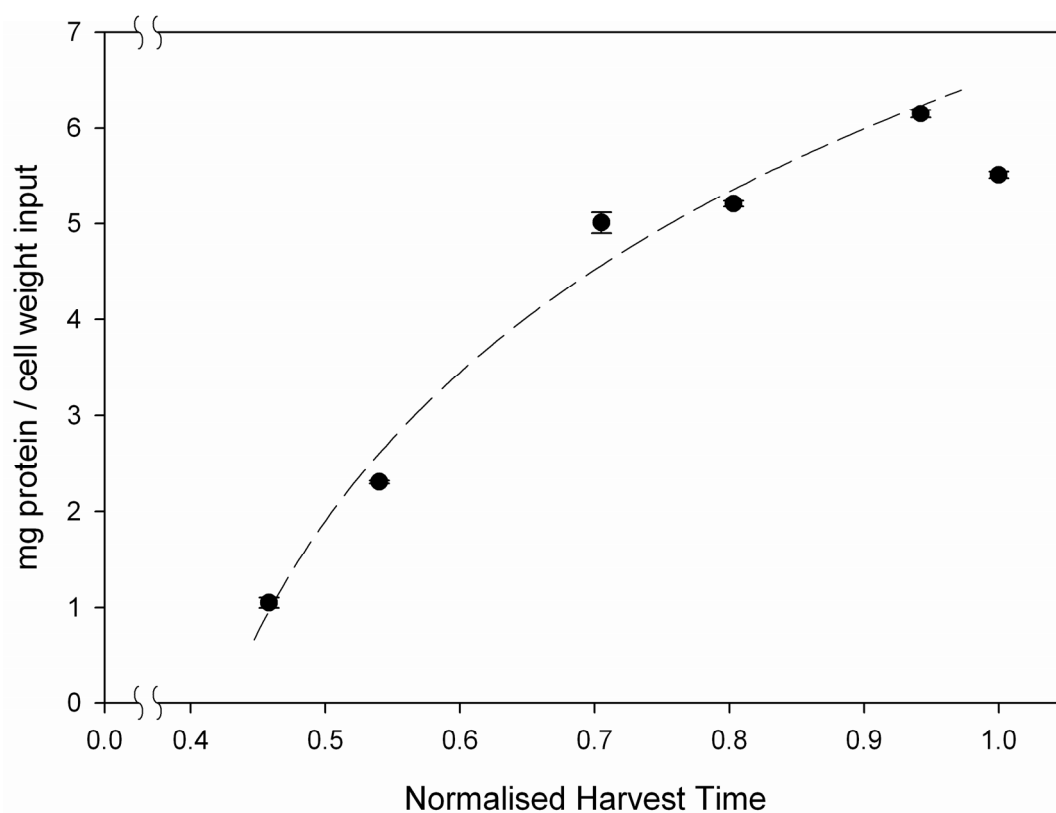


**Figure 7.10.** Final chromatographic recovery through the microscale VLP purification as a function of fermentation harvest time. Recovery is expressed as the total protein recovered following the second column (CHT) per unit cell weight input, and harvest time is normalised to the final harvest time (harvest time / final harvest time). (These units were selected to protect Merck intellectual property while retaining the scientific importance of the data.) The five harvest timepoints prior to the final harvest time are fit with an empirical line of best fit (3-parameter logarithmic function):  $y = y_0 + a \ln(x - x_0)$ .

**Table 7.6.** Experimental throughput and labour of the AFA cell disruption method (+/- lytic enzyme) when used as a component of the microscale HPV VLP purification (for evaluating yeast fermentation conditions). These calculations are shown relative to the laboratory-scale homogenisation.

	<b>AFA Disruption - Lytic Enzyme</b>	<b>AFA Disruption + Lytic Enzyme</b>	<b>Lab-Scale Disruption</b>
System Set-up / Clean-up Time (hr)	0.5	0.5	0.5
Batch Size (number of pastes/run)	12 <sup>a</sup>	12 <sup>a</sup>	1
Run Time (hr)	2.25 <sup>b</sup>	0.85 <sup>c</sup>	0.5
Number Runs / 8-hr Day <sup>d</sup>	2	4	12
Cell Preparation Time <sup>e</sup> (hr) / 8-hr Day	1.5	1.5	1.5
Pre-treatment Time (hr) / 8-hr Day	0	2.5	0
<b>Throughput (pastes processed / 8-hr day)</b>	<b>24</b>	<b>48</b>	<b>12</b>
<b>Total Labour (hr)<sup>f</sup></b>	<b>2.5</b>	<b>3.5</b>	<b>8</b>

a) 3 X 4 configuration using the 16 X 100 mm borosilicate glass tubes

b) 10-minute run time / paste + 15 min post-run sample handling

c) 3-minute run time / paste + 15 min post-run sample handling

d) Accounts for system and cell preparation times as well as run time

e) Includes dilution, transfer to treatment vessel, enzyme addition (when applicable). Excludes cell thawing time.

f) Includes system set-up/clean-up, cell preparation, and post-run sample handling (15 min/run) times. For laboratory-scale disruption, also includes run time.

The VLP purification is typically a two-day process, with the cell disruption carried out on the first day, followed by an overnight incubation and subsequent centrifugation and chromatographic purification on the second day. The throughput projected for the downstream chromatographic purification is about 32 pastes per day, when the chromatography is carried out in duplicate (Table 6.3). By using the AFA cell disruption technique (in combination with enzyme pre-treatment), the cell disruption is no longer the bottleneck and is able to keep pace with throughput of the

downstream purification. In this way, 32 pastes can be evaluated every two days. However, this calculation does not account for the time required for analysis, and often it is the analysis of these large experimental sets that can become a bottleneck.

## **7.7. Summary**

Having low volume methods for yeast cell breakage that are capable of disrupting the rigid cell wall is critical to the miniaturisation of bioprocesses that use these expression systems. Adaptive Focused Acoustics offers a small-scale technique for yeast cell disruption that is comparable to high pressure homogenisation with respect to soluble protein release and performance through the downstream chromatography. The addition of a lytic enzyme significantly decreases processing time and consequently increases throughput. No adverse effects on the product (HPV VLPs) are observed under the exposure times required for yeast cell lysis by AFA.

The AFA microscale cell disruption technique (Wenger et al., 2008) facilitates integrated microscale process development strategies for proteins produced intracellularly, alongside microscale techniques for fermentation (Micheletti and Lye, 2006), microfiltration (Jackson et al., 2006), centrifugation (Hutchinson et al., 2006), and chromatography (Bensch et al., 2005; Wenger et al., 2007; Bergander et al., 2008; Coffman et al., 2008). Interactions between upstream and downstream operations can be studied, and representative feed material for the downstream chromatography can be produced for high-throughput experiments. Although a completely automated downstream purification sequence is not demonstrated in this thesis, a robotic interface on a new model of the Covaris AFA instrument (model E210R) makes integration with a liquid-handling workstation feasible, enabling not only a fully microscale process, but also a fully automated one.

## 8. CONCLUSIONS AND FUTURE DIRECTIONS

### 8.1. Conclusions

The next generation of bioprocess development depends on the seamless integration of microscale bioprocessing techniques into its routine workflow to cope with the many challenges facing it. Automated microscale techniques allow bioprocess information to be obtained efficiently with microlitre sample volumes, thus reducing manual intervention, improving product understanding, and accelerating process development. Because chromatography is usually an integral part of protein purification processes, the capacity to deploy microscale chromatography can make an important contribution towards the development of robust processes. Micro-tip chromatography is therefore a key element to an integrated, high-throughput process development strategy. In this thesis, the technique was demonstrated as a tool for adsorbent characterisation, as an integral component of a high-throughput workflow, and as a small-scale mimic of a laboratory-scale purification that evaluates the interactions between fermentation processes and the downstream chromatography. Acquiring such knowledge will become increasingly important as industry seeks to understand the consequence of how upstream process changes can affect the performance of downstream operations.

#### *8.1.1. Micro-Tip Chromatography as a Platform for Microscale Chromatography*

Micro-tip chromatography is operated with bi-directional (up, down) flow through a small bed height of packed adsorbent. An important advantage of the micro-tip format over other microscale chromatographic techniques is that it provides a simple path to full walk-away automation, without the requirement to manipulate loose adsorbent slurries by mixing and filtration in the way that is required for other approaches such as micro-batch incubation. As with traditional packed beds, dynamic flow of the mobile phase is employed through the micro-tip column, but without the multiple plates (separation stages) seen in a conventional chromatography column. Consequently, both column residence time and contact time (total loading time) are key operational parameters that must be considered, and these in turn are a function of aspiration-dispense cycle number, sample volume, column size, and flow rate. For the test IgG proteins used in this thesis, uptake onto micro-tip columns containing preparative porous cation-exchange adsorbents was found to be primarily a function of total resin-sample contact time and not the

column residence time. It is postulated that this occurs because intra-particle mass transfer is rate limiting in the case of globular proteins such as immunoglobulin (Helfferich, 1965; Ruthven, 2000; Dziennik et al, 2003 and 2005), whereas film mass transfer is presumably rate determining for much larger viral particles which are excluded from the adsorbent pore volume.

#### *8.1.2. Adsorbent Characterisation by Micro-Tip Chromatography*

Obtaining fundamental knowledge about the equilibrium and mass transport properties of an adsorbent for a particular protein can assist in the development of a Quality by Design (QbD)-based approach to process characterisation and the late-stage definition of manufacturing design space. As shown in this thesis, micro-tip columns can be used to obtain thermodynamic and kinetic data, employing methods for performing equilibrium adsorption isotherms, finite-bath batch uptake experiments, and shallow-bed chromatography. Finite-bath methods for adsorption isotherm and uptake experiments were used primarily in this thesis, with micro-tip results found to agree well with those obtained from micro-batch (static-mixing) methods. This agreement was expected for the adsorption isotherm data since they are carried out at (or close to) equilibrium conditions. In the case of the kinetic experiments, although the external mass transport conditions differ significantly between the formats, the similarity of the results can be attributed to the fact that intra-particle pore diffusion is the main rate limiting factor governing the adsorption of comparatively small proteins inside porous adsorbents. Shallow-bed chromatography also appears to be a feasible approach for micro-tip chromatography, providing an alternative to finite-bath methods, although there is a constraint on the lower range of sample concentration that may be used. Therefore, this approach was not pursued further in this thesis.

Although a qualitative comparison of adsorption kinetics is useful for resin screening, ultimately a more quantitative measurement of column dynamic binding capacity (DBC) is required in order to define the productivity and process economics of the step. Modelling DBC from microscale data can help to conserve limited materials and resources, and in this thesis, two data-driven models were evaluated. The goal here was not to predict the full shape of the breakthrough curve or elucidate the underlying mechanisms of mass transfer, but simply to predict column  $DBC_{10\%}$

from micro-tip data sets. The modelling approaches used in this thesis were selected because they are primarily data-driven and do not require complex mass transport models and mathematics. Given the finding above that micro-tip batch uptake data is analogous to micro-batch adsorption when pore diffusion is rate limiting, the first model used an approach applied by Bergander et al. (2008) to micro-batch adsorption data, in which shrinking-core pore-diffusion behaviour was assumed. The approach showed reasonable agreement between the predicted and experimental column data, with errors ranging from 5 to 29% across the 10-fold flow-rate range examined. The second approach employed a simple staged-reaction model, analogous to that used by Chase (1984), but with the model parameters obtained instead from *pre-equilibrium* adsorption isotherm data. The predicted values of this approach showed very good agreement with the laboratory-scale experimental data, with all errors  $\leq 12\%$ . However, one limitation of this approach is that it requires a column calibration experiment to be performed in order to relate micro-tip contact time to that of the column.

#### *8.1.3. Micro-Tip Chromatography Applied to High-Throughput Process Development*

Micro-tip chromatography was demonstrated in this thesis as an element of high-throughput process development for two different applications. In the first, a microscale workflow was applied to the development of a mixed mode chromatography step in the purification of a monoclonal antibody from cell filtrate. Conditions were defined in days instead of weeks and with only milligram quantities of feed material. More significantly, the examination of a wide operating space revealed conditions where the mixed mode chromatography might be used as an alternative to Protein A chromatography in order to reduce cost, clean with sodium hydroxide, and eliminate the low-pH elution step. The batch microscale results were subsequently verified in the dynamic column mode using a 1-mL laboratory-scale column (a 100-fold scale-up), with the results in agreement in terms of yield, impurity clearance, and adsorbent capacity.

In the second application, a two-step chromatographic purification of VLPs was miniaturised by 1000-fold with micro-tip columns. This purification was used to inform upstream yeast fermentation development by examining the effect that

fermentation changes have upon the downstream chromatography. As in the mixed-mode chromatography example, the microscale purification was predictive of the laboratory-scale purification in terms of yield and purity, although an empirical correction factor was applied in this case to correct for a consistent offset in recovery. This offset was shown to be due to the deliberately shortened loading times of the second tip chromatography step, serving as an example of the trade-off that sometimes needs to be made between experimental throughput and predictive performance. The micro-tip chromatography increased the overall productivity of the purification (number of fermentation pastes purified per hour of labour) by  $\geq 12$ -fold.

#### *8.1.4. Adaptive Focused Acoustics for Microscale Cell Disruption*

The miniaturisation of the VLP purification necessitated the need for a small-scale disruption method for yeast cells, with the goal being to provide representative feed material for the microscale chromatography. This was achieved using a relatively new technology known as Adaptive Focused Acoustics. With this method, the total soluble protein release was equivalent to that of laboratory-scale homogenisation, and cell disruption was evident by light microscopy. The recovery of VLPs through a microscale chromatographic purification following AFA cell disruption differed by  $\leq 10\%$  from that obtained using homogenisation, with equivalent product purity observed. The addition of a yeast lytic enzyme prior to cell disruption reduced processing times by nearly three-fold and further improved the comparability of the lysate to that of the laboratory-scale homogenate. In addition, unlike conventional sonication methods, sample heating was minimised ( $\leq 8\text{ }^{\circ}\text{C}$  increase), even when using the maximum power settings required for yeast cell disruption. The small-scale disruption method improved the overall productivity of the microscale VLP purification by an additional factor of six or more, while reducing the amount of cell input by nearly 100-fold. Together the microscale cell disruption and micro-tip techniques facilitate integrated microscale strategies and enable the scale-down of additional process steps including the fermentation.

## 8.2. Future Directions

### 8.2.1. *Future Directions in Micro-Tip Chromatography*

Within process development groups, there can be debate over which microwell chromatographic format to implement (micro-batch adsorption, micro-tip chromatography, or miniature columns). Yet, these formats are not necessarily mutually exclusive and often can be employed in a complementary manner. The batch methods (micro-batch adsorption and micro-tip chromatography) lend themselves well to high-throughput screening of adsorbents and mobile phase conditions, especially in early development. While these batch methods also can potentially be validated for the prediction of specific aspects of large-scale operation, the mini-column format appears to provide the best opportunity for a validated scale-down model, although it too has some important differences from laboratory-scale columns with respect to bed height and wall effects. Even between the two batch methods, there are clear differences. Micro-batch adsorption provides very high throughput, ease of use in a manual or semi-automated manner, and the lowest cost. Consequently, this format can be deployed easily across a wide number of end users, especially when there are no automation capabilities available. On the other hand, micro-tip chromatography is much simpler to automate and, therefore, is better suited for automated laboratories wanting to achieve full walk-away automation. Moreover, it enables additional capabilities such as shallow-bed chromatography and potentially more predictive column lifetime experiments.

Although in this thesis micro-tip experiments were performed with only eight micro-tip columns at a time, the micro-tip format should be capable of performing 96 parallel experiments in a single run. To do so, though, requires the availability of 96-channel arms that can accommodate 1-mL pipette tips, in order to maintain the operational flexibility of the format. Currently, most conventional 96-channel liquid-handling arms are made for 200- $\mu$ L pipette tips. However, recently some robotic manufacturers such as Hamilton Robotics (Reno, NV, USA) and Tecan have introduced 96-channel pipetting heads that can accommodate larger pipette tips (0.5-1.0 mL pipetting volume), and other manufacturers are sure to follow. This increases the throughput over an eight-channel micro-tip experiment by a factor of 12, and because the micro-tip format is fully automated and requires no resin manipulation, it potentially offers greater throughput than 96-well micro-batch adsorption.

Furthermore, an additional advantage of 96-channel liquid-handling arms over the 8-channel Tecan arm used in this thesis is that they typically operate by positive displacement. This means that no system liquid is required, thereby avoiding the chance of water dripping into the tip. Furthermore, the delay times after pipetting may be reduced. Developing 96-channel micro-tip methods is therefore an important area of future work for enhancing the throughput and robustness of the technique.

#### *8.2.2. Need for High-Throughput Assays and a Comprehensive Analytical Strategy*

The mainstream implementation of high-throughput microscale methods depends on a well-coordinated analytical strategy; otherwise, analytical resources risk being overwhelmed. This analytical strategy must be capable of handling very high sample numbers and low-microlitre sample volumes. Therefore, development and refinement of such a strategy is an important area for future contribution.

A number of assays used in this thesis were automated on a Tecan workstation, including the host-cell protein ELISA, the BCA total protein assay, and the PicoGreen DNA assay. This automation improved throughput and reduced labour. Yet, even with these high-throughput methods, analytical resources were still sometimes overwhelmed, especially if there was not careful planning and close collaboration with the analytical testing groups. One way of alleviating this problem is to run the automated assays on the same robotic deck as that of the purification experiments, thereby eliminating the logistics of sample transfer. Moreover, in addition to automated assays, new assay technologies, like the ForteBio (Menlo Park, CA, USA) Octet, provide a path to low-volume, parallel testing. Microfluidic technologies (Ohno et al., 2008) also present opportunities for rapid, low-volume testing, with an example being the Caliper (Hopkinton, MA, USA) Labchip for protein electrophoresis. These new technologies when combined with automated procedures can potentially eliminate the analytical bottleneck in high-throughput process development.

#### *8.2.3. Experimental Design to Best Utilise Increased Experimental Throughput*

In addition to a well-planned analytical strategy, the smart experimental design of microscale experiments is another important means to avoiding analytical gridlock and improving the overall efficiency of process development. Options for

experimental design may include simple brute-force approaches like the one used in Chapter 5, conventional DoE methodologies such as factorial and central composite designs, and complex iterative approaches such as simplex and genetic algorithms. A particularly fascinating concept known as the 'Robot Scientist' has recently emerged (Whelan and King, 2004; King et al., 2009) with respect to experimental design. A Robot Scientist borrows from techniques in the field of artificial intelligence and consists of programmable hardware and intelligent software. This software integrates the physical experimentation with results analysis, formation of a hypothesis, and subsequent experimental design. King et al. (2009) recently demonstrated a Robot Scientist known as 'Adam' for the identification of genes encoding orphan enzymes in *Saccharomyces cerevisiae*. Some have criticised this concept by arguing that what is discovered by the Robot Scientist is often implicit in the formulation of the problem. However, for the empirical optimisation typical of bioprocess development, this may not necessarily be problematic. Clearly then, the Robot Scientist concept offers an exciting opportunity for automated microscale bioprocessing, but is just emerging as an area of future work.

#### 8.2.4. *A Vision for Microscale Bioprocess Development*

Microscale techniques hold the promise of transforming bioprocess development, but the fulfilment of this promise depends on their routine integration into the workflow for both early- and late-stage development. Early-stage integration is straightforward, with these methods used to acquire information about likely trends in output variables across the operating space that can be used subsequently to minimise the scope of the ensuing laboratory-scale development. However, their integration into late-stage development is considerably more difficult, since to be of most value, these techniques must be validated for their capacity to accurately predict the absolute values of process-scale outputs.

##### 8.2.4.1. High-Throughput Examination of the Parameter Space

In the simplest scenario, microscale experiments are used to rapidly locate optimal ranges for the ensuing laboratory studies, as outlined in Figure 1.6. This strategy was used for the mixed mode chromatography development described in Chapter 5 and also in the high-throughput approaches published by Coffman et al. (2008) and Chhatre et al. (2009). The advantage of this strategy is that although the microscale

technique needs be predictive of trends in large-scale operation, it does not have the burden of needing to be a fully validated scale-down model. The disadvantage though is that some laboratory-scale experiments are still required. This strategy is analogous to an explorer searching for a lost city on an island out at sea. In this analogy, high-throughput microscale methods are used to narrow the search, i.e. 'find the island in the sea'. A few focused laboratory-scale experiments are then performed to verify the microscale results and locate the optimum, i.e. 'verify that you have landed upon the right island and then find the city on the island'. Although laboratory-scale experiments are not entirely eliminated, this approach nevertheless builds in improved quality by increasing knowledge of the operating window, even if these data cannot be formally used from a regulatory perspective to support process validation ranges.

#### 8.2.4.2. Validated Micro Scale-Down Models

Achieving the full potential of microscale bioprocessing techniques ultimately depends on having validated methods which can be used to quantitatively predict pilot- or manufacturing-scale performance, without the need for intermediate laboratory-scale verification. To do so, these validated microscale techniques may have to rely on the use of predictive modelling or engineering correlations. The microscale multi-step VLP purification described in this thesis is an example of one such opportunity. While correlation of the micro-tip data with the laboratory scale results was established with respect to purity and recovery, such a correlation with pilot and manufacturing scales was not examined. Another possible opportunity comes from the ultra scale-down work by Hutchinson et al. (2006) in which shear stresses on cells in the feed zone of an industrial-scale continuous centrifuge were examined using a small-scale shear device. These researchers used these data in combination with laboratory-scale test tube centrifuge studies to successfully predict the performance in the large-scale centrifuge. For a chromatography step, this same research group (Hutchinson et al., 2009) demonstrated an ultra scale-down approach in which a 1-mL laboratory-scale protein A column was used to predict the elution profile of an 18.3-L pilot-scale column. This was achieved by applying empirical correction factors derived from changes in the conductivity profile to account for differences in dispersion and retention between the scales.

Having validated scale-down techniques for late-stage development enables their formal use in setting process validation ranges and supporting the definition of a manufacturing design space. However, developing these methods and subsequently validating them is a formidable task, especially in the highly regulated environment of biopharmaceuticals. Therefore, this remains an important but very challenging area of future work.

#### 8.2.4.3. An Integrated Strategy for Bioprocess Development

A strategy for the full integration of microscale bioprocess techniques into routine process development is proposed in Figure 8.1. This strategy includes the use of screening methods for early-stage development as well as validated scale-down methods for late-stage process definition. Instead of following a linear sequence, as the one shown in Fig 1.6, this strategy is more dynamic, with information flowing back and forth between stages. A typical workflow might first use high-throughput microscale techniques to screen a wide range of conditions in order to guide laboratory-scale development, with the details of the experimental design depending on prior experience, expert knowledge, the number of potential variables, and the DoE methodology employed. The results of the microscale experiments would then be verified and optimised at the laboratory scale. However, additional microscale experiments might sometimes be required if there were any unexpected findings at the laboratory scale, especially if this meant performing a large number of follow-up experiments. After these additional microscale experiments, laboratory-scale verification would again ensue, followed by scale-up to the pilot and manufacturing scales. Any unforeseen issues at the production scale, as well as initiatives for process improvement, might trigger additional microscale and laboratory-scale experiments.

As an alternative to this workflow, validated microscale methods might be used, allowing conventional laboratory-scale development to be bypassed all together. The validated methods would then be used to define optimal process ranges at the pilot or manufacturing scale, and later on, to troubleshoot unforeseen issues that arise at these scales. High-throughput screening methods might still precede the use of these validated microscale methods if doing so improved the overall efficiency of process development. In this way, microscale techniques become an integral element of the

process development workflow, with a number of paths available for achieving a robust final manufacturing process. The further refinement and implementation of this vision for microscale process development is an important area of future work.

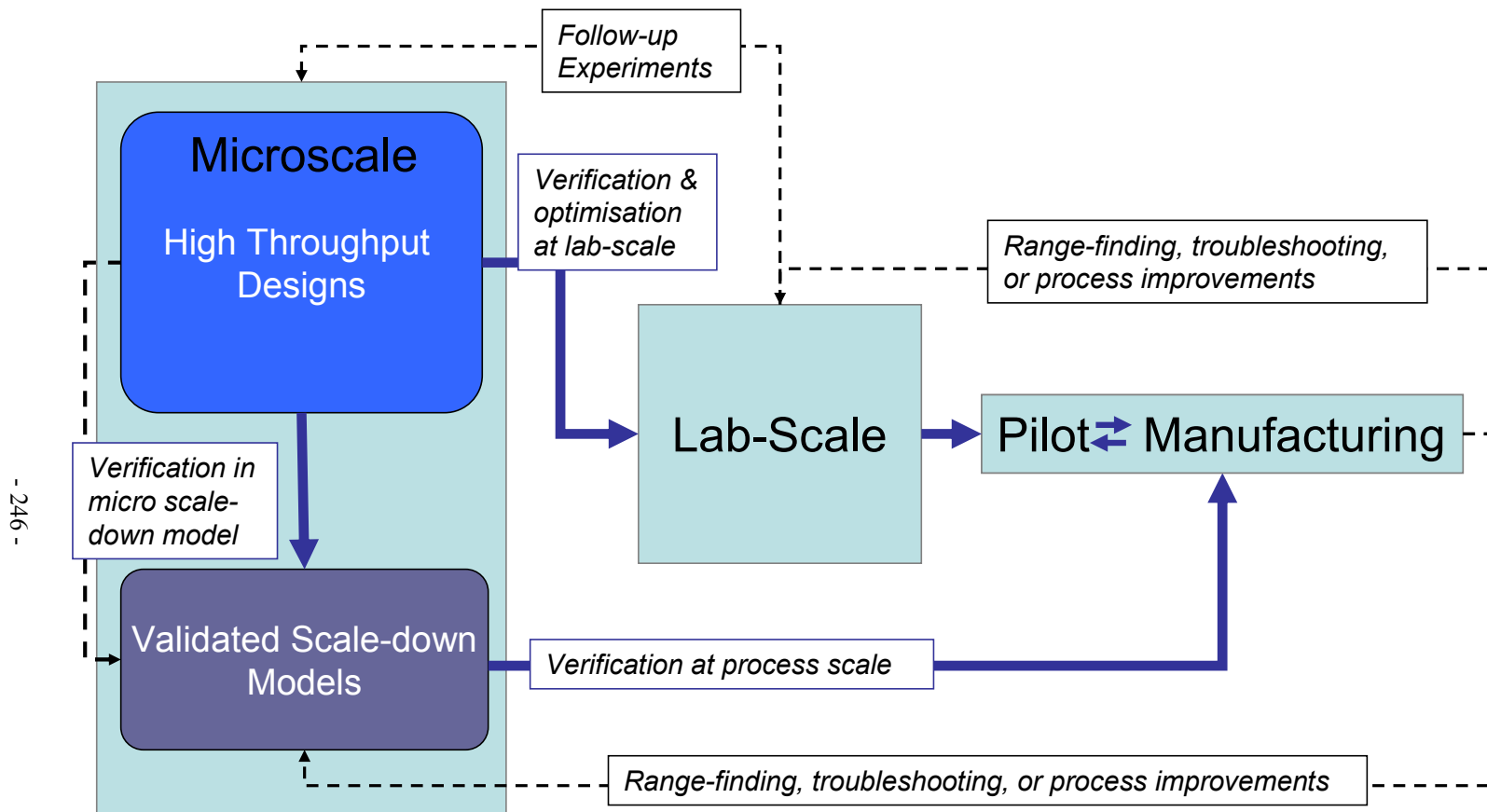


**Figure 8.1.** Integration of microscale bioprocess techniques into the process development workflow. Microscale experiments can be used for early-stage development and late-stage range finding, troubleshooting, or process development experiments. This integrated approach facilitates quality-by-design process development.

## REFERENCES

1. Abdiche, Y., D. Malashock, A. Pinkerton, and J. Pons. 2008. Determining kinetics and affinities of protein interactions using a parallel real-time label-free biosensor, the Octet. *Anal. Biochem.* 377, 209-217.
2. Afeyan, N.B., N.F. Gordon, I. Mazsaroff, L. Varady, S.P. Fulton, Y.B. Yang, and F.E. Regnier. 1990. Flow-through particles for the high-performance liquid chromatographic separation of biomolecules: Perfusion chromatography. *J. Chromatogr. A.* 519, 1-29.
3. Aggarwal, S. 2009. What's fueling the biotech engine - 2008. *Nat. Biotechnol.* 27, 987-993.
4. Agrawal, P.B. and A.B. Pandit. 2003. Isolation of  $\alpha$ -glucosidase from *Saccharomyces cerevisiae*: Cell disruption and adsorption. *Biochem. Eng. J.* 15, 37-45.
5. Aguerro, A. 2003. ProCreator: Automating the Creation of Buffer Matrices for Protein Crystallization. *J. Assoc. Lab. Auto.* 8, 52-54.
6. Amari, J.V. and I. Mazsaroff. 1996. Analysis of recombinant human interleukin-11 fusion protein derived from *Escherichia coli* lysate by combined size-exclusion and reversed-phase liquid chromatography. *J. Chromatogr. A.* 729, 113-124.
7. Arnold, F.H., H.W. Blanch, and C.R. Wilke. 1985. Analysis of affinity separations I.: Predicting the performance of affinity adsorbers. *Chem. Eng. J.* 30, B9-B23.
8. Arve, B.H. and A.I. Liapis. 1987. Modeling and analysis of biospecific adsorption in a finite bath. *AIChE J.* 33, 179-193.
9. Asenjo, J.A. and B.A. Andrews. 1990. Enzymatic cell lysis for product release. *Bioprocess Technol.* 9, 143-175.
10. Asenjo, J.A., A.M. Ventom, R.B. Huang, and B.A. Andrews. 1993. Selective release of recombinant protein particles (VLPs) from yeast using a pure lytic glucanase enzyme. *Nat. Biotechnol.* 11, 214-217.
11. Bak, H., O.R.T. Thomas, and J. Abildskov. 2007. Lumped parameter model for prediction of initial breakthrough profiles for the chromatographic capture of antibodies from a complex feedstock. *J. Chromatogr. B Analyt. Technol. Biomed. Life Sci.* 848, 131-141.
12. Baker, T.S., W.W. Newcomb, N.H. Olson, L.M. Cowser, C. Olson, and J.C. Brown. 1991. Structures of bovine and human papillomaviruses. Analysis by cryoelectron microscopy and three-dimensional image reconstruction. *Biophys. J.* 60, 1445-1456.

13. Bannister, D., A. Wilson, L. Prowse, M. Walsh, R. Holgate, L. Jermutus, and T. Wilkinson. 2006. Parallel, high-throughput purification of recombinant antibodies for in vivo cell assays. *Biotechnol. Bioeng.* 94, 931-937.
14. Barut, M., A. Podgornik, L. Urbas, B. Gabor, P. Brne, J. Vidic, S. Plevcak, and A. Strancar. 2008. Methacrylate-based short monolithic columns: Enabling tools for rapid and efficient analyses of biomolecules and nanoparticles. *J. Sep. Sci.* 31, 1867-1880.
15. Belter, P., E. Cussler, and W. Hu. 1988. *Bioseparations: Downstream Processing for Biotechnology.* John Wiley and Sons: New York
16. Bensch, M., P. Schulze Wierling, E. von Lieres, and J. Hubbuch. 2005. High throughput screening of chromatographic phases for rapid process development. *Chem. Eng. Technol.* 28, 1274-1284.
17. Bergander, T., K. Nilsson-Välimaa, K. Oberg, and K.M. Lacki. 2008. High-throughput process development: Determination of dynamic binding capacity using microtiter filter plates filled with chromatography resin. *Biotechnol. Prog.* 24, 632-639.
18. Berrill, A., S.V. Ho, and D.G. Bracewell. 2008. Ultra scale-down to define and improve the relationship between flocculation and disc-stack centrifugation. *Biotechnol. Prog.* 24, 426-431.
19. Betts, J.I. and F. Baganz. 2006. Miniature bioreactors: Current practices and future opportunities. *Microbial Cell Factories.* 5, 21-35.
20. Beyzavi, K. 1999. Adsorbents, inorganic. In *Encyclopedia of Bioprocess Technology: Fermentation, Biocatalysis, and Bioseparation*; M.C. Flickinger and S.W. Drew, Eds.; John Wiley and Sons: New York, 13-19.
21. Bhikhabhai, R., A. Sjöberg, L. Hedkvist, M. Galin, P. Liljedahl, T. Frigard, N. Pettersson, M. Nilsson, J.A. Sigrell-Simon, and C. Markeland-Johansson. 2005. Production of milligram quantities of affinity tagged-proteins using automated multistep chromatographic purification. *J. Chromatogr. A.* 1080, 83-92.
22. Bierau, H., Z. Zhang, and A. Lyddiatt. 1999. Direct process integration of cell disruption and fluidised adsorption for the recovery of intracellular proteins. *J. Chem. Technol. Biotechnol.* 74, 208-212.
23. Boardman, N.K. and S.M. Partridge. 1955. Separation of neutral proteins on ion-exchange resins. *Biochem. J.* 59, 543-552
24. Boschetti, E. 1994. Advanced sorbents for preparative protein separation purposes. *J. Chromatogr. A.* 658, 207-236.

25. Bracewell, D.G., R.A. Brown, and M. Hoare. 2004. Addressing a whole bioprocess in real-time using a biosensor – Formation and purification of antibody fragments from a recombinant *E. coli* host. *Bioproc. Biosys. Eng.* 26, 271-282.
26. Brenac, V., V. Ravault, P. Santambien, and E. Boschetti. 2005. Capture of a monoclonal antibody and prediction of separation conditions using a synthetic multimodal ligand attached on chips and beads. *J. Chromatogr. B Analyt. Technol. Biomed. Life Sci.* 818, 61-66.
27. Brooks, C.A. and S.M. Cramer. 1992. Steric mass-action ion exchange: Displacement profiles and induced salt gradients. *AIChE. J.* 38, 1969-1978.
28. Burton, S.C and D.R.K Harding. 1998. Hydrophobic charge induction chromatography: Salt independent protein adsorption and facile elution with aqueous buffers. *J. Chromatogr. A.* 814, 71-81.
29. Carta, G., A.R. Ubiera, and T.M. Pabst. 2005. Protein mass transfer kinetics in ion-exchange media: Measurements and interpretations. *Chem. Eng. Technol.* 28, 1252-1264.
30. Carta, G. 2006. Mass transfer in liquid chromatography. PREP2006 Workshop Course Handbook
31. Chae, Y.K., W. Jeon, and K.S. Cho. 2002. Rapid and simple method to prepare functional pfuDNA polymerase expressed in *Escherichia coli* periplasm. *J. Microbiol. Biotech.* 12, 841-842.
32. Chan, G., A.J. Booth, K. Mannweiler, and M. Hoare. 2006. Ultra scale-down studies of the effect of flow and impact conditions during *E. coli* processing. *Biotechnol. Bioeng.* 95, 671-683.
33. Chang, C. and A.M. Lenhoff. 1998. Comparison of adsorption isotherms and uptake rates in preparative cation-exchange materials. *J. Chromatogr. A.* 827, 281-293.
34. Chapman, T. 2005. Protein purification: Pure but not simple. *Nature.* 434, 795-798.
35. Charlton, H., B. Galarza, K. Leriche, and R. Jones. 2006. Chromatography process development using 96-well microplate formats. *BioPharm International.* 19, 20-26, 42.
36. Chase, H.A. 1984. Prediction of the performance of preparative affinity chromatography. *J. Chromatogr. A.* 297, 179-202.
37. Chase, H.A. 1994. Purification of proteins by adsorption chromatography in expanded bed. *Trends Biotechnol.* 12, 296-303.

38. Chen, J., J. Tetrault, and A. Ley. 2008A. Comparison of standard and new generation hydrophobic interaction chromatography resins in the monoclonal antibody purification process. *J. Chromatogr. A.* 1177, 272-281.
39. Chen, J., T. Yang, and S.M. Cramer. 2008B. Prediction of protein retention times in gradient hydrophobic interaction chromatographic systems. *J. Chromatogr. A.* 1177, 207-214.
40. Chhatre, S. and N.J. Titchener-Hooker. 2009. Review: Microscale methods for high-throughput chromatography development in the pharmaceutical industry. *J. Chem. Technol. Biotechnol.* 84, 927-940.
41. Chhatre, S., D.G. Bracewell, N.J. Titchener-Hooker. 2009. A microscale approach for predicting the performance of chromatography columns used to recover therapeutic polyclonal antibodies. *J. Chromatogr. A.* 1216, 7806-7815.
42. Choi, J.H. and S.Y. Lee. 2004. Secretory and extracellular production of recombinant proteins using *Escherichia coli*. *Appl. Microbiol. Biotechnol.* 64, 625-635.
43. Ciccolini, L., P. Taillandier, A.M. Wilhem, H. Delmas, and P. Strehaiano. 1997. Low frequency thermo-ultrasonication of *Saccharomyces cerevisiae* suspensions: Effect of temperature and of ultrasonic power. *Chem. Eng. J.* 65, 145-149.
44. Clarke, P.R. and C.R. Hill. 1970. Physical and chemical aspects of ultrasonic disruption of cells. *J Acoust. Soc. Am.* 47, 649-653.
45. Clarkson, A.I., P. Lefevre, and N.J. Titchener-Hooker. 1993. A study of process interactions between cell disruption and debris clarification stages in the recovery of yeast intracellular products. *Biotechnol. Prog.* 9, 462-467.
46. Clonis, Y.D. 2006. Affinity chromatography matures as bioinformatic and combinatorial tools develop. *J. Chromatogr. A.* 1101, 1-24.
47. Coffman, J.L., J.F. Kramarczyk, and B.D. Kelley. 2008. High-throughput screening of chromatographic separations: I. Method development and column modeling. *Biotechnol. Bioeng.* 100, 605-618.
48. Cook, J.C., J.G. Joyce, H.A. George, L.D. Schultz, W.M. Hurni, K.U. Jansen, R.W. Hepler, C. Ip, R.S. Lowe, P.M. Keller, and E.D. Lehman. 1999. Purification of virus-like particles of recombinant human papillomavirus type 11 major capsid protein L1 from *Saccharomyces cerevisiae*. *Protein Expr. Purif.* 17, 477-484.
49. Craig, L.C. 1944. Identification of small amounts of organic compounds by distribution studies: II. Separation by counter-current distribution. *J. Biol. Chem.* 155, 519-534.

50. Cramer, S.M. and G. Jayaraman. 1993. Preparative chromatography in biotechnology. *Curr. Opin. Biotechnol.* 4, 217-225.
51. Cruz, P.E., A. Cunha, C.C. Peixoto, J. Clemente, J.L. Moreira, and M.J.T. Carrondo. 1998. Optimization of the production of virus-like particles in insect cells. *Biotechnol. Bioeng.* 60, 408-418.
52. Davies, R. 1959. Observations on the use of ultrasound waves for the disruption of micro-organisms. *Biochim. Biophys. Acta.* 33, 481-493.
53. DePhillips, P. and A.M. Lenhoff. 2000. Pore size distributions of cation-exchange adsorbents determined by inverse size-exclusion chromatography. *J. Chromatogr. A.* 883, 39-54.
54. DePhillips, P. and A.M. Lenhoff. 2001. Determinants of protein retention characteristics on cation-exchange adsorbents. *J. Chromatogr. A.* 933, 57-72.
55. DePhillips, P. and A.M. Lenhoff. 2004. Relative retention of the fibroblast growth factors FGF-1 and FGF-2 on strong cation-exchange sorbents. *J. Chromatogr. A.* 1036, 51-60.
56. DeVault, D. 1942. The theory of chromatography. *J. Am. Chem. Soc.* 65, 532-540.
57. Doulah, M.S. 1977. Mechanism of disintegration of biological cells in ultrasonic cavitation. *Biotechnol. Bioeng.* 19, 649-660.
58. Dziennik, S.R., E.B. Belcher, G.A. Barker, M.J. DeBergalis, S.E. Fernandez, and A.M. Lenhoff. 2003. Nondiffusive mechanisms enhance protein uptake in ion exchange particles. *PNAS.* 100, 420-425.
59. Dziennik, S.R., E.B. Belcher, G.A. Barker, and A.M. Lenhoff. 2005. Effects of ionic strength on lysozyme uptake rates in cation exchangers. I: Uptake in SP Sepharose FF. *Biotechnol. Bioeng.* 91, 139-153.
60. Felinger, A. and G. Guiochon. 1996. Multicomponent interference in overloaded gradient elution chromatography. *J. Chromatogr. A.* 724, 27-37.
61. Feliu, J.X., R. Cubarsi, and A. Villaverde. 1998. Optimized release of recombinant proteins by ultrasonication of *E. coli* cells. *Biotechnol. Bioeng.* 58, 536-540.
62. Fernandez, M.A. and G. Carta. 1996. Characterization of protein adsorption by composite silica-polyacrylamide gel anion exchangers I. Equilibrium and mass transfer in agitated contractors. *Chromatogr. A.* 746, 185-198.

63. Fernandez, M.A., W.S. Laughinghouse, and G. Carta. 1996. Characterization of protein adsorption by composite silica-polyacrylamide gel anion exchangers II. Mass transfer in packed columns and predictability of breakthrough behavior. *Chromatogr. A.* 746, 185-198.
64. Fiercebiotech at [www.fiercebiotech.com](http://www.fiercebiotech.com) (2008). IMS Health statistics quoted.
65. Firon, A., G. Lesage, and H. Bussey. 2004. Integrative studies put cell wall synthesis on the yeast functional map. *Curr. Opin. Microbiol.* 7, 617-623.
66. Fisher, K.L. and J.P. Woods. 2000. Determination of beta-glucosidase enzymatic function of the *Histoplasma capsulatum* H antigen using a native expression system. *Gene.* 247, 191-197.
67. Follows, M., P. J. Hetherington, P. Dunnill, and M. D. Lilly. 1971. Release of enzymes from bakers' yeast by disruption in an industrial homogenizer. *Biotechnol. Bioeng.* 13, 549-560.
68. Freire, T., J. D'Alayer, and S. Bay. 2006. Efficient monitoring of enzymatic conjugation reaction by surface-enhanced laser desorption/ionization time of flight mass spectrometry for process optimization. *Bioconjugate Chem.* 17, 559-564.
69. Gallant, S., A. Kundu, and S. Cramer. 1995. Modeling non-linear elution of proteins in ion-exchange chromatography. *J. Chromatogr. A.* 702, 125-142.
70. Garcia, F.A.P. 1999. Cell disruption and lysis. In *Encyclopedia of Bioprocess Technology: Fermentation, Biocatalysis, and Bioseparation*; M.C. Flickinger and S.W. Drew, Eds.; John Wiley and Sons: New York, 493-504.
71. GE Healthcare Product Bulletin. 2008. High-Throughput Process Development with PreDicator Plates. Bulletin No. 28-9403-58AA.
72. Gerngross, T.U. 2004. Advances in the production of human therapeutic proteins in yeasts and filamentous fungi. *Nat. Biotechnol.* 22, 1409-1414.
73. Ghosh, R. 2002. Protein separation using membrane chromatography: Opportunities and challenges. *J. Chromatogr. A.* 952, 13-27.
74. Gjerde, D. and C. Hanna. 2009. Low dead volume extraction column device. US Patent 7,482,169.
75. Gritti, F., G. Gotmar, B.J. Stanley, and G. Guiochon. 2003. Determination of single component isotherms and affinity energy distribution by chromatography. *J. Chromatogr. A.* 988, 185-203.
76. Gu, T., G.J. Tsai, and G.T. Tsao. 1993. Modeling of nonlinear multicomponent chromatography. *Adv. Biochem. Eng.* 49, 46-71.

77. Guiochon, G., T. Farkas, H. Guan-Sajonz, J.-H. Koh, M. Sarker, B.J. Stanley, and M. Yun. 1997. Consolidation of particle beds and packing of chromatographic columns. *J. Chromatogr. A.* 762, 83-88.
78. Guiochon, G. 2002. Preparative liquid chromatography. *J. Chromatogr. A.* 965, 129-161.
79. Guiochon, G. and B. Lin. 2003. Modeling for Preparative Chromatography. Academic Press, San Diego, CA, USA.
80. Guiochon, G., A. Felinger, D. Shirazi, and A.M. Katti. 2006. Fundamentals of Preparative and Nonlinear Chromatography, 2<sup>nd</sup> edition. Elsevier Academic Press, San Diego, CA, USA.
81. Hagel, L., M. Ostberg, and T. Andersson. 1996. Apparent pore size distribution of chromatography media. *J. Chromatogr. A.* 743, 33-42.
82. Hahn, R., A. Tscheliessnig, A. Zöchling, and A. Jungbauer. 2005A. Shallow bed adsorption: Theoretical background and applications. *Chem. Eng. Technol.* 28, 1241-1251.
83. Hahn, R., P. Bauerhansl, K. Shimahara, C. Wizniewski, A. Tscheliessnig, and A. Jungbauer. 2005B. Comparison of protein A affinity sorbents II: Mass transfer properties. *J. Chromatogr. A.* 1093, 98-110.
84. Hall, K.R., L.C. Eagleton, A. Acrivos, and T. Vermeulen. 1966. Pore- and solid-diffusion kinetics in fixed-bed adsorption under constant-pattern conditions. *Ind. Eng. Chem. Fundam.* 5, 212-223.
85. Harrison, R., P. Todd, S. Rudge, and D. Petrides. 2003. Bioseparation Science and Engineering. Oxford University Press: New York.
86. Hatti-Kaul, R. and B. Mattiasson. 2003. Release of protein from biological host. In *Isolation and Purification of Proteins*; R. Hatti-Kaul and B. Mattiasson, Eds.; Marcel Dekker: New York, 1-27.
87. Helfferich, F.G. 1965. Ion-exchange kinetics. V. Ion-exchange accompanied by reactions. *J. Phys. Chem.* 69, 1178-1187.
88. Helfferich, F.G. 1990. Models and physical reality in ion-exchange kinetics. *React. Polym.* 13, 191-194.
89. Hermann, R., M. Lehmann, and J. Buchs. 2003. Characterization of gas-liquid mass transfer phenomena in microtiter plates. *Biotechnol. Bioeng.* 81, 178-186.
90. Herrmann, T., M. Schroder, and J. Hubbuch. 2006. Generation of equally sized particle plaques using solid-liquid suspension. *Biotechnol. Prog.* 22, 914-918.

91. Ho, C.W., T.K. Chew, T.C. Ling, S. Kamaruddin, W.S. Tan, and B.T. Tey. 2006. Efficient mechanical cell disruption of *Escherichia coli* by an ultrasonicator and recovery of intracellular hepatitis B core antigen. *Proc. Biochem.* 41, 1829-1834.
92. Hofmann, K.J., J.C. Cook, J.G. Joyce, D.R. Brown, L.D. Schultz, H.A. George, M. Rosolowsky, K.H. Fife, and K.U. Jansen. 1995. Sequence determination of human papillomavirus type 6a and assembly of virus-like particles in *Saccharomyces cerevisiae*. *Virology*. 209, 506-518.
93. Hofmann, K.J., M.P. Neeper, H.Z. Markus, D.R. Brown, M. Mueller, and K.U. Jansen. 1996. Sequence conservation within the major capsid protein of human papillomavirus (HPV) type 18 and formation of HPV-18 virus-like particles in *Saccharomyces cerevisiae*. *J. Gen. Virol.* 77, 465-468.
94. Hofmeister, F. 1888. On the understanding of the effects of salts. *Arch. Exp. Pathol. Pharmacol.* 24, 247-260.
95. Holz, C., B. Prinz, N. Bolotina, V. Sievert, K. Büsow, B. Simon B, U. Stahl, and C. Lang. 2003. Establishing the yeast *Saccharomyces cerevisiae* as a system for expression of human proteins on a proteome-scale. *J. Struct. Funct. Genomics.* 4, 97-108.
96. Hopkins, T.R. 1991. Physical and chemical cell disruption for the recovery of intracellular proteins. In *Purification and Analysis of Recombinant Proteins*; R. Seetharam and S.K. Sharma, Eds.; Marcel Dekker: New York, 57-83.
97. Horvath, C. and H.-J. Lin. 1978. Band spreading in liquid chromatography. General plate height equation and a method for the evaluation of the individual plate height contributions. *J. Chromatogr.* 149, 43-70.
98. Huang, R.B., B.A. Andrews, and J.A. Asenjo. 1991. Differential product release (DPR) of proteins from yeast: A new technique for selective product recovery from microbial cells. *Biotechnol. Bioeng.* 38, 977-985.
99. Hubbuch, J., T. Linden, E. Knieps, A. Ljunglof, J. Thommes, and M.R. Kula. 2003A. Mechanism and kinetics of protein transport in chromatographic media studied by confocal laser microscopy. Part I. The interplay of sorbent structure and fluid phase conditions. *J. Chromatogr. A.* 1021, 93-104.
100. Hubbuch, J., T. Linden, E. Knieps, J. Thommes, and M.-R. Kula. 2003B. Mechanism and kinetics of protein transport in chromatographic media studied by confocal laser microscopy. Part II. Impact on chromatographic separations. *J. Chromatogr. A.* 1021, 105-115.
101. Hummel, W. and M.R. Kula. 1989. Simple method for small-scale disruption of bacteria and yeast. *J. Microbiol. Met.* 9, 201-209.

102. Hunter, J.B. and J.A. Asenjo. 1988. A structured mechanistic model of the kinetics of enzymatic lysis and disruption of yeast cells. *Biotechnol. Bioeng.* 31, 929-943.
103. Hunter, A.K. and G. Carta. 2002. Protein adsorption on novel acrylamido-based polymeric ion-exchangers. IV. Effects of protein size on adsorption capacity and rate. *J. Chromatogr. A.* 971, 105-116.
104. Hutchinson, N., N. Bingham, N. Murrell, S. Farid, and M. Hoare. 2006. Shear stress analysis of mammalian cell suspensions for prediction of industrial centrifugation and its verification. *Biotechnol. Bioeng.* 95, 483-491.
105. Hutchinson, N., S. Chhatre, H. Baldascini, J.L. Davies, D.G. Bracewell, and M. Hoare. 2009. Ultra scale-down approach to correct dispersive and retentive effects in small-scale columns when predicting larger scale elution profiles. *Biotechnol. Prog.* 25, 1103-1110.
106. Indge, K.J. 1968. The effects of various anions and cations on the lysis of yeast protoplasts by osmotic shock. *J. Gen. Microbiol.* 51, 425-432.
107. Jackson, N.B, J.M. Liddell, and G.J. Lye. 2006. An automated microscale technique for the quantitative and parallel analysis of microfiltration operations. *J. Membrane Sci.* 276, 31-41.
108. James, C.J., W.T. Coakley, and D.E. Hughes. 1972. Kinetics of protein release from yeast sonicated in batch and flow systems at 20 kHz. *Biotechnol. Bioeng.* 14, 33-42.
109. Johansson, B.L., M. Belew, S. Eriksson, G. Glad, O. Lind, J.L Maloisel, and N. Norrman. 2003A. Preparation and characterization of prototypes for multi-modal separation media aimed for capture of negatively charged biomolecules at high salt conditions. *J. Chromatogr. A.* 1016, 21-33.
110. Johansson, B.L., M. Belew, S. Eriksson, G. Glad, O. Lind, J.L Maloisel, and N. Norrman. 2003B. Preparation and characterization of prototypes for multi-modal separation aimed for capture of positively charged biomolecules at high-salt conditions. *J. Chromatogr. A.* 1016, 35-49.
111. Jungbauer, A. 1993. Preparative chromatography of biomolecules. *J. Chromatogr. A.* 639, 3-16.
112. Jungbauer, A. and O. Kaltenbrunner. 1996. Fundamental questions in optimizing ion-exchange chromatography of proteins using computer-aided process design. *Biotechnol. Bioeng.* 52, 223-236.
113. Jungbauer, A. and O. Kaltenbrunner. 1999. Chromatography, computer-aided design. In *Encyclopedia of Bioprocess Technology: Fermentation, Biocatalysis, and Bioseparation*; M.C. Flickinger and S.W. Drew, Eds.; John Wiley and Sons: New York, 585-600.

114. Kalyanpur, M. 1999. Membrane separations. In *Encyclopedia of Bioprocess Technology: Fermentation, Biocatalysis, and Bioseparation*; M.C. Flickinger and S.W. Drew, Eds.; John Wiley and Sons: New York, 493-504.
115. Kapucu, H., N. Gulsoy, and U. Mehmetoglu. 2000. Disruption and protein release kinetics by ultrasonication of *Acetobacter peroxydans* cells. *Biochem. Eng. J.* 5, 57-62.
116. Kelley, B., S. Tobler, P. Brown, J. Coffman, R. Godavarti, T. Iskra, M. Switzer, and S. Vunnum. 2008A. Weak partitioning chromatography for anion exchange purification of monoclonal antibodies. *Biotechnol. Bioeng.* 101, 553-566.
117. Kelley, B., M. Switzer, P. Bastek, J. Kramarczyk, K. Molnar, T. Yu, and J. Coffman. 2008B. High-throughput screening of chromatographic separations: IV. Ion-exchange. *Biotechnol. Bioeng.* 100, 950-963.
118. Kempe, H., A. Axelsson, B. Nilsson, and G. Zacchi. 1999. Simulation of chromatographic process applied to separation of proteins. *J. Chromatogr. A.* 846, 1-12.
119. Kim, J., S.H. Jang, J. Guangyao, J.V. Zoval, N.A. Da Silvab, and M. J. Madou. 2004. Cell lysis on a microfluidic CD (compact disc). *Lab Chip.* 4, 516-522.
120. King, R.D., J. Rowland, S.G. Oliver, M. Young, W. Aubrey, E. Byrne, M. Liakata, M. Markham, P. Pir, L.N. Soldatova, A. Sparkes, K.E. Whelan, and A. Clare. 2009. The automation of science. *Science.* 324, 85-89.
121. Klis, F.M., P. Mol, K. Hellingwerf, and S. Brul. 2002. Dynamics of cell wall structure in *Saccharomyces cerevisiae*. *FEMS Microbiol. Rev.* 26, 239-256.
122. Klis, F.M., A. Boorsma, and P.W. De Groot. 2006. Cell wall construction in *Saccharomyces cerevisiae*. *Yeast.* 23, 185-202.
123. Knox, J.H., G.R. Laird, and P.A. Raven. 1976. Interaction of radial and axial dispersion in liquid chromatography in relation to the "infinite diameter effect". *J. Chromatogr. A.* 122, 129-145.
124. Knox, J.H. 1999. Band dispersion in chromatography – a new view of A-term dispersion. *J. Chromatogr. A.* 831, 3-15.
125. Kollar, R., B.B. Reinhold, E. Petrakova, H.J. Yeh, G. Ashwell, J. Drgonova, J.C. Kapteyn, F.M. Klis, and E. Cabib. 1997. Architecture of the yeast cell wall.  $\beta(1\rightarrow6)$ -glucan interconnects mannoprotein,  $\beta(1\rightarrow3)$ -glucan, and chitin. *J. Biol. Chem.* 272, 17762-17775.

126. Kramarczyk, J.F., B.D. Kelley, and J.L. Coffman. 2008. High-throughput screening of chromatographic separations: II. Hydrophobic interaction. *Biotechnol. Bioeng.* 100, 707-720.
127. Kula, M.R. and H. Schutte. 1987. Purification of proteins and the disruption of microbial cells. *Biotechnol. Prog.* 3, 31-42.
128. Ladisch, H. 2001. *Bioseparations Engineering: Principles, Practice, and Economics*, Wiley-Interscience: New York.
129. Laugharn, J.A. and B.S. Garrison. 2004. Apparatus and method for controlling sonic treatment. US Patent 6,719,449 B1.
130. Lawrence, S. 2007. Billion dollar babies- Biotech drugs as blockbusters. *Nature Biotechnol.* 25, 380-382.
131. Lenhoff, A. 1987. Significance and estimation of chromatographic parameters. *J. Chromatogr. A.* 384, 285-299.
132. Lesage, G. and H. Bussey. 2006. Cell wall assembly in *Saccharomyces cerevisiae*. *Microbiol. Mol. Biol. Rev.* 70, 317-343.
133. LeVan, M.D., G. Carta, and C.M. Yon. 2008. Absorption and Ion Exchange. In *Perry's Chemical Engineers' Handbook, 8<sup>th</sup> Edition*; D.W. Green and R.H. Perry, Eds.; McGraw-Hill: New York, Chapter 16.
134. Lewus, R.K. and G. Carta. 2001. Protein transport in constrained anionic hydrogels: Diffusion and boundary layer mass transfer. *Ind. Eng. Chem. Res.* 40, 1548-1558.
135. Li, H., N. Sethuraman, T. A. Stadheim, D. Zha, B. Prinz, N. Ballew, P. Bobrowicz, B.-K. Choi, W. J. Cook, M. Cukan, N.R. Houston-Cummings, R. Davidson, B. Gong, S. R. Hamilton, J.P. Hoopes, Y. Jiang, N. Kim, R. Mansfield, J.H. Nett, S. Rios, R. Strawbridge, S. Wildt, and T.U. Gerngross. 2006. Optimization of humanized IgGs in glycoengineered *Pichia pastoris*. *Nat. Biotechnol.* 24, 210-215.
136. Lightfoot, E.N. and J.S. Moscariello. 2004. Bioseparations. *Biotechnol. Bioeng.* 87, 259-273.
137. Linden, T., A. Ljunglof, M.-R. Kula, and J. Thommes. 1999. Visualizing two-component protein diffusion in porous adsorbents by confocal scanning laser microscopy. *Biotechnol. Bioeng.* 65, 622-630.
138. Londo, T., P. Lynch, T. Kehoe, M. Meys, and N. Gordon. 1998. Accelerated recombinant protein purification process development automated, robotics-based integration of chromatographic purification and analysis. *J. Chromatogr. A.* 798, 73-82.

139. Lyddiatt, A. and D.A. O'Sullivan. 1998. Biochemical recovery and purification of gene therapy vectors. *Curr. Opin. Biotechnol.* 9, 177-185.
140. Lyddiatt, A. 2002. Process chromatography: Current constraints and future options for the adsorptive recovery of bioproducts. *Curr. Opin. Biotechnol.* 13, 95-103.
141. Mach, H., D.B. Volkin, R.D. Troutman, B. Wang, Z. Luo, K.U. Jansen, and L. Shi. 2006. Disassembly and reassembly of yeast-derived recombinant human papillomavirus virus-like particles. *J. Pharm. Sci.* 95, 2195-2206.
142. Mandenius, C.F., and A. Brundin. 2008. Bioprocess optimization using design-of-experiments methodology. *Biotechnol. Prog.* 24, 1191-1203.
143. Mannall, G.J., J.P. Myers, J. Liddell, N. J. Titchener-Hooker, and P. A. Dalby. 2008. Ultra scale-down of protein refold screening in microwells: Challenges, solutions and application. *Biotechnol. Bioeng.* 103, 329-340.
144. Maranga, L., T.F. Brazão, and M.J.T. Carrondo. 2003. Virus-like particle production at low multiplicities of infection with the baculovirus insect cell system. *Biotechnol. Bioeng.* 84, 245-253.
145. Marques, M.P.C, J.M.S. Cabral, and P. Fernandes. 2009. High throughput in biotechnology: From shake-flasks to fully instrumented microfermentors. *Recent Pat. Biotechnol.* 3, 124-140.
146. Martin, A.J.P. and R.L.M. Synge. 1941. A new form of chromatogram employing two liquid phases. *Biochem. J.* 35, 1358-1368.
147. McCarthy, M.P., W.I. White, F. Palmer-Hill, S. Koenig, and J.A. Suzich. 1998. Quantitative disassembly and reassembly of human papillomavirus type 11 viruslike particles *in vitro*. *J. Virol.* 72, 32-41.
148. Melander, W., Z.E. Rassi, and C. Horvath. 1989. Interplay of hydrophobic and electrostatic interactions in biopolymer chromatography: Effect of salts on the retention of proteins. *J. Chromatogr. A.* 469, 3-27.
149. Micheletti, M. and G.J. Lye. 2006. Microscale bioprocess optimisation. *Curr. Opin. Biotechnol.* 17, 611-618.
150. Middelberg, A.P.J. 1995. Process-scale disruption of microorganisms. *Biotech. Adv.* 3, 491-551.
151. Milavec, P., A. Podgomik, R. Stravs, and T. Koloini. 2002. Effect of experimental error on the efficiency of different optimization methods for bioprocess media optimization. *Bioprocess Biosyst. Eng.* 25, 69-78.
152. Miozzari G.F., P. Niederberger P, and R. Hütter. 1978. Permeabilization of microorganisms by Triton X-100. *Anal. Biochem.* 90, 220-233.

153. Muller, E. 2005. Properties and characterization of high capacity resins for biochromatography. *Chem. Eng. Technol.* 28, 1295-1305.
154. Murphy, J.C., M.A. Winters, and S.L. Sagar. 2006. Large-scale, nonchromatographic purification of plasmid DNA. *Methods Mol Med.* 127, 351-362.
155. Nealon, A.J., R.D O'Kennedy, N.J. Titchener-Hooker, and G.J. Lye. 2006. Quantification and prediction of jet macro-mixing times in static microwell plates. *Chem. Eng. Sci.* 61, 4860-4870.
156. Neeper, M.P., K.J. Hofmann, and K.U. Jansen. 1996. Expression of the major capsid protein of human papillomavirus type 11 in *Saccharomyces cerevisiae*. *Gene.* 180, 1-6.
157. Ng, P.K., J. He, and P. Gagnon. 2007. Mechanistic model for adsorption of immunoglobulin on hydroxyapatite. *J. Chromatogr. A.* 1142, 13-18.
158. Nguyen, H., B. Martinez, N. Oganessian, and R. Kim. 2004. An automated small-scale protein expression and purification screening provides beneficial information for protein production. *J. Struct. Funct. Genomics.* 5, 23-27.
159. Nti-Gyabaah, J., I. Ikechukwu, M.E. Dahlgren, M. Iammarino, D. Roush, and T. Linden. 2009. Application of high-pressure liquid-chromatography for purification of therapeutic proteins to reduce cycle time. Abstracts of Papers, 238th ACS National Meeting, Washington, DC, United States, August 16-20.
160. Ohno, K., K. Tachikawa, and A. Manz. 2008. Microfluidics: Application for analytical purposes in chemistry and biochemistry. *Electrophoresis.* 29, 4443-4453.
161. Park, L.J., C.H. Park, C. Park, and T. Lee. 1997. Application of genetic algorithms to parameter estimation of bioprocesses. *Med. Biol. Eng. Comput.* 35, 47-49.
162. Polson, A. 1950. Some aspects of diffusion in solution and a definition of a colloidal particle. *J. Phys. Colloid Chem.* 54, 649-652.
163. Prather, K.J., S. Sagar, J. Murphy, and M. Chartrain. 2003. Industrial scale production of plasmid DNA for vaccine and gene therapy: Plasmid design, production, and purification. *Enz. Microbiol. Technol.* 33, 865-883.
164. Prinz, B., J. Schultchen, R. Rydzewski, C. Holz, M. Boettner, U. Stahl, and C. Lang. 2004. Establishing a versatile fermentation and purification procedure for human proteins expressed in the yeasts *Saccharomyces cerevisiae* and *Pichia pastoris* for structural genomics. *J. Struct. Funct. Genomics* 5, 29-44.
165. Rathore, A.S. and H. Winkle. 2009. Quality by design for biopharmaceuticals. *Nat. Biotechnol.* 27, 26-34.

166. Redaelli, L., F. Zolezzi, V. Nardese, B. Bellanti, V. Wanke, D. Carettoni. 2005. A platform for high-throughput expression of recombinant human enzymes secreted by insect cells. *J. Biotechnol.* 120, 59-71.
167. Rege, K., M. Pepsin, B. Falcon, L. Steele, and M. Heng. 2006. High-throughput process development for recombinant protein purification. *Biotechnol. Bioeng.* 93, 618-630.
168. Regnier, F. and I. Mazsaroff. 1987. A theoretical examination of adsorption processes in preparative liquid chromatography of proteins. *Biotechnol. Progress.* 3, 22-26.
169. Regnier, F. 1991. Perfusion chromatography. *Nature.* 350, 634-635.
170. Reichert, J.M. 2008. Monoclonal antibodies as innovative therapeutics. *Curr. Pharm. Biotechnol.* 9, 423-430.
171. Retallack, D, J.C. Schneider, J. Mitchell, L. Chew, and H. Liu. 2007. Transport of heterologous proteins to the periplasmic space of *Pseudomonas fluorescens* using a variety of native signal sequences. *Biotechnol. Lett.* 29, 1483-1491.
172. Reynolds, O. 1883. An experimental investigation of the circumstances which determine whether the motion of water shall be direct or sinuous, and of the law of resistance in parallel channels. *Philosophical Transactions of the Royal Society.* 174, 935-982.
173. Reynolds T., M. Boychyn, T. Sanderson, M. Bulmer, J. More, and M. Hoare. 2003. Scale-down of continuous filtration for rapid bioprocess design: Recovery and dewatering of protein precipitate suspensions. *Biotechnol. Bioeng.* 83, 454-464.
174. Rhodes, M. 2008. Fluid Flow through a Packed Bed of Particles. In *Introduction to Particle Technology*; John Wiley & Sons: West Sussex, England, 153-168.
175. Rios, S., E. M. Giaccone, and T.U. Gerngross. 2007. Rapid screening of chromatography resins for the purification of proteins. In *Methods in Molecular Biology*; J. M. Cregg, Ed.; Humana Press Inc.: Totowa, NJ, 99-106.
176. Roque, A.C., G. Gupta, and C.R. Lowe. 2005. Design, synthesis, and screening of biomimetic ligands for affinity chromatography. *Methods Mol. Biol.* 310, 43-62.
177. Rose, R.C., W. Bonnez, R.C. Reichman, and R.L. Garcea. 1993. Expression of human papillomavirus type-11 L1 protein in insect cells: In vivo and in vitro assembly of viruslike particles. *J. Virol.* 67, 1936-1944.

178. Rossi, J.L., L. Gissmann, K. Jansen, and M. Muller. 2000. Assembly of infectious human papillomavirus type 16 virus-like particle in *Saccharomyces cerevisiae*. *Hum. Gene Ther.* 11, 1165-1176.
179. Rouf, S.A., P.L. Douglas, M. Moo-Young, and J.M. Scharer. 2001. Computer simulation for large scale bioprocess design. *Biochem. Eng. J.* 8, 229-234.
180. Rounds, M.A and F.E. Regnier. 1984. Evaluation of a retention model for high-performance ion-exchange chromatography using two different displacing salts. *J. Chromatogr. A.* 283, 37-45.
181. Ruthven, D. M. 2000. The rectangular isotherm model for adsorption kinetics. *Adsorption.* 6, 287-291.
182. Salazar, O. and J.A. Asenjo. 2007. Review: Enzymatic lysis of microbial cells. *Biotechnol. Lett.* 29, 985-994.
183. Schmidt, F.R. 2004. Recombinant expression systems in the pharmaceutical industry. *Appl. Microbiol. Biotechnol.* 65, 363-372.
184. Shalliker, R.A., B.S. Broyles, and G. Guiochon. 2000. Physical evidence of two wall effects in liquid chromatography. *J. Chromatogr. A.* 888, 1-12.
185. Shalliker, R.A., B.S. Broyles, and G. Guiochon. 2003. Axial and radial diffusion coefficients in a liquid chromatography column and bed heterogeneity. *J. Chromatogr. A.* 994, 1-12.
186. Shank-Retzlaff, M.L., Q. Zhao, C. Anderson, M. Hamm, K. High, M. Nguyen, F. Wang, N. Wang, B. Wang, M. Washabaugh, R. Sitrin, and L. Shi. 2006. Evaluation of the thermal stability of Gardasil®. *Hum. Vaccine.* 2, 147-154.
187. Shapiro, M., S.J. Haswell, G.J. Lye, and D.G. Bracewell. 2009. Design and characterization of a microfluidic packed bed system for protein breakthrough and dynamic binding capacity determination. *Biotechnol. Prog.* 25, 277-285.
188. Sharma, B.P. Cell Separation, Sedimentation. 1999. In *Encyclopedia of Bioprocess Technology: Fermentation, Biocatalysis, and Bioseparation*; M.C. Flickinger and S.W. Drew, Eds.; John Wiley and Sons: New York, 548-553.
189. Shi, L., G. Sanyal, A. Ni, Z. Luo, S. Doshna, B.Wang, T.L. Graham, N. Wang, and D. Volkin. 2005. Stabilization of human papillomavirus virus-like particles by non-ionic surfactants. *J. Pharm. Sci.* 94, 1538-1551.

190. Shukla, A.A., B. Hubbard, T. Tressel, S. Guhan, and D. Low. 2007A. Downstream processing of monoclonal antibodies: Application of platform approaches. *J. Chromatogr. B. Analyt. Technol. Biomed. Life Sci.* 848, 28-39.
191. Shukla, A.K., M.M. Shukla, and A.M. Shukla. 2007B. Incision-based filtration/ separation pipette tip. US Patent 7,276,158.
192. Skidmore, G.L., B.J. Horstmann, and H.A. Chase. 1990. Modeling single-component protein adsorption to the cation exchanger S Sepharose FF. *J. Chromatogr. A.* 498, 113-128.
193. Smith, A.E., Z. Zhang, C.R. Thomas, K.E. Moxham, and A.P.J. Middelberg. 2000. The mechanical properties of *Saccharomyces cerevisiae*. *Proc. Natl. Acad. Sci. USA.* 97, 9871-9874.
194. Smith, C. 2005. Striving for purity: Advances in protein purification. *Nature Methods.* 2, 71-76.
195. Soriano, E., N. Borth, H. Katinger, and D. Mattanovich. 2002. Optimization of recombinant protein expression level in *Escherichia coli* by flow cytometry and cell sorting. *Biotechnol. Bioeng.* 80, 93-99.
196. Stromberg, P., J. Rotticci-Mulder, R. Bjornestedt, and S.R. Schmidt. 2005. Preparative parallel protein purification (P4). *J. Chromatogr. B Analyt. Technol. Biomed. Life Sci.* 818, 11-18.
197. Sun, S., L.H.T. Nguyen, O.H. Ross, G.F. Hollis, and R. Wynn. 2002. Quantitative analysis of c-myc-tagged protein in crude cell extracts using fluorescence polarization. *Anal. Biochem.* 307, 287-296.
198. Teo, W. and D. Ruthven. 1986. Adsorption of water from aqueous ethanol using 3-Å molecular sieves. *Ind. Eng. Chem. Proc. Des. Dev.* 25, 17-21.
199. Thiemann, J., J. Jankowski, J. Rykl, S. Kurzawski, T. Pohl, B. Wittmann-Liebold, and H. Schlüter. 2004. Principle and application of the protein-purification-parameter screening system. *J. Chromatogr. A* 1043, 73-80.
200. Thomas, H.C. 1944. Heterogeneous ion exchange in a flowing system. *J. Amer. Chem. Soc.* 66, 1664-1666.
201. Titchener-Hooker, N.J., P. Dunnill, and M. Hoare. Micro biochemical engineering to accelerate the design of industrial-scale downstream processes for biopharmaceutical proteins. 2008. *Biotechnol. Bioeng.* 100, 473-487.
202. Tswett, M. 1906. *Ber. Dtsch. Botan. Ges.* 24, 384-393.
203. Tuft Center for the Study of Drug Development. Outlook 2009. [www.csdd.tufts.edu](http://www.csdd.tufts.edu)

204. Tugcu, N., M. Song, C.M. Breneman, N. Sukumar, K.P. Bennett, and S.M. Cramer. 2003. Prediction of the effect of mobile-phase salt type on protein retention and selectivity in anion exchange systems. *Anal. Chem.* 75, 3563-3572.
205. Tustian A.D., H. Salte, N.A. Willoughby, I. Hassan, M.H. Rose, F. Baganz, M. Hoare, and N.J. Titchener-Hooker. 2007. Adapted ultra scale-down approach for predicting the centrifugal separation behavior of high cell density cultures. *Biotechnol. Prog.* 23, 1404-1410.
206. van Deemter, J.J., F.J. Zuiderweg, and A. Klinkenberg. 1956. Longitudinal diffusion and resistance to mass transfer as causes of non ideality in chromatography. *Chem. Eng. Sci.* 5, 271-289.
207. Varga, E.G., N.J. Titchener-Hooker, and P. Dunnill. 1998. Use of scale-down methods to rapidly apply natural yeast homogenisation models to a recombinant strain. *Bioprocess Eng.* 19, 373-380.
208. Vasquez-Alvarez, E., M.E. Lienqueo, and J.M. Pinto. 2001. Optimal synthesis of protein purification processes. *Biotechnol. Prog.* 17, 685-696.
209. Velayudhan, A. 1990. Studies in nonlinear chromatography. In: *Doctoral Dissertation*, Yale University.
210. Walsh, G. 2006. Biopharmaceutical benchmarks 2006. *Nat. Biotechnol.* 24, 769-774.
211. Wang, M., L.L. Wang, L.F. Chen, Y.H. Han, Y.H. Zou, J.Y. Si, and G.X. Song. 2003. Expression of human papillomavirus type 6 L1 and L2 isolated in China and self assembly of virus-like particles by the products. *Acta Biochim. et Biophys. Sinica* 35, 27-34.
212. Weaver, L.E. and G. Carta. 1996. Protein adsorption on cation exchangers: Comparison of macroporous and gel-composite media. *Biotechnol. Prog.* 12, 342-355.
213. Weinberger, S.R., E. Boschetti, P. Santambien, and V. Brenac. 2002. Surface-enhanced desorption-ionization retentate chromatography mass spectrometry (SELDI-RC-MS): A new method for rapid development of process chromatography conditions. *J. Chromatogr. B. Analyt. Technol. Biomed. Life Sci.* 782, 307-316.
214. Wenger, M.D., P. DePhillips, C.E. Price, and D.G. Bracewell. 2007. An automated microscale chromatographic purification of virus-like particles as a strategy for process development. *Biotechnol. Appl. Biochem.* 47, 131-139.
215. Wenger, M.D., P. DePhillips, and D.G. Bracewell. 2008. A microscale yeast cell disruption technique for integrated process development strategies. *Biotechnol. Prog.* 24, 606-614.

216. Wensel, D.L., B.D. Kelley, and J.L. Coffman. 2008. High-throughput screening of chromatographic separations: III. Monoclonal antibodies on ceramic hydroxyapatite. *Biotechnol. Bioeng.* 100, 839-854.
217. Whelan, K.E. and R.D. King. 2004. Intelligent software for laboratory automation. *Trends in Biotechnol.* 22, 440-445.
218. Whitley, R.D., R. Wachter, F. Liu, and H.-W.L. Wang. 1989. Ion-exchange equilibria of lysozyme, myoglobin, and bovine serum albumin: Effective valence and exchanger capacity. *J. Chromatogr. A.* 465, 137-156.
219. Wicke, E. 1939. Empirische und theoretische Untersuchungen der Sorptionsgeschwindigkeit von Gasen an porösen Stoffen - II. (Empirical and Theoretical Investigations of the Sorption Velocity of Gases on Porous Substances – II. *Kolloid Z.* 86, 295-313.
220. Wiendahl, M., P. S. Wierling, J. Nielsen, D. F. Christensen, J. Krarup, A. Staby, and J. Hubbuch. 2008. High throughput screening for the design and optimization of chromatographic processes – Miniaturization, automation, and parallelization of breakthrough and elution studies. *Chem. Eng. Technol.* 31, 893-903.
221. Wierling, P.S., R. Bogumil, E. Knieps-Grunhagen, and J. Hubbuch. 2007. High throughput screening of packed-bed chromatography coupled with SELDI-TOF MS analysis: Monoclonal antibodies versus host cell protein. *Biotechnol. Bioeng.* 98, 440-450.
222. Willoughby N., P. Martin, and N. Titchener-Hooker. 2004. Extreme scale-down of expanded bed adsorption: Purification of an antibody fragment directly from recombinant *E. coli* culture. *Biotechnol. Bioeng.* 87, 641-647.
223. Wilson, J.N. 1940. A theory of chromatography. *J. Am. Chem. Soc.* 62, 1583-1591.
224. Wilson, E.J. and C.J. Geankoplis. 1996. Liquid mass transfer at very low Reynolds numbers in packed beds. *Ind. Eng. Chem. Fundamen.* 5, 9–14.
225. Wurm, F.M. 2004. Production of recombinant therapeutics in cultivated mammalian cells. *Nat. Biotechnol.* 11, 1393-1398.
226. Yang, K., Q.-H. Shi, and Y. Sun. 2006. Modeling and simulation of protein uptake in cation exchanger visualized by confocal laser scanning microscopy. *J. Chromatogr. A.* 1136, 19-28.
227. Yang, T., M.C. Sundling, A.S. Freed, C.M. Breneman, and S.M. Cramer. 2007A. Prediction of pH-dependent chromatographic behavior in ion-exchange systems. *Anal. Chem.* 79, 8927-8939.

228. Yang, T., C.M. Breneman, and S.M. Cramer. 2007B. Investigation of multi-modal high-salt binding ion-exchange chromatography using quantitative structure-property relationship modeling. *J. Chromatogr. A.* 1175, 96-105.
229. Zhang, Z., S. Burton, S. Williams, E. Thwaites, and A. Lyddiatt. 2001. Design and assembly of solid-phases for the effective recovery of nanoparticulate bioproducts in fluidised bed contactors. *Bioseparation.* 10, 113-132.
230. Zhang, Y. and L.R. Lynd. 2003. Quantification of cell and cellulase mass concentrations during anaerobic cellulose fermentation: Development of an ELISA-based method with application to *Clostridium thermocellum* batch cultures. *Anal. Chem.* 75, 219-227.
231. Zhang, Y. and P.S. Cremer. 2006. Interactions between macromolecules and ions: The Hofmeister series. *Curr. Opin. Biol. Chem.* 10, 658-663.
232. Zhang H., S. Kong, A. Booth, R. Boushaba, M.S. Levy, and M. Hoare. 2007. Prediction of shear damage of plasmid DNA in pump and centrifuge operations using an ultra scale-down device. *Biotechnol. Prog.* 23, 858-865.
233. Zhou, Y.H. and N.J. Titchener-Hooker. 1999. Simulation and optimisation of integrated bioprocesses: a case study. *J. Chem. Technol. Biotechnol.* 74, 289-292.
234. Zhou, X-P., W. Li, Q.-H. Shi, and Y. Sun. 2006. Analysis of mass transport models for protein adsorption to cation exchanger by visualization with confocal laser scanning microscopy. *J. Chromatogr. A.* 1103, 110-117.
235. Zhu, J., A.M. Katti, and G. Guiochon. Comparison of various isotherm models for predicting competitive adsorption data. 1991. *J. Chromatogr. A.* 552, 71-89.